Phenotype-specific store-operated calcium entry and the differentiation response in neuroblastoma cells

Claire Whitworth

Thesis submitted for the degree of Doctor of Philosophy

Institute for Cell and Molecular Biosciences
Faculty of Medical Sciences
Newcastle University

September 2015

Abstract

Understanding the fundamental molecular mechanisms that control the proliferation-differentiation cellular switch and maintenance of the differentiated state is needed to fully harness the therapeutic potential for highly detrimental diseases such as cancer and neurodegenerative disorders. Intracellular free Ca^{2+} plays an essential role in the differentiation process and, more specifically, the ubiquitous Ca^{2+} signalling pathway; store-operated Ca^{2+} entry (SOCE) is altered with differentiation. The SH-SY5Y neuroblastoma cancer cell line was utilised in this study to investigate the role of SOCE in phenotype-specific differentiation responses using morphological, biochemical and functional single cell, Ca^{2+} imaging techniques.

Neuroblastoma is a paediatric malignancy of the sympathetic nervous system that is comprised of immature neural crest cells. Retinoic acid is used to treat neuroblastoma patients however many respond poorly, leading to aggressive disease progression. The SH-SY5Y neuroblastoma-derived cell line consists of three morphologically distinct phenotypes; immature neuroblastic N-type cells, non-neuronal S-type cells and putative intermediate I-type cells, which exhibit variable tumourgenicity and can be induced to differentiate using 9-*cis*-retinoic acid (9*c*RA).

The 9*c*RA-induced differentiation response of N-type and S-type populations involved morphological changes accompanied by an uncoupling of SOCE from Ca^{2+} store release that could be observed from the first day of 9cRA treatment. SOCE down-regulation was attributed to changes in expression and localisation of the CRAC channel protein Orai1 and the Ca^{2+} sensing protein STIM1. The extent of SOCE uncoupling was influenced in N-type and I-type cells but not S-type cells by the predominant background cell environment. Conditioned media from proliferating and differentiating N-type and S-type populations was also able to influence cell phenotype and the associated SOCE responses.

This study describes how the 9*c*RA-induced differentiation response occurred in a multi-step manner in N-type populations and in gradual manner in S-type populations and raises the possibility that SOCE proteins could potentially be utilised as drug targets in neuroblastoma treatment or neurodegenerative disease therapy.

Acknowledgements

First, I thank my supervisor Dr Tim Cheek for providing me with the opportunity to undertake this research in his lab and also for putting up with my antics for the last four years! He has offered me guidance when I was unsure, support when I wanted to push myself and countless friendly chats over the much needed tea breaks! I also thank my co-supervisor Dr Chris Redfern for his profound help at the drop of a hat and, as ever, his unwavering patience with statistics. I don't think I'll ever grasp the complexities so it seems I will forever badger you with numbers and stats complaints!

A huge thank you to Dr Natalie Bell for her excellent guidance at the beginning of this project, continued support and friendship. Thanks also to the lab oracle that is Maureen Sinclair who got me started, offered extensive advice over my first two years and ensured the lab was always in working order (and stocked with tea and biscuits).

I thank Dr Mark Levasseur for the many, many, MANY hours of microscope availability he granted me as well as for his expertise when setting up the new system. This project really wouldn't have taken this angle without it. I also thank Professor Caroline Austin and Lauren Harkin for their collaboration with the RNA sequencing data as well as Dr Simon Cockell and Robert Stones for their bioinformatics support.

To the excel wizard Dr Graham Scholefield, I thank you not only for the collaboration to build the tool for efficient analysis (without it I would have been analysing this data forevermore!) but also for the ridiculous amount of support you have given me over the last couple of years. You've been my go-to for all technical lab issues, pushed me to stay motivated, nurtured my strengths and helped me to recognise them as well as having been a shoulder to cry on when it was all too much!

Finally I would like to thank the amazing PAN!C! One of the aspects of my time in ICaMB that I am truly most proud of stems from co-founding this student network. So many hours of organising, planning, rounding up peers, plastering the walls of ICaMB in posters and, of course, fun and drinking, were totally worth it! Even if it did take me away from the lab bench….

Contents

Chapter 1: Introduction

Mapping the subcellular and molecular changes that accompany cell differentiation is a valuable strategy for the resolution of many global health issues. Understanding the mechanisms that drive and maintain the differentiated state of neuronal cells is of particular importance to fully harness the therapeutic potential for highly detrimental diseases such as neurodegenerative disorders (Berridge 2010) and cancer (Chen 2013). The ability to encourage differentiation of stem cells towards a fully neuronal phenotype is the considered the holy grail of neurobiology. Our laboratory has utilised immature neuroblastic cells as a model for the investigation of neuronal differentiation and related alterations in Ca^{2+} signalling pathways associated with Ca^{2+} entry into the cell (Brown 2005; Riddoch 2007; N. Bell 2013). This model can also be used to study cancer cell differentiation as uncontrolled proliferation of immature neuroblasts manifests as neuroblastoma (Bourdeaut 2008). Manipulation of the Ca^{2+} signalling pathways involved in cancer cell differentiation and defining the associated mechanisms that drive a specific cell population towards a differentiated state could also have significant implications for the development of novel anti-cancer drug targets.

1.1. Neuroblastoma is resilient

Neuroblastoma is a neural crest-derived paediatric malignancy with which primary tumours arise in the sympathetic nervous system, often forming in the adrenal glands. Neuroblastoma represents around ~6% of childhood cancers (Siegel 2013), with highest prevalence occurring in infants under 1 year old which is likely attributed to tumourigenesis taking place during embryonic development (Cancer Research UK 2014). As with the majority of cancers, age and stage at diagnosis, as well as biochemical factors, significantly influence neuroblastoma prognosis. Patients often present with metastatic disease whereby prognosis worsens and recurrence is more likely. Advanced cases are particularly difficult to treat successfully, despite the use of aggressive multimodal therapies. The retinoid 13-cis-retinoic acid (13*c*RA) is administered alongside standard chemotherapeutic agents in order to initiate differentiation of immature neuroblastic cells thereby rendering the tumour benign

and preventing further proliferation and invasion of advanced and residual disease (Barletta 1997). Despite the implementation of retinoid therapy, survival remains fairly poor for these patients (Matthay 2009; Navalkele 2011). Elucidating the mechanistic contributors to the molecular switch from cellular proliferation to differentiation and for maintenance of this differentiated state in cancerous cells is therefore crucial for the advancement of increasingly efficacious therapies to ultimately improve patient survival.

1.2. Tumour heterogeneity influences treatment success

Heterogeneity exists within neoplastic tissue, the composition of which may include numerous cell phenotypes that exhibit a range of proliferative, motile and invasive capabilities (Fidler 1978). The variety of tumourigenic characteristics displayed by cells within a tumour poses a complex and challenging problem in terms of treatment specificity and efficacy towards all neoplastic cells of the disease but could significantly impact the success of a treatment. Since specific cell phenotypes may be more adept at surviving aggressive therapeutic insult or acquire resistance to chemotherapeutic agents, tumour advancement and metastasis would, presumably, be more likely to occur when treatment is only effective against a specific subset of cancerous cells. This complexity is increased further when taking into account the host environment, given that the aggressive nature of cancerous cells and their potential to establish a tumour is also influenced by their microenvironment and local expression of intrinsic factors (Raz 1987; Potter 2007).

Neuroblastoma disease outcome is highly variable, progressing aggressively in some patients whilst spontaneously regressing or maturating to benign ganglioneuromas in others (Pritchard 1994; Nakagawara 1998; Schwab 2003; Hero 2008). This diverse variability in disease outcome may be attributed to the heterogeneity of neuroblastoma cells and their range of characteristics associated with tumourgenicity and treatment resistance (Bernal 1983; Ross 2003; Ross 2004; Walton 2004; Coco 2005).

1.3 Neuroblastoma is comprised of three distinct cell phenotypes

Neuroblastoma tumours consist of several neural crest cell lineages and three distinct cell phenotypes are known to reside in neuroblastoma cell lines (Figure 1.3.1), each with a particular set of morphological and biochemical characteristics and tumour forming capacity. Neuroblastic N-type cells are generally the predominant cell type (Ciccarone 1989) and are identifiable by their small, rounded cell bodies and the presence of short neurite-like processes (Figure 1.3.1). In culture, N-type cells are fast growing, adhere weakly to substrate, form cell aggregates (Figure 1.3.1), and express typical neuronal cell markers such as neurofilament protein (Ciccarone 1989), the neurotransmitter enzyme dopamine β-hydroxylase (Ross 1983; Ciccarone 1989) and the microtubule protein β-tubulin III (Whitworth 2012; N. Bell 2013). N-type cells differentiate towards a neuronal lineage upon exposure to differentiation-inducing compounds such as retinoic acid (RA), developing extended neuritic processes (Whitworth 2012; N. Bell 2013).

Substrate-adherent S-type cells are non-neuronal precursors that form flat monolayers and can be distinguished by their large, flat cell bodies, abundant cytoplasm with the absence of neuritic processes (Figure 1.3.1). In culture, S-type cells are slow growing, adhere strongly to substrate and express proteins characteristic to a range of non-neuronal cell types such as the intermediate filament protein vimentin (Whitworth 2012; N. Bell 2013) which is indicative of Schwann cells, melanocytes and immature glial cells, the extracellular matrix protein fibronectin and the melanocyte marker tyrosinase (Ross 1985; Ciccarone 1989). This expression profile implies that S-type cells may be the embryonic neural crest precursors for Schwann cells, glial cells and melanocytes. Upon RA-induced differentiation, S-type cells become more epithelial-like with a flattened morphology, more abundant cytoplasm and spread cell margins (Whitworth 2012; N. Bell 2013). S-type cells express the neuronal microtubule protein β-tubulin III, which is down-regulated following RA-mediated differentiation (N. Bell 2013). This expression could be indicative of recent transdifferentiation from the N-phenotype and β-tubulin III down-regulation with S-type differentiation implies commitment to a non-neuronal lineage. Since morphological and biochemical phenotypic interconversion can occur spontaneously in neuroblastoma cell culture

(Biedler 1975; Ross 1983; Ciccarone 1989), understanding this phenotypic plasticity may provide reasoning as to why retinoid therapy is not always effective.

Intermediate I-type cells exhibit characteristics of both the N- and S-phenotype, being moderately substrate adherent with an intermediate abundance of cytoplasm and can possess spindly projections comparable to the neurite-like processes of N-type cells (Figure 1.3.1). Given their morphological similarity to the N- and S-type cells, they can be difficult to distinguish in culture. I-type cells may represent a multi-potent progenitor or stem cell population that gives rise to the neuronal N-type or non-neuronal S-type lineage (Ciccarone 1989; Ross 1995) (Figure 1.3.2iii). Alternatively, it has also been shown that bidirectional transdifferentiation occurs between N-type and S-type cells (Ross 1983; Ciccarone 1989) (Figure 1.3.2i), which may take place with the I-type as an intermediate cell type (Figure 1.3.2ii). The I-type population may not actually signify a specific cell population and instead reflect a transient morphology of direct N-type to S-type interconversion associated with the cell phenotype at a particular point mid-transition. At present, the true identity of the putative I-type population and the common pathway for spontaneous transdifferentiation are unclear. Regardless of the I-type identity, persistence of this population following treatment would likely instigate tumour progression.

Of the three cell phenotypes, I-type cells are considerably more tumourigenic than N-type and S-type cells and neuroblastoma tumours with high numbers of I-type cells were associated with the poorest outcomes (Walton 2004). N-type cells are considered to have a greater malignant potential than S-type cells since they form the bulk of most neuroblastoma tumours (Walton 2004), have been shown to cause more aggressive tumour growth *in vivo* and, in response to RA treatment, less apoptosis *in vitro* (Picacentini 1996). This could be reflective of a differentiation-mediated, up-regulation of the anti-apoptotic protein Bcl-2, which promotes cell survival through inhibition of cytochrome c release from the mitochondria (Zhang 1996), and has previously been observed in RA-differentiated SH-SY5Y neuroblastoma cells (Hanada 1993; Lasorella 1995; N. Bell 2013). Bcl-2 up-regulation in this case also correlated with a differentiated phenotype and has been associated with increased chemotherapeutic

drug resilience (Lasorella 1995) compared to neuroblastoma-derived cell lines with low Bcl-2 expression (Hanada 1993). RA-induced Bcl-2 up-regulation in SH-SY5Y cells can also increase resistance to the retinoid analogue fenritinide, which can inhibit proliferation and trigger apoptosis in neuroblastoma cells (Armstrong 2012). Potentially, targeting Bcl-2 to reduce expression or action via the p53 pathway may prevent chemotherapeutic sensitivity and increase response.

Neuroblastoma tumours can spontaneously regress or mature into benign ganglioneuromas (Pritchard 1994; Nakagawara 1998; Schwab 2003; Hero 2008) consisting predominantly of differentiating S-type and N-type cells (Ambros 1996; Nishihira 2000; Liu 2005; Bourdeaut 2008). Tumours consisting of predominantly S-type cells often display a differentiating phenotype and therefore have a more favourable prognosis, whilst predominantly N-type tumours are more likely to be actively proliferating and aggressive, therefore have a poor prognosis(Mora 2001; Liu 2005). Given the ability of N-type and S-type cells to transdifferentiate, the relationship between N-type and S-type cells may impact tumour behaviour (Liu 2005). It has been suggested that immature neuronal and glial precursor cells are able to interact and impact differentiation (Biagiotti 2006; Acosta 2009). The process by which transdiffernetiation occurs is unclear and it is evident that further investigation of this pathway will improve understanding of therapeutic resistance.

It is therefore crucial to determine the cellular pathways that underlie tumour differentiation and the mechanisms associated with proliferation-differentiation switch to a benign phenotype to ensure elucidation of novel drug targets and increase treatment efficacy and patient survival.

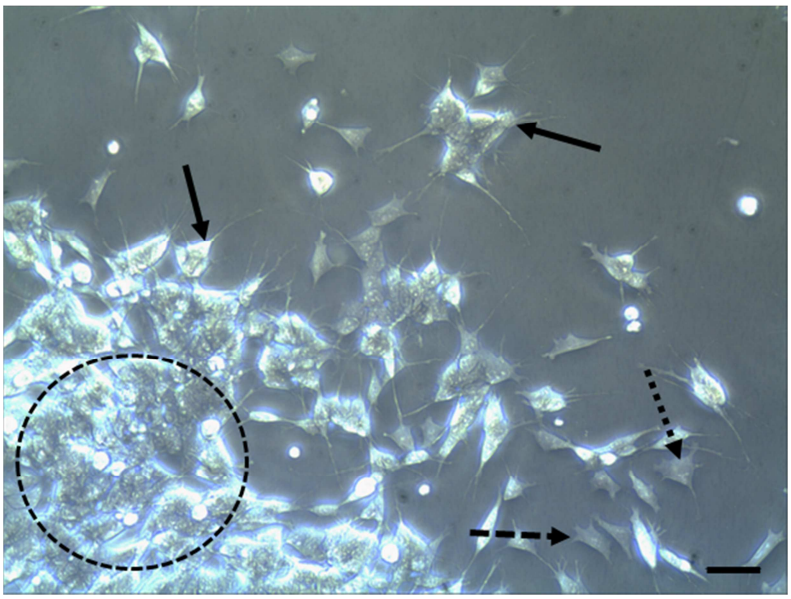

Figure 1.3.1. The SH-SY5Y neuroblastoma cell line is comprised of three cell phenotypes

The SH-SY5Y cell line consists of three distinguishable cell phenotypes; N-type, S-type and I-type. Immature neuroblastic N-type cells (black arrows) are the predominant cell type and possess small rounded cell bodies with short neurite-like processes and can grow in aggregates (dashed circle). Substrate-adherent S-type cells (dashed arrow) are present in smaller numbers and possess more abundant cytoplasm with a flattened morphology but no neuritic processes. I-type cells (dotted arrow) have characteristics of both phenotypes, possessing a flattened morphology and abundant cytoplasm like that of S-type cells but also exhibit neurite-like process similar to that of N-type cells. Scale bar represents 20 µm.

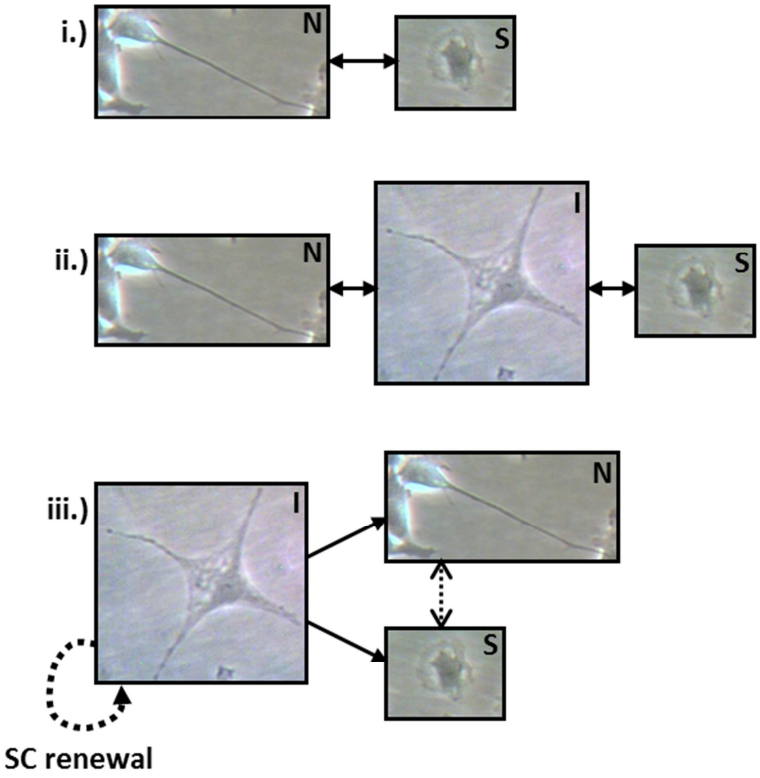

Figure 1.3.2. Phenotypic transdifferentiation may occur between N-type and S-type cells or involve the putative I-type population

Models of possible trans-differentiation stages, adapted from Ciccarone *et al* (1989) with images from MRes dissertation (Whitworth 2012). **i.)** Direct conversion may occur between N-type (N) and S-type (S) cells. **ii.)** Putative I-type (I) cells may act as an intermediate for transient transition between the N- and S-phenotype or may represent a transitional morphology rather than in individual phenotype. **iii)** Putative I-type cells may be a stem cell (SC) population that is capable of self-renewal and/or are progenitors for N-type and S-type cells, which subsequently may or may not trans-differentiate between phenotypes.

1.4. S-type sub-populations are identifiable in culture

Variable S-type cell morphology has been shown to exist between different neuroblastoma cell lines (Ciccarone 1989) and previous work in our laboratory has identified three distinguishable morphological subsets within the S-type population of the SH-SY5Y cell line; outstretched, angular and elongated (Figure 1.4.1) (Whitworth 2012). Outstretched S-type cells (S_O) were the most abundant sub-population (62%) and appeared flatter and more spread out with poorly distinguishable cell membranes (Whitworth 2012). Angular S-type cells (S_A) were present in lower quantities (35%) and tended to be smaller with a more compact morphology and less abundant cytoplasm than S_O cells (Whitworth 2012). Elongated S-type cells (S_E) were present in the lowest numbers (3%) and had a lengthened appearance (Whitworth 2012). These S-type sub-populations may represent variable phenotypes of a single cell lineage or may encompass three specific cell types, therefore, they pose an intriguing aspect for further analysis into the potential variability in biochemical attributes and Ca^{2+} signalling profiles in terms of phenotype and also in relation to their differentiated state.

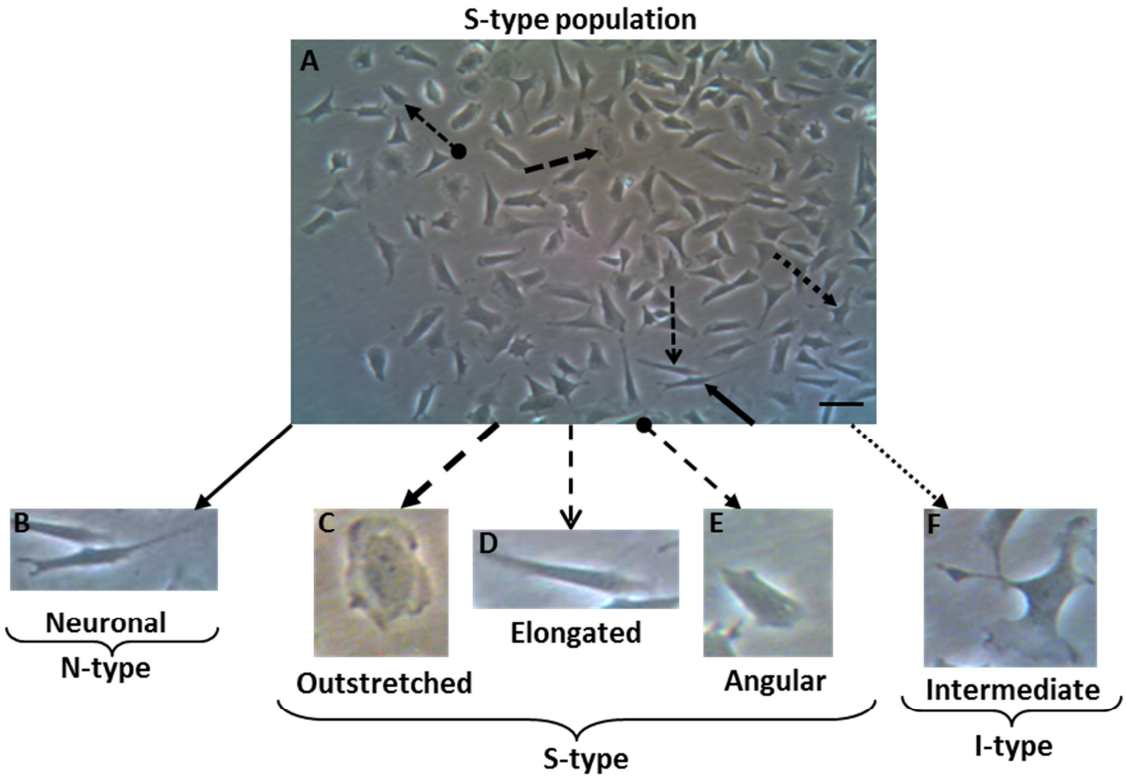

Figure 1.4.1. The S-phenotype is comprised of three distinct morphologies

(A) Five cell phenotypes can be distinguished in the SH-SY5Y cell line and the derived S-type enriched populations; **(B)** neuroblastic N-type cells (black arrow), **(C-E)** substrate-adherent S-type cells (dashed arrows) and **(F)** possible intermediate I-type cells (dotted arrow). Within the S-phenotype, a further three sub-populations can be identified; **(C)** outstretched cells with abundant cytoplasm and a flatter, more spread out appearance (bold, dashed arrow), **(D)** elongated cells with a lengthened morphology (open arrowhead, dashed arrow) and **(E)** angular cells with a shortened, more compact appearance (circle tipped, dashed arrow). Scale bar represents 20 µm. Figure adapted from MRes dissertation (Whitworth 2012)

1.5. Retinoids can induce differentiation

Retinoic acid is a derivative of vitamin A that regulates many cellular mechanisms such as differentiation, growth and gene transcription as well as the proliferation-differentiation switch. There are three main isoforms of RA that have been studied in the context of neuroblastoma differentiation; all-*trans*-retinoic acid (ATRA), 13-*cis*-retinoic acid (13*c*RA) and 9-*cis*-retinoic acid (9*c*RA)(Lovat 1997), of which the latter is the most potent but also the most toxic *in vivo* (Ponthan 2001). High risk neuroblastoma patients can receive 13*c*RA as part of treatment for advanced or minimal residual disease (Matthay 2009) since it is less toxic than other isoforms (Lovat 1997; Ponthan 2001). Although overall survival is improved with 13*c*RA administration in these patients, response remains relatively poor (Finklestein 1992; Smith 1992; Villablanca 1995; Matthay 2009).

The mechanism of action of RA is well documented (Abemayor 1989; Rees 1989; Heyman 1992; Allenby 1993; Redfern 1994; Chambon 1996; Minucci 1997; Reynolds 2003; Schug 2007). RA is transported via cytoplasmic cellular retinoic acid-binding proteins (CRABPs) and cellular retinol binding proteins (CRBPs) into the nucleus (Abemayor 1989; Redfern 1994) and binds heterodimers of retinoic acid receptor (RAR) and retinoid X receptor (RXR) (Redfern 1994; Minucci 1997; Reynolds 2003; Shaw 2003; Schug 2007; E. Bell 2013), each of which has an α, β and γ isoform (Rees 1989; Redfern 1994; Chambon 1996). This complex then associates with retinoic acid response elements (RAREs) upstream of promoters that regulate transcription of genes involved with cell proliferation and differentiation (Reynolds 2003; Shaw 2003; Schug 2007; E. Bell 2013).

All three of the discussed isoforms of RA can bind RARs but the 13*c*RA isoform that is used in patients has a very low affinity for RARs (Redfern 1994; Lovat 1997) which may contribute to its poor efficacy. Only 9*c*RA is capable of RXR binding (Heyman 1992; Allenby 1993; Minucci 1997), which may influence its efficacy with differentiation compared to other isoforms (Lovat 1997; Ponthan 2001). Variability of expression of RARs and RXRs (Rees 1989; Mollard 2000) as well as varying affinities of RA may contribute to treatment resistance.

The effects of RA as a differentiation inducer have been extensively demonstrated in neuroblastoma cells (Pahlman 1984; Lovat 1997; Simpson 2001; Mora 2001; Reynolds 2003; Voigt 2003; Dubey 2004; Brown 2005; Constantinescu 2007; N. Bell 2013). RA-induced differentiation can alter oncogene expression as has been demonstrated with the observation that N-myc and p53 are down-regulated in differentiated neuroblastoma cells and may instigate the differentiation process (Abemayor 1989). Varying effects of RA have been observed in neuroblastoma cells, with short-term (1-3 days) treatment enhancing migration and invasion of SH-SY5Y cells and long-term (≥5 days) treatment inducing differentiation (Joshi 2006), perhaps due to differential interactions with RARs and RXRs. Ca^{2+} signalling changes have also been associated with altered oncogene expression in differentiating neuroblastoma cells as well as other cancers (Macara 1985; Morgan 1986; Okazaki 1986; Reboulleau 1986; Abemayor 1989). Additionally, 9*c*RA-induced differentiation alters methacholine-stimulated Ca^{2+} entry and causes down-regulation of store-operated Ca^{2+} entry (SOCE), possibly to maintain the differentiated state (Brown 2005).

Retinoic acid-induced differentiation of neuroblastoma cells is also used as a model to investigate neuronal differentiation (da Rocha 2015) and in the context of neurodegenerative disorders, such as Parkinson's Disease (PD) (Constantinescu 2007; Cheung 2009) and Alzheimer's Disease (AD) (Petratos 2008).

1.6. Neuroblastoma cells are used to study neurodegenerative disorders

As previously discussed (Introduction 1.3 and 1.5), the SH-SY5Y neuroblastoma cell line consists predominantly of immature neuroblastic cells that can differentiate towards a neuronal phenotype. For this reason, both proliferating and differentiated SH-SY5Y cells have been widely used for *in vitro* investigations of neurotoxicity and as a model for the exploration of neurodegenerative disorder pathology and treatment (K. Nakamura 2000; Misonou 2000; Brill 2003; Jamsa 2004; Zheng 2006; Cheung 2009; Korecka 2013). Systems genomic characterisation of SH-SY5Y cells revealed that the majority of Parkinson's Disease (PD)-associated genes and Alzheimer's Disease (AD)-associated genes, were intact (Krishna 2014), demonstrating the relevance of this cell line in the study of neurodegenerative disorders.

Degeneration of dopaminergic neurons is a hallmark of PD and all-*trans*-retinoic acid (ATRA)-differentiated SH-SY5Y cells have been found to exhibit a predominantly dopaminergic-like phenotype (Korecka 2013) making them suitable for the study of genetic targets or compounds for PD treatment. The neurotoxin MPP(+)inhibits complex I in the mitochondrial electron transport chain causing ATP depletion and formation of reactive oxygen species (ROS), which leads to loss of dopaminergic neurons and mimics symptoms of PD (K. Nakamura 2000; Korecka 2013). MPP(+) treatment of SH-SY5Y cells was also shown to induce oxidative stress and cell death (Brill 2003). Similarly, 6-hydroxydopamine (6-OHDA) is a toxin used in experimental models of PD as it accumulates intracellularly, causing oxidative stress and cell death, thereby mimicking the pathology of PD (Lopes 2010). 6-OHDA induces SH-SY5Y cell death, which is enhanced in ATRA-differentiated SH-SY5Y cells (Lopes 2010).

The formation of amyloid β protein (Aβ) plaques and ROS accumulation leading oxidative stress are contributing factors in the development of Alzheimer's Disease (AD)(Zheng 2006) and oxidative stress induced by hydrogen peroxide treatment has been shown to increase Aβ formation in SH-SY5Y cells (Misonou 2000). It is suspected that Aβ accumulation in neurons precedes plaque formation in AD and it has been found that Aβ is able to accumulate in the lysosomes of ATRA-differentiated SH-SY5Y cells, a process that was enhanced by ROS induced oxidative stress (Zheng 2006).

Phosphorylated tau is the main component of neurofibrillary tangles, the formation of which is also associated with AD development, and an increase in phosphorylated tau has been observed in SH-SY5Y cells differentiated with ATRA and brain-derived neurotrophic factor (BDNF) (Jamsa 2004).

Whilst the SH-SY5Y neuroblastoma differentiation model investigated in this study has noteworthy applicability for neurodegenerative disorders, the focus of this study is the phenotype-specific comparisons which can be drawn from the heterogeneity of the cell line with regard to neuroblastoma disease, therefore the context of neurodegenerative disorders will not be further discussed in depth.

1.7. Ca^{2+} is a fundamental intracellular signalling molecule

Intracellular free Ca^{2+} is a ubiquitous signalling molecule that plays a key role in many physiological pathways, such as cell differentiation, proliferation and apoptosis (Hanada 1993; Lasorella 1995; Berridge 1998; Bootman 2001; Sammels 2010; Smyth 2010). Ca^{2+} signal spiking is involved in differentiation, including during neuronal development (Berridge 2000). Ca^{2+} homeostasis is therefore crucial for the maintenance of these pathways and correct cell functioning. There are several Ca^{2+} transporting mechanisms that utilise Ca^{2+} binding proteins to allow Ca^{2+} entry and release, allowing for maintenance of cytosolic Ca^{2+} concentration at ~10-100 nM at rest as well as for induction of spatially and temporally versatile Ca^{2+} signals where cytosolic Ca^{2+} concentration can rise 10-100-fold (Berridge 1998; Berridge 2000; Bootman 2001; Putney 2001).

Ca^{2+} signals can be generated from extracellular Ca^{2+} entry or internal Ca^{2+} stores that include the endoplasmic reticulum (ER) or sarcoplasmic reticulum (SR) in muscle cells (Berridge 2000; Bootman 2001; Mekahli 2011), lyososomes (Galione 2010) and mitochondria (Rizzuto 2012). Ryanodine receptors (RyRs) and inositol 1,4,5-trisphosphate receptors (IP_3Rs) located at the ER/SR membrane can be activated by Ca^{2+} itself and, in the process of Ca^{2+}-induced Ca^{2+} release (CICR), raise $[Ca^{2+}]_i$ by releasing Ca^{2+} from ER/SR stores (Carafoli 1987; Berridge 2000; Parekh 2005). Mechanisms that allow Ca^{2+} entry into the cell via the plasma membrane (PM) include store-operated Ca^{2+} channels (SOCs), receptor-operated Ca^{2+} channels (ROCs) and voltage-operated Ca^{2+} channels (VOCs). SOCs are activated by ER Ca^{2+} store depletion and are ubiquitously expressed (Berridge 2000; Bootman 2001). ROCs open upon binding extracellular agonists such as glutamate, acetylcholine or ATP and are highly prevalent on secretory cells and at nerve terminals (Berridge 2000; Bootman 2001). VOCs are stimulated by membrane depolarisation and are present in electrically excitable cells such as neuronal and muscle cells (Berridge 2000; Bootman 2001; Parekh 2005). All of these channels are localised to the PM and function to allow an increase in $[Ca^{2+}]_i$ via Ca^{2+} entry from the extracellular environment (Carafoli 1987; Berridge 2000). Cytosolic Ca^{2+} sensors, including calmodulin and troponin C, are able to

activate downstream effects such as muscle contraction, gene transcription and metabolism (Berridge 2000).

The main mechanisms that serve to reduce $[Ca^{2+}]_i$ act through either extracellular Ca^{2+} release via the plasma membrane, which includes the PM Ca^{2+} ATPase (PMCA) and the Na^+/Ca^{2+} exchanger, or through reuptake at the ER/SR membrane by the sarco/endoplasmic reticulum Ca^{2+} ATPase (SERCA) (Carafoli 1987; Berridge 2000) and mitochondrial sequestration by uniporters at mitochondrial membranes (Berridge 2000; Bootman 2001). Cytosolic Ca^{2+} buffers such as parvalbumin and calretinin also offer a further route for regulation of the spatial and temporal Ca^{2+} signalling which can be utilised to ensure localisation to precise intracellular regions or organelles (Berridge 2000).

Due to its presence in many biological systems, aberrant Ca^{2+} signalling has been implicated in many pathological conditions such as neurodegenerative disorders and cancer (Parekh 2005; Berridge 2010; Sammels 2010; Chen 2013; Calì 2014). Ca^{2+} signalling is involved in cell migration, a key feature of cancer cell metastasis, and plays a role in mechanisms for cell motility, such as focal adhesion and cytoskeleton rearrangement (Prevarskaya 2011; Chen 2013). Ca^{2+} homeostasis is remodelled in cancer to increase cell proliferation and angiogenesis (Chen 2013), both of which are required for tumour establishment. Mutations found in familial Alzheimer's disease (FAD) can disrupt Ca^{2+} homeostasis (Targos 2005). In PD, aggregates of α-synuclein protein are thought to affect Ca^{2+} permeability, increasing Ca^{2+} influx and inducing toxicity (Calì 2014). Similarly, knockdown of the PD-associated mitochondrial protein PINK1 has been shown to cause an increase in mitochondrial Ca^{2+} in neuroblastoma cells through inhibition of the Na^+/Ca^{2+} exchanger which led to ROS accumulation and vulnerability to cell death (Gandhi 2009). The Ca^{2+} signalling network therefore poses a target under much investigation for its role in cancer and neurodegenerative disorder progression.

1.8. SOCE is a key pathway for Ca^{2+} entry

SOCE (Figure 1.9.1) is a ubiquitous Ca^{2+} entry pathway that has a role in many cellular processes such as proliferation, differentiation, apoptosis and motility (Bootman 2001; Targos 2005). Initiation of ER Ca^{2+} store release can be triggered by binding of extracellular ligands, such as hormones, growth factors and neurotransmitters to cell surface G-protein coupled receptors. This leads to binding of phosphatidylinositol to phosphatidylinositol transfer proteins, which in turn activates phospholipase C (PLC) mediated conversion of phosphatidylinositol 4,5-bisphosphate (PIP_2) to diacylglycerol (DAG) and inositol trisphosphate ($InsP_3$) (Berridge 2000; Bootman 2001). Ca^{2+} is then released into the cytosol from the ER lumen upon $InsP_3$ binding its receptor on the ER membrane (Berridge 2000). $InsP_3$Rs, as well as ryanodine receptors (RyRs), can be activated by Ca^{2+} itself in the process of Ca^{2+}-induced Ca^{2+} release and also cause ER Ca^{2+} store release (Berridge 2000). ER Ca^{2+} store depletion triggers the opening of SOCs at the PM that allow for Ca^{2+} entry into the cell, which is transported into the ER via the action of the SERCA to replenish the depleted ER Ca^{2+} store (Berridge 2000; Bootman 2001; Putney 2011). This process of SOCE (Figure 1.9.1) is crucial for replenishing depleted intracellular Ca^{2+} stores and for prolonging the Ca^{2+} response for downstream signalling (Putney 1986; Bootman 2001; Parekh 2005; Putney 2011).

The current underlying SOCE; Ca^{2+} release-activated Ca^{2+} current (I_{CRAC}), is highly Ca^{2+} selective, mediated by electrostatic repulsion of monovalent ions by bound Ca^{2+} (Prakriya 2006; Smyth 2010), and single CRAC channel conductance is extremely low (Prakriya 2006). CRAC channel kinetics are slow and governed by the rate of transition from an inactive to a highly active state (Prakriya 2006). I_{CRAC} is inhibited by Ca^{2+} itself whereby Ca^{2+} flux through individual channels feeds back to rapidly inactivate I_{CRAC} over milliseconds, without affecting I_{CRAC} of other local channels (Zweifach 1995), and intracellular Ca^{2+} feeds back to slowly inactivate I_{CRAC} over tens of seconds due to Ca^{2+} store refilling (Zweifach 1995; Prakriya 2006).

SOCE remodelling has been associated with cancer cell proliferation, migration and invasion (Targos 2005; Chen 2013) therefore SOCE pathway components could potentially be targeted as a means of neuroblastoma therapy. SOCE down-regulation

in human prostate cancer cells was shown to protect cells from apoptosis and reinstating SOCE activity restored apoptosis (Flourakis 2010). SOCE was associated with breast cancer cell migration *in vitro* and breast cancer invasion in mice and inhibiting SOCE reduced tumour invasion in mice (Yang 2009). In breast cancer cells, carboxyamido-triazole (CAI) treatment caused an inhibition of Ca^{2+} uptake and prevented tumour cell growth and invasion (Sherbert 2001). Targeting the Ca^{2+} signalling pathways involved in differentiation could therefore have implications for cancer therapy. SOCE dysfunction has also been associated with neurodegenerative diseases such as PD and Huntington's disease (Majewski 2015). In Alzheimer's Disease (AD), altered ER Ca^{2+} storage and store release has been observed and affects SOCE (Targos 2005). Reduced SOCE has been found in cells with mutated presenilin protein, a known cause of early-onset AD (Bojarski 2009).

Ca^{2+} entry via SOCs is closely associated with intracellular Ca^{2+} store depletion and three proteins have thus far been implicated in the integration of these signalling events; STIM, Orai and TRPC1.

1.9. STIM

RNAi screens have identified two mammalian stromal interaction molecule (STIM) homologues; STIM1 and STIM2 (Liou 2005; Roos 2005). Structurally, STIM1 and STIM2 share >60% sequence homology (Williams 2001; Zheng 2008). STIM1 and STIM2 are both type 1 transmembrane proteins that are expressed in the ER, with C-terminal domains in the cytoplasm and N-terminal domains in the ER lumen (Zheng 2008), and both possess an EF-hand domain that is able to bind Ca^{2+} in the ER lumen (Williams 2001; Liou 2005; Zhang 2005; Wu 2006; Brandman 2007; Zheng 2008) with binding affinity in the normal 250-600 µM range for ER [Ca^{2+}] (Stathopulos 2006; Zheng 2008).

STIM1 is a 77kDa single pass ER membrane spanning protein (Liou 2005; Zhang 2005; Wu 2006; Zheng 2008) that is also found at the PM (Zhang 2005; Manji 2000; Soboloff 2006; Zheng 2008). The level of STIM1 expression has been extensively associated with extent of SOCE activity. STIM1 knockdown causes a reduction in SOCE whilst overexpression increases SOCE in many cell types including HeLa cells (Liou 2005), Jurkat T cells (Roos 2005; Huang 2006), Drosophila S2 cells (Roos 2005), HEK293 cells (Mercer 2006; Abdullaev 2008), endothelial cells (Abdullaev 2008), vascular smooth muscle cells (Takahashi 2007; Aubart 2009; Potier 2009), endothelial progenitor cells (Kuang 2010; Shin 2010) and SH-SY5Y neuroblastoma cells (Abdullaev 2008; Bell 2011). STIM2 has also been found to induce Ca^{2+} entry in a predominantly constitutive store-independent manner but also in a calmodulin-regulated, transient store-dependent manner and (Parvez 2008). Although STIM2-mediated activation of SOCE has been observed, STIM2 has a lower Ca^{2+} sensitivity than STIM1, being activated at higher ER Ca^{2+} concentrations than STIM1 and found to be a regulator of basal cytosolic and ER Ca^{2+} concentration (Brandman 2007). Knockdown of STIM2 in HeLa cells caused a reduction in SOCE (Liou 2005) but has also been shown to have no effect in Jurkat T cells (Roos 2005), therefore STIM2 may have a role in SOCE but only under certain conditions.

STIM1 phosphorylation at multiple serine residues has been identified (Manji 2000; Smyth 2009; Sundivakkam 2012; Pozo-Guisado 2013; Sundivakkam 2013) and shown to have a role in STIM1 activation during ER Ca^{2+} store depletion (Lopez 2012; Pozo-

guisado 2013) as well as inhibit SOCE (Smyth 2009; Sundivakkam 2013). STIM1 can also be glycosylated (Manji 2000; Dziadek 2007), which can affect PM localisation (Williams 2002). Therefore, as well as expression level, modification of STIM1 affect the role of STIM1 in SOCE. Similarly, STIM1 has recently been found to exist as two isoforms; STIM1S and STIM1L (Darbellay 2011; Sauc 2015). The shorter STIM1S isoform has been extensively studied as the predominant STIM1 isoform whilst the longer STIML isoform has only recently been identified (Darbellay 2011) and is able to activate SOCE in cells lacking STIM1S (Sauc 2015). STIM1L is able to induce SOCE quicker than STIM1S (Darbellay 2011; Horinouchi 2012) which may be utilised by the cell to regulate SOCE activity accordingly.

Since STIM1 has a role in SOCE activity, expression of STIM1 was explored in this thesis (Chapter 5). The function of STIM1 in SOCE is discussed further in 1.11.

1.10. Orai

There are three human homologues of the calcium release-activated calcium channel protein Orai; Orai1, Orai2 and Orai3. Orai1 is a 33kDa tetra-pass PM spanning protein that forms the SOC pore (Prakriya 2006; Gwack 2007; Kawasaki 2009; Yuan 2012). Loss of I_{CRAC} attributed to depletion of Orai1 was first identified in SCID patients, where a point mutation in Orai1 caused defective SOCE activity in patient T cells and reinstated expression of wildtype Orai1 in these cells restored SOCE activity and I_{CRAC} (Feske 2006). Orai1 has since been shown to have a role in SOCE in many other cell types, as knockdown of Orai1 induced a down-regulation of SOCE activity in neuroblastoma cells (N. Bell 2013), neural progenitor cells (Hao 2014), acinar cells (Hong 2011), osteoclasts (Zhou 2011), endothelial cells (Abdullaev 2008), Jurkat T cells (Gwack 2007) and HEK293 cells (Gwack 2007; Kawasaki 2010). Orai1 overexpression was also shown to cause an increase in SOCE in HEK293 cells (Fukushima 2012) and restore SOCE in SCID T cells and fibroblasts (Gwack 2007) and differentiating neuroblastoma cells (Bell 2011).

Structurally, Orai1, Orai2 and Orai3 have a high degree of conservation (>80%) however they possess some regions of dissimilarity, including at the cytosolic N- and C-termini, which may be involved in channel activation (Takahashi 2007; Shuttleworth 2012). Indeed, Orai3 has been observed to have a distinct role from that of Orai1 and Orai2 (Shuttleworth 2012). For example, co-expression of Orai1 or Orai2 with STIM1 results in an increase in I_{CRAC}, though to a lesser extent or no effect with Orai2 expression (Mercer 2006; Lis 2007; Takahashi 2007), whilst co-expression of Orai3 with STIM1 does not produce detectable Ca^{2+} selective currents (Mercer 2006; DeHaven 2007). Similarly, in cells expressing STIM1, siRNA-induced Orai1 knockdown reduced SOCE whilst Orai3 knockdown had no effect on SOCE (Mercer 2006; DeHaven 2007; Lis 2007). Orai3 overexpression did restore Ca^{2+} entry in cells with knockdown of Orai1 and stable STIM1 expression, although the magnitude of response was reduced to that observed with Orai1 expression (Mercer 2006; DeHaven 2007; Lis 2007). This suggests that, whilst Orai3 has a minimal function in SOCE, Orai3 may play a compensatory role in SOCE when the usual means of SOCE are compromised.

Since Orai1 co-expression with STIM1 has consistently been shown to increase SOCE activity to a greater extent than seen with Orai2 or Orai3 expression (Mercer 2006; Peinelt 2006; Soboloff 2006; Takahashi 2007), this suggests that the Orai1 isoform has a more prominent role in SOCE. The cytosolic N-terminus of Orai1 is structurally different to that of Orai2 and Orai3 and has been shown to contribute to its superior role in SOCE over Orai2 and Orai3 (Takahashi 2007). Co-expression of STIM1 with Orai1 that had the Orai2 N-terminal tail only marginally increased SOCE whilst co-expression of STIM1 with Orai2 containing the Orai1 N-terminus dramatically increased SOCE to levels observed with Orai1-STIM1 co-expression (Takahashi 2007). These results provided evidence for a STIM1-Orai1 association to promote SOCE activity and it has since been found that SOCE is in fact, for the most part, governed by STIM1-Orai1 mediated interactions.

Since Orai1 has a role in SOCE activity, expression of Orai1 was investigated in this thesis (Chapter 5). The function of Orai1 in SOCE is discussed further in 1.11.

1.11. STIM1 and Orai1 mediate SOCE

Interaction between STIM1 and Orai1 is known to facilitate SOCE (Figure 1.11.1). STIM1 is a Ca^{2+} sensor that alters the gating of SOCs at the PM to allow Ca^{2+} entry for replenishment of depleted Ca^{2+} stores (Liou 2005; Roos 2005). The N-terminus of STIM1 resides in the ER lumen and contains an EF-hand Ca^{2+} binding domain (Hodeify 2015) and sterile α motif (SAM) domain (Zheng 2008). In its Ca^{2+} bound state when the ER Ca^{2+} store is full, STIM1 monomers are sequestered in the ER (Stathopulos 2009). However, in its unbound state when Ca^{2+} stores are depleted, STIM1 oligomerises which induces localisation into puncta at ER/PM junctions (Luik 2008) mediated by its sterile alpha motif (SAM) domain (Liou 2005; Park 2009; Yuan 2012). These puncta reside in close proximity (~20 nm) to the PM (Wu 2006; Hodeify 2015) so that STIM1 can then interact with the C-terminus of Orai1, which forms the SOC pore (Kawasaki 2009; Yuan 2012). Clustering alone does not induce SOCE (Park 2009); STIM1 interacts with PM phosphoinositides via the polybasic domain (Lewis 2011) and STIM1 interacts with the coiled-coil region of the Orai1 C-terminus via the Orai1-activating region (SOAR)/CRAC activating domain (CAD) (Kim 2011) within the STIM1 C-terminal ezrin/radixin/moesin (ERM) domain (Kawasaki 2009; Lewis 2011; Yuan 2012). As around half Orai1 cycles between intracellular and PM pools, this STIM1 interaction traps Orai1 at the PM and sequesters Orai1 into cortical STIM1 clusters (Hodeify 2015), inducing a conformational change in Orai1 that allows opening of the SOC and an influx of Ca^{2+} to ensue. It is thought that 8 STIM1s bind to each CRAC channel for maximal SOCE activity (Lewis 2011). STIM1 also inactivates SOCE through interaction of the CRAC-modulating domain/Ca^{2+}-dependent inactivation (CDM/CDI) region with Orai1 (Mullins 2009; Yuan 2012). Upon replenishment of the ER Ca^{2+} store and inactivation of SOCE, STIM1 dissociates from Orai1 and translocates back to the ER membrane (Liou 2007).

STIM1 is therefore essential for the gating of Orai1, as has been shown by knockdown experiments in which SOCE was significantly down-regulated (Roos 2005; DeHaven 2009; N. Bell 2013). STIM1 has been observed to redistribute to the PM and co-localise with Orai1 upon Ca^{2+} store depletion in sinoatrial node cells (Liu 2015), *Xenopus* oocytes (Courjaret 2014) and HEK293 cells (Fukushima 2012). Similarly, STIM1

association with the ER and redistribution of STIM1 into punctate structures forming within 100 nm of the PM following Ca^{2+} store depletion has been observed in HeLa cells whilst a STIM1 mutant lacking an EF-hand binding domain failed to reorganise into puncta following Ca^{2+} store depletion (Liou 2005).

Alterations in STIM1-Orai1 mediated Ca^{2+} entry is involved in cancer cell proliferation, migration and invasion (Chen 2013) therefore this pathway is a potential therapeutic target. For example, RNAi of STIM1 and Orai1 expression in highly metastatic breast cancer reduced tumour invasion in animal models (Yang 2009). Similarly, Orai1 down-regulation and dampened SOCE was associated with reduced apoptosis in human prostate cancer cells and restoring Orai1 expression and SOCE activity promoted apoptosis (Flourakis 2010).

The role of STIM1, Orai1 and SOCE within the phenotype-specific differentiation response of neuroblastoma cells was investigated in this thesis.

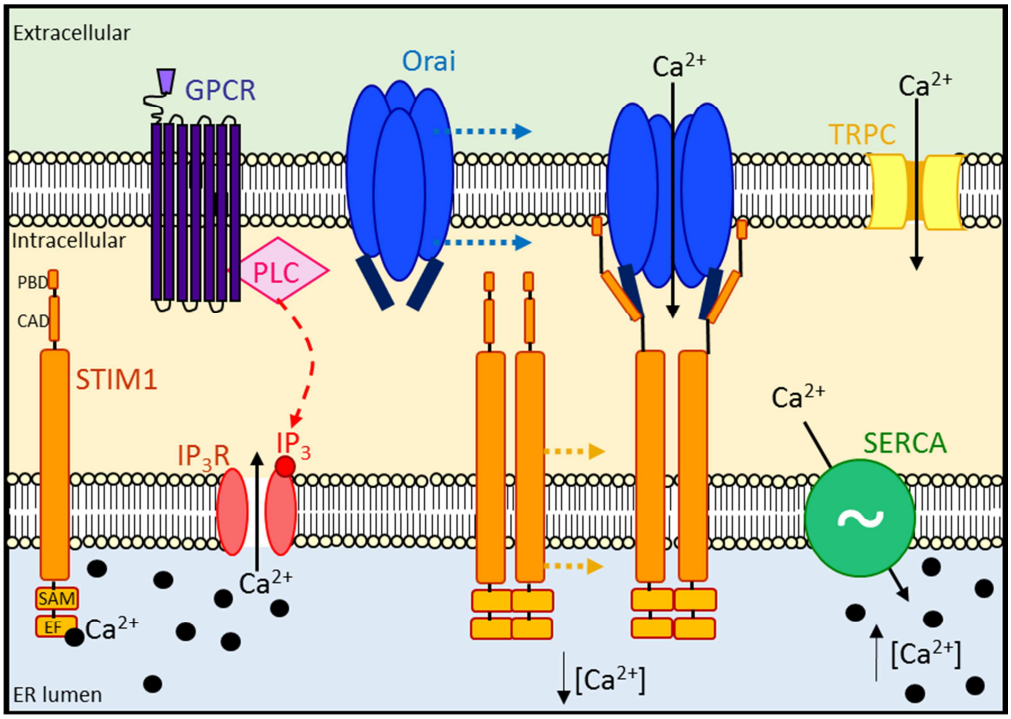

Figure 1.11.1. Store-operated Ca^{2+} entry (SOCE)

When ER Ca^{2+} stores are full, the Ca^{2+} sensing protein STIM1 (orange) at the ER membrane binds Ca^{2+} (black) through the EF-hand domain in the ER lumen. To initiate Ca^{2+} store release, extracellular ligands, such as hormones, growth factors and neurotransmitters bind to cell surface G-protein coupled receptors (purple), activating phospholipase C (PLC, pink) mediated conversion of phosphatidylinositol 4,5-bisphosphate (PIP_2) to diacylglycerol (DAG) and inositol trisphosphate ($InsP_3$). $InsP_3$ triggers inositol trisphosphate receptor (IP_3R) channels opening (red). Ca^{2+} can then flow down its concentration gradient from the ER into the cytosol. Store depletion is detected by STIM1 monomers which oligomerise in their unbound state (orange). STIM1 and store-operated Orai1 channels at the PM membrane (blue) translocate and associate at ER/PM junctions, forming puncta. Upon STIM1 binding to Orai1 through the CRAC-activating domain (CAD) and interacting with PM phosphoinositides via the polybasic domain (PBD), Orai1 channels open and Ca^{2+} enters the cytosol. Ca^{2+} is then transferred to the ER via the sarco/endoplasmic reticulum Ca^{2+} ATPase (SERCA, green) to replenish the depleted ER Ca^{2+} stores. TRPC1 (yellow) is a non-selective Ca^{2+} channel that can also be activated by SOCE, in a STIM1-dependent and independent manner, as well as by other pathways. Figure adapted from Lewis 2011.

1.12. TRPC may function as a SOC

Transient receptor potential cation 1 (TRPC1) channels are non-selectively permeable to Ca^{2+} and involved in cation transport in a variety of biological processes (Yuan 2003). TRPC1 is a 90 kDa protein that has been found to have a role in SOCE and was originally thought to be the primary SOC involved in SOCE before the discovery of Orai1 (Parekh 2005). For example, knockdown of TRPC1 in mouse acinar cells causes a reduction in SOCE (Liou 2007). TRPC1 has been found to function as a SOC via interactions with STIM1 (Yuan 2007; Alicia 2008; Jardin 2008) and through STIM1-mediated insertion of TRPC1 into lipid raft domains (LRDs) (Alicia 2008). LRDs also play a role in TRPC1-Orai interactions, as has been shown in human platelets where disruption of LRDs reduced SOCE by preventing TRPC1-Orai1 interactions (Jardin 2008). However, TRPC1 may also function as a SOC without the requirement of STIM1 interactions (DeHaven 2009) and can be activated by other non-SOCE pathways (Putney 2007).

Up-regulation of TRPC1 expression was associated with reduced SOCE in neuroblastoma differentiation (N. Bell 2013), myoblast differentiation (Louis 2008; Zanou 2012) and hippocampal neuronal cell differentiation (Wu 2004). However, inhibition of TRPC1 was found to suppress proliferation of A549 lung cancer cells whereas overexpression of TRPC1 enhanced proliferation (Jiang 2013). Similarly, knockdown of TRPC1 in keratinocytes caused a reduction in SOCE and inhibited differentiation (Cai 2006). This conflicting evidence supports that TRPC1 has some role in SOCE but the TRPC1 function in SOCE activity is unclear.

Aims

The aims of this thesis were to investigate proliferating and 9cRA-induced differentiating N-type and S-type cells at the single cell level by combining morphological, biochemical (protein expression and localisation) and functional (Ca^{2+} signalling) markers to establish a phenotype-specific 'signature' of the differentiation process. These aims were met through:

- Confirmatory studies of the cellular changes associated with the differentiation response of neuroblastoma cells (Chapter 3 and 4)

- Establishment and optimisation of single cell Ca^{2+} signalling data collection and analysis within the SHSY5Y cell line that was comparable to previous analysis at the population level using the Ca^{2+} add-back technique (Chapter 4)

- Investigations revealing the complexity of phenotype-specific differentiation response that underlie those observed at the population level and the effects of the predominant phenotype on phenotype-specific Ca^{2+} signals (Chapter 4)

- Determination of the expression and localisation patterns of two key SOCE proteins; STIM1 and Orai1 (Chapter 5)

- Study of the relationship of these changes over the time-course of the differentiation response (Chapter 6)

- Investigation into the effects of conditioned media on phenotype-specific differentiation profiles (Chapter 4 and 5)

Chapter 2: Materials and Methods

2.1. Materials

SH-SY5Y cells were supplied by Professor R. Ross (Fordham University, NY, USA). All chemicals were from Sigma-Aldrich (Dorset,UK) unless stated otherwise.

2.2. Cell culture

SH-SY5Y cells were cultured in Dulbecco's Modified Eagles Medium (DMEM)/F12:1 with GlutaMAX^{TM} (Life Technologies, Paisley, UK) supplemented with Fetal Calf Serum (10% v/v), penicillin (100IU.ml-1) and streptomycin (100IU.ml-1) and incubated at 37°C in a humidified 5% CO_2 atmosphere. Cells were grown in 75 cm^2 flasks (Corning, Flintshire, UK) and passaged once a week when approximately 90% confluent and were not used beyond passage 25.

For passage, cells were washed with pre-warmed phosphate buffered saline (PBS) and incubated in 0.02% ethylenediaminetetracetic acid (EDTA) for 5 minutes at 37°C to disrupt cell surface adherence proteins. Flasks were agitated to aid cell detachment and cells re-suspended in complete media following three flask surface washes to fully detach cells. The cell suspension (10 ml) was centrifuged at 1,000rpm for 5 minutes, the supernatant removed and pellet re-suspended in complete media for seeding.

2.3. Establishment of N- and S-type cell populations

SH-SY5Y cells consist predominantly (66%) of N-type cells but with S-type (26%) and I-type (8%) cells also present (Whitworth 2012). These cell types possess different substrate adherent properties, allowing selection and enrichment for either and N- or S-phenotype. Since an N-type enriched population is comparable to the mixed population (Bell 2011), the SH-SY5Y cell population is now used by our laboratory for N-type population studies.

In order to establish S-type populations, the SH-SY5Y neuroblastoma cell line was S-enriched through removal of less adherent N-type cells (Whitworth 2012; Bell 2011).

This was achieved through washing of SH-SY5Y cells in 10 ml pre-warmed PBS, incubating for ~3 minutes in 4 ml PBS then the culture flask was agitated. The flask was then washed in 10 ml PBS to remove nay loosely adhered cells and the remaining strongly adherent S-type cells were cultured. This process was repeated, when cells were ~80% confluent, four times to produce an S-type population (Figure 2.3.1). Enrichment of SH-SY5Y cells for S-type cells in this way produces a predominantly (81% Figure 2.3.2) S-type population and the enrichment process does not select for a particular sub-phenotype (Figure 2.3.3) (Whitworth 2012). Further enrichment did not significantly increase the proportion of S-type cells in the population (Whitworth 2012) and enrichment to S4 rather than S3 was used as this provided a larger quantity of cells to be obtained for seeding therefore S-enrichment to S4 was deemed appropriate for use in experiments to represent S-type populations.

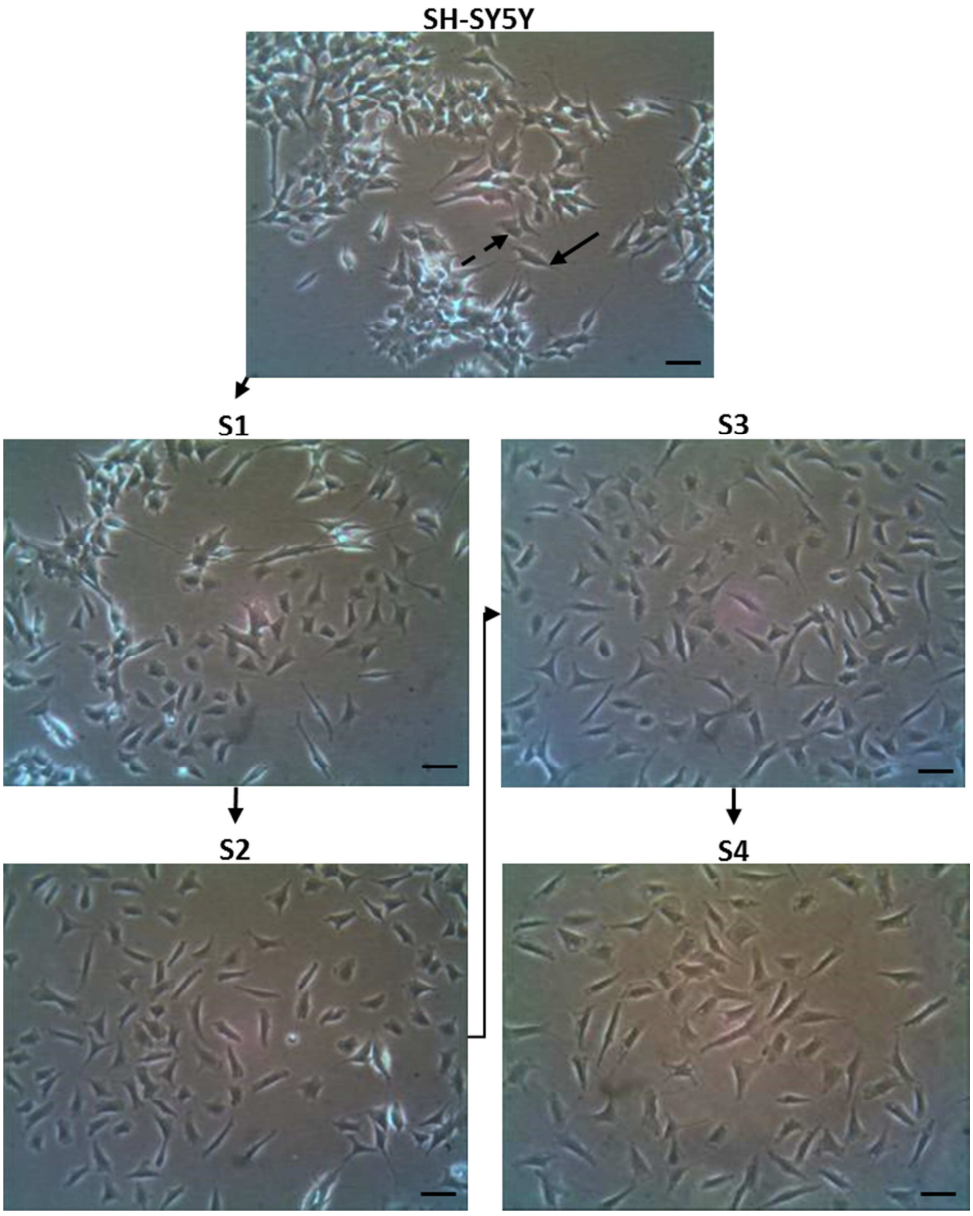

Figure 2.3.1. S-type populations can be enriched based on substrate adherence

Figure adapted from MRes dissertation (Whitworth 2012). The SH-SY5Y neuroblastoma cell line consists primarily of N-type cells (black arrow). Adherence-based S-type enrichment causes S-type cells (dashed arrow) to become more predominant with each level of enrichment (S1-S4). Enrichment to S4 was used in experiments to represent an S-type population. Scale bars represent 20 µm.

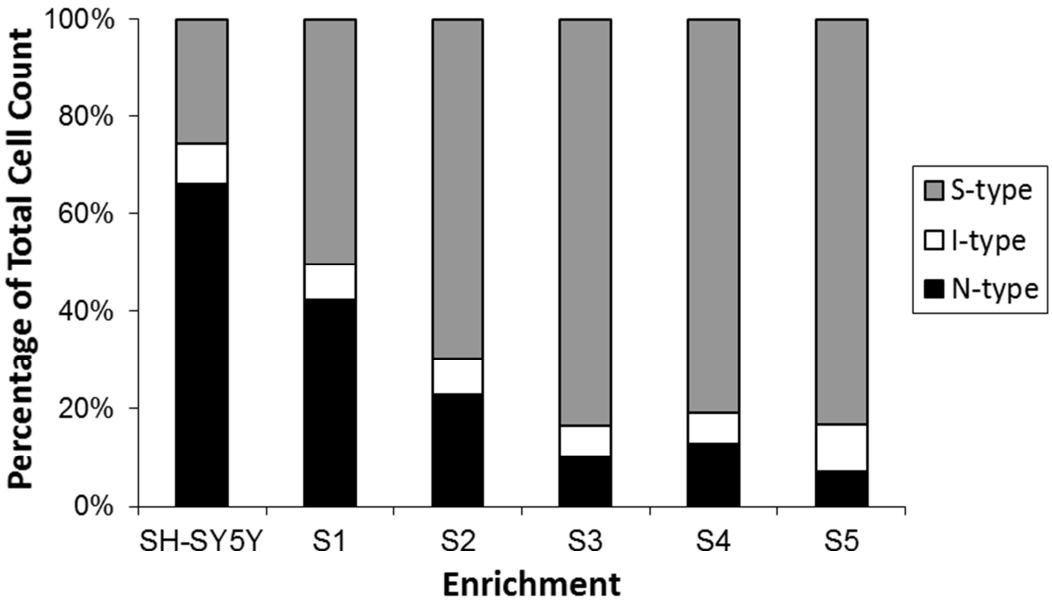

Figure 2.3.2. Enrichment for S-type cells produces predominantly S-type populations
Results from MRes dissertation (Whitworth 2012). SH-SY5Y populations are predominantly composed of N-type cells (66%) with S-type cells (26%) and I-type cells (8%) also present. At each enrichment stage, S-type cells become more predominant. S-enrichment to S1 doubles the S-type population proportion (54%, P=0.0193). Enrichment to S2 produces a predominantly S-type population (70%). Enrichment to S3 significantly increases the S-type population proportion (83%) compared to S1 enrichment (P=0.0225) however this was not increased with further enrichment to S4 (P=0.6795) and S5 (P=0.9996). Therefore S-enrichment to S4 was deemed sufficient for use in experiments since higher cell quantities could be obtained compared to S3. I type cells were consistently present with each enrichment (~8%, P=0.3966). N≥5 for each enrichment stage.

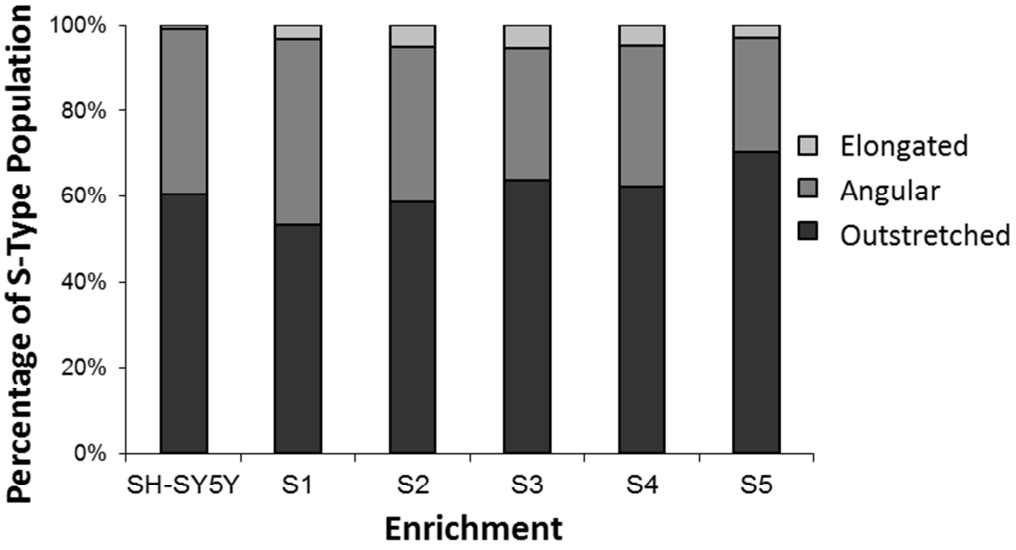

Figure 2.3.3. S-type enrichment does not affect the proportion of S_O, S_A or S_E cells

Figure adapted from MRes dissertation results (Whitworth 2012). The proportion of each individual S-type sub-population was determined as a percentage of the total S-type population at each enrichment stage. These proportions remain consistent with each S-enrichment; ~62% outstretched (S_O), ~35% angular (S_A) and ~3% elongated (S_E). N≥5 for each enrichment stage.

2.4. Cell counts

A Neubauer haemocytometer (VWR International, Leicestershire, UK) with chamber depth of 0.1 mm was used for counting cells. The haemocytometer was cleaned with EtOH and a glass coverslip was fixed in place. Cell suspension was added to the chamber and cells in the four corner squares (1 mm^2 each) were counted. Cells touching the left and upper lines of each grid were counted and those touching the right and lower right lines were not counted. To determine cell numbers per ml suspension, the average number of cells per square was calculated and multiplied by 10^4 as the volume of each square is 0.1 µl and the required number of cells were seeded.

2.5. Differentiation

Cells were seeded onto sterile 10 mm Ø glass coverslips in 35 mm Ø tissue culture dishes or 24 well tissue culture plates for fluorimetry and immunofluorescence experiments, 20mm Ø glass coverslips in 6 well tissue culture plates for single cell Ca^{2+} add-back experiments or 60mm Ø tissue culture dishes for imaging and protein harvesting at least 24 hours before treatment to allow sufficient cell adhesion. 9*c*RA (1 mg) was dissolved in AnaLar EtOH for a stock of 10 mM which was aliquoted and stored at -20°C. A new aliquot was used each week and stocks were replaced each month. Cells were treated with 1 µM 9*c*RA in complete media to induce differentiation or 0.01% EtOH was used as a control for proliferating cells. Differentiation and control media were replaced every 2 days and cells were used for experiments following 7 days of treatment.

2.6. CRAC inhibition

Cells were seeded onto sterile 20mm Ø glass coverslips in 6 well tissue culture plates for single cell Ca^{2+} add-back experiments or 60mm Ø tissue culture dishes for imaging and protein harvesting at least 24 hours before treatment to allow sufficient cell adhesion. The CRAC channel inhibitor N-[4-[3,5-Bis(trifluoromethyl)-1H-pyrazol-1-yl]phenyl]-4-methyl-1,2,3-thiadiazole-5-carboxamide (BTP2) was made up to a stock concentration of 20 mM in DMSO. Cells were treated with varying concentrations (0.1

μM – 20 μM) of BTP2 in complete media to induce CRAC inhibition, or DMSO was used as a control. Cells were used for experiments after 24 hours of treatment.

2.7. Imaging

An Optik XDS-2 microscope with 20x objective was used to capture phase contrast images. An Axiovert 200M microscope (Carl Zeiss Ltd) coupled to a laser scanning confocal microscope system (LSM 510, Carl Zeiss Ltd) using a 40x or 63x objective and helium-neon (HeNe) laser (633nm) was used for differential interference contrast (DIC) images and immunofluorescence images. For DIC images, cells were either live in PBS or fixed in paraformaldehyde (PFA, 4% w/v) and attached to slides with FluorSave Reagent (Calbiochem,Merck KGaA, Germany) overnight. Slides were kept at 4°C until imaging.

Phase contrast and DIC images were used to determine the average neurite length and percent differentiation of N-type cells and the diameter of S_O and S_A cells and the length of S_E cells (Figure 2.7.1). To calculate the percent differentiation of N-type cells, the total number of N-type cells and total number of differentiated cells (possessing one or more neurites ≥50 μm in length) were counted. The total number of differentiated cells was divided by the total number of cells and multiplied by 100 to convert to a percentage.

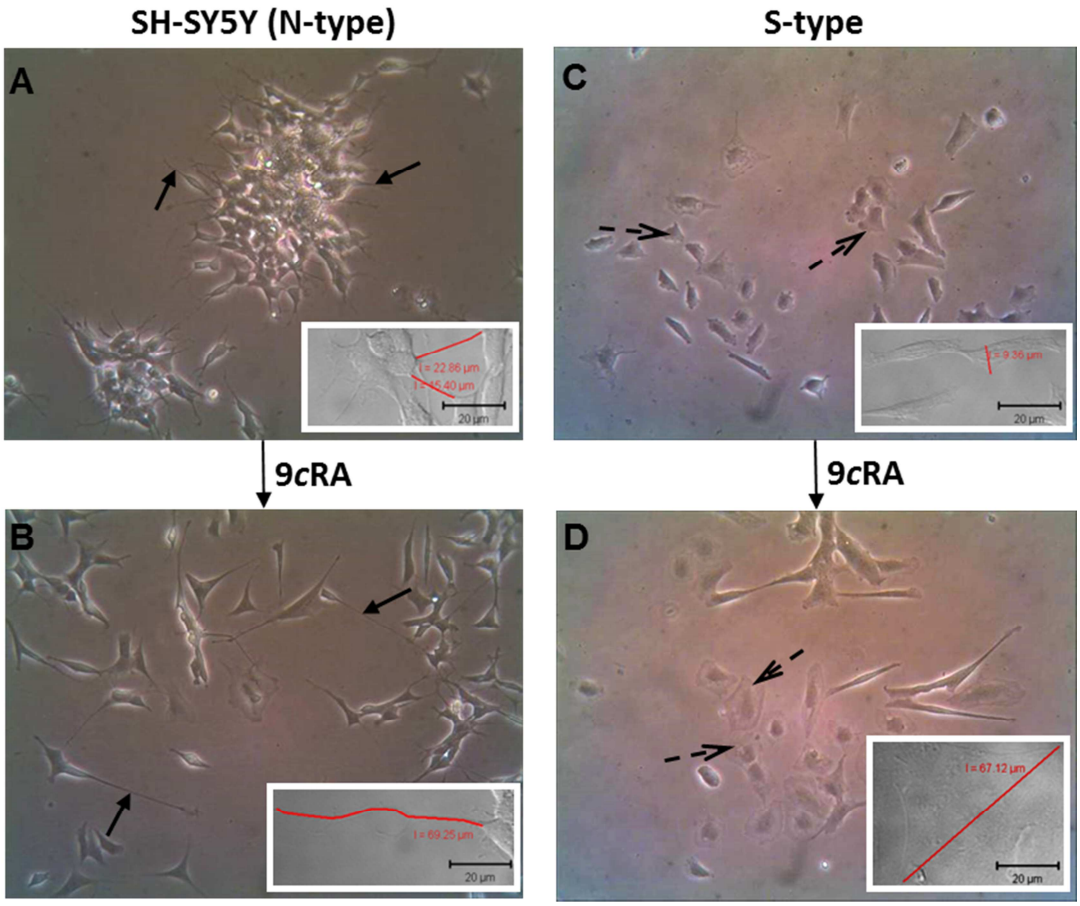

Figure 2.7.1. N-type neurite length and S-type diameter or length were measured to determine the extent of morphological differentiation

Figure adapted from MRes dissertation (Whitworth 2012). Phase contrast (main images) and DIC images (insets) were used to for cell counts and cell measurements using Metamorph and LSM Image Browser software respectively. The length of **(A)** proliferating and **(B)** differentiating N-type neurite-like process in SH-SY5Y populations were used to characterise the extent of morphological neuronal differentiation. The cell diameter of **(C)** proliferating and **(D)** differentiating S_O and S_A cells and the cell length of S_E cells were measured to characterise the extent of non-neuronal morphological differentiation. Scale bars representative of 50µm.

2.8. Immunofluorescence of protein localisation

Cells on glass coverslips were washed with PBS then fixed with PFA (4% w/v) for 10 minutes at RT, washed with PBS then permeabilised using Triton X-100 (0.1% v/v) for 10 minutes at RT and then wash with PBS and blocked with bovine serum albumin (BSA, 5% w/v) for 30 minutes at 4°C. Coverslips were incubated for 2 hours in at 4°C with primary antibody from Table 2.8.1 diluted in BSA. Following incubation with unconjugated antibodies, coverslips were washed and incubated for 1 hour at 4°C with secondary antibody Table 2.8.1 diluted in BSA. Conjugated fluorophores are summarised in Table 2.8.2. Cells were then washed in PBS and incubated with nucleic acid specific ethidium homodimer-1 (EthD-1, Table 2.8.1 and 2.8.2) diluted in PBS for 10 minutes at RT. Control cells were incubated with BSA only, primary antibody only and secondary antibody only. Coverslips were washed in PBS then dH_2O, fixed with FluorSave Reagent (Merck, Darmstadt, Germany) overnight and kept in the dark at 4°C until imaging.

For imaging, excitation and emission wavelengths of the fluorophores used in experiments are shown in Table 2.8.2. Fluorophores with overlapping emission were collected separately using multi-track configuration (as opposed to single-track) to prevent cross-talk. Images were acquired with 12 bit data depth, a frame size of 512 x 512 and a scan speed of 9.

Antibody	Concentration	Use	Species	Supplier
β-actin	1/10,000	WB	Mouse	abcam, UK
β-tubulin III	1/200	WB, IF	Mouse	Covance, USA
β-tubulin III (alexa-fluor 488)	1/50	IF	Mouse	Covance, USA
vimentin	1/200	WB, IF	Mouse	Santa Cruz, USA
vimentin (alexa-fluor 647)	1/50	IF	Mouse	Santa Cruz, USA
Bcl-2	1/200	WB	Mouse	Santa Cruz, USA
CD133	1/1,000, 1/50	WB, IF	Mouse	Millipore, USA
MiTF	1/500, 1/100	WB, IF	Rabbit	abcam, UK
SOX10	1/200	WB, IF	Rabbit	abcam, UK
GFAP	1/20,000	WB, IF	Rabbit	abcam, UK
STIM1	1/200, 1:50	WB, IF	Mouse	BD Biosciences, USA
Orai1	1/200, 1/100	WB, IF	Rabbit	Sigma Aldrich, USA
TRPC1	1/200	WB	Rabbit	Alamone Labs, Israel
EthD-1	1/500	IF	-	Sigma Aldrich, USA
***Mouse - HRP**	1/5,000	WB	Rabbit	Dako, Denmark
***Rabbit - HRP**	1/5,000	WB	Swine	Dako, Denmark
***Mouse - FITC**	1/500	IF	Goat	Santa Cruz, USA
***Rabbit - TRITC**	1/500	IF	Rabbit	Sigma Aldrich, USA

Table 2.8.1. Antibodies used in immunofluorescence and Western blotting experiments

Antibodies used in Western blotting (WB) and immunofluorescence (IF) experiments. *denotes secondary antibody.

Fluorophore	Excitation wavelength	Emission wavelength	Laser used	Filters used
FITC (Fluorescein Isothiocyanate) or alexa-fluor 488	490	525	Argon 488	NFT 635 NFT 545 BP 505-550
TRITC (Tetramethyl Rhodamine Isothiocyanate)	557	576	HeNe 543	NFT 635 NFT 545 BP 560-615
EthD-1	510	595	Argon 488	NFT 635 NFT 545 BP 560-615
alexa-fluor 647	650	665	HeNe 633	NFT 635 LP 650

Table 2.8.2. Fluorophores conjugated to secondary antibodies used for immunofluorescence experiments

2.9. Protein extraction and concentration

Cells were lysed with buffer containing; 10% (v/v) Triton X-100, 2 mM Tris (pH 7.6), 1.28 mM sucrose, 1 mM EGTA (pH 8), 1 mM EDTA (pH 8) and 1 protease inhibitor cocktail tablet (Roche Diagnostics, Indianapolis, USA) per 10 ml. Cells were scraped into the lysis buffer, homogenised using a 20 gauge needle and centrifuged at 12,000 rpm for 10 minutes at 4°C. Supernatent was aliquot and stored at -20°C.

Bradford assays were used to determine protein concentration in cell samples. Various amounts of bovine serum albumin (BSA; 0-40 µg) were used for protein standards. BSA standards and protein samples (3 or 5 µ) were made up to 40 µl with dH_2O. Protein Assay Dye Reagent Concentrate (1 ml; BioRad, Herfordshire, UK) was added to the standards and samples which were briefly vortexed and left for 15 minutes at RT. The Coomassie Brilliant Blue G-250 dye within the reagent binds to protein causing a shift in maximum absorption from 465nm to 595nm, with a corresponding change in colour from blue to brown. The absorbance measurements from BSA standards at 595nm were plotted to form a standard curve to which a line of best fit was added (Figure 2.9.1). The absorbance measured from the 0 µg BSA standard was subtracted from each reading. The value of the slope (Y) from the line of best fit, was used to calculate the concentration of triplicate measurements from protein samples. The average absorbance from the protein samples was divided by the number of µl used and thereby the slope (Y) of the standard curve. This provided an estimate of protein concentration in µg/µl which was used to calculate the volume required to load samples onto gels.

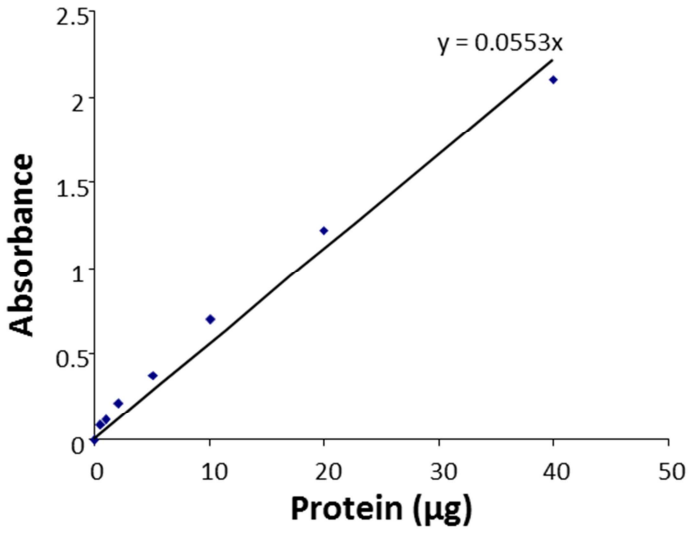

Figure 2.9.1. Example of BSA standard for Bradford Assay

Figure from MRes dissertation (Whitworth 2012). The average absorbance of BSA standard duplicates were calculated. Values were used to produce a trend line with intercept=0. The equation value for the line slope was applied to determine unknown sample protein concentrations.

2.10. Chloroform/methanol protein precipitation

The chloroform/methanol method (Wessel 1984) was used to precipitate proteins if concentrations were too low for SDS-PAGE as determined by Bradford assay. 20 µg of protein sample was made up to 100 µl in dH_2O before the addition of methanol (4 volumes), chloroform (1 volume) and dH_2O (3 volumes) were added. Samples were vortexed between each addition then spun down at 13,000 rpm for 2 mins. The aqueous supernatant above the protein layer was discarded. Methanol (3 volumes) was added and samples were inverted gently to allow mixing. The samples were spun at 13,000rpm for 2 minutes. The supernatant was discarded and the protein pellets allowed to air dry for ~5 minutes. Samples were re-suspended in 12 µl or 20 µl dH_2O and used for western blotting.

2.11. Western Blotting

20 µg of protein sample (12 µl or 20 µl in dH_2O) was incubated at 95°C with sodium dodecyl sulfate (SDS) sample buffer (3 µl or 5 µl respectively; 2% w/v SDS, 5% v/v 2-Mercaptoethanol, 10% w/v glycerol, pinch bromophenol blue in 60mM Tris (pH 6.8)). SDS is an anionic detergent that denatures proteins by disrupting noncovalent bonds and coats proteins with a negative charge relative to molecular weight whilst Mercaptoethanol reduces disulfide bonds. Heating helps denature the proteins and enhances SDS binding. Glycerol increases protein sample viscosity to weigh down samples in wells before the current is applied. Bromophenol blue is a small molecule dye added to allow visualisation of protein separation in SDS-PAGE which migrates through the gel quickly.

Protein samples were centrifuged for ~10 seconds at 12,000 g to remove condensation on the underside of the lid before being separated by gel electrophoresis through NuPAGE 10% Bis-Tris gels (1.0 mm, 10 well or 15 well, Invitrogen). NuPAGE MOPS SDS Running Buffer was used with the addition of NuPAGE Antioxidant (both Life Technologies) to the inner chamber to maintain the reduced state of proteins during electrophoresis. Gel wells were rinsed with running buffer before sample loading. Precision Plus Dual Colour Protein Standards (BioRad) to determine molecular weight.

Electrophoresis was carried out at a constant voltage of 200 V for ~1 hour or until dye reached the bottom of the gel. The electric field applied to the negatively charged proteins causes them to migrate toward the positive electrode at the bottom of the gel tank. Proteins are separated based on their molecular weight where small proteins move through the porous polyacylamide gel quickly and large proteins move through the gel more slowly.

Separated proteins were transferred to a nitrocellulose membrane (Bio-Rad, UK) at constant voltage of 50 V for ~2 hours. The transfer cassette (BioRad) was pre-equilibrated in transfer buffer (25mM Tris, 192mM glycine, 20% v/v methanol) and loaded in an orientation so that the gel was closest to the negative electrode and the nitrocellulose membrane was closest to the positive electrode. Therefore, when the electric field was applied, the negatively charged proteins moved towards the positive electrode and were bound to the nitrocellulose membrane. An ice pack was placed in the transfer tank to prevent overheating during transfer (Bio-Ice Cooling Unit). Transfer tanks were then placed on a magnetic stir plate to ensure buffer was continuously stirred throughout transfer.

The membrane was washed in PBS and blocked in a mix of Blotting-Grade Blocker non-fat dry milk powder (5% w/v) with Triton X-100 (0.02% v/v) in PBS for 1 hour at RT with gentle agitation to block unoccupied sites on membranes and prevent non-specific binding of antibodies.

2.12. Immunodetection of protein expression

Nitrocellulose membranes (Methods 2.11) were placed in 50 ml falcon tubes with the side that was in contact with the gel facing inwards and incubated with the primary antibodies in Table 2.8.1 diluted in incubation buffer (2.5% w/v non-fat dried milk in PBS) overnight at 4˚C. Membranes were washed in wash buffer (2.5% w/v non-fat dried milk, 0.2% v/v Triton X-100 in PBS) for 3 x 5 minutes at RT to remove unbound antibody. Membranes were then incubated with horseradish peroxidase (HRP) conjugated secondary antibodies (Table 2.8.1) for 1 hour at RT. The blot was washed in

wash buffer for 3 x 10 minutes at RT and, once slightly dry, protein standard bands were dotted with secondary anti-rabbit antibody (Table 2.8.1).

For chemiluminescence, blots were placed in a solution of 1.25 mM luminol in 0.1 M Tris-HCL (pH 8.5), 0.09 mM p-coumaric acid in dimethyl sulfoxide (DMSO) and 0.09% v/v hydrogen peroxide) for 1 minute. Membranes were wrapped in saran wrap, placed in a film cassette and exposed to x-ray film (HyperfilmTM, GE Healthcare, Amersham, Buckinghamshire, UK) for various times (10 seconds - 30 minutes) depending on the primary antibody used. Regions of film that are exposed to light (from HRP) darken. Exposed film was placed in Kodak Developer until immunoreactive bands were visible, briefly washed in water and then placed in Kodak fix for 2 minutes.

Bands were analysed by densitometry using ImageJ software to measure the intensity of each band signal (Figure 2.12.1). The integrated pixel density (sum of pixel values in selected area) of each band was measured and the selection area remained constant for each set of bands analysed. A background value was also subtracted from each band intensity. Values were expressed as a ratio of β-actin in order to determine the expression levels of proteins.

2.13. Determination of $[Ca^{2+}]_i$ through Ca^{2+}-addback in cell populations

Cells were washed 3 times with Ca^{2+}-containing Krebs buffer; (10 mM HEPES (pH7.4), 4.2 mM $NaHCO_3$, 1.2 mM $MgSO_4$, 1.2 mM KH_2PO_4, 4.7M m KCl, 118 mM NaCl, 10 mM glucose, 2 mM $CaCl_2$, 800 µM sulfinpyrazone) and then loaded with 3 µM of the Ca^{2+}-sensitive fluorescent dye, fura-2/AM (Calbiochem, Germany), for 45 minutes in the dark at RT.

Fura-2/AM is plasma membrane permeable and Ca^{2+} insensitive until cleavage of its acetoxymethyl (AM) esters within the cytosol. Cleaved fura-2 is Ca^{2+}-sensitive due to exposed carboxylate groups. Fura-2 is polar and therefore unable to diffuse out of the cell via the PM. However, it may still be transported either out of the cell or into cytoplasmic organelles via organic ion transporters. Sulfinpyrazone is an inhibitor of organic anion transporters and is therefore added to the Krebs buffer in order to prevent this fura-2 transport from the cytosol that could result in poor loading.

After fura-2 loading, cells were washed 3 times in 2ml Ca^{2+}-containing Krebs buffer and incubated in 2ml Ca^{2+}-containing Krebs buffer for 30 minutes in the dark at RT to allow complete fura-2/AM de-esterification. Individual coverslips were washed 3 times in 2ml Ca^{2+}-free Krebs buffer and fixed into a coverslip holder (Perkin Elmer, Beaconsfield, UK) which was placed in a Hellma fluorescence UV Quartz 10 mm cuvette (Scientific Laboratory Supplies, Nottingham, UK) containing 1.5 ml Ca^{2+}-free Krebs buffer and a magnetic stirrer. The loaded cuvette was transferred to a fluorimeter (PerkinElmer, LS-50B) and an excitation wavelength scan (250-450 nm) was carried out prior to each experiment so that coverslips with poor fura-2 loading and/or confluency could be discarded (Figure 2.13.1).

For measurements of intracellular Ca^{2+} store depletion and SOCE, Ca^{2+}-addback experiments were performed in which fura-2 fluorescence was recorded every 20 seconds at an excitation wavelength of 340 nm and emission wavelength of 510 nm (Figure 2.13.2). The trace was allowed to reach a steady baseline before 200 nm thapsigargin (TG; Calbiochem) was added to the cuvette. TG is a SERCA inhibitor that causes Ca^{2+} to leak from ER stores into the cytoplasm, increasing $[Ca^{2+}]_i$ and therefore

fura-2 fluorescence. Stock TG was made up in DMSO therefore traces from cells with an equivalent volume of vehicle DMSO added in place of TG were used as a control. Once the TG or DMSO response returned to baseline, 2 mM $CaCl_2$ was added to the cuvette, which causes Ca^{2+} entry representing SOCE to refill ER Ca^{2+} stores. This leads to a rise in $[Ca^{2+}]_i$ and fura-2 fluorescence due to SOCE.

Upon return to a steady baseline, 50 µM ionomycin (Calbiochem) was added to the cuvette. Ionomycin is a Ca^{2+} ionophore that alters Ca^{2+} membrane permeability and causes a large Ca^{2+} influx that saturates fura-2, producing maximal fluorescence (F_{max}). Following this sharp increase in fura-2 fluorescence, 1 mM $MnCl_2$ was added to the cuvette which quenches the fura-2, leading to a sharp decrease in fluorescence and generation of the autofluorescence (AF) value, which can be used to calculate the minimal fluorescence (F_{min}) value.

WinLab software (Perkin Elmer) was used to calculate $[Ca^{2+}]_i$ for which the Grynkiewicz formula is used and assumes a dissociation constant (K_d) of 224 nM and an instrument constant (IC) of 3. The individual traces were then calibrated (Figure 2.13.3) using the F_{max} and F_{min} values in order to convert the fluorescence changes into changes in $[Ca^{2+}]_i$ using the following equations:

$$F_{min} = 1 / IC\ (F_{max} - AF)$$

$$[Ca^{2+}]_i = K_d\ (F - F_{min}) / (F_{max} - F)$$

The area under the curve for TG and Ca^{2+} responses were calculated using WinLab software to determine the amount of Ca^{2+} entry into the cytosol as a reflection of Ca^{2+} store depletion and SOCE, respectively (Figure 2.13.3). For each dish (4 coverslips), 1 coverslip was used as a DMSO control and the others were used to determine the TG response. Average DMSO control trace values were subtracted from the average of the typical response values. All data presented throughout this thesis are basal-subtracted (i.e. DMSO response) and are therefore response to stimulus only. Extent of changes in SOCE were calculated taking any changes in Ca^{2+} store release into account and assuming a linear relationship.

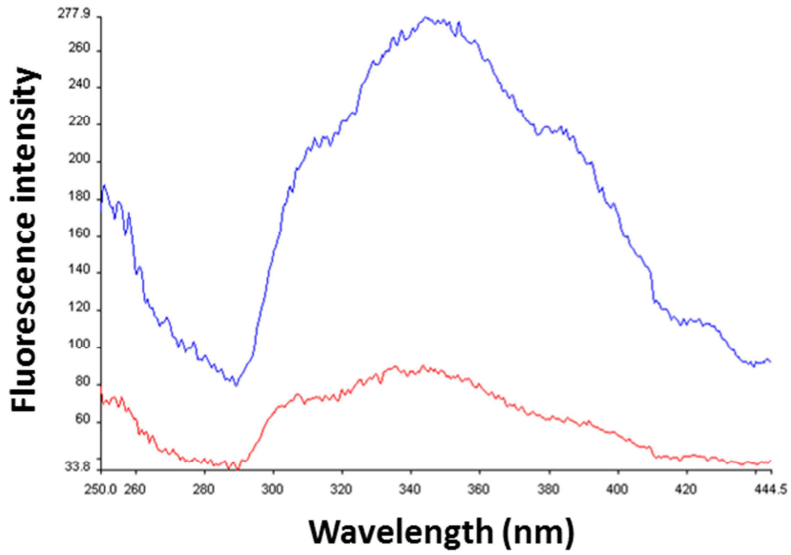

Figure 2.13.1. Wavelength scans were performed before each fluorimetry based experiment

Figure from MRes dissertation (Whitworth 2012). Excitation wavelength scans were carried out before each Ca^{2+}-addback experiment to ensure cells were loaded with fura-2/AM dye. Correct loading produced a trace with a high peak (>150) and small left hand shoulder (blue trace). Poor loading resulted in a small peak (<150) and high left hand shoulder (red trace).

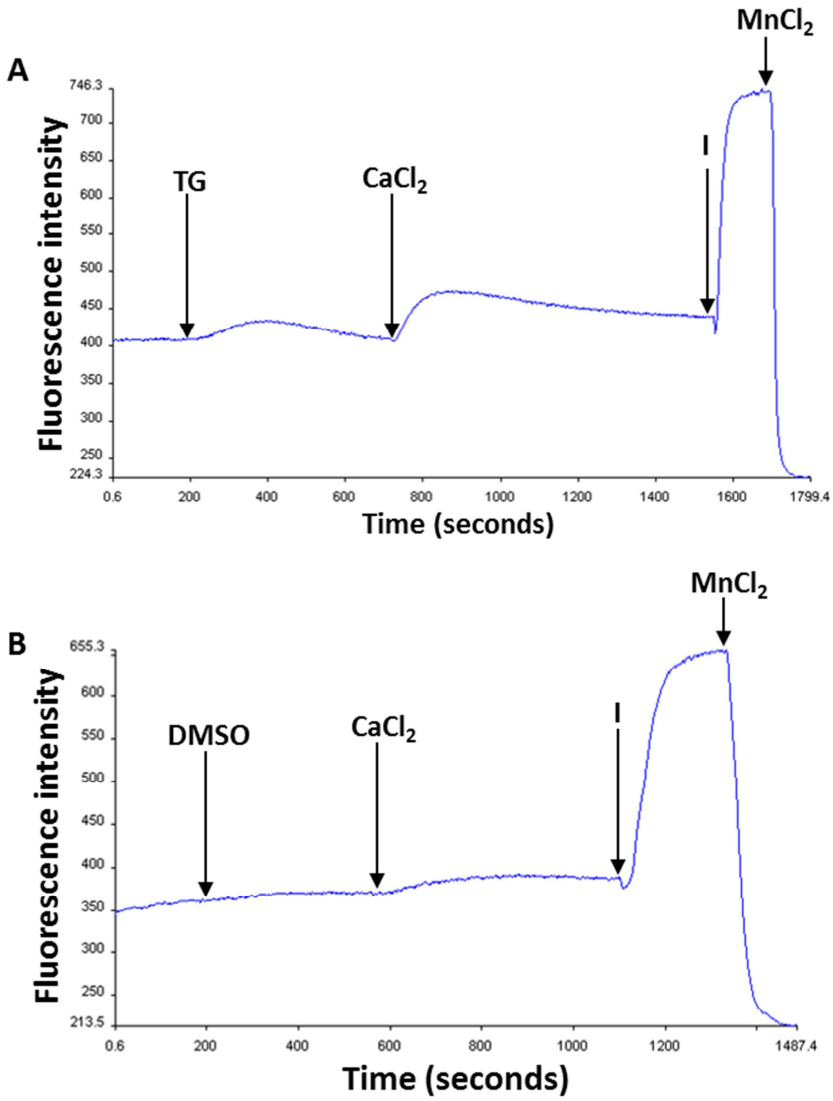

Figure 2.13.2. Typical Ca^{2+}-addback traces from fluorimetry based experiments

Figure from MRes dissertation (Whitworth 2012). **(A)** Typical Ca^{2+}-addback trace. Addition of 200 nM thapsigargin (TG) causes Ca^{2+} store depletion and therefore increases fura-2 fluorescence intensity. Ca^{2+}-addback (2 mM $CaCl_2$) produces a second, larger increase in fura-2 fluorescence intensity due to SOCE. Addition of 50 µM ionomycin (I) causes fura-2 saturation and a sharp increase in fura-2 fluorescence intensity to its maximal value (F_{max}) whilst addition of 1 mM manganese ($MnCl_2$) queches fura-2 and causes a sharp decrease in fura-2 fluorescence intensity to minimal autofluorescence (AF). The two responses are used to calibrate the trace. **(B)** Typical control Ca^{2+}-addback trace with DMSO added in place of TG which causes no change or a slight increase in fura-2 fluorescence intensity. Response to Ca^{2+}-addback is also reduced. Arrows represent addition of chemical.

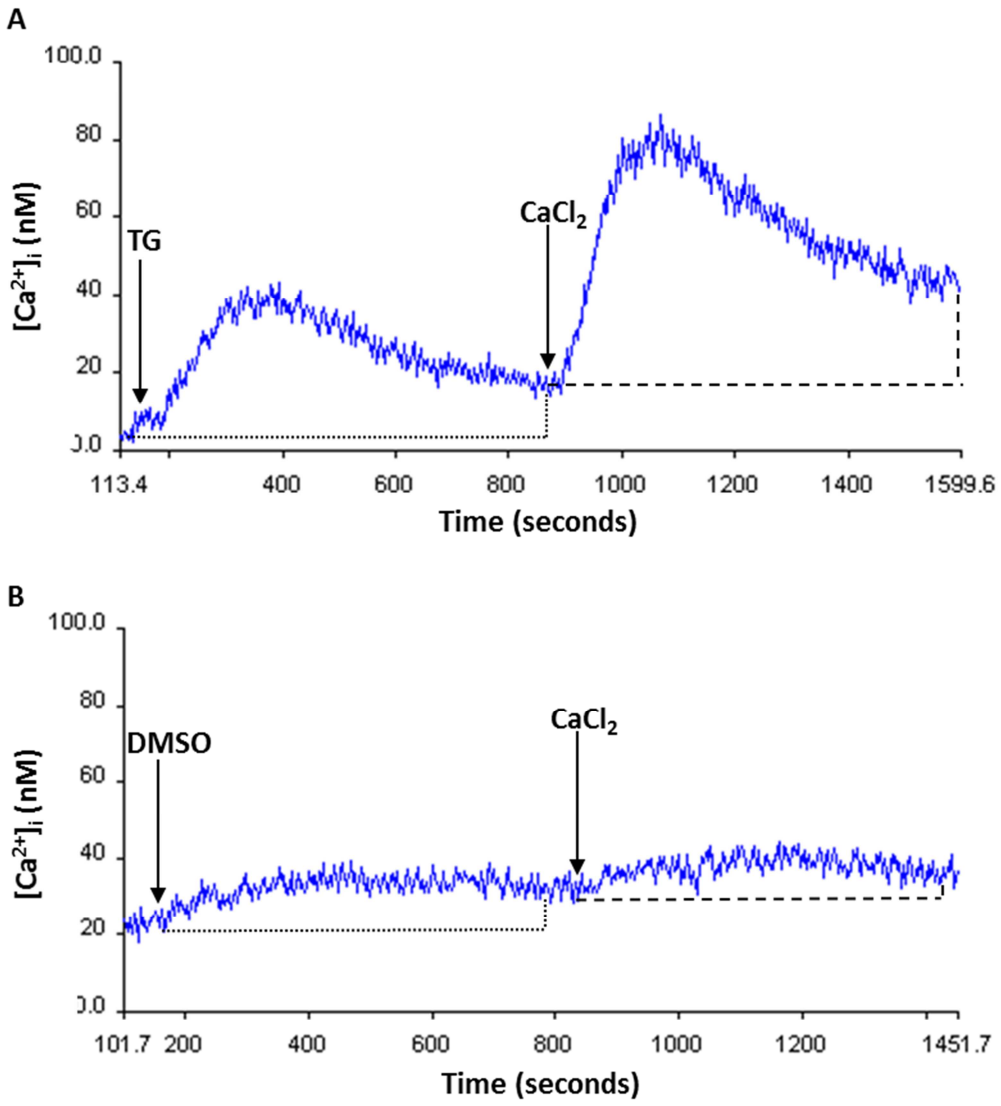

Figure 2.13.3. Determining $[Ca^{2+}]_i$ using calibrated Ca^{2+} addback traces from fluorimetry based experiments

Figure adapted from MRes dissertation (Whitworth 2012). **(A)** Typical Ca^{2+}-addback trace. Addition of 200 nM thapsigargin (TG) causes Ca^{2+} store depletion and therefore increases fura-2 fluorescence intensity. The change in $[Ca^{2+}]_i$ representative of Ca^{2+} store release was determined through calibration of the area under the curve (bound by dotted lines and trace peak). Ca^{2+}-addback (2 mM $CaCl_2$) produces a second, larger increase in fura-2 fluorescence intensity. The change in $[Ca^{2+}]_i$ representative of SOCE was determined through calibration of the area under the curve (bound by dashed lines and trace peak). **(B)** Typical control Ca^{2+}-addback trace with DMSO added in place of TG which causes no change or a slight increase in fura-2 fluorescence intensity. The change in $[Ca^{2+}]_i$ was determined through calibration of the area under the curve

(bound by dotted lines and trace peak). Response to Ca^{2+}-addback is reduced in DMSO controls. The change in $[Ca^{2+}]_i$ representative of basal SOCE was determined through calibration of the area under the curve (bound by dashed lines and trace peak). Arrows represent addition of chemical.

2.14. Single cell Ca^{2+}-addback experiments

Cells were loaded with fura-2/AM as described above (Methods 2.13). After loading and washing, individual coverslips were fixed into a coverslip holder (custom made), producing a chamber in which Ca^{2+}-free Krebs buffer was added. Measurements of relative changes in $[Ca^{2+}]_i$ were recorded using ratiometric imaging through detection of fura-2 fluorescence at an excitation wavelength of 340 nm and 380 nm and an emission wavelength of 510 nm using an Olympus IX70 fluorescent microscope or a Nikon Eclipse TE300 microscope. Images were obtained with a charge-coupled device (CCD) camera (MicroMax, Sony Interline Chip, Princeton Instruments, Trenton, NJ) and using a 20x objective lens.

MetaFluor software (Universal Imaging, Marlow, UK) was used to record data and calculate the ratio between 340 nm and 380 nm fluorescence intensity (FR) as a representation of $[Ca^{2+}]_i$. Ratiometric measurements take advantage of the dual excitability of fura-2, which shifts its absorbance maximum to lower wavelengths in its Ca^{2+} bound form. Alternating excitement at 340 nm and 380 nm ensures a maximal difference between the fluorescence emission of fura-2 in its unbound and Ca^{2+} bound state. This normalises for changes in fluorescence intensity that are unrelated to changes in $[Ca^{2+}]_i$, such as unequal fura-2 distribution, uneven cell thickness or noise introduced by the detection equipment (e.g. changes in illumination intensity).

To establish a new system for single cell Ca measurements, the optimum exposure times for 340 nm and 380 nm excitation were determined using a range of exposure times (Figure 2.14.1). The optimum exposure times were 300 ms for 340 nm excitation and 80 ms for 380 nm as these exposure times did not cause photobleaching over the time of the experiment (Figure 2.14.1B) but still provided ample maximal difference between the responses at the two wavelengths of excitation.

Regions of interest were drawn around ~10 cells before each experiment to track the response over the Ca^{2+}-addback experiment (Figure 2.14.2). Following establishment of a steady trace baseline, 200 nM TG (Calbiochem) was added to induce ER Ca^{2+} store release and a rise in $[Ca^{2+}]_i$ represented as a peak in FR (Figure 2.14.3A), or an

equivalent volume of DMSO as a control was added (Figure 2.14.3B). Following return to a steady baseline, 2 mM $CaCl_2$ was added to induce SOCE and a rise in $[Ca^{2+}]_i$ represented as second peak in FR (Figure 2.14.2).

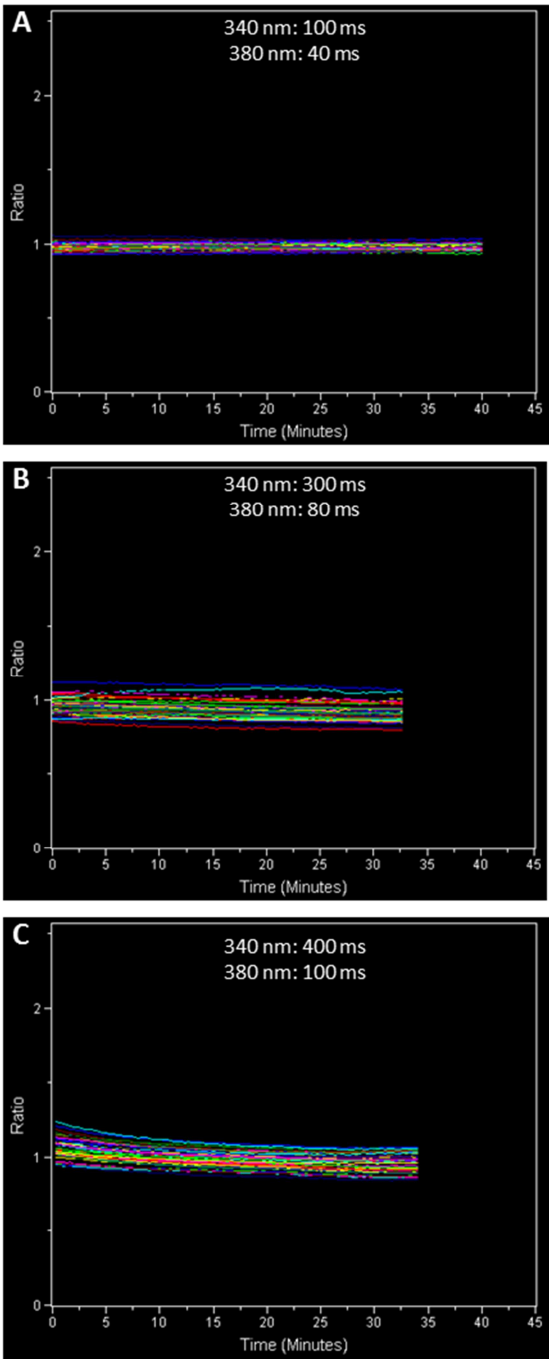

Figure 2.14.1. Optimum exposure times to prevent photobleaching in single cell based experiments

Ratiometric imaging through detection of fura-2 fluorescence at an excitation wavelength of 340 nm and 380 nm and an emission wavelength of 510 nm was performed using an Olympus IX70 fluorescent microscope or a Nikon Eclipse TE300 microscope. Measurements of changes in fluorescence intensity over time were recorded to determine optimum exposure times for 340 nm and 380 nm excitation. A range of exposure times were used, upwards from **(A)** 100 ms for 340 nm excitation with 40 ms for 380 nm excitation. Optimum exposure times were observed at **(B)** 300 ms for 340 nm excitation with 80 ms for 380 nm excitation since there was no change in fluorescence intensity over the time-course like that in (A) and increasing exposure time further to **(C)** 400 ms for 340 nm excitation with 100 ms for 380 nm excitation caused a slight decrease over the time-course due to photobleaching.

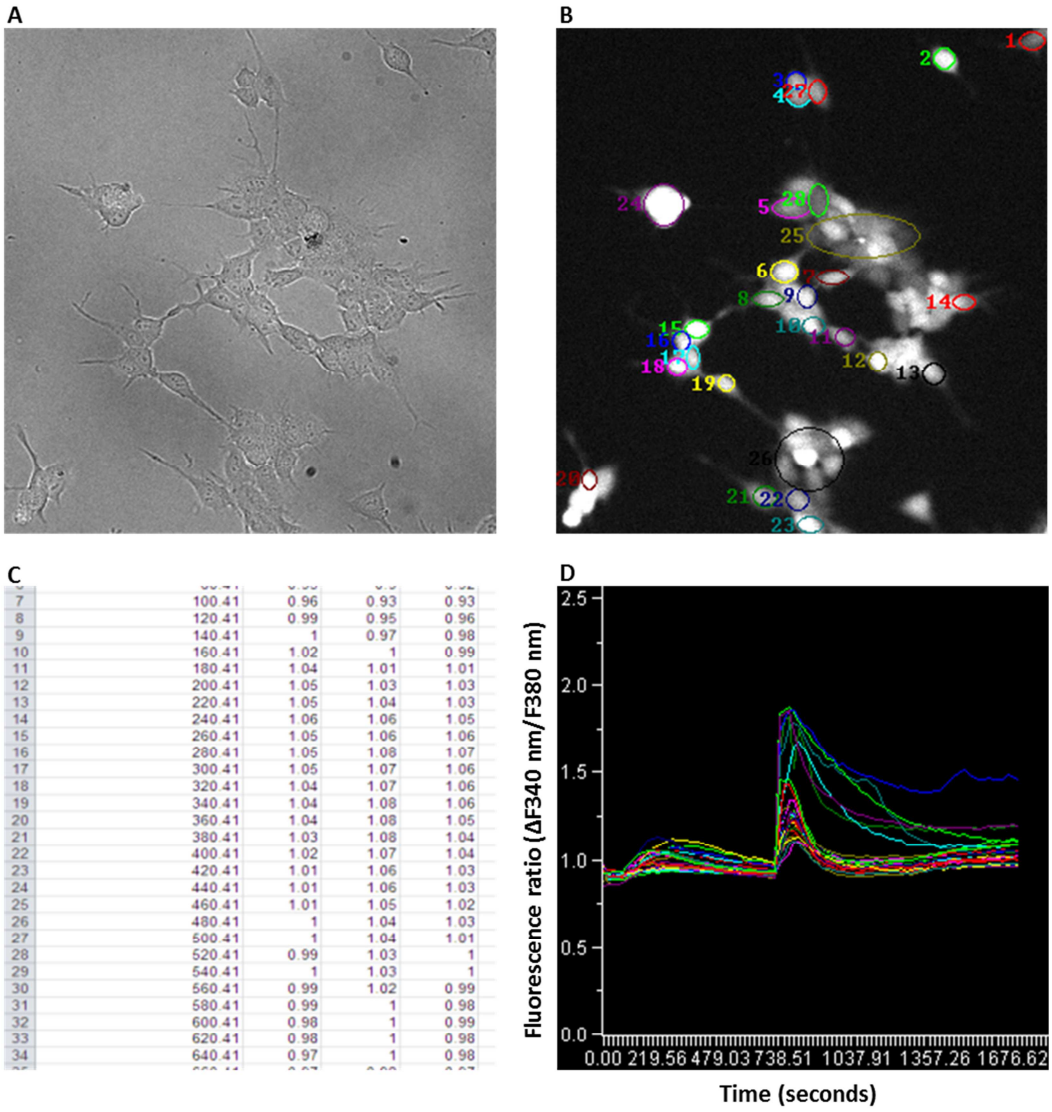

7	100.41	0.96	0.93	0.93
8	120.41	0.99	0.95	0.96
9	140.41	1	0.97	0.98
10	160.41	1.02	1	0.99
11	180.41	1.04	1.01	1.01
12	200.41	1.05	1.03	1.03
13	220.41	1.05	1.04	1.03
14	240.41	1.06	1.06	1.05
15	260.41	1.05	1.06	1.06
16	280.41	1.05	1.08	1.07
17	300.41	1.05	1.07	1.06
18	320.41	1.04	1.07	1.06
19	340.41	1.04	1.08	1.06
20	360.41	1.04	1.08	1.05
21	380.41	1.03	1.08	1.04
22	400.41	1.02	1.07	1.04
23	420.41	1.01	1.06	1.03
24	440.41	1.01	1.06	1.03
25	460.41	1.01	1.05	1.02
26	480.41	1	1.04	1.03
27	500.41	1	1.04	1.01
28	520.41	0.99	1.03	1
29	540.41	1	1.03	1
30	560.41	0.99	1.02	0.99
31	580.41	0.99	1	0.98
32	600.41	0.98	1	0.99
33	620.41	0.98	1	0.98
34	640.41	0.97	1	0.98

Figure 2.14.2. Typical Ca^{2+}-addback experiment using a single cell based approach

Ca^{2+} addback experiments were recorded using ratiometric imaging through detection of fura-2 fluorescence at an excitation wavelength of 340 nm and 380 nm and an emission wavelength of 510 nm using an Olympus IX70 fluorescent microscope. Images were obtained with a charge-coupled device (CCD) camera (MicroMax, Sony Interline Chip, Princeton Instruments, Trenton, NJ) and using a 20x objective lens. Cells were identified morphologically using **(A)** bright field and **(B)** fluorescence images. **(B)** Regions of interest were created over each cell in the field of view. Example includes individual N-type cells (#1-23) and cell clumps (#24-26). **(C and D)** The experiment was run to capture fluorescence ratio data values in Excel (time-points and data from 3 cells depicted) and produce a trace for each region of interest corresponding to a specific cell phenotype and differentiation status.

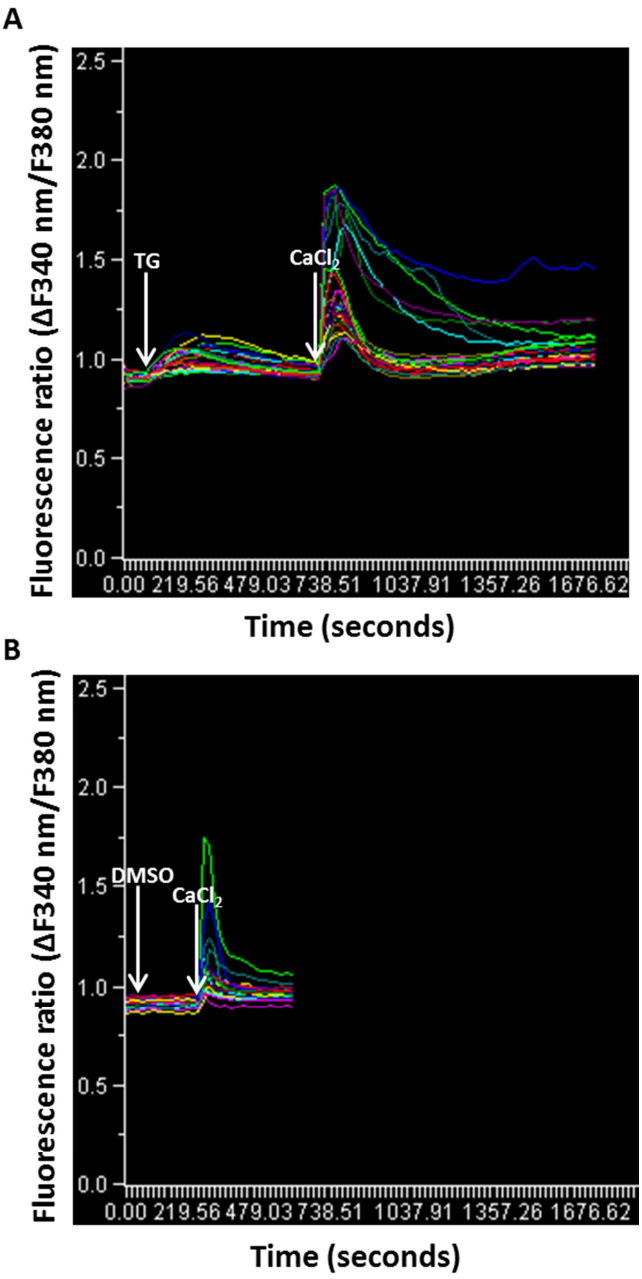

Figure 2.14.3. Typical Ca^{2+}-addback traces using single cell based experiments

(A) Addition of 200 nM thapsigargin (TG) causes an increase in fura-2 fluorescence and the fluorescence ratio between the two excitation wavelengths, representative of a rise in $[Ca^{2+}]_i$ due to release of Ca^{2+} from intracellular ER stores. Ca^{2+}-addback (2 mM $CaCl_2$) causes a second increase in fura-2 fluorescence and the fluorescence ratio between the two excitation wavelengths, representative of a rise in $[Ca^{2+}]_i$ due to SOCE. **(B)** DMSO addition as a control for TG does not increase fura-2 fluorescence and the subsequent Ca^{2+}-add-back response is reduced, is representative of basal Ca^{2+} entry.

2.15. Analysis of relative changes in $[Ca^{2+}]_i$ in single cells

MetaFluor and MetaMorph software (Universal Imaging) were used to record data and calculate the fluorescence ratio (FR) as a representation of $[Ca^{2+}]_i$. Regions of interest (ROI) were applied to individual cells and the experiments recorded (Methods 2.14) were re-ran to produce a trace for every cell or cell aggregate in the field of view (Figure 2.14.1). The fluorescence ratio data was recorded in Microsoft Excel for each region of interest that could be related to morphological phenotype and differentiation status (Figure 2.15.1A).

The peak height (PH), rate of rise (ROR), rate of decline (ROD) and area under the curve (AUC) for TG and Ca^{2+} responses were calculated using Excel functions in a template spread sheet, custom built under a collaboration with Dr Graham Scholefield, so that only three cell values needed to be altered manually for each data set (Figure 2.15.1A).

The minimum and maximum fluorescence ratio values in the TG and Ca^{2+} range were calculated to determine the peak height of each response (Figure 2.15.1). To eliminate the possibility of finding a minimum value at the end of the Ca^{2+} response, the function finds the minimum within the rising phase of the peak, defined as data preceding the maximum value.

The rate of rise (ROR) function determines the row number of the dataset at the minimum and maximum values in the TG or Ca^{2+} range and minuses the minimum row number from the maximum row number (Figure 2.15.1). This value is multiplied by 20 to give the time value of the TG or Ca^{2+} response range, since the time lapse between measurements is 20 seconds. The peak height is then divided by the time range to provide the ROR (Figure 2.15.1).

The rate of decline (ROD) function determines the row number of the dataset at the maximum value and the minimum value following the peak in the TG or Ca^{2+} range and minuses the maximum row number from the minimum row number (Figure 2.15.1). This value is multiplied by 20 to give the time value of the TG or Ca^{2+} response range,

since the time lapse between measurements is 20 seconds. The peak height is then divided by the time range to provide the total ROD (Figure 2.15.1). Since the ROD for the Ca^{2+} often consisted of two phases, the initial and late ROD was also determined. The initial ROD function uses the calculations described above but finds and uses the time-point at 300 secs following the peak of the Ca^{2+} response instead of the minimum value to determine the time range (Figure 2.15.1). The late ROD function uses the calculations described above but finds and uses the time-point at 300 secs following the peak of the Ca^{2+} response instead of the maximum value and still uses the minimum value to determine the time range (Figure 2.15.1).

The AUC function finds the area bound by the graph and within a specified time region above the specified minimum value (Figure 2.15.1). This function multiplies the minimum value by the time range and minuses this from the maximum to account for changes in baseline.

The cell type (N-, S-, or I-type and S_O, S_A or S_E) and differentiation status (proliferating or differentiating) were defined morphologically as previously described (Introduction 1.3 and 1.4) and manually attributed to each ROI dataset (Figure 2.15.1A). Data from the Excel spreadsheet described above was then automagically extracted to a custom built VBA coded Excel tool, developed in collaboration with Dr Graham Scholefield. The tool was able to extract and group data together based on the characteristics described above, as well as by experiment date and type, and, by use of data filters, could average the grouped data, subtract grouped DMSO control data from experimental data and perform Student's t-tests.

Average DMSO control trace values were subtracted from the average of the typical response values. All data presented throughout this thesis are basal-subtracted (i.e. DMSO response) and are therefore response to stimulus only. Extent of changes in SOCE were calculated taking any changes in Ca^{2+} store release into account and assuming a linear relationship.

A

	A	B	C	D	E	F	G	H	I	J
1	ONLY EDIT **BOLD** VALUES							**Cell Type: 1 N**		**2 N**
2	DO NOT EDIT VALUES IN *ITALICS*									
3		Time Calcium added =	**940**	sec				*Region #:*	*R1 R1*	*R2 R1*
4		Time between each image =	**20**	sec				*TG Range*	*Data!$B$3:$B$44*	*Data!$C$3:$C$44*
5		First time row number (in data tab) =	**3**					*Ca Range*	*Data!$B$45:$B$95*	*Data!$C$45:$C$95*
6		Last time row number (in data tab) =	**95**				TG	*Min*	*1.03*	*1*
7							TG	*Max*	*1.25*	*1.14*
8		Name of data sheet=	*Data*				TG	*Height of peak*	*0.22*	*0.14*
9		Time Range =	*Data!$A$3:$A$95*				TG	*Rate of rise*	*0.001571429*	*0.001*
10		TG Lower Time =	*100.34*	sec			TG	*Area under peak*	*94.8*	*50.4*
11		TG Upper Time =	*920.34*	sec				*Ca 'Peak Rise' Range*	*Data!$B$45:$B$51*	*Data!$C$45:$C$51*
12		Ca Lower Time =	*940.34*	sec			Ca	*Min*	*1.07*	*0.99*
13		Ca Upper Time =	*1940.34*	sec			Ca	*Max*	*1.77*	*1.22*
14							Ca	*Height of peak*	*0.7*	*0.23*
15							Ca	*Rate of rise*	*0.005833333*	*0.001916667*
16							Ca	*Area under peak*	*367.8*	*139.8*
17										
18							TG	*ROD till CA*	0.000257143	0.000214286
19							Ca	*ROD to 1240.34 secs*	0.000266667	0.0002
20							Ca	*ROD to 1940.34 secs*	0.00059	0.00016
21							Ca	*ROD from 1240.34 to 1*	0.000728571	0.000142857
22										

Analysis Formulas

New Formulas

B

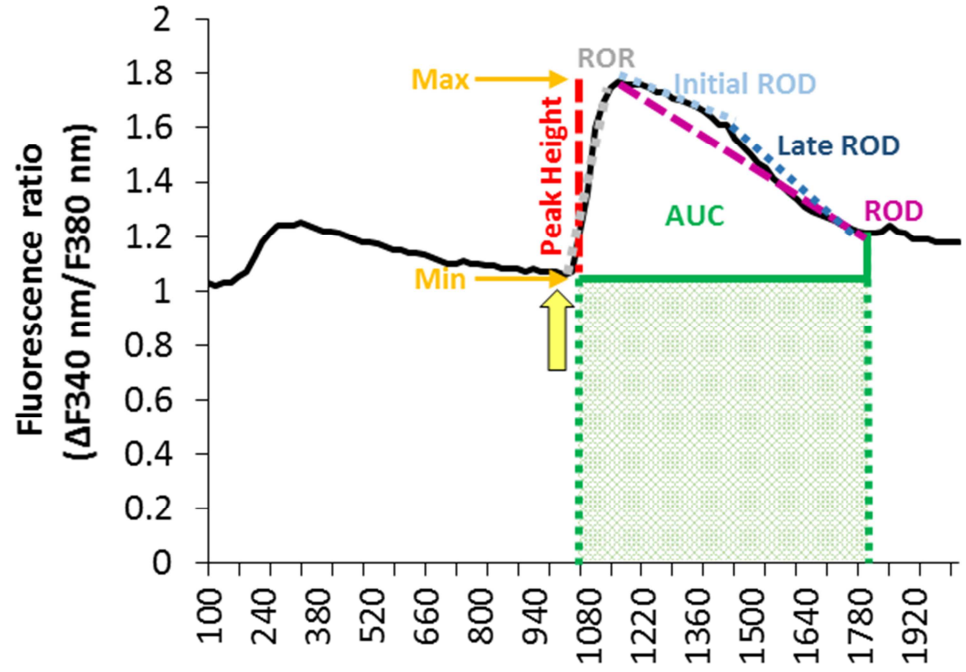

Figure 2.15.1. Determining relative changes in $[Ca^{2+}]_i$ using Ca^{2+}-addback traces from single cell based experiments

(A) Example of template spread sheet with trace values attributed to each ROI defined by morphology (Row 1). Colours correspond to those on the **(B)** example data set depicting spread sheet function calculations for SOCE peak. The time of $CaCl_2$ addition is used as the start of the SOCE response (yellow). For each region of interest (ROI) data set, the minimum value is subtracted from the maximum value (orange) to find peak height (red). The area under the curve (AUC) function finds the area that is bound

by the graph within a specified time region (dotted green lines) and above the specified minimum value (solid green line). The function also multiplies the minimum value (orange) by the time range (dotted green lines) and minuses this from the maximum (i.e. subtracts dotted green area from total AUC) to provide the AUC (bound by solid green line and trace). The rate of rise (ROR) function determines the row number of the dataset at the minimum and maximum values (orange) and minuses the minimum row number from the maximum row number. This value is multiplied by 20 to give the time value of the response range (dotted green lines), since the time lapse between measurements is 20 seconds. The peak height (red) is then divided by the time range to provide the ROR (grey). The rate of decline (ROD) function determines the row number of the dataset at the maximum value and the minimum value (orange) following the peak and minuses the maximum row number from the minimum row number. This value is multiplied by 20 to give the time value of the response range (dotted green lines), since the time lapse between measurements is 20 seconds. The peak height is then divided by the time range to provide the total ROD (purple dashed line). Since the ROD for SOCE often consisted of two phases, the initial and late ROD was also determined. The initial ROD function uses the calculations described above but finds the time-point at 300 secs following the peak of the Ca^{2+} response instead of using the minimum value to determine the time range (light blue dotted line). The late ROD function uses the calculations described above but finds the time-point at 300 secs following the peak of the Ca^{2+} response instead of using the maximum value whilst still using the minimum value to determine the time range (dark blue dotted line).

2.16. RNA extraction and sequencing

Total RNA extraction was performed by Lauren Harkin using the QIAgen RNeasy mini kit (QIAgen, West Sussex, UK) according to the manufacturer's protocol. This procedure allows all RNA molecules >200 nucleotides to be purified, thereby enriching for mRNA. Briefly, cells were lysed and homogenised in the presence of a denaturing guanidine-isothiocyanate buffer which inactivates RNases to prevent RNA degradation. Ethanol (70%, 1 volume) was added to samples to promote binding to RNeasy silica-membranes. Samples were transferred to an RNeasy spin column in a collection tube. Samples were centrifuged at 10,000 rpm for 15 seconds to wash away contaminants. Flow-through was discarded and wash buffer was added to the samples, which were centrifuged at 10,000 rpm for 15 seconds to wash the spin column membrane. This was repeated twice and samples were centrifuged for two minutes a third time to dry the spin column membrane and ensure ethanol was not transferred in the RNA elution. RNase-free water was added to the spin column membrane and centrifuged at 10,000 rpm for 1 minute to elute the RNA. Purified RNA was stored at -20°C in RNase-free water until being sent for sequencing.

2.17. Statistical Analysis

Data are representative of mean ± S.E.M of N total number of experiment days and n total number of cells. Microsoft Excel and GraphPad Prism 3 and 6 were used to analyse all data using, for unpaired groups, two-tailed Student's t-tests or, for groups of three or more, one-way analysis of variance (ANOVA). Statistical significance was accepted as $P \leq 0.05$. The level of significance is indicated in figures as P<0.05*, P<0.01**, P<0.001***, P<0.0001****.

Chapter 3: The 9-*cis*-retinoic acid-induced differentiation response

Chapter 3 - Introduction

Induction of neuroblastoma differentiation by retinoic acid administration alongside standard chemotherapy is used to treat patients with end stage or residual neuroblastoma (Matthay 2009). There are several isoforms of retinoic acid, of which 9*c*RA is the most potent for differentiation induction (Han 1995; Lovat 1997). It has previously been shown that 9cRA-induced morphological differentiation of N-type cells causes elongation of neurite-like processes (Brown 2005; Cheung 2009; N. Bell 2013) and that morphological changes occur in S-type cells (N. Bell 2013) however these have yet to be fully defined. The aim of this chapter was to characterise the phenotype-specific 9cRA-induced differentiation profile of SH-SY5Y neuroblastoma cells morphologically and biochemically.

Chapter 3 - Results

3.1. 9cRA induces a lineage-specific morphological change in neuroblastoma cells

Treatment of SH-SY5Y cells (N-type populations) and S-enriched SH-SY5Y cells (S-type populations) for 7 days with 1 µM 9*c*RA induced morphological changes that were used to distinguish a differentiating phenotype from a proliferating (EtOH treated) phenotype (Figure 3.1.1). Proliferating N-type cells possess small, rounded cell bodies with short neurite-like processes and grow over one another, forming aggregates (Figure 3.1.1A). With 9cRA treatment, N-type cells differentiate towards a neuronal lineage developing extended neuritic processes (Figure 3.1.1A and B). Neurite length has been extensively used as a marker of N-type cell differentiation and cells possessing one or more neurites over 50 µm in length are generally regarded as differentiated (N. Bell 2013; Brown 2005; Simpson 2001). Compared to EtOH treated cells, the percentage of differentiated cells increased with 9*c*RA treatment (6% to 18%, respectively, $P<0.0001$, Figure 3.1.2A). The average neurite length was also significantly increased in 9cRA treated cells (28 µm to 36 µm, $P=0.0002$, Figure 3.1.2B).

Proliferating S-type cells have abundant cytoplasm with no neuritic processes and develop a more flattened and spread out morphology with differentiation (Figure 3.1.1C and D). The S-phenotype consists of three sub-populations; outstretched (S_O), angular (S_A) and elongated (S_E), which all undergo morphological changes with differentiation. Since no standardised morphological marker of differentiation has been established for S-type cells, cell diameter for S_O and S_A cells and cell length for S_E cells was used to quantify the effect of 9cRA-induced differentiation. Cell measurements of all three sub-phenotypes increased with 9*c*RA treatment (Figure 3.1.3). The diameter of EtOH treated S_O and S_A cells (33.60 µm and 16.85 µm, respectively, Figure 3.1.3) increased with 9cRA treatment (46.94 µm, P=0.0018 and 24.00 µm, P=0.212, respectively, Figure 3.1.3). The length of S_E cells also increased significantly with 9cRA treatment (from 56.76 µm to 86.02 µm, P=0.001, Figure 3.1.3). The proportions of cell phenotypes within S-type populations were not significantly altered with differentiation (Figure 3.1.4), although it is noteworthy that there was a greater than two-fold increase in the proportion of S_E cells upon differentiation. 9*c*RA-induced differentiation also causes a reduction in the proliferation rates of N-type and S-type cells.

I –type cells in EtOH treated populations exhibited morphological characteristics of both N-type and S-type cells, with abundant cytoplasm and neurite-like processes (Figure 3.1.1A). In 9cRA treated populations, I-type cell processes appeared more elongated and cell bodies more spread out (Figure 3.1.1B).

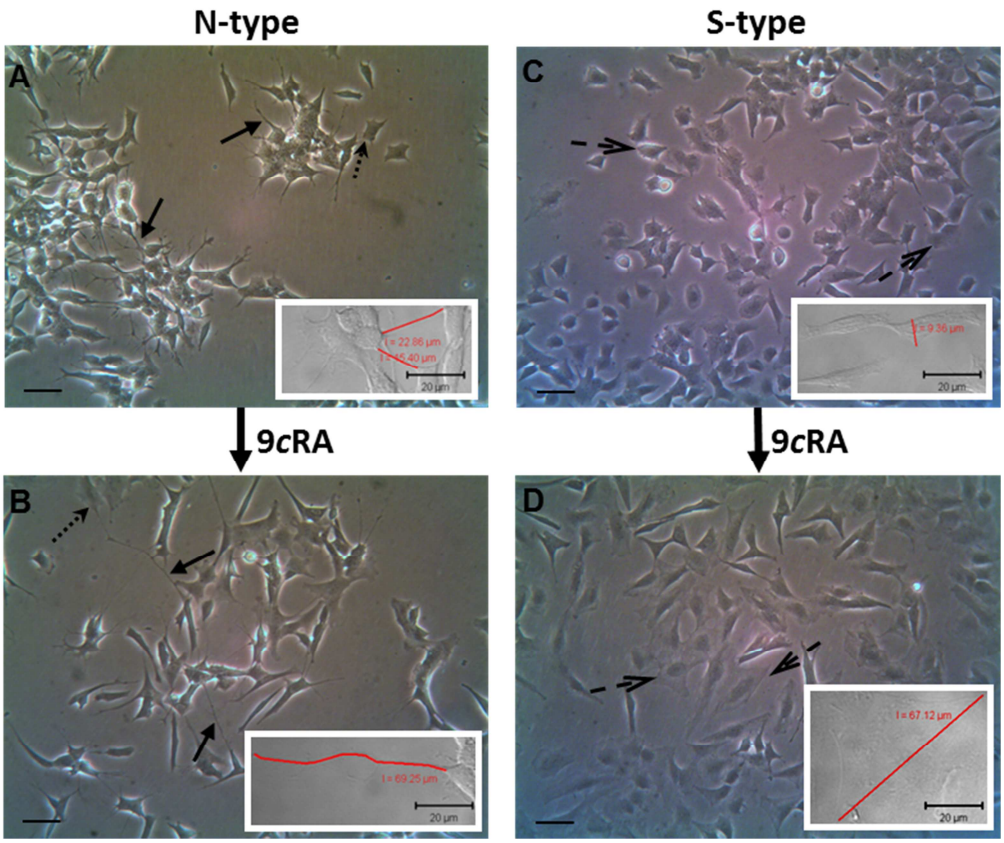

Figure 3.1.1. Treatment of N-type and S-type populations with 9*c*RA induces morphological differentiation

N-type and S-type cell populations were treated for 7 days with 1 µM 9*c*RA to induce differentiation or with an equivalent volume of EtOH as a control to maintain proliferation. Inset DIC images show the measurement of changes in cell morphology. **(A)** Proliferating N-type cells possess short neurite-like processes (black arrows and inset) and **(B)** upon differentiation, neurites become elongated (arrows and inset). **(C)** Proliferating S-type cells have abundant cytoplasm and a flattened morphology (dashed arrows and inset) and **(D)** become more flattened and spread out with differentiation, with an increased diameter (dashed arrows and inset). I-type cells in proliferating populations **(A)** possess abundant cytoplasm and neurite-like processes (dotted arrow) and in differentiating populations **(B)**, I-type processes become elongated like that of N-type cells and cell bodies become more spread out like that of S-type cells (dotted arrow). Scale bars of main phase contrast images represents 50 µm and DIC inset images represent 20 µm.

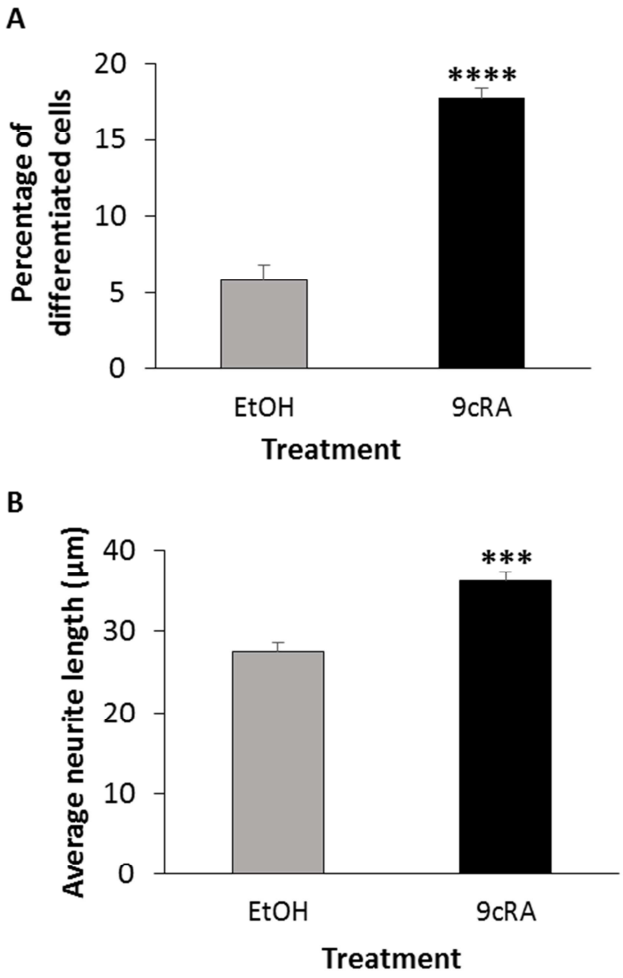

Figure 3.1.2. Treatment of N-type cells with 1 µM 9*c*RA causes elongation of neurites
N-type cell populations were treated for 7 days with 1 µM 9*c*RA to induce differentiation or with an equivalent volume of EtOH as a control to maintain proliferation. Phase contrast or DIC images were used for neurite measurements using Metamorph and LSM Image Browser, respectively. (A) Neurite length was used to classify N-type cells as morphologically proliferating or differentiated. Cells possessing one or more neurites >50µm in length were classed as differentiated. Percentage of differentiated cells was 5.84% in control EtOH treated cells and was significantly higher in 9*c*RA treated cells (17.76%, P<0.0001****) therefore 9cRA treatment for 7 days alters N-type morphology to a differentiating phenotype. (B) The neurites of N-type cells were significantly shorter in EtOH treated cells (27.57µm) than those of 9*c*RA treated cells (36.29µm, P=0.0002***). EtOH treated n=6394, 9cRA treated n=2694. N=6.

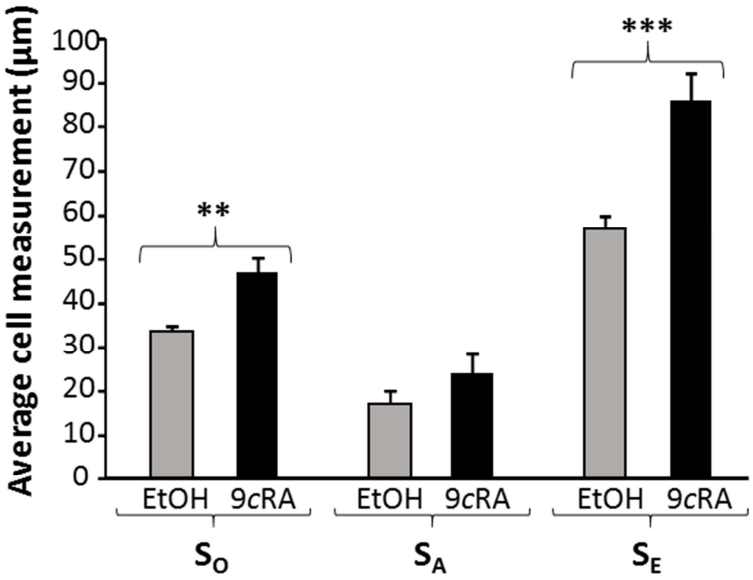

Figure 3.1.3. 9*c*RA-induced differentiation of S-type cells develop increased cell dimensions

Treatment with 1 µM 9*c*RA for 7 days induces morphological changes in the three S-type sub-populations compared to EtOH treated cells. Phase contrast or DIC images were used for neurite measurements using Metamorph and LSM Image Browser, respectively. **(A)** The diameter of proliferating (P) outstretched (S_O) cells significantly increased with 9*c*RA-induced differentiation (D, 33.60 µm to 46.94 µm, P=0.0018**). The diameter of proliferating angular (S_A) cells (16.85 µm) cells increased with differentiation (24.00 µm, P=0.212). The length of elongated cells (S_E) significantly increased with differentiation (from 56.76 µm to 86.02 µm, P=0.001***). Proliferating S_O n=2055, S_A n=1144, S_E n=126. Differentiating S_O n=1492,S_A n=563, S_E n=146. N=7.

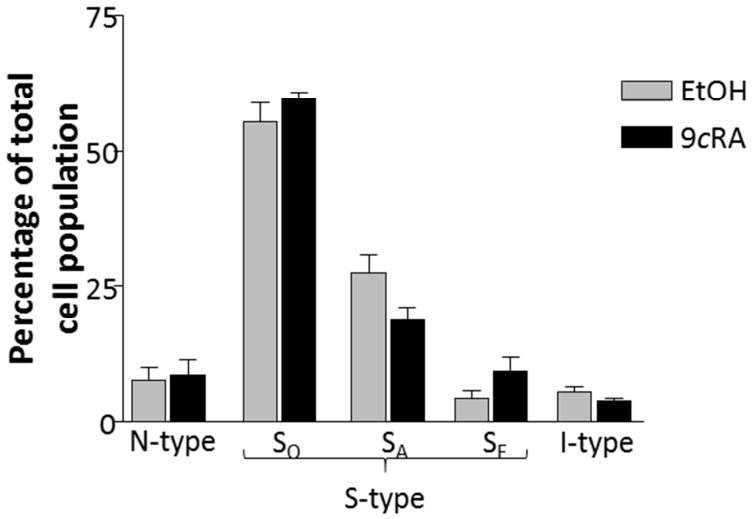

Figure 3.1.4. Cell phenotype proportions do not change with differentiation of S-type cell populations.

S-type cell populations were treated for 7 days with 1 µM 9*c*RA or equivalent volume of EtOH as a control to induce morphological. Phase contrast or DIC images were used for neurite measurements using Metamorph and LSM Image Browser, respectively. Compared to EtOH treated S-type populations, in 9*c*RA treated S-type populations there was no significant difference in the percentage of proliferating N-type (7% and 9%, respectively, P=0.8101), S_O (57% and 59%, respectively, P=0.3030), S_A (27% and 21%, respectively, P=0.0641), S_E (3% and 7%, respectively, P=0.1153) or I-type cells (5% and 4%, respectively, P=0.1293). EtOH treated n=3274, 9cRA treated n=2138. N=5.

3.2 Increases in 9cRA concentration do not increase morphological differentiation of N-type neuroblastoma cells

As the extent of differentiation is variable between studies and between batches of cells, it is important to confirm the maximum dose of 9*c*RA in this study. Therefore, dose-response experiments were performed in N-type populations (Figure 3.2.1 and 3.2.2) to determine the optimal 9*c*RA concentration for a sufficient morphological differentiation response.

Previously in this laboratory, treatment with 1 µM 9*c*RA over 7 days has been deemed an appropriate concentration to induce significant differentiation of neuroblastoma cells (Bell *et al*., 2013). As expected, treatment of N-type populations with 1 µM 9*c*RA for 7 days caused a significant increase in percentage of differentiation compared to EtOH treated control cells (from 3% to 14%, P=0.0161, Figure 3.2.2A) and neurite length was significantly increased (from 26 µm to 34 µm, P=0.0112, Figure 3.2.1B and 3.2.2B). There was no further significant increase in the percentage of differentiated cells with subsequent increases in 9*c*RA concentration up to 20 µM (P>0.05, Figure 3.2.2A). There was, however, a significant increase in average neurite length between 1 µM and 10 µM 9*c*RA treatment (34 µm and 39 µm, respectively, *P*=0.0335, Figure 3.2.2B). This increase was marginal and treatment at a concentration of 10 µM 9*c*RA appeared to lie close to limit of inhibition, since the percentage differentiation and average neurite length appeared to fall slightly with 20 µM 9*c*RA (Figure 3.2.2A and B). Consistent with a possible inhibitory dose of 9*c*RA, 20 µM 9cRA also appeared to reduce cell numbers (Figure 3.2.1F). This provided rationale for continuing to use a concentration of 1 µM 9*c*RA as the differentiating medium. Cells treated with 1µM 9*c*RA will therefore be referred to as differentiating cells whilst cells treated with the equivalent volume of EtOH as a control will be referred to as proliferating cells.

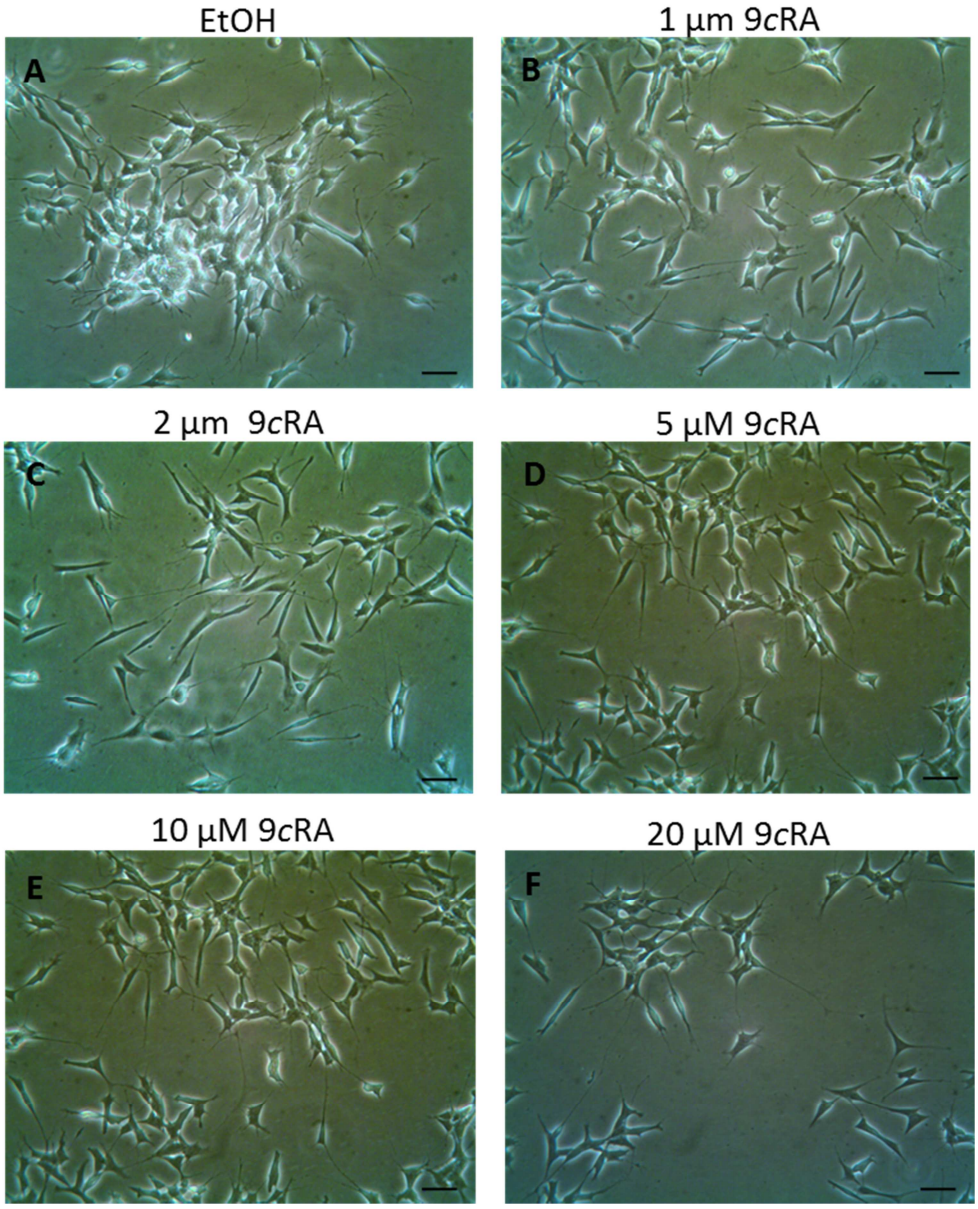

Figure 3.2.1. Treatment of N-type cells with 9*c*RA induces elongation of neurite-like processes

N-type populations were treated with a range of concentrations of 9*c*RA for 7 days to induce differentiation or equivalent volume of EtOH as a control for proliferation. **(A)** Proliferating N-type cells have short neurite-like processes and **(B)** upon differentiation with 1 µM 9*c*RA for 7 days, their neurites become elongated. Treatment with a higher concentration of 9*c*RA also caused elongation of neurite-like processes at **(C)** 2 µM **(D)** 5 µM **(E)** 10 µM **(F)** 20 µM 9*c*RA. Scale bar of phase contrast images represents 50 µm.

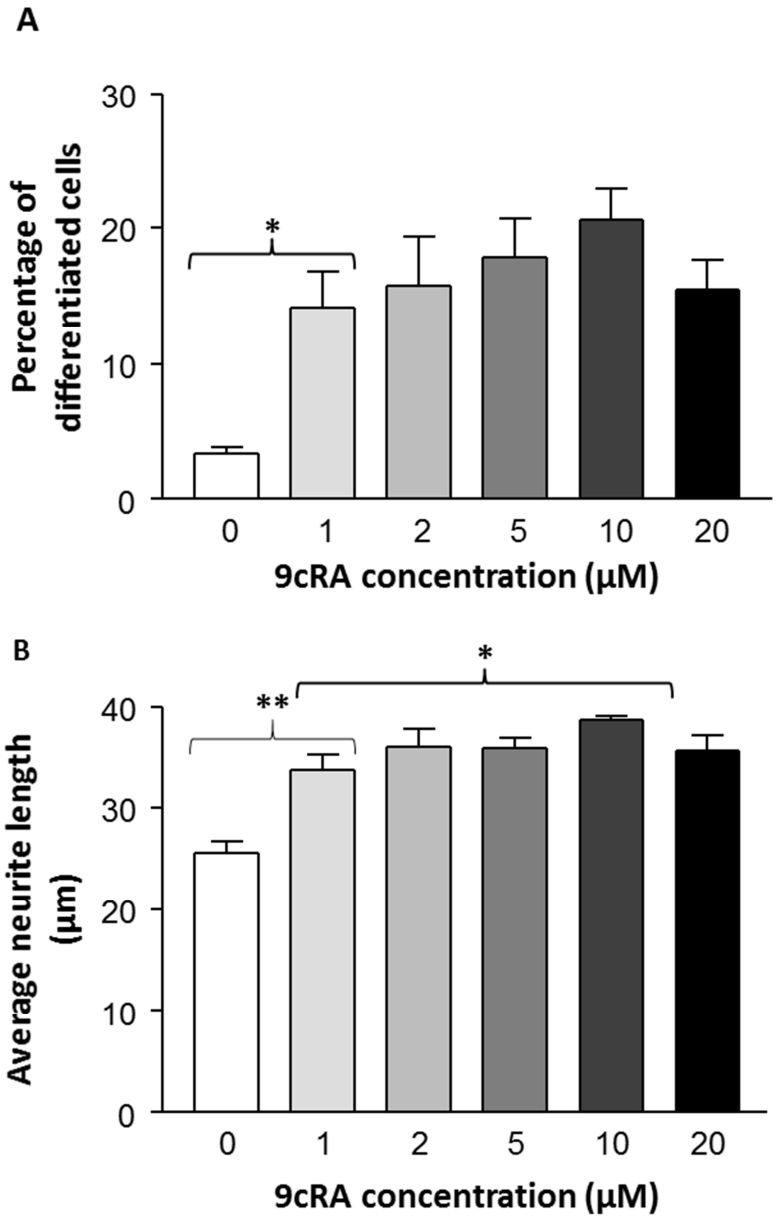

Figure 3.2.2. Treatment of N-type cells with 1 µM 9*c*RA induces maximal phenotypic differentiation

Cells were treated for 7 days with a range of 9*c*RA concentrations to induce differentiation or EtOH as a control for proliferation. Neurite lengths were measured from DIC images using LSM Image Browser. **(A)** Compared to proliferating cells (0 µM 9*c*RA, EtOH treated control), there was a significant increase in the percentage differentiation with 1 µM 9*c*RA treatment (3.30% to 14.17% respectively, P=0.0161*). There was no further significant increase in percentage differentiation when treating N-type cells with concentrations of 9*c*RA above 1 µM (P>0.05). **(B)** Compared to

proliferating cells, average neurite length was significantly increased with 1 µM 9*c*RA treatment (25.59 µm to 33.82 µm respectively, P=0.0063**). There was a further significant increase in neurite length between 1 µm and 10 µM 9*c*RA treatment (from 33.82 µm to 38.71 µm, P=0.0335*). There was no significant difference in neurite length between cells treated with 1 µm and 2 µm, 5 µm or 20 µm 9*c*RA (P>0.05). 0 µm n=3844, 1 µm n=2085, 2 µm n=1549, 5 µm n=1557, 10 µm n=1527, 20 µm n=1320. N=3.

3.3. N-type and S-type populations express a neuronal and a non-neuronal marker

The neuronal microtubule protein β-tubulin III has been shown to be expressed in N-type cells whilst the non-neuronal type III intermediate filament protein vimentin has been shown to be expressed in S-type cells (Whitworth 2012; N. Bell 2013). These two markers were used to distinguish between N-type and S-type populations.

β-tubulin III was expressed by proliferating N-type populations and expression was not significantly altered with differentiation (P=0.740, Figure 3.3.1A and B). β-tubulin III was also expressed by proliferating S-type populations and expression was not significantly altered with differentiation (P=0.838, Figure 3.3.1A and B). Proliferating S-types exhibited 35% less expression of β-tubulin III compared to N-type cells, but this was not significant (P=0.159, Figure 3.3.1A and B).

Vimentin was predominantly expressed by both proliferating S-type populations and expression was increased by 85% with differentiation, but this was not significant (0.509, Figure 3.3.1A and C). Vimentin expression was minimal in proliferating N-type populations and was expression was increased by over ~2 fold with differentiation, however this was not significant (P=0.346, Figure 3.3.1A and C). Vimentin expression was over ~7 fold greater in differentiating S-type cells compared to proliferating N-type populations, but this was not significant (P=0.077, Figure 3.3.1C).

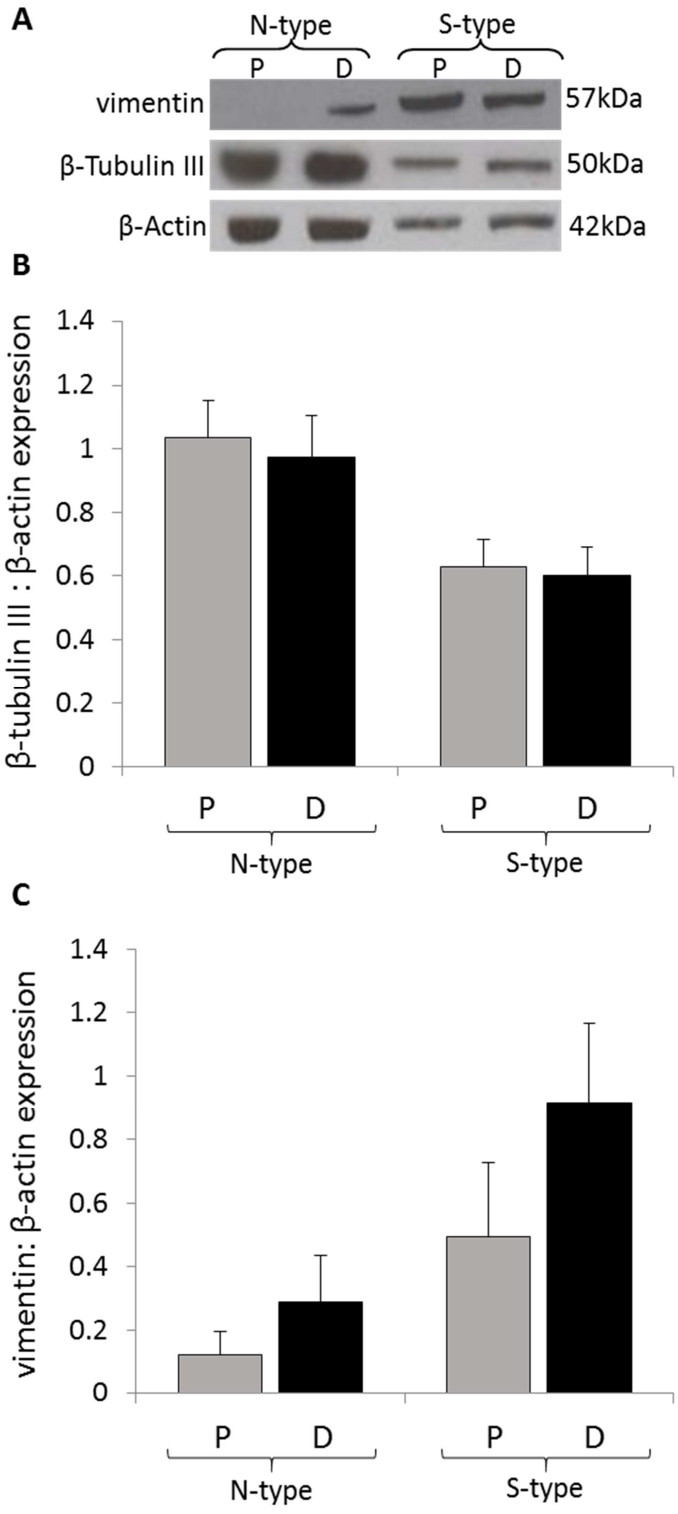

Figure 3.3.1. The expression of β-tubulin III and vimentin are not significantly altered with differentiation

Western blots were performed on protein extracts from SH-SY5Y (N-type) and S-enriched (S-type) cell populations following treatment for 7 days with 1 µM 9cRA (D, differentiating) or equivalent volume of EtOH as a control (P, proliferating). Blots were

probed with anti-β-tubulin III antibody which detected a band at 50 kDa, anti-vimentin antibody which detected a band at 57 kDa and re-probed with anti-β-actin antibody as a loading control which detected a band at 42 kDa. Quantitative band measurements were performed using densitometry in ImageJ. **(A)** β-tubulin III was expressed by both proliferating and differentiating N-type populations and appeared to be expressed to a lesser extent in S-type populations. Vimentin was expressed minimally by proliferating N-type populations with an apparent increase in band intensity with differentiation. Vimentin appeared to be expressed to a greater extent in S-type populations and band intensity similar between proliferating and differentiating S-type populations. **(B)** β-tubulin III expression was expressed as a ratio of β-actin. β-tubulin III expression was not significantly altered with differentiation of N-type populations (P=0.740, N=5) or S-type populations (P=0.838, N=3). Although β-tubulin III expression was 39.34% higher in proliferating N-type compared to proliferating S-type populations, this was not significant (P=0.159). **(C)** Vimentin expression was expressed as a ratio of β-actin. Vimentin expression was >2 fold higher in differentiating N-type compared to proliferating N-type populations, but this was not significant (P=0.346, N=6). Vimentin expression was 84.85% higher in differentiating S-type populations compared to proliferating S-type populations, but this was not significant (P=0.509, N=5). Although vimentin expression was >7 fold higher in S-type compared to N-type populations, this was not significant (P=0.077).

3.4. Bcl-2 expression is a differentiation marker in N-type populations

The anti-apoptotic protein Bcl-2 is known to be up-regulated with differentiation of neuroblastoma cells (Hanada 1993) and has previously been used to determine biochemical differentiation in SH-SY5Y cells (Riddoch 2007; N. Bell 2013). Bcl-2 was therefore used in this study as a biochemical marker of differentiation.

Bcl-2 was expressed in proliferating N-type populations and significantly up-regulated with differentiation ($P=0.0003$, Figure 3.4.1A and B). Compared to N-type populations, Bcl-2 was expressed at significantly lower levels in proliferating S-type populations ($P=0.017$) and expression was non-significantly down-regulated by 34% with S-type population differentiation ($P=0.121$, Figure 3.4.1A and B). This up-regulation of Bcl-2 expression in differentiating N-type cells may correspond with the neuroblastic cells becoming more neuronal-like whilst a down-regulation with S-type population differentiation may imply a shift away from the neuronal phenotype towards a different cell lineage.

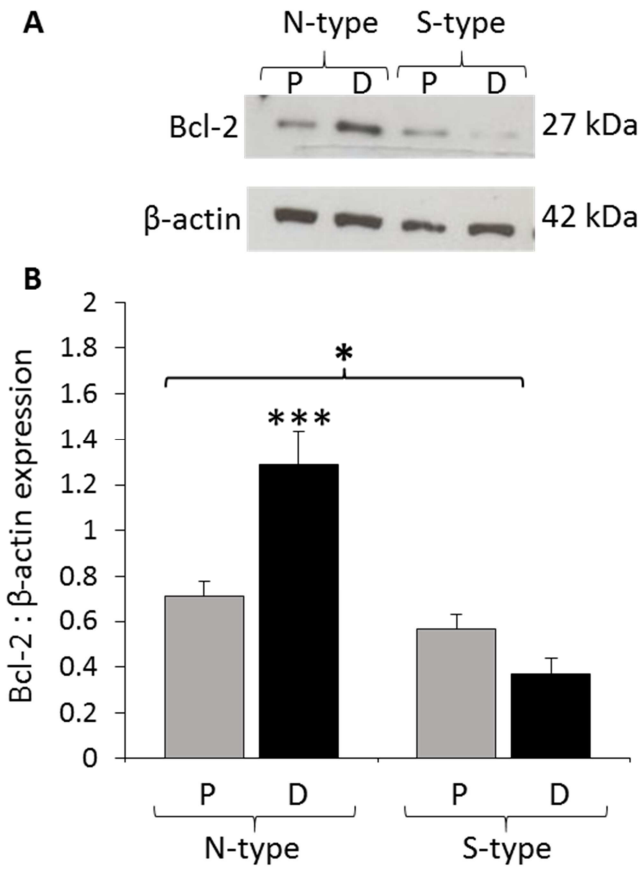

Figure 3.4.1. Bcl-2 expression is altered with differentiation of N-type and S-type populations.

Western blots were performed on protein extracts from SH-SY5Y (N-type) and S-enriched (S-type) cell populations following treatment for 7 days with 1 µM 9cRA (D, differentiating) or equivalent volume of EtOH as a control (P, proliferating). Blots were probed with anti-Bcl-2 antibody which detected a band at 27 kDa and re-probed with anti-β-actin antibody as a loading control which detected a band at 42 kDa. **(A)** Bcl-2 was expressed by both proliferating and differentiating N-type populations and to a lesser extent in S-type populations. With differentiation, there was an increase in band intensity in N-type populations and a decrease in band intensity in S-type populations. **(B)** Quantitative band measurements were performed using densitometry in ImageJ. Bcl-2 expression was expressed as a ratio of β-actin. Bcl-2 expression was significantly lower in proliferating S-type populations compared to proliferating N-type populations (P=0.0166*). There was a significant increase in Bcl-2 expression with differentiation of N-type populations (87%, P=0.0003***, N=14). Bcl-2 expression was non-significantly down-regulated in S-type populations with differentiation (34%, P=0.121, N=13).

3.5. Proliferating and differentiating N- and S-type cells express a stem cell and melanocyte marker

Western blotting and immunofluorescence techniques were used to further characterise N-type and S-type cell populations biochemically and potentially identify the sub-phenotypes within the S-type population. To characterise the cells, the expression of several markers associated with Schwann cells, glial cells and melanocytes were investigated, since they are thought to exist within the S-type population. The expression of a stem cell marker was also studied given that there is heterogeneity in the 9*c*RA-induced differentiation response (Brown 2005).

The neural crest stem cell marker, CD133 (prominin-1) is a cell surface glycoprotein that has been identified as a cancer stem cell marker in a variety of malignancies (Collins 2005; Olempska 2007; Ricci-Vitiani 2007; Yin 2007). CD133 was expressed by both proliferating and differentiating N-type populations and also by S-type populations, though to a generally lesser extent (Figure 3.5.1A and B). This may reflect the tumourigenic nature of N-type cells over S-type cells. There were no significant changes in expression with 9*c*RA-induced differentiation of N- or S-type cells, however it is noteworthy that there was a 40% decrease in CD133 expression in differentiating S-type cells and that this was close to significance (P=0.068, Figure 3.5.1B). CD133 was observed throughout the cytoplasm of N- and S-type cells and there were no significant differences observed in the distribution between proliferating and differentiating N- or S-type cells (Figure 3.5.2).

The micropthalmia-associated transcription factor (MiTF) is a known inducer of melanocyte differentiation (Tachibana 1996; Li 2003; Loercher 2005; Levy 2006) and was investigated in this study given the unclear identity of S-type cells. MiTF was expressed by N-type and, unexpectedly to a lesser extent, S-type populations (Figure 3.5.1A and C). MiTF was observed throughout the cytoplasm of both proliferating and differentiating N- and S-type cells (Figure 3.4.3). Surprisingly, there was no significant effect of differentiation on MiTF expression (Figure 3.5.2C) or distribution (Figure 3.5.3).

There was no expression detected of two glial cell markers; the intermediate filament protein, GFAP and the neural crest transcription factor, SOX10, observed in either N- or S-type populations (data not shown). These proteins are normally expressed in precursor glial cells however there is the possibility that N- and S-type cells perhaps may be too immature for these proteins to be expressed.

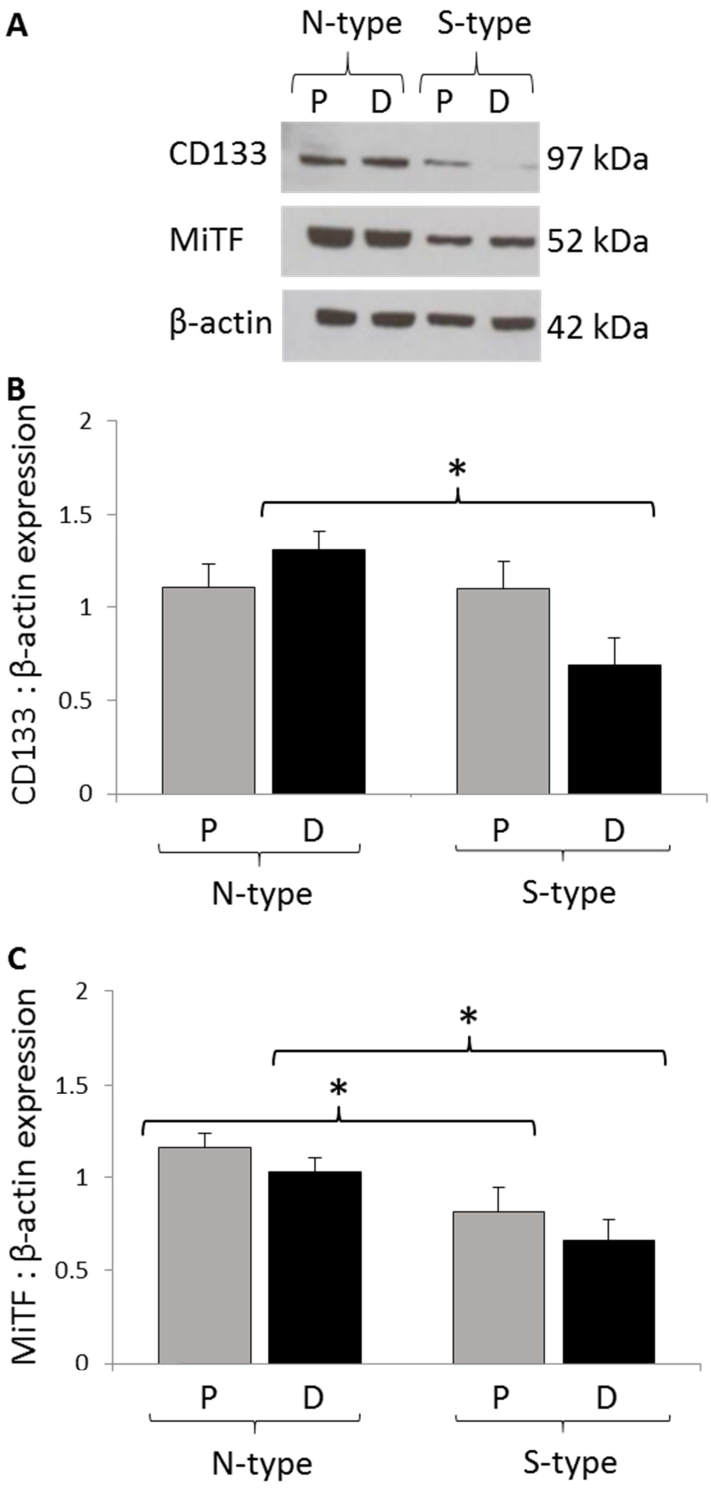

Figure 3.5.1. N-type and S-type populations express a stem cell and melanocyte marker

Western blots were performed on protein extracts from SH-SY5Y (N-type) and S-enriched (S-type) cell populations following treatment for 7 days with 1 µM 9cRA (D, differentiating) or equivalent volume of EtOH control (P, proliferating). **(A)** Blots were

probed with anti-CD133 antibody which detected a band at 97 kDa or anti-MiTF antibody which detected a band at 52 kDa. Blots were re-probed with anti-β-actin antibody as a loading control which detected a band at 42 kDa. The stem cell surface glycoprotein, CD133, and the transcription factor, MiTF were expressed by both proliferating and differentiating N-type and S-type populations. **(B)** There was no change in expression of CD133 in differentiating N-type populations (P=0.237, N=9) and a slight but non-significant decrease by 40% in differentiating S-type populations (P=0.068, N=8). There was no difference in expression of CD133 between proliferating N-type and S-type populations (P=0.673) but CD133 expression was significantly less in differentiating S-type populations compared to differentiating N-type populations (P=0.0478*). (C) There was no significant change in the expression of MiTF between proliferating and differentiating N-type populations (P=0.244, N=9) or S-type populations (P=0.370, N=9). Compared to N-type populations, expression of MiTF was significantly down-regulated by 24% in proliferating (P=0.0342*) and differentiating (P=0.0175*) S-type populations.

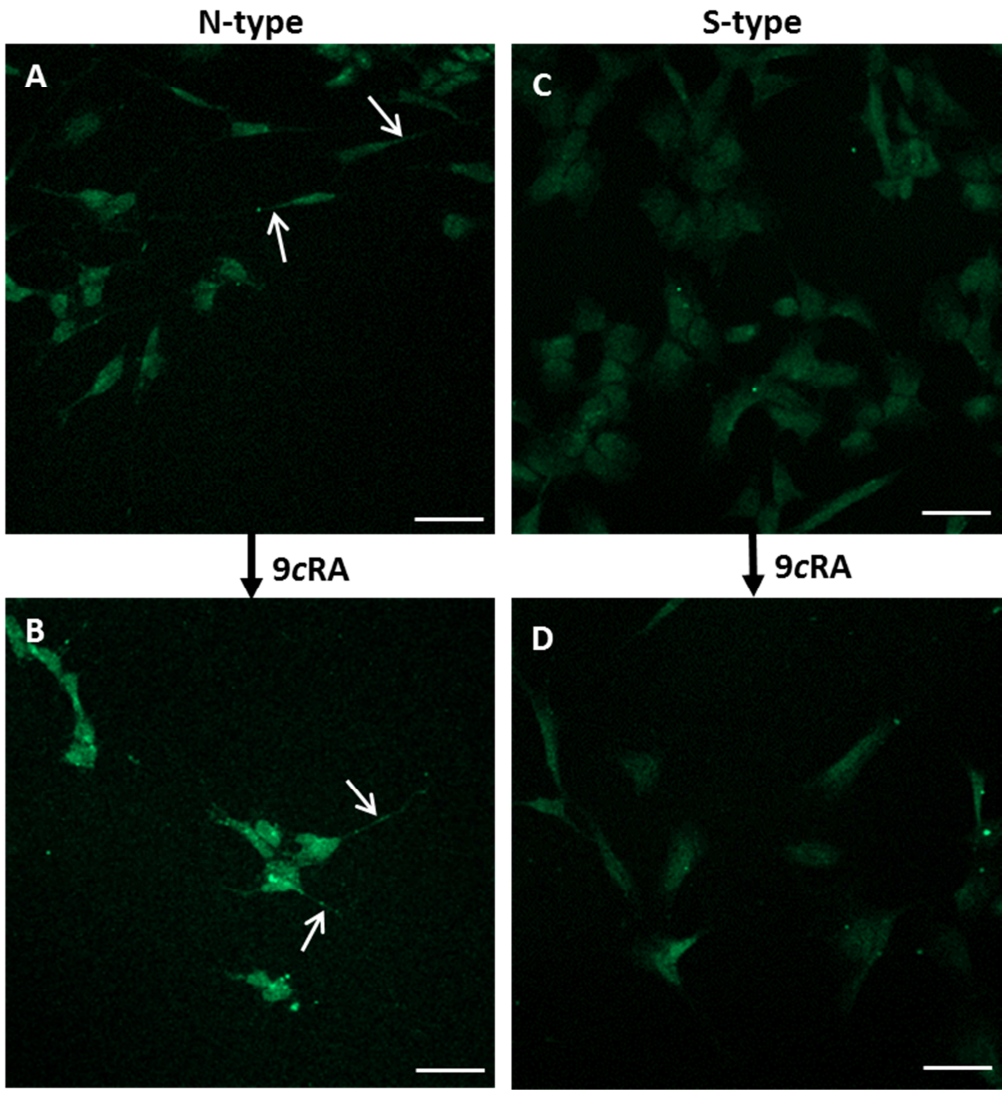

Figure 3.5.2. Proliferating and differentiating N- and S-type cells express CD133 throughout their cytoplasm

Cells were stained with CD133 antibody (green). Images were captured using laser scanning confocal microscopy. **(A)** Proliferating and **(B)** differentiating N-type cell populations stain positively for CD133 throughout their cytoplasm and neurite-like processes (white arrows). **(C)** Proliferating and **(D)** differentiating S-type cell populations stain positively for CD133 throughout their cytoplasm. There was no apparent change in localisation with differentiation of N-type or S-type populations. Scale bars represent 20 µm. Images representative of >20 images. N=2.

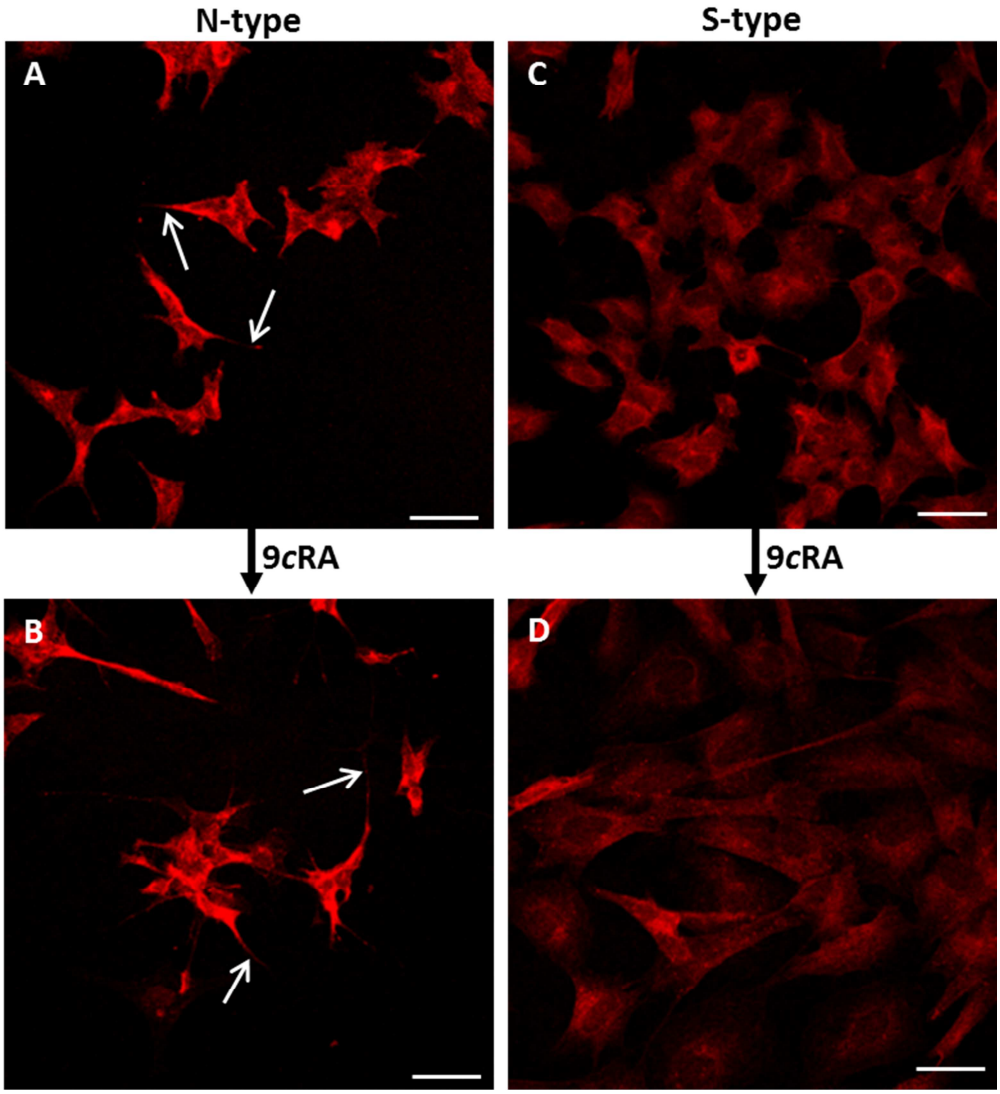

Figure 3.5.3. Proliferating and differentiating N- and S-type cells express MiTF throughout their cytoplasm

Cells were stained with MiTF antibody (red). Images were captured using laser scanning confocal microscopy **(A)** Proliferating and **(B)** differentiating N-type cell populations stain positively for MiTF throughout their cytoplasm and neurite-like processes (white arrows). **(C)** Proliferating and **(D)** differentiating S-type cell populations stain positively for MiTF throughout their cytoplasm. There was no apparent change in localisation with differentiation of N-type or S-type populations. Scale bars represent 20 µm. Images representative of >20 images. N=2.

Chapter 3 - Discussion

Retinoic acid has been used as a treatment alongside standard chemotherapy in neuroblastoma patients with end stage or residual disease (Matthay 2009). However, given the heterogeneity of the disease and cell responses, this treatment is not always effective and survival is poor in these patients (Matthay 2009). The SH-SY5Y neuroblastoma cell line consists of N-type, S-type and I-type cells, which exhibit varying levels of tumourigenicity *in vivo* (Picacentini 1996; Walton 2004) and thereby may possess potential differences in retinoic acid-induced differentiation responses. Determining variations in the differentiation responses between cell phenotypes may help identify sub-populations of cells that are able to evade proliferation-halting therapies and will contribute to our understanding of acquired resistance that may facilitate disease progression. In this chapter, the phenotype-specific differentiation responses of neuroblastoma cells were characterised as a prelude to the phenotype-specific Ca^{2+} signalling studies presented in subsequent chapters.

Treatment of SH-SY5Y (N-type) cell populations and S-enriched (S-type) populations with 1 µM 9*c*RA for 7 days induced both morphological and biochemical differentiation, with N-type cells becoming more neuronal-like and S-type cells becoming more epithelial-like. This is consistent with previous studies, including from this laboratory (Bell *et al.,* 2013), which have shown that N-type cells differentiate towards a neuronal phenotype, (Lovat 1997; Simpson 2001; Brown 2005; Armstrong 2012; Dwane 2013; N. Bell 2013) that express neuronal markers such as β-tubulin III and NF-68 (Messi 2008; N. Bell 2013). In the present study, there was a significant increase in the extent of N-type cell neurite outgrowth and an increase in the percentage of differentiated N-type cells. The percentage of differentiation in 9cRA treated cells (18%) was, however, likely to be underestimated since only cells with fully visible neurites were measured and so neurites with cells that had grown over them will not have been included. There were areas of cells that continued to proliferate and grow in aggregates despite 9*c*RA treatment, which has previously been observed (Brown 2005) even in cells that were treated over a longer time period (N. Bell 2013). This implies that neuroblastoma cells can respond differently to 9*c*RA or even fail to respond altogether. This heterogeneity is a characteristic feature of neuroblastoma cell

lines (Biedler 1973; Ciccarone 1989; Acosta 2009) and of neuroblastoma disease (Valent 1999; Coco 2005), however the underlying reasons are unknown. Heterogeneity in response to retinoic acid treatment may be, at least in part, caused by the heterogeneic nature of neuroblastoma cells, particularly when considering that neuroblastoma cell phenotypes are known to transdifferentiate in culture (Ciccarone 1989; Gaitonde 2001; Cimmino 2015).

This study attempted to define and quantify sub-populations of S-type cells based on their morphology. Although S-type cell populations have been shown to become more flattened with differentiation (Bell et al. 2013) this is the first time, to our knowledge, that morphological changes in sub-populations of S-type cells have been reported. There are three sub-populations of S-type cells that can be distinguished morphologically; S_O, S_A and S_E (Introduction 1.4). The diameter of S_O cells as well as the length of S_E cells were significantly increased with differentiation, demonstrating that these morphological changes can be used as a morphological marker of differentiation in the S-phenotype. S-type cells have previously been shown to differentiate to Schwann cells (Tsokos 1987) and melanocytes (Tsokos 1987; Ciccarone 1989). Non-neuronal neural crest cells such as Schwann and glial cells express the intermediate filament protein vimentin (Ciccarone 1989), which is also expressed by S-type cells (N. Bell 2013), indicating their non-neuronal nature. However, S-type cells also express the neuronal microtubule component β-tubulin III and the neurofilament protein NF-68 (Messi 2008; Acosta 2009; N. Bell 2013) and β-tubulin III expression becomes down-regulated with differentiation of S-type cells (N. Bell 2013). These protein expression profiles indicate that proliferating S-type cells share some biochemical characteristics with immature, neuronal-like N-type cells but commit to a non-neuronal lineage by differentiating away from the neuronal phenotype that is seen with N-type differentiation.

I-type cells are difficult to morphologically distinguish and characterise given that they possess characteristics of both N-type and S-type cells. In differentiating conditions, I-type cell cytoplasm became more abundant and cell margins spread out like that of S-type cells whilst processes became elongated like that of N-type cells. I-type cells are

recognised as a potential multipotent progenitor or cancer stem cell population in neuroblastoma cells that give rise to the neuronal N-type or non-neuronal S-type lineage (Ciccarone 1989; Ross 1995; Walton 2004). They are the most malignant phenotype in culture and *in vivo* (Picacentini 1996; Walton 2004) and retinoic acid resistance has been observed in these cells (Lasorella 1995; Messi 2008). It has also been shown that bidirectional transdifferentiation occurs between N- and S-phenotype (Ross 1983; Ciccarone 1989) and this may come about with the I-type as an intermediate cell type. The I-phenotype may not actually signify a specific cell population and instead reflect a transient morphology of direct N- and S-type interconversion associated with the cell phenotype at a particular point mid-transition. The observation in this study that I-type cells exhibited morphological characteristics of both N-type and S-type cells would be consistent with this notion. At present, the true identity of the putative I-type population is unclear as is the common pathway for spontaneous transdifferentiation, however this may play a role in the heterogeneic nature of the retinoic acid-induced differentiation response.

The neuronal marker β-tubulin III and non-neuronal marker vimentin have previously been used to distinguish N-type and S-type cells, respectively (Whitworth 2012; Bell 2011). Expression of both markers was not altered with differentiation of N-type or S-type populations suggesting that these markers are unable to distinguish between the differentiation state of each cell phenotype.

Bcl-2 is a proto-oncogene and its product, the anti-apoptotic protein Bcl-2, promotes cell survival by preventing mitochondrial cytochrome c release (Zhang *et al*., 1996). Bcl-2 expression has previously been shown to be regulated during differentiation of neuroblastoma cells (Hanada *et al*., 2010) and to directly regulate the differentiation of neural crest cells (Zhang 1996; Liang 2003) and neuronal cells (Middleton 1998; Suzuki 1998). Bcl-2 expression was increased with differentiation of N-type populations, consistent with previous studies in these cells (Lasorella 1995; Riddoch 2007; N. Bell 2013), and was expressed at much lower levels in both proliferating and differentiating S-type populations, as shown in other S-type neuroblastoma cell lines (Hanada 1993). Bcl-2 was slightly down-regulated with differentiation of S-type cells. Hence, Bcl-2 was

used as a biochemical marker of differentiation in this study. Differentiation of neuroblastoma cell lines with phorbol ester also increased Bcl-2 expression (Hanada 1993), indicating that changes in Bcl-2 expression is associated with differentiation rather than as a direct effect of treatment used. It is noteworthy that Bcl-2 up-regulation, which has been observed in differentiated N-type populations and associated with lability of caffeine-sensitive ER Ca^{2+} store depletion (Riddoch 2007), has also been shown to decrease activity of the SERCA pump (Dremina 2004), increase ER membrane Ca^{2+} permeability (Foyouzi-Youssefi 2000), as well as down-regulate SOCE (Pinton 2000; Abeele 2002). This will be discussed in more depth in the next chapter (Discussion 4).

The cell surface glycoprotein CD133 (prominin-1) is a known neuronal and cancer stem cell marker in a variety of malignancies (Collins 2005; Olempska 2007; Ricci-Vitiani 2007; Yin 2007) and has been shown to suppress neuroblastoma differentiation and regulate proliferation (Takenobu 2011). Interestingly, we found a 40% decrease in CD133 expression in differentiating S-type populations. Although marginally non-significant, a down-regulation as S-type cells differentiate towards a lineage specific, mature population would be consistent with a role for CD133 as a possible suppressor of differentiation in this multi-potent precursor cell population. Since there was no change in CD133 expression with differentiation of N-type cell populations, this could correspond to the N-phenotype possessing more tumourigenic characteristics or being closer to the stem cell I-phenotype which, again, may influence the efficacy of retinoic acid.

The micropthalmia-associated transcription factor (MiTF) is known to induce melanocyte differentiation (Tachibana 1996; Li 2003; Loercher 2005; Levy 2006) and we hypothesised that MiTF expression would increase with S-type differentiation since these cells are thought to be melanocyte precursors (Tsokos 1987; Ciccarone 1989). However, MiTF was found to be expressed by both N-type and, to a lesser extent, S-type populations, with no significant effect of differentiation on MiTF expression. This could be explained by MiTF actually consisting of several isoforms, of which only MiTF-M is melanocyte specific (Tachibana 1996; Li 2003). Other isoforms of MiTF could be

down-regulated with differentiation which may obscure a simultaneous up-regulation of MiTF-M expression however at present, there are no readily available MiTF-M specific antibodies to investigate this further.

Using the morphological and biochemical differentiation markers specific to N-type and S-type cells discussed in this chapter, it was possible to investigate phenotype-specific Ca^{2+} signals associated with the differentiation response.

Chapter 4: SOCE in N-type, S-type and I-type cells

Chapter 4 – Introduction

SOCE is the process by which Ca^{2+} enters the cell via plasma membrane SOCs to replenish depleted ER Ca^{2+} stores. SOCE has previously been shown to be down-regulated in differentiating SH-SY5Y and N-type enriched populations (N. Bell 2013; Brown 2005), with no change in differentiating S-type enriched populations (N. Bell 2013). Since SH-SY5Y populations consist predominantly of N-type cells (Introduction) and there was no difference in Ca^{2+} signals or differentiation response of SH-SY5Y populations and N-type enriched populations (Bell 2011), this study has used SH-SY5Y populations to represent N-type populations. SH-SY5Y populations that are S-enriched four times (Methods) consist predominantly of S-type cells (Introduction) and there was no difference in the Ca^{2+} signals or differentiation response of S-type enriched populations enriched between four and up to twelve times (Bell 2011) therefore S4 populations were used to represent S-type populations. N-type and S-type populations were treated for 7 days with 1 µM 9cRA to induce a differentiating phenotype or with an equivalent volume of EtOH as a control for a proliferating phenotype.

Given the heterogeneity in the SH-SY5Y neuroblastoma cell line and the differences in differentiation response between N-type and S-type populations, this chapter aimed to dissect the differentiation-associated phenotype-specific Ca^{2+} signalling responses underlying N-type and S-type population differentiation responses and determine the effect of predominant cell environment on Ca^{2+} signals through establishment and utilisation of live, single cell fura-2 imaging.

All experiments in this chapter were performed on N-type or S-type populations that had been treated for 7 days with 1 µM 9*c*RA (differentiating) or an equivalent volume of EtOH as a control (proliferating). Proliferating N-type and S-type populations will be referred to as P_N and P_S, respectively, whilst differentiating N-type and S-type populations will be referred to as D_N and D_S, respectively. Proliferating and differentiating cell populations were loaded with the Ca^{2+} indicator dye, fura-2/AM, to allow measurements of intracellular Ca^{2+} during Ca^{2+}-addback experiments. Under

Ca^{2+}-free conditions, TG (200 nM) was applied to trigger ER Ca^{2+} store release whilst subsequent $CaCl_2$ (2 mM) 'addback' induced SOCE to replenish depleted Ca^{2+} stores.

Overall Ca^{2+} responses as well as dynamics of the Ca^{2+} responses were also investigated through analysis of trace characteristics. The area under the trace peaks for Ca^{2+} store release and SOCE were used to determine total cytosolic Ca^{2+} entry. Peak height was used to determine maximal cytosolic Ca^{2+} entry. Any changes in Ca^{2+} store release must be taken into account when determining alterations in SOCE activity as Ca^{2+} store release and SOCE are closely related. The response to TG and $CaCl_2$ was calculated as a relative measure of SOCE. The response value from proliferating cells was taken as 100% and the ratio from differentiating cells was determined as a percentage of SOCE activity in proliferating cells. Total rate of rise and decline of Ca^{2+} store release and SOCE were used to determine the speed and efficiency of cytosolic Ca^{2+} entry and deactivation of the response. Given that there were often two phases of SOCE decay, the initial rate of decline from the first 300 seconds following maximal SOCE response and the late rate of decline of the SOCE response following this initial 300 seconds were determined. All measurements were conducted over a similar time-course therefore any changes in rate reflect a change in duration of response.

Chapter 4 - Results

4.1. SOCE is down-regulated in differentiating N-type and S-type populations

Initially, population analysis was utilised to confirm previous findings using the fluorimetry technique (Methods: 2.13). In N-type populations, Ca^{2+}-addback traces of changes in fura-2 fluorescence that were calibrated to show $[Ca^{2+}]_i$ indicated that there was a reduction in SOCE in differentiating compared to proliferating N-type populations (Figure 4.1.1A). There was a 49% increase in $Ca^{2=}$ store release in differentiating N-type populations (14.71 ± 1.62 μMs) however, this was non-significant compared to proliferating N-type populations (9.87 ± 1.74 μMs, P=0.148, Figure 4.1.1B). Nevertheless, taking Ca^{2+} store size into account (see Introduction, above), SOCE was reduced by 34% in differentiating N-type populations (Figure 4.1.1B). These results indicate that 9*c*RA-induced differentiation of N-type populations causes an uncoupling of Ca^{2+} release and SOCE, corresponding with previous findings (Brown 2005; Whitworth 2012; N. Bell 2013).

In S-type populations, Ca^{2+}-addback traces indicated an increase in Ca^{2+} store release and a reduction in SOCE in differentiating S-type populations compared to proliferating S-type populations (Figure 4.1.2A). Ca^{2+} store release was significantly up-regulated by 94% in differentiating S-type populations (19.88 ± 4.01 μMs) compared to proliferating S-type populations (10.23 ± 2.04 μMs, P=0.049) and total SOCE was down-regulated by 41% (Figure 4.1.2B). These results indicate that 9cRA-induced differentiation of S-type populations causes an uncoupling of Ca^{2+} release and SOCE and are in contrast to those described previously (N. Bell 2013).

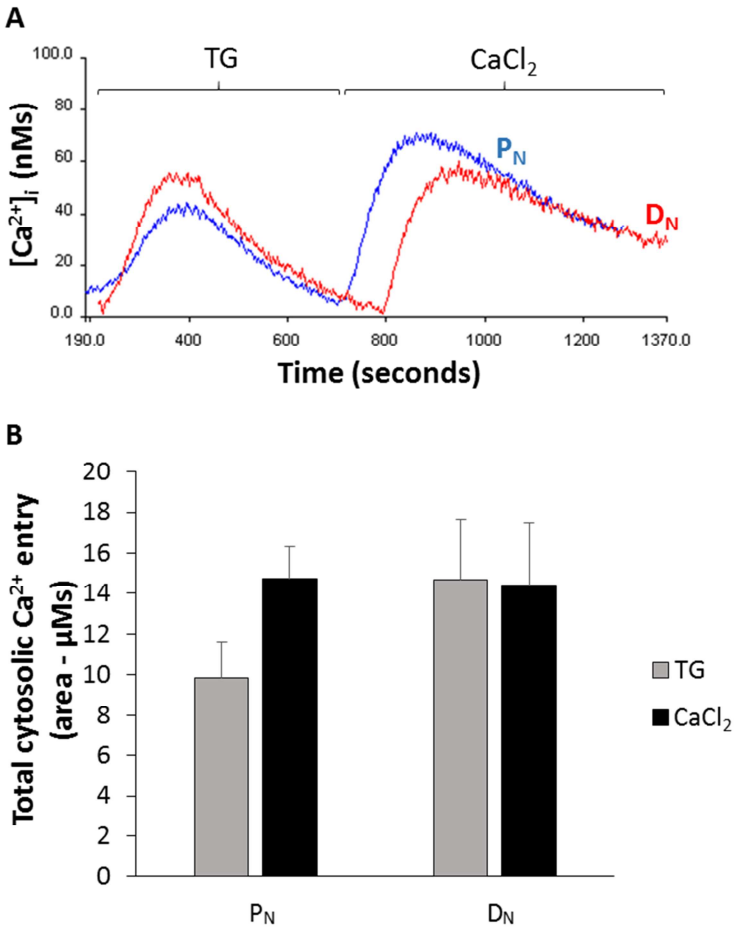

Figure 4.1.1. SOCE is down-regulated in differentiating N-type populations

N-type populations were treated for 7 days with EtOH (P_N, proliferating) or 1 µM 9*c*RA (D_N, differentiating). **(A)** Typical calibrated Ca^{2+}-addback traces from P_N (blue trace) and D_N (red trace) populations. $[Ca^{2+}]_i$ was determined by measuring fura-2 fluorescence at an excitation wavelength of 340 nm and an emission wavelength of 510 nm. Following addition of thapsigargin (TG, first peak) there was increase in $[Ca^{2+}]_i$ in P_N and D_N populations indicating Ca^{2+} store release. Subsequent Ca^{2+} addback ($CaCl_2$, second peak) caused an increase in $[Ca^{2+}]_i$ in P_N and D_N populations, indicating SOCE to replenish depleted stores. **(B)** The Grynkiewicz formula was used to calibrate fluorimetry measurements using Perkin Elmer WinLab software and DMSO (TG control) measurements were deducted from the experimental data. Total Ca^{2+} store release was increased by 49.04% in D_N populations compared to P_N populations (14.71 ± 1.62 µMs and 9.87 ± 1.74 µMs, respectively, P=0.148). Taking into account the increase in store release, total SOCE was down-regulated by 34.36% in D_N populations compared to P_N populations. N=12.

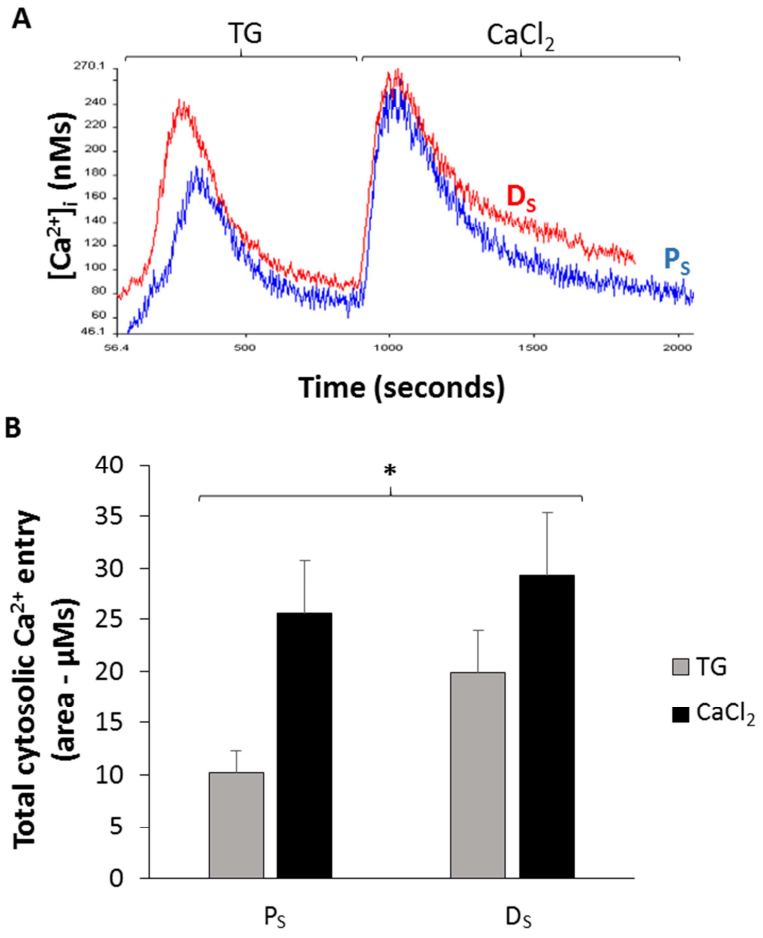

Figure 4.1.2 SOCE is down-regulated in differentiating S-type populations

S-type populations were treated for 7 days with EtOH (P_S, proliferating) or 1 µM 9cRA (D_S, differentiating). **(A)** Typical calibrated Ca^{2+}-addback traces from P_S (blue trace) and D_S (red trace) populations. $[Ca^{2+}]_i$ was determined by measuring fura-2 fluorescence at an excitation wavelength of 340 nm and an emission wavelength of 510 nm. Following addition of thapsigargin (TG, first peak) there was increase in $[Ca^{2+}]_i$ in P_S and D_S populations indicating Ca^{2+} store release. Subsequent Ca^{2+} addback ($CaCl_2$, second peak) caused an increase in $[Ca^{2+}]_i$ in P_S and D_S populations, indicating SOCE to replenish depleted stores. **(B)** The Grynkiewicz formula was used to calibrate fluorimetry measurements using Perkin Elmer WinLab software and DMSO (TG control) measurements were deducted from the experimental data. Total Ca^{2+} store release was increased by 94.33% in D_S populations compared to P_S populations (19.88 ± 4.01 µMs and 10.23 ± 2.04 µMs respectively, P=0.049*). Taking into account the increase in store release, total SOCE was down-regulated by 41.06% in D_S populations compared to P_S populations. N=11.

4.2. Single cell Ca^{2+} signals reflect that obtained using population based data collection

A method for single cell fura-2 imaging acquisition and data analysis has been established and optimised in our laboratory for this study (Methods 2.14 and 2.15). The previous Ca^{2+} add-back method for cell population studies using fluorimetry was adapted and applied to a single cell ratiometric technique using epifluorescence. The ratiometric technique involves use of two excitation wavelengths (340 nm and 380 nm) from which changes in ratio reflects changes in cytosolic Ca^{2+}, whilst reducing error from noise due to uneven cell loading and illumination variations (Methods 2.14 and 2.15). Fluorimetry analyses the cell population as a whole whilst epifluorescence analyses single cells within a cell population. Analysis at the single cell level was used to identify Ca^{2+} signalling changes with the differentiation response specific to N-type, S-type and I-type cells within N-type and S-type predominant populations. This section has investigated single cell fura-2 imaging in single cells and analysis is of the N-type and S-type population as a whole.

In N-type populations, which are SH-SH5Y cells consisting predominantly of N-type cells but with S-type and I-type cells present, Ca^{2+}-addback traces of changes in fura-2 fluorescence ratio indicated that the SOCE response was dampened and of shorter duration in D_N populations compared to P_N populations (Figure 4.2.1A). Total Ca^{2+} store release was slightly reduced in D_N populations relative to P_N populations (54.89 ± 1.22 and 58.73 ± 1.20 FRUs, respectively; P=0.026, Figure 4.2.1B). Taking the change in Ca^{2+} store size into account, total SOCE was reduced by 54% in D_N populations relative to P_N populations (67.02 ± 2.91 and 158.59 ± 5.54 FRUs, respectively, Figure 4.2.1B). These results indicate an uncoupling of Ca^{2+} store release and SOCE in D_N populations with a similar profile to that which was previously found using a fluorimetry-based cell population approach (Figure 4.1.1).

This profile was further confirmed by analysing maximal (as opposed to total) Ca^{2+} store release, using measurements of peak height (Figure 4.2.2A). Maximal Ca^{2+} store release in D_N populations was reduced slightly compared to P_N populations (P=0.001, Figure 4.2.2A), while maximal SOCE was down-regulated by 29% (Figure 4.2.2A).

Additional analysis revealed that there was a 23% decrease in rate of Ca^{2+} store release ($P<0.0001$) and a 15% increase in rate of SOCE ($P<0.0001$) in D_N populations compared to P_N populations (Figure 4.2.2B). There was no significant difference in Ca^{2+} store release decline rate between P_N populations and D_N populations ($P=0.915$, Figure 4.2.2C). The total SOCE decline rate was reduced by 13% in differentiating N-type populations compared to proliferating populations ($P<0.0001$, Figure 4.2.2C). When SOCE decline rate was further analysed, the initial SOCE decline rate was found to increase by 12% in D_N populations compared to P_N populations ($P=0.0006$, Figure 4.2.2C) whereas the late decline rate was reduced by 59% in D_N populations compared to P_N populations ($P<0.0001$, Figure 4.2.2C).

This single cell data not only confirm previous population-based data (Figure 4.2.1; Bell et al 2013) that Ca^{2+} release and SOCE become uncoupled in D_N compared to P_N populations, but extend these findings by showing that the reduction in SOCE in D_N populations is accompanied by increases in the rates at which SOCE is activated and deactivated, leading to a shorter and smaller SOCE response compared to P_N populations.

In S-type populations, consisting of predominantly S-type cells but N-type and I-type cells were also present, Ca^{2+}-addback traces of changes in fura-2 fluorescence ratio indicated that the SOCE response was dampened and of shorter duration in D_S populations relative to P_S populations (Figure 4.2.3A). Total Ca^{2+} store release in D_S populations (47.76 ± 1.19 FRUs) was 26% higher compared to P_S populations (38.05 ± 0.79 FRUs, $P<0.0001$, Figure 4.3.2B). In addition, total SOCE was down-regulated by 66% in D_S compared to P_S populations (54.56 ± 2.87 and 127.73 ± 3.47 FRUs, respectively, Figure 4.2.3B). These results indicate an uncoupling of Ca^{2+} store release and SOCE in D_S populations using single cell analysis with a similar profile to that which was previously found using a fluorimetry-based cell population approach (Figure 4.1.3).

This profile was examined further by analysing maximal (as opposed to total) Ca^{2+} store release, using measurements of peak height (Figure 4.2.4A). Maximal Ca^{2+} store

release in D_S populations was 27% higher compared to P_S populations ($P<0.0001$, Figure 4.2.4A) while maximal SOCE was down-regulated by 59% (Figure 4.2.4A). Additional analysis revealed that there was a 28% increase in rate of Ca^{2+} store release ($P<0.0001$) and a 10% increase in rate of SOCE ($P<0.0001$) in D_S populations compared to P_S populations (Figure 4.2.4.B). There was an 18% increase in Ca^{2+} store release decline rate in D_S compared to P_S populations ($P<0.0001$, Figure 4.2.4C). The total SOCE decline rate was reduced by 9% in D_S compared to P_S populations ($P=0.0017$, Figure 4.2.4C). When SOCE decline rate was further analysed, the initial SOCE decline rate was reduced by 18% in D_S compared to P_S populations ($P<0.0001$, Figure 4.2.4C) and the late decline phase was reduced by 26% in D_S compared to P_S populations ($P<0.0001$, Figure 4.2.4C).

This single cell data not only confirms previous population-based data (Figure 4.1.3) that Ca^{2+} release and SOCE become uncoupled in D_S compared to P_S populations, but extend these findings by showing that the rates at which SOCE is activated seem to be faster than that in P_S populations, whilst the rates of SOCE deactivation appear to be slower. Thus, although the SOCE response in D_S populations is smaller than that in P_S populations, it is maintained for longer. In addition, this single cell data also indicates that differentiation of S-type populations leads to increases in the amount of Ca^{2+} store release and the rate at which the store is depleted. This suggests a potential increase in the size of the ER Ca^{2+} store and/or an increased sensitivity to TG.

In light of the previous analysis, the single cell technique can be used to analyse Ca^{2+} signals related to specific cell types and sub-phenotypes, allowing for potential detection of a sub-population of cells that may exhibit different Ca^{2+} signalling characteristics. Given that both N- and S-type populations consist of three individual cell types; N-type, S-type and I-type, as well as possible S sub-phenotypes; S_O, S_A and S_E, it is unsurprising that there is wide variability in the Ca^{2+} signalling response between individual cells within an experiment. Observing the responses of five cells within one experiment highlights this variability within a particular cell type and potentially could be attributed to specific sub-phenotypes (Figure 4.2.1A and 4.2.3A). Phenotype-specific Ca^{2+} signals were therefore investigated (Results 4.3 and 4.4).

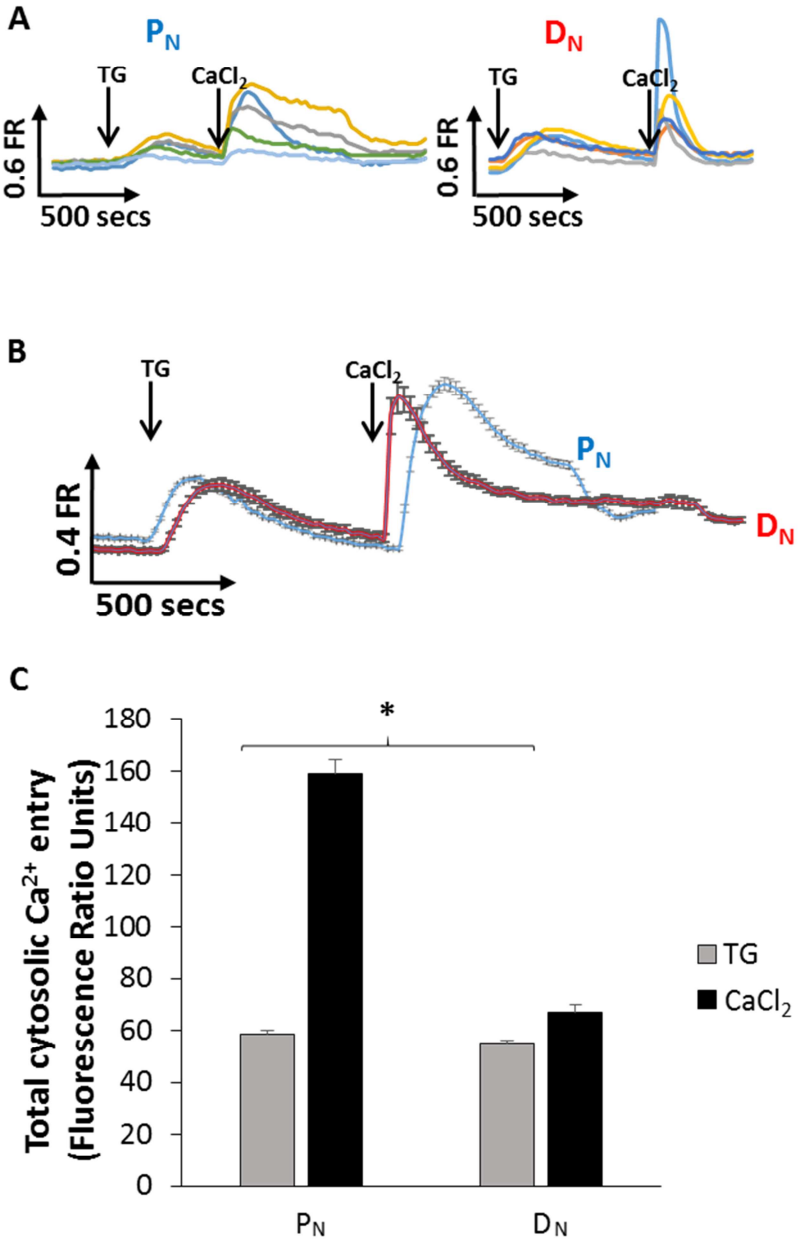

Figure 4.2.1. Single cell Ca^{2+} signals from N-type populations similar to those previously observed using a population analysis technique

N-type populations were treated for 7 days with EtOH (P_N, proliferating) or 1 µM 9*c*RA (D_N, differentiating). TG represents the addition of the SERCA inhibitor thapsigargin to induce Ca^{2+} store release and $CaCl_2$ represents Ca^{2+} addback to induce SOCE. **(A)** Typical Ca^{2+}-addback traces from 5 individual cells within one experiment in P_N (blue) and D_N populations (red) exhibit variability in Ca^{2+} responses. **(B)** Typical average Ca^{2+}-addback traces from P_N (blue trace) and D_N (red trace) populations. Traces represent an average from 20 cells ± S.E.M from one experiment. Fura-2 fluorescence was

measured at excitation wavelengths of 340 nm and 380 nm and an emission wavelength of 510 nm, with changes in fluorescence ratio (FR) reflective of changes in $[Ca^{2+}]_i$. Following addition of thapsigargin (TG, first peak) there was increase in FR in P_N and D_N populations indicating Ca^{2+} store release. Subsequent Ca^{2+}-addback ($CaCl_2$, second peak) caused an increase in FR in P_N and D_N populations, indicating SOCE to replenish depleted stores. The SOCE response was dampened and shorter in D_N cells. **(C)** DMSO (TG control) measurements were deducted from the experimental data. Fluorescence ratio units (FRUs) represent a change in $[Ca^{2+}]_i$. There was a 6.54% decrease in total Ca^{2+} store release in D_N populations compared to P_N populations (54.89 ± 1.22 and 58.73 ± 1.20 FRUs, respectively, P=0.0264*). Taking this change in Ca^{2+} store release into account, total SOCE was down-regulated by 54.79% in D_N populations compared to P_N populations (67.02 ± 2.91 and 158.59 ± 5.54 FRUs, respectively). P_N: n=783, D_N: n=911. N=6.

A

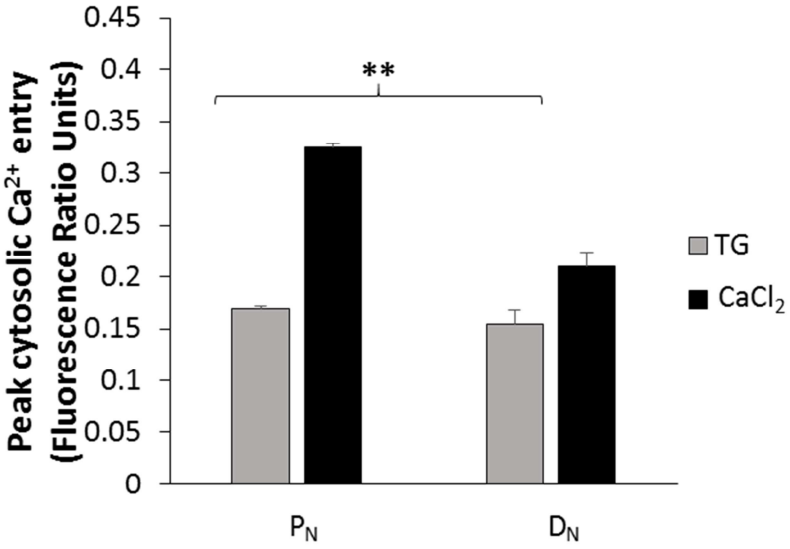

B

	Rate of rise (FRUs x 10^{-4})		
	Proliferating	Differentiating	
TG	13.00 ± 0.26	9.99 ± 0.20	****
$CaCl_2$	49.20 ± 1.90	56.74 ± 1.70	****

C

	Rate of decline (FRUs x 10^{-4})		
	Proliferating	Differentiating	
TG	2.60 ± 0.04	2.59 ± 0.07	
$CaCl_2$ (Total)	3.21 ± 0.06	2.81 ± 0.06	****
$CaCl_2$ (Initial)	6.58 ± 0.18	7.38 ± 0.15	***
$CaCl_2$ (Late)	1.98 ± 0.07	0.81 ± 0.04	****

Figure 4.2.2. There is a change in SOCE dynamics with differentiation of N-type populations

N-type populations were treated for 7 days with EtOH (P_N, proliferating) or 1 µM 9*c*RA (D_N, differentiating). Changes in fluorescence ratio units (FRUs) are reflective of changes in $[Ca^{2+}]_i$ following addition of thapsigargin (TG) indicating Ca^{2+} store release and subsequent Ca^{2+}-addback ($CaCl_2$) indicating SOCE to replenish depleted stores. **(A)** DMSO (TG control) measurements were deducted from the experimental data. There was an 11.76% decrease in maximal Ca^{2+} store release in D_N populations compared to P_N populations (0.15 ± 0.003 and 0.17 ± 0.002 FRUs, respectively, P=0.001**). Taking this change in Ca^{2+} store release into account, maximal SOCE was down-regulated by 29.04% in D_N populations compared to P_N populations (0.21 ± 0.01 and 0.33 ± 0.01 FRUs, respectively). **(B)** There was a 23.15% decrease in rate of Ca^{2+}

store release (P<0.0001****) and a 15.33% increase in rate of SOCE (P<0.0001****) in D_N populations compared to P_N populations. **(C)** There was no change in Ca^{2+} store release decline rate with differentiation of N-type populations (P=0.915). The total SOCE decline rate was reduced by 12.46% in D_N populations (P<0.0001****). The initial SOCE decline rate was increased by 12.14% (P=0.0006***) whilst the later decline phase was reduced by 59.12% (P<0.0001****) in D_N populations. P_N: n=783, D_N: n=911. N=6.

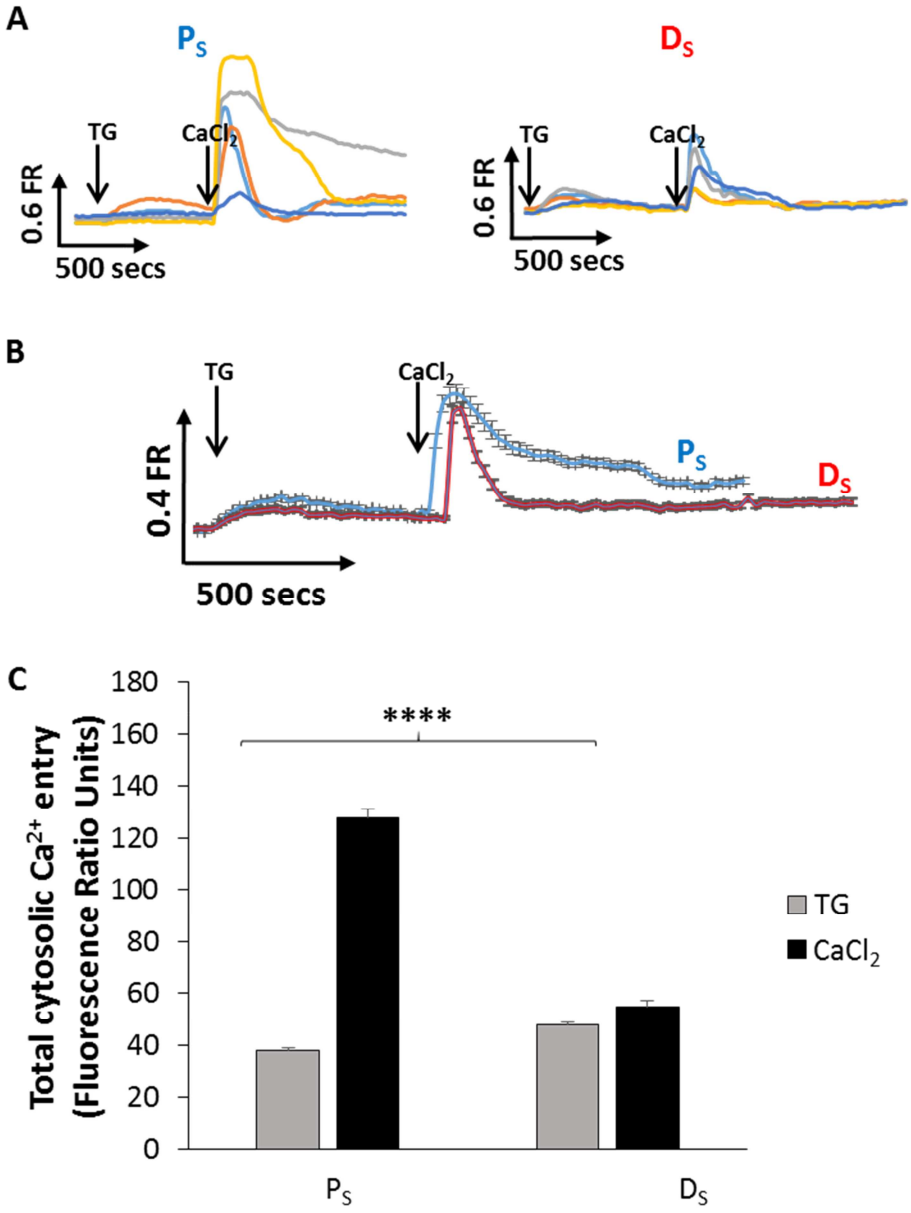

Figure 4.2.3. Single cell analysis of S-type populations exhibit Ca^{2+} signals similar to those previously observed using a population analysis technique

S-type populations were treated for 7 days with EtOH (P_S, proliferating) or 1 µM 9*c*RA (D_S, differentiating). TG represents the addition of the SERCA inhibitor thapsigargin to induce Ca^{2+} store release and $CaCl_2$ represents Ca^{2+} addback to induce SOCE. **(A)** Typical Ca^{2+}-addback traces from 5 individual cells within one experiment in P_S (blue) and D_S populations (red) exhibit variability in Ca^{2+} responses. **(B)** Typical Ca^{2+}-addback traces from P_S (blue trace) and D_S (red trace) populations. Traces represent an average from 20 cells ± S.E.M from one experiment. Fura-2 fluorescence was measured at

excitation wavelengths of 340 nm and 380 nm and an emission wavelength of 510 nm, with changes in fluorescence ratio (FR) reflective of changes in $[Ca^{2+}]_i$. Following addition of thapsigargin (TG, first peak) there was increase in FR in P_S and D_S populations indicating Ca^{2+} store release. Subsequent Ca^{2+}-addback ($CaCl_2$, second peak) caused an increase in FR in P_S and D_S populations, indicating SOCE to replenish depleted stores. The SOCE response was dampened and shorter in D_S cells. **(C)** DMSO (TG control) measurements were deducted from the experimental data. Fluorescence ratio units (FRUs) represent a change in $[Ca^{2+}]_i$. There was a 25.52% increase in total Ca^{2+} store release in D_S populations compared to P_S populations (47.76 ± 1.19 and 38.05 ± 0.79 FRUs, respectively, P<0.0001****). Taking this change in Ca^{2+} store release into account, total SOCE was down-regulated by 65.97% in D_S populations compared to P_S populations (54.56 ± 2.87 and 127.73 ± 3.47 FRUs, respectively). Proliferating n=1092, differentiating n=1002. N=8.

A

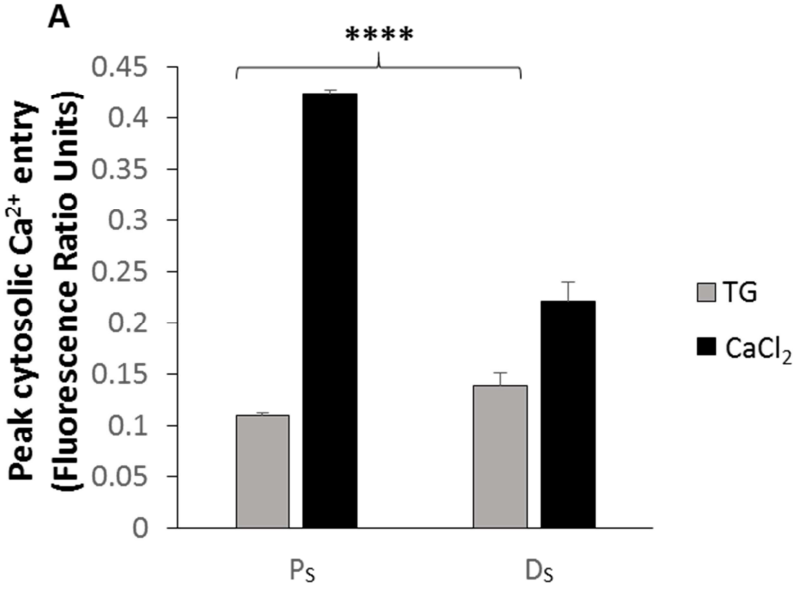

B

	Rate of rise (FRUs x 10^{-4})		
	Proliferating	Differentiating	
TG	9.07 ± 0.23	11.57 ± 0.28	****
$CaCl_2$	89.87 ± 2.44	98.50 ± 3.53	****

C

	Rate of decline (FRUs x 10^{-4})		
	Proliferating	Differentiating	
TG	2.13 ± 0.04	2.52 ± 0.05	****
$CaCl_2$ (Total)	4.38 ± 0.08	3.98 ± 0.10	**
$CaCl_2$ (Initial)	11.72 ± 0.22	9.65 ± 0.23	****
$CaCl_2$ (Late)	0.97 ± 0.05	0.72 ± 0.03	****

Figure 4.2.4. There is a change in SOCE dynamics with differentiation of S-type populations

S-type populations were treated for 7 days with EtOH (P_S, proliferating) or 1 µM 9*c*RA (D_S, differentiating). Changes in fluorescence ratio units (FRUs) are reflective of changes in $[Ca^{2+}]_i$ following addition of thapsigargin (TG) indicating Ca^{2+} store release and subsequent Ca^{2+}-addback ($CaCl_2$) indicating SOCE to replenish depleted stores. **(A)** DMSO (TG control) measurements were deducted from the experimental data. There was a 27.27% increase in maximal Ca^{2+} store release in D_S populations compared to P_S populations (0.14 ± 0.003 and 0.11 ± 0.002 FRUs, respectively, P<0.0001****). Taking this change in Ca^{2+} store release into account, maximal SOCE was down-regulated by 58.58% in D_S populations compared to P_S populations (0.17 ± 0.02 and 0.43 ± 0.03

FRUs, respectively). **(B)** There was a 27.57% increase in rate of Ca^{2+} store release (P<0.0001****) and a 9.61% increase in rate of SOCE (P<0.0001****) in D_S populations compared to P_S populations. **(C)** There was an 18.00% increase in Ca^{2+} store release decline rate with differentiation of S-type populations (P<0.0001****). In D_S populations, there was a reduction in total (by 9.05%, P=0.0017**), initial (by 17.70%, P<0.0001****) and late (by 26.05% P<0.0001****) SOCE decline rates. P_S: n=1092, D_S: n=1002. N=8.

4.3. There is an effect of predominant cell environment on SOCE differentiation responses

Thus far, single cell Ca^{2+} signals have been measured from all cell types within a predominantly N-type environment and in a predominantly S-type environment. Despite establishment of N-type and S-type predominant populations, N-type, S-type and I-type cells were always present (Methods 2.3). This could be reflective of transdifferentiation or a need for all three phenotypes to be present to support growth, for example S-type enrichment has been found to reduce cell growth and result in cell death (Acosta 2009). It may be that it is simply not possible to completely eliminate other phenotypes from the population, particularly given the presence of I-type cells which are thought to represent a stem cell population that may give rise to N-type or S-type cells within an S-type population or N-type population respectively. Changes in phenotype-specific Ca^{2+} signal responses may therefore be influenced by the environment in which the cells are grown (i.e an N-type or S-type predominant environment). One advantage of the single cell technique is that it can be used to analyse Ca^{2+} signals related to specific phenotypes (or sub-phenotypes) within the background environment. The effect of background environment on the Ca^{2+} signal response with differentiation was therefore investigated. The area under the trace peaks for Ca^{2+} store release and SOCE were used to determine total relative Ca^{2+} entry into the cytosol expressed as fluorescence ratio units (FRUs). The results discussed below are summarised in Table 4.3.

4.3.1. Ca^{2+} signals in single cells in an N-type predominant cell environment

For N-type cells grown within N-type populations, total Ca^{2+} store release was reduced by 12% in D_N N-type compared to P_N N-type cells (P=0.0007, Figure 4.3.1) and total SOCE was reduced by 53% (Figure 4.3.1). Consistent with this, there was a 14% decrease in maximal Ca^{2+} store release in D_N N-type compared to P_N N-type cells (P<0.0001, Figure 4.3.2A) and maximal SOCE was down-regulated by 21% (Figure 4.3.2A). There was a 29% decrease in rate of Ca^{2+} store release (P<0.0001) and a 19% increase in rate of SOCE (P=0.0016) in D_N N-type compared to P_N N-type cells (Figure 4.3.2B) with no change in Ca^{2+} store release decline rate (P=0.387, Figure 4.3.2C). The total and late SOCE decline rate were reduced in D_N N-type cells (16% and 66%

respectively, both P<0.0001, Figure 4.3.2C). The initial SOCE decline rate was increased by 20% in D_N N-type cells compared to P_N N-type cells (P<0.0001, Figure 4.3.2C).

These results are consistent with those previously seen with single cell analysis of N-type populations as a whole (Results 4.2) which show that, although Ca^{2+} store release remains unchanged or is slightly reduced, it becomes uncoupled from SOCE. This is unsurprising given that previous measurements were also made in an N-type background which consists of 66% N-type cells (Introduction 1.3).

For S-type cells grown within N-type populations, there was no difference in total Ca^{2+} store release between P_N S-type and D_N S-type cells (P=0.331, Figure 4.3.1) and there was a 60% reduction in total SOCE in D_N S-type compared to P_N S-type cells (P<0.0001, Figure 4.3.1). Consistent with this, there was no difference in maximal Ca^{2+} store release between P_N S-type and D_N S-type cells (P=0.056, Figure 4.3.2A) and maximal SOCE was significantly down-regulated by 55% in D_N S-type compared to P_N S-type cells (P<0.0001, Figure 4.3.2A). There was an 18% decrease in rate of Ca^{2+} store release (P=0.0002) but no change in rate of SOCE (P=0.750) in D_N S-type compared to P_N S-type cells (Figure 4.3.2B). Ca^{2+} store release decline rate and total SOCE decline rate were reduced in D_N S-type compared to P_N S-type cells (14%, P=0.0038 and 16%, P<0.0004, respectively, Figure 4.3.2C). There was no significant difference in the initial SOCE decline rate between P_N S-type and D_N S-type cells (P=0.072) whilst the later decline phase was reduced by 47% (P<0.0001) in D_N S-type cells (Figure 4.3.2C).

Interestingly, these results differ from single cell analysis of the S-type population as a whole (Results 4.2). In D_S populations, Ca^{2+} store release was increased compared to P_S populations (Figures 4.1.3 & 4.2.3), whereas in single S-type cells in an N-type environment, Ca^{2+} store release in is unchanged (Figure 4.3.1). This observation indicates that S-type cells may display a plasticity that can be influenced by the background environment. The reasons underlying this putative plasticity in Ca^{2+} store release are investigated further in Section 4.4. The reduction in SOCE that was seen in D_S populations (Results 4.1 and 4.2) was also present in D_N S-type cells (Figure 4.3.1),

indicating that Ca^{2+} release and SOCE are uncoupled in S-type cells in an N-type environment, as well as in an S-type environment.

For I-type cells grown within N-type populations, total Ca^{2+} store release in D_N I-type cells was 51% greater than that of P_N I-type cells ($P<0.0001$, Figure 4.3.1) and D_N I-type cells had a 63% reduction in total SOCE compared to P_N I-type cells (Figure 4.3.1). Consistent with this, maximal Ca^{2+} store release was increased by 52% in D_N I-type compared to P_N I-type cells ($P<0.0001$, Figure 4.3.2A). Taking this change in Ca^{2+} store release into account, maximal SOCE was down-regulated by 53% in D_N I-type compared to P_N I-type cells (Figure 4.3.2A). There was a 24% increase in rate of Ca^{2+} store release ($P=0.020$) and a 50% increase in rate of SOCE ($P=0.024$) in D_N I-type compared to P_N I-type cells (Figure 4.3.2B). Ca^{2+} store release decline rate and total SOCE decline were significantly increased by 50% and 40% respectively in D_N I-type compared to P_N I-type cells ($P=0.0003$ and $P<0.0007$, respectively, Figure 4.3.2C). The initial SOCE decline rate was increased by 35% in D_N I-type cells compared to P_N I-type cells ($P<0.0001$) but there was no difference in late SOCE decline rate ($P=0.571$, Figure 4.4.2C). These results show that overall Ca^{2+} store release in I-type cells is increased and that rate of activation and emptying is faster in D_N conditions, indicating a potential increase in store size or sensitivity to TG, in contrast to the N-type and S-type cell response. The extent of SOCE down-regulation in D_N I-type cells was greater than that of N-type cells and similar to that of S-type cells in the same environment. The rate of SOCE activation and deactivation was increased with differentiation, suggesting a smaller and shorter SOCE response.

4.3.2. Ca^{2+} signals in single cells in an S-type predominant cell environment

For N-type cells grown within S-type predominant populations, total Ca^{2+} store release in D_S N-type cells was increased by 65% compared to P_S N-type cells ($P<0.0001$, Figure 4.3.3) and total SOCE in D_S N-type cells was reduced by 68% compared to P_S N-type cells (Figure 4.3.3). Consistent with this, there was a 68% increase in maximal Ca^{2+} store release in D_S N-type compared to P_S N-type cells ($P<0.0001$) and maximal SOCE was down-regulated by 62% in D_S N-type compared to P_S N-type cells (Figure 4.3.4A). There was an increase in Ca^{2+} store release rate (66%, $P<0.0001$, Figure 4.3.4B), decline

rate (51%, P<0.0001, Figure 4.3.4C) and rate of SOCE (25%, P=0.0039, Figure 4.3.4B) in D_S N-type compared to P_S N-type cells. There was no difference in total (P=0.122) or initial (P=0.768) SOCE decline rate between P_S N-type and D_S N-type cells, however, the late decline phase was reduced by 27% (P=0.0088) in D_S N-type cells (Figure 4.3.4C).

These results differ from an N-type population and single N-type cells grown in an N-type environment (Results 4.2 and 4.3.1). In an N-type environment, total Ca^{2+} store release was unchanged or slightly reduced with differentiation (Results 4.2, Figure 4.3.1), whereas for N-type cells grown in an S-type environment, total Ca^{2+} store release is significantly increased (Figure 4.3.2). In addition, the Ca^{2+} store has higher rates of activation and emptying in D_S conditions, suggesting an increase in store size or an increased sensitivity to TG. This observation indicated that N-type cells may display a plasticity in Ca^{2+} store release that can be influenced by the background environment. The reduction in SOCE that was seen in D_N N-type cells (Figure 4.3.1) was also present in D_S N-type cells (Figure 4.3.2), indicating that Ca^{2+} release and SOCE are uncoupled in N-type cells in an S-type environment, as well as an N-type environment.

For S-type cells grown within S-type populations, there was no change in total Ca^{2+} store release between P_S S-type and D_S S-type cells (P=0.973, Figure 4.3.3) and a 68% reduction in total SOCE in D_S S-type compared to P_S S-type cells (P<0.0001, Figure 4.3.3). There was no difference in maximal Ca^{2+} store release between P_S S-type and D_S S-type cells (P=0.845, Figure 4.3.4A) and maximal SOCE was significantly down-regulated by 61% in D_S S-type compared to P_S S-type cells (P<0.0001, Figure 4.3.4A). There was no change in rate of Ca^{2+} store release (P=0.456), rate of SOCE (P=0.127) or Ca^{2+} store release decline rate (P=0.502) between D_S S-type and P_S S-type cells (Figure 4.3.4B and C). Total, initial and late SOCE decline rate were reduced by 23% (P<0.0001), 30% (P<0.0001) and 23% (P=0.0086), respectively in D_S S-type cells compared to P_S S-type cells (Figure 4.3.4C).

These results show that Ca^{2+} store release is unaffected in S-type cells within D_S conditions. Interestingly, this result differs from those observed previously in S-type predominant populations, where there was an increase in Ca^{2+} store release in

differentiated cells (Figures 4.1.2 & 4.2.3). This indicates a variability in S-type response that is independent from, but additional to, that caused by background environment (Results 4.3.1). This variability is investigated further in Results 4.4. This also suggests that the N-type cells within the S-type predominant population may be driving the Ca^{2+} store release increase observed at the population level. The reduction in SOCE that was seen in D_N S-type cells (Figure 4.3.1) was also present in D_S S-type cells (Figure 4.3.3), indicating that Ca^{2+} release and SOCE are uncoupled in S-type cells in an S-type environment, as well as in an N-type environment.

For I-type cells grown within S-type populations, there was no difference in total Ca^{2+} store release between to P_S I-type and D_S I-type cells (P=0.568, Figure 4.3.3) and total SOCE was reduced by 61% in D_S I-type compared to P_S I-type cells (P<0.0001, Figure 4.3.3). Consistent with this, there was no difference in maximal Ca^{2+} store release between P_S I-type and D_S I-type cells (P=0.709, Figure 4.3.4A) and maximal SOCE was down-regulated by 47% in D_S I-type compared to P_S I-type cells (P=0.0006, Figure 4.3.4A). There was no change in rate of Ca^{2+} store release (P=0.344) and a 32% increase in rate of SOCE (P=0.027) in D_S I-type cells compared to P_S I-type cells (Figure 4.3.4B). There was no difference Ca^{2+} store release decline rate between P_S I-type cells and D_S I-type cells (P=0.247, Figure 4.3.4C). Total, initial and late SOCE decline rates were reduced by 22% (P=0.0012), 28% (P<0.0001) and 39% (P=0.006), respectively in D_S I-type cells compared to P_S I-type cells (Figure 4.3.4C).

These results differ from I-type cells in an N-type environment. In an N-type environment, total Ca^{2+} store release was significantly increased with differentiation (Figure 4.3.1), whereas in an S-type environment total Ca^{2+} store release is unchanged with differentiation (Figure 4.3.3). This observation indicates that I-type cells may display a plasticity in Ca^{2+} store release that can be influenced by the background environment. The reduction in SOCE that was seen in D_N I-type cells (Figure 4.3.1) was also present in D_S I-type cells (Figure 4.3.3), indicating that Ca^{2+} release and SOCE are uncoupled in I-type cells in an S-type environment, as well as in an N-type environment.

	N-type	S-type	I-type
D_N	Ca^{2+} release: slightly reduced SOCE: decreased	Ca^{2+} release: no change SOCE: decreased	Ca^{2+} release: increased SOCE - decreased
D_S	Ca^{2+} release: increased SOCE: decreased	Ca^{2+} release: no change SOCE: decreased	Ca^{2+} release: no change SOCE: decreased

Table 4.3. Summary of N-type, S-type and I-type single cell Ca^{2+} signals determined by predominant background environment

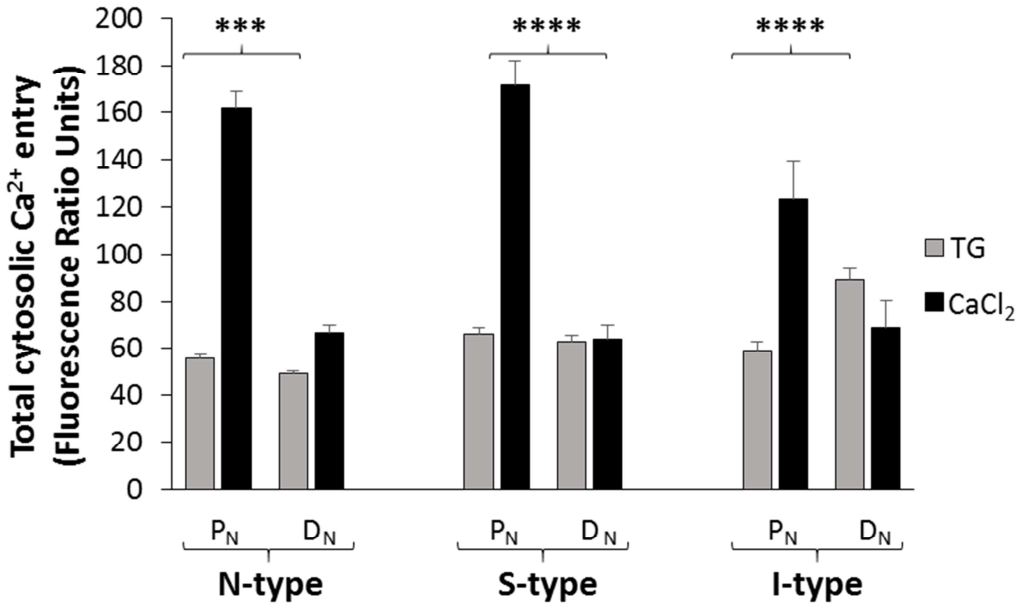

Figure 4.3.1. An uncoupling of Ca^{2+} store release and SOCE occurs with differentiation of N-, S- and I-type cells grown in an N-predominant environment

N-type populations were treated for 7 days with EtOH (P_N, proliferating) or 1 µM 9cRA (D_N, differentiating). Changes in fluorescence ratio units (FRUs) are reflective of changes in $[Ca^{2+}]_i$ following addition of thapsigargin (TG) indicating Ca^{2+} store release and subsequent Ca^{2+}-addback ($CaCl_2$) indicating SOCE to replenish depleted stores. There was a significant down-regulation of total Ca^{2+} store release by 12.10% in D_N N-type cells compared to P_N N-type cells (49.34 ± 1.33 and 56.13 ± 1.49 FRUs, respectively, P=0.0007***). Taking this change in store release into account, total SOCE ($CaCl_2$) was reduced by 53.23% in D_N N-type cells compared to P_N N-type cells (66.56 ± 3.44 and 161.92 ± 7.11 FRUs, respectively). Proliferating n=509, differentiating n=668. Compared to P_N S-type cells, D_N S-type cells showed no change in total Ca^{2+} store release (66.35 ± 2.48 and 62.72 ± 2.80 FRUs, respectively, P=0.331) and a 60.44% reduction in total SOCE (171.50 ± 10.39 and 64.14 ± 5.95 FRUs, respectively, P<0.0001****). P_N S-type n=187, D_N S-type n=163. Compared to P_N I-type cells, D_N I-type cells had a 50.47% increase in total Ca^{2+} store release (59.10 ± 3.73 and 88.93 ± 4.80 FRUs, respectively, P<0.0001****) and a 62.85% reduction in total SOCE (123.17 ± 16.22 and 68.85 ± 11.40 FRUs, respectively). P_N I-type n=72, D_N I-type n=73. N=6.

A

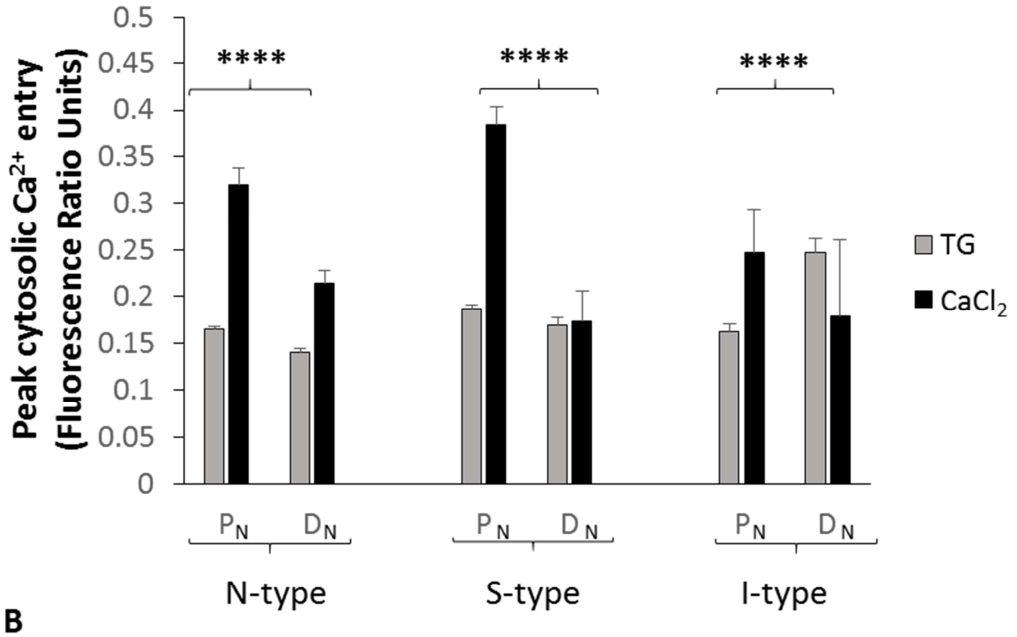

B

	Rate of rise (FRUs x 10^{-4})					
	P_N N-type	D_N N-type	P_N S-type	D_N S-type	P_N I-type	D_N I-type
TG	12.50 ± 0.30	9.00 ± 0.20	14.74 ± 0.50	12.04 ± 0.50	12.07 ± 0.70	14.94 ± 1.00
$CaCl_2$	45.24 ± 1.82	54.00 ± 1.98	59.30 ± 5.10	57.28 ± 3.37	53.08 ± 9.08	79.76 ± 7.45

C

	Rate of decline (FRUs x 10^{-4})					
	P_N N-type	D_N N-type	P_N S-type	D_N S-type	P_N I-type	D_N I-type
TG	2.63 ± 0.05	2.54 ± 0.08	2.62 ± 0.07	2.25 ± 0.11	2.39 ± 0.10	3.59 ± 0.31
$CaCl_2$ (Total)	3.11 ± 0.08	2.60 ± 0.07	3.61 ± 0.11	3.05 ± 0.11	2.97 ± 0.20	4.16 ± 0.28
$CaCl_2$ (Initial)	5.99 ± 0.20	7.16 ± 0.17	7.83 ± 0.39	6.95 ± 0.27	7.56 ± 0.74	10.24 ± 0.80
$CaCl_2$ (Late)	2.07 ± 0.09	0.70 ± 0.04	2.03 ± 0.14	1.08 ± 0.08	1.29 ± 0.16	1.18 ± 0.11

Figure 4.3.2 SOCE dynamics with differentiation of N-, S- and I-type cells grown in an N-predominant environment

N-type populations were treated for 7 days with EtOH (P_N, proliferating) or 1 µM 9*c*RA (D_N, differentiating). Changes in fluorescence ratio units (FRUs) are reflective of changes in $[Ca^{2+}]_i$ following addition of thapsigargin (TG) indicating Ca^{2+} store release and subsequent Ca^{2+}-addback ($CaCl_2$) indicating SOCE to replenish depleted stores. **(A)** DMSO (TG control) measurements were deducted from the experimental data. There was a slight but significant decrease in maximal Ca^{2+} store release in D_N N-type cells (0.14 ± 0.004 FRUs) compared to P_N N-type cells (0.16 ± 0.14 FRUs, P<0.0001****). Taking this change in Ca^{2+} store release into account, maximal SOCE was down-regulated by 21.40% in D_N N-type cells (0.22 ± 0.01 FRUs) compared to P_N N-

type cells (0.32 ± 0.02 FRUs). There was no difference in maximal Ca^{2+} store release between P_N S-type cells (0.19 ± 0.01 FRUs) and D_N S-type cells (0.17 ± 0.01 FRUs, P=0.056) . Maximal SOCE was significantly down-regulated by 54.94% in D_N S-type cells (0.17 ± 0.03 FRUs) compared to P_N S-type cells (0.39 ± 0.02 FRUs, P<0.0001****). Maximal Ca^{2+} store release was significantly increased in D_N I-type cells (0.25 ± 0.02 FRUs) compared to P_N I-type cells (0.16 ± 0.01 FRUs, P<0.0001****). Taking this change in Ca^{2+} store release into account, maximal SOCE was down-regulated by 52.64% in D_N I-type cells (0.18 ± 0.08 FRUs) compared to P_N I-type cells (0.25 ± 0.05 FRUs). **(B)** There was a significant decrease in rate of Ca^{2+} store release (P<0.0001) and a significant increase in rate of SOCE (P=0.0016) in D_N N-type cells compared to P_N N-type cells. There was a significant decrease in rate of Ca^{2+} store release (P=0.0002) but no change in rate of SOCE (P=0.750) in D_N S-type cells compared to P_N S-type cells. There was a significant increase in rate of Ca^{2+} store release (P=0.020*) and a significant increase in rate of SOCE (P=0.024*) in D_N I-type cells compared to P_N I-type cells. **(C)** There was no change in Ca^{2+} store release decline rate between P_N N-type cells and D_N N-type cells (P=0.387). The total SOCE decline rate was significantly reduced in D_N N-type cells (P<0.0001). The initial SOCE decline rate was significantly increased in D_N N-type cells compared to P_N N-type cells (P<0.0001) whilst the later decline phase was significantly reduced (P<0.0001) in D_N N-type cells. Ca^{2+} store release decline rate and total SOCE decline rate were significantly reduced in D_N S-type cells compared to P_N S-type cells (P=0.0038 and P<0.0004, respectively). There was no difference in the initial SOCE decline rate was between P_N S-type cells and D_N S-type cells (P=0.072) whilst the later decline phase was significantly reduced (P<0.0001) in D_N S-type cells. Ca^{2+} store release decline rate and total SOCE decline were significantly increased in D_N I-type cells compared to P_N I-type cells (P=0.0003 and P<0.0007, respectively). The initial SOCE decline rate was significantly increased in D_N I-type cells compared to P_N I-type cells (P<0.0001) but there was no difference in late SOCE decline rate (P=0.571).
In P_N populations: N-type n=509, S-type n=187, I-type n=72.In D_N populations: N-type n=668, S-type n=163, I-type n=73. N=6.

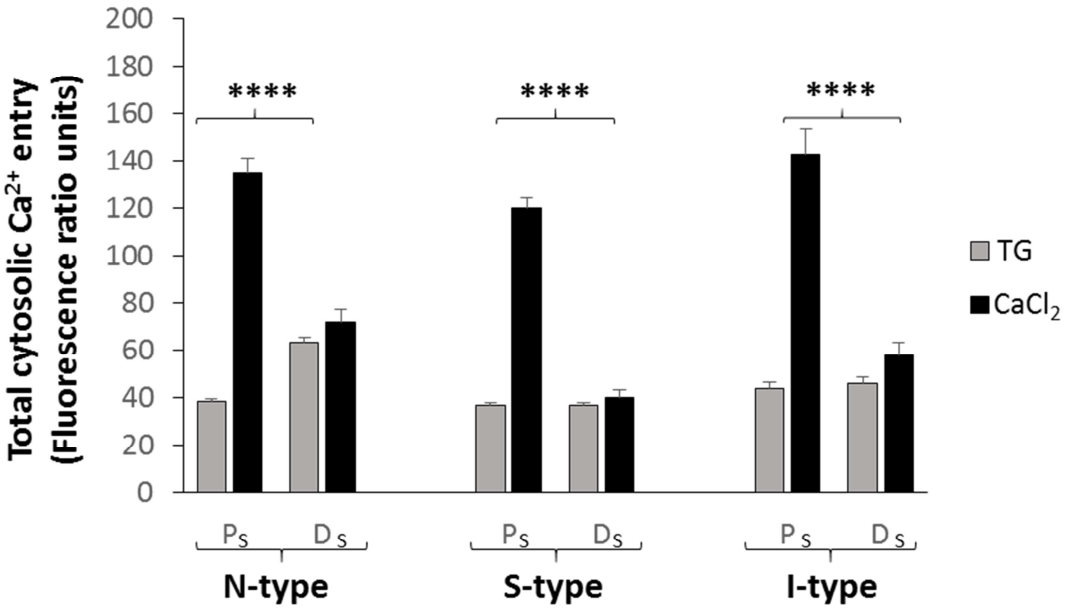

Figure 4.3.3. An uncoupling of Ca^{2+} store release and SOCE occurs with differentiation of N-, S- and I-type cells grown in an S-predominant environment

S-type populations were treated for 7 days with EtOH (P_S, proliferating) or 1 µM 9cRA (D_S, differentiating). Changes in fluorescence ratio units (FRUs) are reflective of changes in $[Ca^{2+}]_i$ following addition of thapsigargin (TG) indicating Ca^{2+} store release and subsequent Ca^{2+}-addback ($CaCl_2$) indicating SOCE to replenish depleted stores. Compared to P_S N-type cells, in D_S N-type cells there was a 65.12% increase in total Ca^{2+} store release (38.31 ± 1.44 and 63.25 ± 2.45 FRUs, respectively, P<0.0001****) and taking this change into account, total SOCE was reduced by 67.54% (134.57 ± 6.56 and 72.12 ± 5.47 FRUs, respectively). P_S N-type cells n=397, D_S N-type cells n=346. Compared to P_S S-type cells, D_S S-type cells showed no change in total Ca^{2+} store release (36.86 ± 0.99 and 36.80 ± 1.30 FRUs, respectively, P=0.973) and a 67.54% reduction in total SOCE (120.28 ± 4.21 and 40.02 ± 3.66 FRUs, respectively, P<0.0001****). P_S S-type cells n=586, D_S S-type cells n=468. Compared to P_S I-type cells, D_S I-type cells showed no change in total Ca^{2+} store release (44.03 ± 2.70 and 46.17 ± 2.37 FRUs, respectively, P=0.568) and total SOCE was reduced by 61.13% (142.47 ± 11.13 and 58.07 ± 5.41 FRUs, respectively, P<0.0001****). P_S I-type cells n=106, D_S I-type cells n=186. N=8.

A

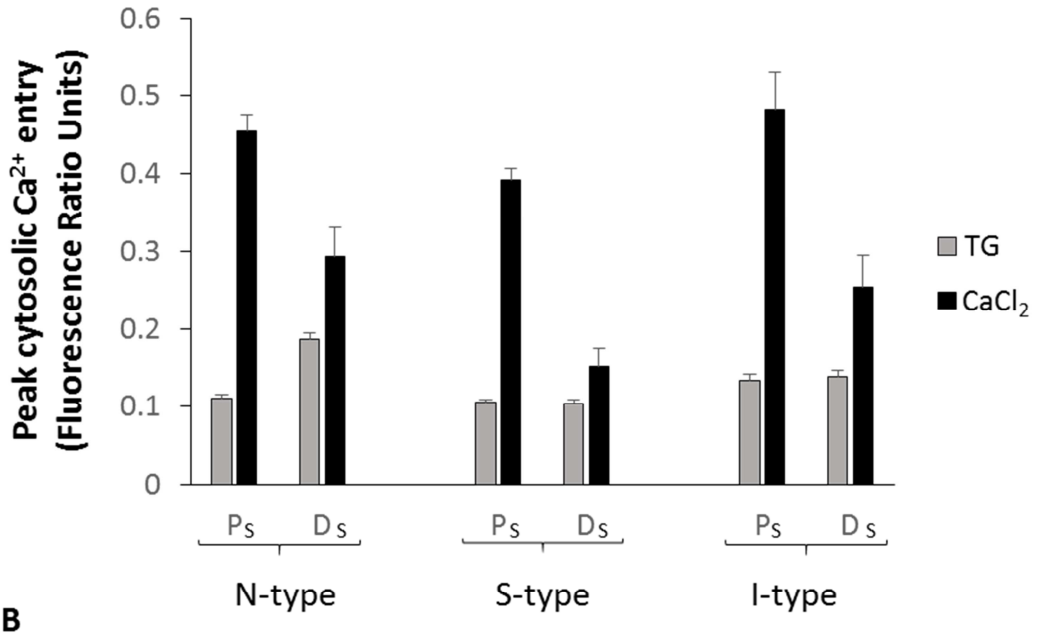

B

	Rate of rise (FRUs x 10^{-4})					
	P_S N-type	**D_S N-type**	**P_S S-type**	**D_S S-type**	**P_S I-type**	**D_S I-type**
TG	9.15 ± 0.38	15.18 ± 0.56	8.87 ± 0.30	9.20 ± 0.32	9.95 ± 0.82	10.85 ± 0.55
$CaCl_2$	92.92 ± 4.52	116.32 ± 6.9	89.42 ± 3.22	81.39 ± 4.29	82.43 ± 5.24	109.04 ± 8.54

C

	Rate of decline (FRUs x 10^{-4})					
	P_S N-type	**D_S N-type**	**P_S S-type**	**D_S S-type**	**P_S I-type**	**D_S I-type**
TG	2.26 ± 0.07	3.42 ± 0.09	1.96 ± 0.06	1.91 ± 0.05	2.62 ± 0.15	2.39 ± 0.13
$CaCl_2$ (Total)	4.88 ± 0.15	5.26 ± 0.20	3.89 ± 0.10	3.01 ± 0.10	5.23 ± 0.27	4.06 ± 0.22
$CaCl_2$ (Initial)	12.35 ± 0.38	12.18 ± 0.45	10.84 ± 0.28	7.54 ± 0.26	14.33 ± 0.79	10.28 ± 0.59
$CaCl_2$ (Late)	1.16 ± 0.10	0.85 ± 0.06	0.82 ± 0.05	0.63 ± 0.04	1.11 ± 0.15	0.67 ± 0.08

Figure 4.3.4 SOCE dynamics with differentiation of N-, S- and I-type cells grown in an N-predominant environment

S-type populations were treated for 7 days with EtOH (P_S, proliferating) or 1 µM 9*c*RA (D_S, differentiating). Changes in fluorescence ratio units (FRU) are reflective of changes in $[Ca^{2+}]_i$ following addition of thapsigargin (TG) indicating Ca^{2+} store release and subsequent Ca^{2+}-addback ($CaCl_2$) indicating SOCE to replenish depleted stores.

(A) DMSO (TG control) measurements were deducted from the experimental data. There was a significant increase in maximal Ca^{2+} store release in D_S N-type cells (0.19 ± 0.008 FRUs) compared to P_S N-type cells (0.11 ± 0.01 FRUs, P<0.0001****). Taking this change in Ca^{2+} store release into account, maximal SOCE was down-regulated by

61.76% in D_S N-type cells (0.29 ± 0.04 FRUs) compared to P_S N-type cells (0.46 ± 0.02 FRUs). There was no difference in maximal Ca^{2+} store release between P_S S-type cells (0.10 ± 0.004 FRUs) and D_S S-type cells (0.11 ± 0.003 FRUs, P=0.845). Maximal SOCE was significantly down-regulated by 61.16% in D_S S-type cells (0.15 ± 0.02 FRUs) compared to P_S S-type cells (0.39 ± 0.01 FRUs, P<0.0001****). There was no difference in maximal Ca^{2+} store release between P_S I-type cells (0.14 ± 0.01 FRUs) and D_S I-type cells (0.13 ± 0.01 FRUs, P=0.709). Maximal SOCE was down-regulated by 47.38% in D_S I-type cells (0.25 ± 0.04 FRUs) compared to P_S I-type cells (0.48 ± 0.05 FRUs, P=0.0006***). **(B)** There was a significant increase in rate of Ca^{2+} store release (P<0.0001) and rate of SOCE (P=0.0039) in D_S N-type cells compared to P_S N-type cells. There was no change in rate of Ca^{2+} store release (P=0.456) or in rate of SOCE (P=0.127) in D_S S-type cells compared to P_S S-type cells. There no change in rate of Ca^{2+} store release (P=0.344) and a significant increase in rate of SOCE (P=0.027) in D_S I-type cells compared to P_S I-type cells. **(C)** There was a significant increase in Ca^{2+} store release decline rate in D_S N-type cells compared to P_S N-type cells (P<0.0001). There was no difference in total SOCE decline rate between P_S N-type cells and D_S N-type cells (P=0.122). There was no difference in the initial SOCE decline rate (P=0.768) however, the late decline phase was significantly reduced (P=0.0088) in D_S N-type cells. There was no difference in Ca^{2+} store release decline rate between P_S S-type cells and D_S S-type cells rate (P=0.502). Total SOCE decline rate was significantly reduced in D_S S-type cells compared to P_S S-type cells (P<0.0001).The initial and late SOCE decline rate was significantly reduced in D_S S-type cells compared to P_S S-type cells (P<0.0001 and P=0.0086, respectively). There was no difference Ca^{2+} store release decline rate between P_S I-type cells and D_S I-type cells (P=0.247). Total SOCE decline was significantly decreased in D_S I-type cells compared to P_S I-type cells (P=0.0012). The initial and late SOCE decline rates were significantly reduced in D_S I-type cells compared to P_S I-type cells (P<0.0001 and P=0.006, respectively). In P_S populations: N-type n=397, S-type n=586, I-type n=106.In D_S populations: N-type n=346, S-type n=468, I-type n=186. N=8.

4.4. Sub-populations of S-type cells exhibit variable SOCE responses in N-type and S-type predominant environments

The S-phenotype is comprised of three sub-populations; S_O, S_A and S_E (Introduction 1.4). The overall S-type Ca^{2+} signalling response may therefore be influenced by sub-population-specific Ca^{2+} signals. Since Ca^{2+} signals can be influenced by background environment (section 4.3), sub-population Ca^{2+} signals may in turn also be influenced by the environment in which the cells are grown (i.e an N-type or S-type predominant environment). We investigated whether sub-population-specific Ca^{2+} signals and background environment could play a role in the responses of S-type cells, including the observed variability (Figure 4.2.3A).

4.4.1. Ca^{2+} signals in S_O, S_A and S_E cells in an N-type predominant cell environment

In N-type predominant populations, total Ca^{2+} store release was increased by 17% in D_N S_O compared to P_N S_O cells (P=0.034) and total SOCE was reduced by 66% (Figure 4.4.1). There was no difference in maximal Ca^{2+} store release in D_N S_O compared to P_N S_O cells (P=0.375), whilst maximal SOCE was down-regulated by 55% in D_N S_O compared to P_N S_O cells (P<0.0001, Figure 4.4.2A). There was no difference in rate of Ca^{2+} store release (P=0.217), rate of SOCE (P=0.132), total (P=0.426) or initial (P=0.709) SOCE decline rate between P_N S_O and D_N S_O cells (Figure 4.4.2A and B). There was a decrease in Ca^{2+} store release decline rate (by 12%, P=0.031) and late SOCE decline rate (by 34%, P=0.0089) in D_N S_O compared to P_N S_O cells (Figure 4.4.2C). These results show for S_O cells, Ca^{2+} store release was increased and there was a slower rate of store emptying in D_N conditions suggesting a prolonged store release and possible increase in store size or TG sensitivity. SOCE was down-regulated in D_N conditions however the rate of activation and de-activation and were unaffected except a reduced late SOCE decline phase, therefore response duration was shortened.

D_N S_A cells had a 22% decrease in total Ca^{2+} store release compared to P_N S_A cells (P=0.015) and total SOCE was reduced by 53% (Figure 4.4.1). Consistent with this, there was a 21% decrease in maximal Ca^{2+} store release in D_N S_A compared to P_N S_A cells (P=0.003) and maximal SOCE was down-regulated by 39% (Figure 4.4.2A). There was a 26% decrease in rate of Ca^{2+} store release (P=0.0005) but no difference in rate of

SOCE (P=0.735) in D_N S_A compared to P_N S_A cells (Figure 4.4.2B). There was a reduction in Ca^{2+} store release decline rate (by 16%, P=0.041), total SOCE decline rate (by 17%, P<0.049) and late SOCE decline rate (by 55%, P<0.0001) in D_N S_A cells compared to P_N S_A cells (Figure 4.4.2C). There was no difference in initial SOCE decline rate between P_N S_A cells and D_N S_A cells (P=0.540, Figure 4.4.2C). Overall, D_N S_A cells have reduced Ca^{2+} store release with reduced rate of store release and emptying, indicating a reduced store size or decrease in TG sensitivity with differentiation. SOCE was down-regulated in D_N S_A cells to a greater extent than D_N S_O cells and, whilst the rate of SOCE activation and early de-activation was unaffected, late SOCE decline rate was reduced, suggesting a shortened SOCE response.

Compared to P_N S_E cells, D_N S_E cells had a 42% reduction in total Ca^{2+} store release (P=0.064) and total SOCE was reduced by 61% (Figure 4.4.1). There was no difference in maximal Ca^{2+} store release between P_N S_E compared to D_N S_E cells (P=0.212) and maximal SOCE was down-regulated by 73% in D_N S_E compared to P_N S_E cells (P=0.005, Figure 4.4.2A). There was no difference in rate of Ca^{2+} store release (P=0.129) or rate of SOCE (P=0.176) in P_N S_E compared to D_N S_E cells (Figure 4.4.2B). There was no difference in Ca^{2+} store release decline rate between P_N S_E and D_N S_E cells (P=0.681) and there was a reduction in total SOCE decline rate (by 52%, P=0.0021), initial (by 42%, P=0.046) and late (by 70%, P<0.0001) SOCE decline rate in D_N S_E compared to P_N S_E cells (Figure 4.4.2C). Taken together, these results show that, whilst Ca^{2+} store release was reduced in D_N S_E cells, indicating a reduction of store size, there was no change in speed of activation or store emptying. SOCE was down-regulated in D_N S_E cells and, whilst there no change in rate of activation, de-activation rate was reduced which indicates a smaller but longer SOCE response.

All of this data confirms that S_O, S_A and S_E cells can be identified by sub-population specific Ca^{2+} signals (Table 4.4).

4.4.2. Ca^{2+} signals in S_O, S_A and S_E cells in an S-type predominant cell environment

In S-type predominant populations, compared to P_S S_O cells, there was no change in total Ca^{2+} store release in D_S S_O cells (P=0.092) and total SOCE was reduced by 64%

(P<0.0001, Figure 4.4.3). Consistent with this, maximal Ca^{2+} store release was reduced by 15% in D_S S_O compared to P_S S_O cells (P=0.025) and maximal SOCE was down-regulated by 53% in D_S S_O compared to P_S S_O cells (Figure 4.4.4A). There was a decrease in rate of Ca^{2+} store release (14%, P=0.042) and rate of SOCE (24% P=0.0018) in D_S S_O compared to P_S S_O cells (Figure 4.4.4B). There was a 21% decrease in Ca^{2+} store release decline rate in D_S S_O compared to P_S S_O cells (P<0.0001) and a reduction in total and initial SOCE decline rate in D_S S_O compared to P_S S_O cells (by 37.02% and 48.42% respectively, both P<0.0001, Figure 4.4.4C). There was no difference in late SOCE decline rate between P_S S_O and D_S S_O cells (P=0.560, Figure 4.4.4C). This unchanged Ca^{2+} release response of S_O cells in D_S conditions differs from that seen in D_N conditions, where total Ca^{2+} store release was increased (Figure 4.4.1). In addition, the rate of Ca^{2+} release was reduced in D_S conditions, perhaps suggesting a reduced sensitivity to TG. The reduction in SOCE that was seen in D_N conditions (Figure 4.4.1) was also present in D_S conditions, though it was a shortened response (Figure 4.4.4) indicating that Ca^{2+} release and SOCE are uncoupled in S_O cells in an S-type environment, as well as in an N-type environment.

Compared to P_S S_A cells, there was no change in total Ca^{2+} store release in D_S S_A compared to P_S S_A cells (P=0.087) and total SOCE was reduced by 73% (P<0.0001, Figure 4.4.3). Consistent with this, there was no difference in maximal Ca^{2+} store release between P_S S_A and D_S S_A cells (P=0.097) and maximal SOCE was down-regulated by 71% in D_S S_A compared to P_S S_A cells (P<0.0001, Figure 4.4.4A). There was a 27% increase in rate of Ca^{2+} store release (P=0.0009) but no difference in rate of SOCE (P=0.274) between D_S S_A and P_S S_A cells (Figure 4.4.4B). Ca^{2+} store release decline rate was increased by 17% in D_S S_A compared to P_S S_A cells (P=0.061) whilst there was no difference in the total SOCE decline rate between P_S S_A and D_S S_A cells (P=0.329, Figure 4.4.4C). The initial and late SOCE decline rates were both reduced (by 11.60%, P=0.061 and 22.31%, P=0.098, respectively) in D_S S_A cells compared to P_S S_A cells (Figure 4.4.4C). The unchanged Ca^{2+} release response of S_A cells in D_S conditions differs from that seen in D_N conditions, where total Ca^{2+} store release was decreased (Figure 4.4.1). In addition, the rate of Ca^{2+} release was reduced in D_S conditions. The reduction in SOCE that was seen in D_N conditions (Figure 4.4.1) was also present in D_S conditions, though

it was a shorter response (Figure 4.4.4), indicating that Ca^{2+} release and SOCE are uncoupled in S_O cells in an S-type environment, as well as in an N-type environment.

Compared to P_S S_E cells, there was no change in total Ca^{2+} store release in D_S S_E cells (P=0.663) and total SOCE was reduced by 65% (P<0.0001, Figure 4.4.3). There was no difference in maximal Ca^{2+} store release between P_S S_E compared to D_S S_E cells (P=0.908) and maximal SOCE was down-regulated by 51% in D_S compared to P_S S_E cells (P=0.00016, Figure 4.4.4A). There was no significant difference in rate of Ca^{2+} store release (P=0.369) between P_S S_E and D_S S_E cells but there was a 31% decrease in rate of SOCE in D_S S_E compared to P_S S_E cells (P=0.086 Figure 4.4.3B). There was no difference in Ca^{2+} store release decline rate between P_S S_E and D_S S_E cells (P=0.447) however, compared to P_S S_E cells, D_S S_E cells had significantly reduced total SOCE decline rate (by 41.30%, P=0.0003), initial SOCE decline rate (by 34.02%, P=0.0049) and late SOCE decline rate (by 60.80%, P=0.0011, Figure 4.4.4C). The unchanged Ca^{2+} release response of S_E cells in D_S conditions differs from that seen in D_N conditions, where total Ca^{2+} store release was decreased (Figure 4.4.1). The reduction in SOCE that was seen in D_N conditions (Figure 4.4.1) was also present in D_S conditions, though it was a smaller, slower and extended response (Figure 4.4.4). This indicates that Ca^{2+} release and SOCE are uncoupled in S_O cells in an S-type environment, as well as in an N-type environment.

All of this data confirms that sub-population-specific Ca^{2+} signals in S_O, S_A and S_E cells can each be influenced by background cell environment (Table 4.4).

	S_O	S_A	S_E
D_N	Ca_{2+} release: increased SOCE: decreased	Ca^{2+} release: decreased SOCE: decreased	Ca^{2+} release: decreased SOCE: decreased
D_S	Ca^{2+} release: no change SOCE: decreased	Ca^{2+} release: no change SOCE: decreased	Ca^{2+} release: no change SOCE: decreased

Table 4.4. Summary of S_O, S_A and S_E single cell Ca^{2+} signals determined by predominant background environment

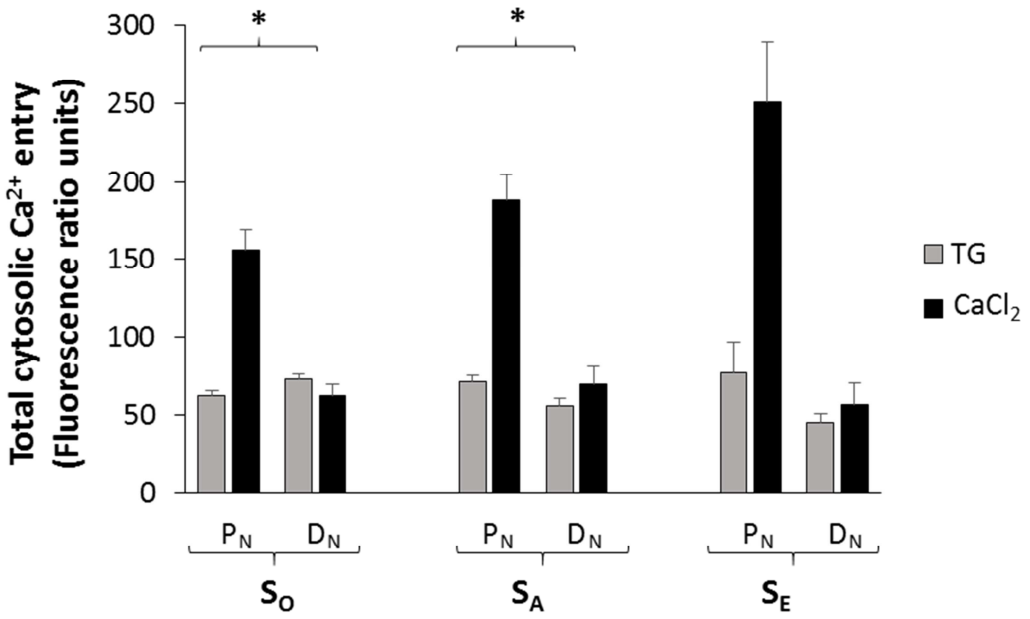

Figure 4.4.1. An uncoupling of Ca^{2+} store release and SOCE occurs with differentiation of S_O, S_A and S_E cells grown in an N-type predominant environment

N-type populations were treated for 7 days with EtOH (P_N, proliferating) or 1 µM 9cRA (D_N, differentiating). Changes in fluorescence ratio units (FRUs) are reflective of changes in $[Ca^{2+}]_i$ following addition of thapsigargin (TG) indicating Ca^{2+} store release and subsequent Ca^{2+}-addback ($CaCl_2$) indicating SOCE to replenish depleted stores. Compared to P_N S_O cells, D_N S_O cells had a 16.58% increase in total Ca^{2+} store release (62.42 ± 3.08 and 72.77 ± 3.80 FRUs, respectively, P=0.034*) and, taking this change into account, total SOCE was reduced by 65.70% (155.80 ± 13.64 and 62.29 ± 7.77 FRUs, respectively). Compared to P_N S_A cells, D_N S_A cells had a 21.77% decrease in total Ca^{2+} store release (71.46 ± 4.15 and 55.91 ± 4.73 FRUs, respectively, P=0.015*) and total SOCE was reduced by 52.93% (188.28 ± 16.36 and 69.33 ± 11.79 FRUs, respectively). Compared to P_N S_E cells, D_N S_E cells had a 42.17% reduction in total Ca^{2+} store release (77.10 ± 20.02 and 44.58 ± 6.07 FRUs, respectively, P=0.064) and total SOCE was reduced by 61.38% (251.18 ± 38.17 and 56.09 ± 14.06 FRUs, respectively). P_N: S_O n=108, S_A n=75, S_E n=4. D_N: S_O n=82, S_A n=57, S_E n=24. N=6.

A

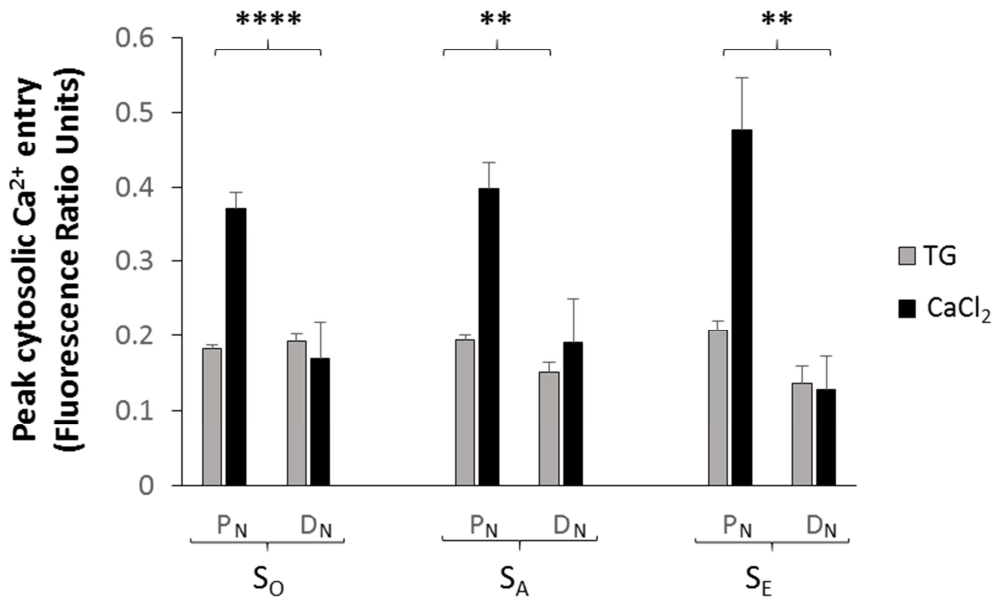

B

	Rate of rise (FRUs x 10^{-4})					
	$P_N S_O$	$D_N S_O$	$P_N S_A$	$D_N S_A$	$P_N S_E$	$D_N S_E$
TG	14.30 ± 0.70	13.07 ± 0.70	15.26 ± 0.70	11.29 ± 0.80	16.80 ± 0.90	10.31 ± 1.70
$CaCl_2$	53.11 ± 2.25	60.17 ± 4.47	68.66 ± 12.30	63.49 ± 6.51	50.71 ± 4.91	32.65 ± 5.17

C

	Rate of decline (FRUs x 10^{-4})					
	$P_N S_O$	$D_N S_O$	$P_N S_A$	$D_N S_A$	$P_N S_E$	$D_N S_E$
TG	2.61 ± 0.09	2.29 ± 0.12	2.64 ± 0.11	2.21 ± 0.19	2.66 ± 0.46	2.26 ± 0.38
$CaCl_2$ (Total)	3.54 ± 0.11	3.40 ± 0.14	3.72 ± 0.22	3.10 ± 0.21	3.69 ± 0.33	1.77 ± 0.22
$CaCl_2$ (Initial)	8.02 ± 0.50	7.78 ± 0.33	7.62 ± 0.67	7.08 ± 0.49	6.58 ± 1.76	3.83 ± 0.38
$CaCl_2$ (Late)	1.84 ± 0.19	1.21 ± 0.11	2.26 ± 0.22	1.03 ± 0.14	2.54 ± 0.38	0.77 ± 0.14

Figure 4.4.2 SOCE dynamics with differentiation of S_O, S_A and S_E cells grown in an N-predominant environment

N-type populations were treated for 7 days with EtOH (P_N, proliferating) or 1 µM 9cRA (D_N, differentiating). Changes in fluorescence ratio units (FRUs) are reflective of changes in $[Ca^{2+}]_i$ following addition of thapsigargin (TG) indicating Ca^{2+} store release and subsequent Ca^{2+}-addback ($CaCl_2$) indicating SOCE to replenish depleted stores. **(A)** DMSO (TG control) measurements were deducted from the experimental data. There was no difference in maximal Ca^{2+} store release in $D_N S_O$ cells (0.19 ± 0.01 FRUs) compared to $P_N S_O$ cells (0.18 ± 0.01 FRUs, P=0.375). Maximal SOCE was down-regulated by 54.52% in $D_N S_O$ cells (0.17 ± 0.05 FRUs) compared to $P_N S_O$ cells (0.37 ± 0.02 FRUs, P<0.0001****). There was a significant 21.43% decrease in maximal Ca^{2+} store release in $D_N S_A$ cells (0.15 ± 0.01 FRUs) compared to $P_N S_A$ cells (0.19 ± 0.01 FRUs,

P=0.003**). Taking this change into account, maximal SOCE was down-regulated by 39.34% in $D_N S_A$ cells (0.19 ± 0.03 FRUs) compared to $P_N S_A$ cells (0.40 ± 0.03 FRUs). There was no difference in maximal Ca^{2+} store release between $P_N S_E$ cells (0.21 ± 0.01 FRUs) compared to $D_N S_E$ cells (0.14 ± 0.02 FRUs, P=0.212). Maximal SOCE was down-regulated by 73.25% in $D_N S_E$ cells (0.13 ± 0.04 FRUs) compared to $P_N S_E$ cells (0.48 ± 0.07 FRUs, P=0.005**). **(B)** There was no significant change in rate of Ca^{2+} store release (P=0.217) or rate of SOCE (P=0.132) between $P_N S_O$ cells and $D_N S_O$ cells. There was a significant 26.04% decrease in rate of Ca^{2+} store release (P=0.0005) but no significant change in rate of SOCE (P=0.735) in $D_N S_A$ cells compared to $P_N S_A$ cells. There was no significant difference in rate of Ca^{2+} store release (P=0.129) or rate of SOCE (P=0.176) in $P_N S_E$ cells compared to $D_N S_E$ cells. **(C)** There was a significant 12.33% decrease in Ca^{2+} store release decline rate in $D_N S_O$ cells compared to $P_N S_O$ cells (P=0.031). There was no difference in total or initial SOCE decline rate (P=0.426, P=0.709, respectively) between $P_N S_O$ cells and $D_N S_O$ cells. Late SOCE decline rate was significantly reduced by 34.19% (P=0.0089) in $D_N S_O$ cells compared to $P_N S_O$ cells. Ca^{2+} store release decline rate and total SOCE decline rate were both significantly reduced by 16.16% and 16.51% in $D_N S_A$ cells compared to $P_N S_A$ cells (P=0.041 and P<0.049, respectively). There was no difference in the initial SOCE decline rate between $P_N S_A$ cells and $D_N S_A$ cells (P=0.540) whilst the late decline rate was significantly reduced by 54.47% (P<0.0001) in $D_N S_A$ cells. There was no difference in Ca^{2+} store release decline rate between $P_N S_E$ cells and $D_N S_E$ cells (P=0.681) and total SOCE decline rate was significantly reduced by 52.19% in $D_N S_E$ cells compared to $P_N S_E$ cells (P=0.0021). The initial and late SOCE decline rate was significantly reduced by 41.77% and 69.54% respectively in $D_N S_E$ cells compared to $P_N S_E$ cells (P=0.046 and P<0.0001, respectively). In P_N populations: S_O n=108, S_A n=75, S_E n=4. In D_N populations: S_O n=82, S_A n=57, S_E n=24. N=6.

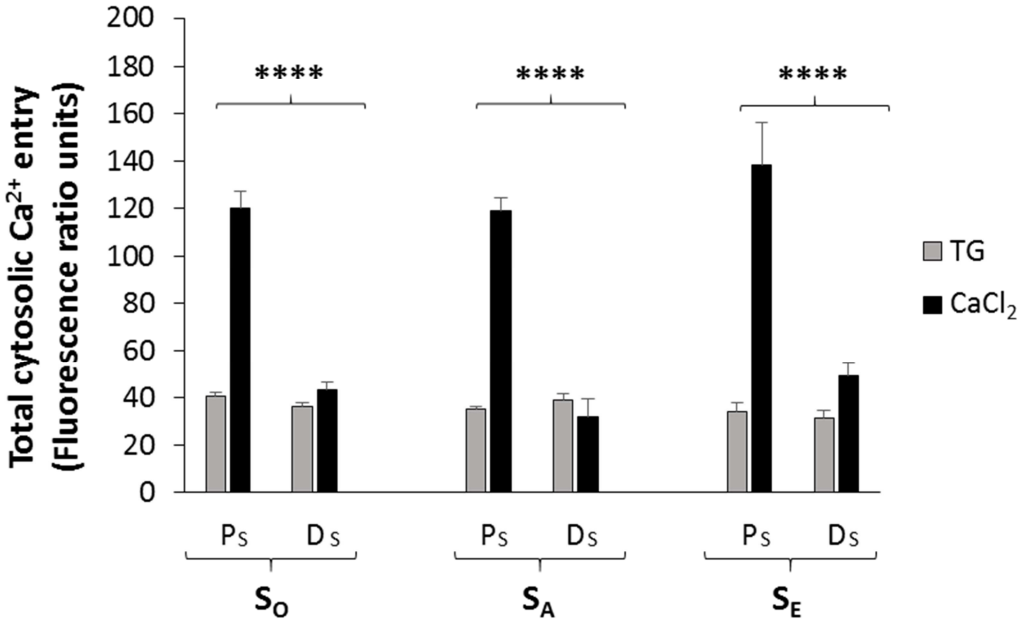

Figure 4.4.3. An uncoupling of Ca^{2+} store release and SOCE occurs with differentiation of S_O, S_A and S_E cells grown in an S-predominant environment

S-type populations were treated for 7 days with EtOH (P_S, proliferating) or 1 µM 9cRA (D_S, differentiating). Changes in fluorescence ratio units (FRUs) are reflective of changes in $[Ca^{2+}]_i$ following addition of thapsigargin (TG) indicating Ca^{2+} store release and subsequent Ca^{2+}-addback ($CaCl_2$) indicating SOCE to replenish depleted stores. Compared to P_S S_O cells, there was no change in total Ca^{2+} store release in D_S S_O cells (40.54 ± 1.82 and 36.50 ± 1.55 FRUs, respectively, P=0.092) and total SOCE was reduced by 63.85% (120.04 ± 7.14 and 43.40 ± 3.35 FRUs, respectively, p<0.0001****). Compared to P_S S_A cells, there was no change in total Ca^{2+} store release in D_S S_A cells (35.05 ± 1.22 and 39.19 ± 2.39, respectively FRUs, P=0.087) and total SOCE was reduced by 72.88% (118.79 ± 5.42 and 32.22 ± 7.45 FRUs, respectively, p<0.0001****). Compared to P_S S_E cells, there was no change in total Ca^{2+} store release in D_S S_E cells (34.04 ± 3.83 and 31.62 ± 3.19, respectively FRUs, P=0.663) and total SOCE was reduced by 64.52% (138.28 ± 17.99 and 49.07 ± 5.37 FRUs, respectively, P<0.0001****). P_S: S_O n=199, S_A n=356, S_E n=31. D_S: S_O n=200, S_A n=190, S_E n=75. N=8.

A

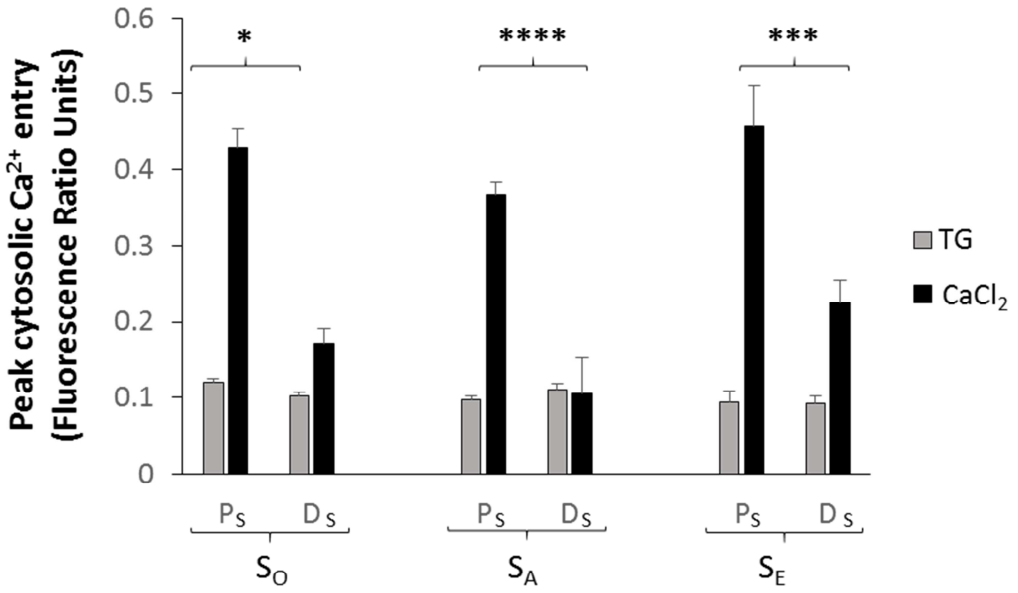

B

	Rate of rise (FRUs x 10^{-4})					
	$P_S S_O$	$D_S S_O$	$P_S S_A$	$D_S S_A$	$P_S S_E$	$D_S S_E$
TG	9.59 ± 0.55	8.26 ± 0.35	8.44 ± 0.36	10.68 ± 0.63	9.31 ± 1.17	8.08 ± 0.73
$CaCl_2$	88.20 ± 4.95	66.98 ± 4.61	87.51 ± 4.18	96.54 ± 8.13	119.21 ± 19.24	82.07 ± 11.27

C

	Rate of decline (FRUs x 10^{-4})					
	$P_S S_O$	$D_S S_O$	$P_S S_A$	$D_S S_A$	$P_S S_E$	$D_S S_E$
TG	2.22 ± 0.10	1.75 ± 0.06	1.82 ± 0.07	2.14 ± 0.09	1.99 ± 0.26	1.79 ± 0.13
$CaCl_2$ (Total)	4.28 ± 0.18	2.69 ± 0.11	3.60 ± 0.12	3.39 ± 0.19	4.81 ± 0.55	2.82 ± 0.26
$CaCl_2$ (Initial)	12.81 ± 0.48	6.61 ± 0.29	9.71 ± 0.35	8.58 ± 0.50	11.16 ± 1.13	7.36 ± 0.71
$CaCl_2$ (Late)	0.69 ± 0.09	0.63 ± 0.05	0.83 ± 0.07	0.65 ± 0.07	1.42 ± 0.32	0.56 ± 0.10

Figure 4.4.4. SOCE dynamics with differentiation of S_O, S_A and S_E cells grown in an S-predominant environment

S-type populations were treated for 7 days with EtOH (P_S, proliferating) or 1 µM 9cRA (D_S, differentiating). Changes in fluorescence ratio units (FRUs) are reflective of changes in $[Ca^{2+}]_i$ following addition of thapsigargin (TG) indicating Ca^{2+} store release and subsequent Ca^{2+}-addback ($CaCl_2$) indicating SOCE to replenish depleted stores. **(A)** DMSO (TG control) measurements were deducted from the experimental data. Maximal Ca^{2+} store release was significantly reduced by 14.61% in D_S S_O cells (0.10 ± 0.01 FRUs) compared to P_S S_O cells (0.12 ± 0.01 FRUs, P=0.025*). Taking this change into account, maximal SOCE was down-regulated by 53.26% in D_S S_O cells (0.17 ± 0.02 FRUs) compared to P_S S_O cells (0.43 ± 0.03 FRUs). There was no significant difference in

maximal Ca^{2+} store release between P_S S_A cells and D_S S_A cells (0.10 ± 0.004 and 0.11 ± 0.01 FRUs, respectively, P=0.097). Maximal SOCE was down-regulated by 71.36% in D_S S_A cells (0.11 ± 0.04 FRUs) compared to P_S S_A cells (0.37 ± 0.02 FRUs, P<0.0001****). There was no difference in maximal Ca^{2+} store between P_S S_E cells (0.09 ± 0.01 FRUs) compared to D_S S_E cells (0.09 ± 0.01 FRUs, P=0.908). Maximal SOCE was down-regulated by 50.72% in D_S S_E cells (0.23 ± 0.03 FRUs) compared to P_S S_E cells (0.46 ± 0.05 FRUs, P=0.00016***). **(B)** There was a significant decrease in rate of Ca^{2+} store release (13.90%, P=0.042) and rate of SOCE (24.05% P=0.0018) in D_S S_O cells compared to P_S S_O cells. There was a significant 26.66% increase in rate of Ca^{2+} store release (P=0.0009) but no significant change in rate of SOCE (P=0.274) in D_S S_A cells compared to P_S S_A cells. There was no significant difference in rate of Ca^{2+} store release (P=0.369) between P_S S_E cells and D_S S_E cells but there was a 31.16% decrease in rate of SOCE in D_S S_E cells compared to P_S S_E cells (P=0.086). **(C)** There was a significant 21.12% decrease in Ca^{2+} store release decline rate in D_S S_O cells compared to P_S S_O cells (P<0.0001). There was a significant reduction in total and initial SOCE decline rate in D_S S_O cells compared to P_S S_O cells (37.02% and 48.42% respectively, both P<0.0001). There was no difference in late SOCE decline rate between P_S S_O cells and D_S S_O cells (P=0.560). Ca^{2+} store release decline rate was significantly increased by 17.32% in D_S S_A cells compared to P_S S_A cells (P=0.061). There was no difference in the total SOCE decline rate was between P_S S_A cells and D_S S_A cells (P=0.329). The initial and late SOCE decline rates were both significantly reduced (by 11.60%, P=0.061 and 22.31%, P=0.098, respectively) in D_S S_A cells. There was no difference in Ca^{2+} store release decline rate between P_S S_E cells and D_S S_E cells (P=0.447). Compared to P_S S_E cells, D_S S_E cells had significantly reduced total SOCE decline rate (by 41.30%, P=0.0003), initial SOCE decline rate (by 34.02%, P=0.0049) and late SOCE decline rate (by 60.80%, P=0.0011). In P_S populations: S_O n=199, S_A n=356, S_E n=31. In D_S populations: S_O n=200, S_A n=190, S_E n=75. N=8.

4.5. There is an effect of media from differentiating N-type and S-type populations

As previously discussed (Results 4.3-4.4) the Ca^{2+} responses of cells within an N-type and S-type population are affected by the surrounding cell environment. This may be due to local effects such as cell-cell contacts or the release of factors by surrounding cells that may alter cell characteristics. To investigate this further, media from proliferating and differentiating S-type populations was applied to N-type populations whilst media from proliferating or differentiating N-type populations was applied to S-type populations.

4.5.1 Applying S-type conditioned media to N-type populations

N-type predominant populations were treated for 7 days with EtOH (P_N, proliferating), 1 µM 9cRA (D_N, differentiating), media from proliferating S-type populations (P_N+P_S), media from differentiating S-type populations (P_N+D_S) or with 1 µM 9cRA plus media from differentiating S-type populations (D_N+D_S). As shown previously, P_N cells possess short neurite-like processes and neurites become elongated with differentiation (Figure 4.5.1A and B). P_N+P_S cells grow in a similar fashion to P_N cells and possess short neurite-like processes whilst P_N+D_S cells and D_N+D_S cells grow in a similar manner to D_N cells and possess elongated neurite-like processes (Figure 4.5.1C, D and E).

Compared to P_N cells, D_N cells had a 20% increase in total Ca^{2+} store release ($P<0.0001$) and total SOCE was reduced by 53% (Figure 4.5.2A and B). Consistent with this, there was a 10% increase in maximal Ca^{2+} store release in D_N compared to P_N cells ($P=0.004$) and maximal SOCE was down-regulated by 61% (Figure 4.5.3A). There was an 11% increase in rate of Ca^{2+} store release ($P=0.003$) but no difference in rate of SOCE ($P=0.948$), Ca^{2+} store release decline rate ($P=0.997$), total SOCE decline rate ($P=0.579$) or initial SOCE decline rate ($P=0.166$, Figure 4.5.3B and C). Late SOCE decline rate was reduced by 19% ($P<0.0001$, Figure 4.5.3C). These results confirm an uncoupling of Ca^{2+} store release and SOCE in D_N populations as described previously (Results 4.2).

Total Ca^{2+} store release in P_N+P_S cells was 13% lower than P_N cells ($P<0.00001$) but there was no change in total SOCE (Figure 4.5.2A and B). There was a 7% increase in maximal Ca^{2+} store release in P_N+P_S compared to P_N cells ($P=0.034$) and maximal SOCE

was down-regulated by 14% (Figure 4.5.3A). There was a 49% increase in rate of Ca^{2+} store release ($P<0.0001$) and 46% down-regulation of SOCE ($P<0.0001$, Figure 4.5.3B). Ca^{2+} store release decline rate was increased by 16% and total SOCE decline rate was reduced by 28% (both $P<0.0001$, Figure 4.5.3C). There was no difference in the initial SOCE decline rate ($P=0.517$) and late SOCE decline rate was reduced by 37% ($P=0.072$, Figure 4.5.3C). These results indicate that treatment of P_N cells with P_S media induces a reduction in Ca^{2+} store release and increases rate of store release activation and rate of store emptying and therefore a smaller, shorter store release that may represent a decrease in store size. Whilst P_s media does not affect the overall extent of P_N SOCE, the activation and late de-activation of SOCE are dampened indicating an extended SOCE response. P_S media therefore, at least in part, maintains the P_N SOCE response.

Compared to P_N cells, total Ca^{2+} store release of P_N+D_S cells was increased by 50% ($P<0.0001$) and total SOCE was reduced by 48% (Figure 4.5.2A and B). Consistent with this, maximal Ca^{2+} store release of P_N+D_S cells was increased by 35% compared to P_N cells ($P<0.0001$) and maximal SOCE was down-regulated by 24% in P_N+D_S (Figure 4.5.3A). There was a 29% increase in rate of Ca^{2+} store release ($P<0.0001$) but no difference in rate of SOCE ($P>0.999$, Figure 4.5.3B). Ca^{2+} store release decline rate was increased by 13% ($P<0.0001$) but there was no difference in total SOCE decline rate ($P=0.268$, Figure 4.5.3C). The initial SOCE decline rate was increased by 97% ($P<0.0001$) whilst late SOCE decline rate was reduced by 39% ($P<0.0001$, Figure 4.5.3C). These results indicate that treatment of P_N cells with D_S media induces an increase in Ca^{2+} store release and rate of store release activation and emptying, suggesting an increase in store capacity and sensitivity to TG, like that seen in D_N cells. Whilst D_s media reduced the overall extent of P_N SOCE, rate of initial SOCE decline was increased, suggesting a smaller, shorter SOCE response. D_S media therefore induces Ca^{2+} responses in P_N cells that more reflect a D_N response than a P_N response.

There was a 25% increase in total Ca^{2+} store release in P_N+D_S cells compared to D_N cells ($P<0.0001$) but no difference in total SOCE (Figure 4.5.2A and B) and an increase in maximal Ca^{2+} store release (22%, $P<0.0001$) and maximal SOCE (93%, Figure 4.5.3A). There was an increase in rate of Ca^{2+} store release (15%, $P<0.0001$) and rate of SOCE

(8%, P<0.0001, Figure 4.5.3B). Ca^{2+} store release decline rate and total SOCE decline rate were significantly increased (12%, P<0.0001 and 15% P=0.019, respectively, Figure 4.6.3C). The initial SOCE decline rate was increased (64%, P<0.0001) whilst late SOCE decline rate was reduced (24%, P<0.0001, Figure 4.5.3C). These results show that treatment of P_N cells with D_S media increases Ca^{2+} store release, rate of activation and emptying to a greater extent than that D_N cells, suggesting an increase in store capacity and sensitivity to TG. There was no difference in extent of SOCE, confirming that D_S media induces SOCE down-regulation in P_N like that of D_N cells. However, this effect is not fully D_N-like since there was an overall shortened SOCE response to a greater extent than that of D_N cells.

Compared to P_N cells, total Ca^{2+} store release in D_N+D_S cells was increased by 14% (P<0.0001) and total SOCE was reduced by 35% (Figure 4.5.2A and B). Consistent with this, maximal Ca^{2+} store release was increased by 22% (P<0.0001) and maximal SOCE was reduced by 36% (Figure 4.5.3A). There was a 67% increase in rate of Ca^{2+} store release (P<0.0001) and 47% decrease in rate of SOCE (P<0.0001, Figure 4.5.3B). There was a reduction in Ca^{2+} store release decline rate (10%), total SOCE decline rate (23%) and late SOCE decline rate (56%, all P<0.0001), whilst initial SOCE decline rate was increased (47%, P<0.0001, Figure 4.5.3C). Treating D_N cells with D_S media therefore induces a similar uncoupling effect to that of P_N cells treated with D_S media, although to a lesser extent, implying that inducing differentiation of N-type cell populations alongside D_S media application somehow dampens the full effect of D_S media. The extent of change in rates of activation and deactivation are also more similar to P_N+P_S cells, with a seemingly increased sensitivity to TG, slower SOCE activation and increased SOCE deactivation.

Total Ca^{2+} store release in D_N+D_S cells was no different to that of D_N cells (P=0.084) and total SOCE was increased by 17% (P=0.028, Figure 4.5.2A and B). Maximal Ca^{2+} store release was increased (10%, P=0.004) and maximal SOCE was increased (62%, Figure 4.5.3A). There was a 50% increase in rate of Ca^{2+} store release (P=0.0001) and 57% decrease in rate of SOCE (P=0.0008, Figure 4.5.3B). There was a reduction in Ca^{2+} store release decline rate (10%, P=0.0008), total SOCE decline rate (18%, P=0.0014) and late

SOCE decline rate (46%, P<0.0001) whilst initial SOCE decline rate was increased (22%, P=0.033, Figure 4.5.3C). These results confirm that the extent of uncoupling when inducing differentiation of N-type cell populations alongside D_S media application dampens the full effect of D_S media.

All of this data confirms that the Ca^{2+} signals of N-type populations can be influenced by S-type conditioned media (Table 4.5.1).

Compared to	P_N	D_N
D_N	Ca^{2+} release: increased SOCE: decreased	- -
$P_N + P_S$	Ca^{2+} release: decreased SOCE: no change	- -
$P_N + D_S$	Ca^{2+} release: increased SOCE: decreased	Ca^{2+} release: increased SOCE: no change
$D_N + D_S$	Ca^{2+} release: increased SOCE: decreased	Ca^{2+} release: no change SOCE: increased

Table 4.5.1. Summary of N-type population single cell Ca^{2+} signals determined by S-type conditioned media

4.5.2 Applying N-type conditioned media to S-type populations

S-type predominant populations were treated for 7 days with EtOH (P_S, proliferating), 1 µM 9cRA (D_S, differentiating), media from proliferating N-type populations (P_S+P_N), media from differentiating N-type populations (P_S+D_N) or with 1 µM 9cRA plus media from differentiating N-type populations (D_S+D_N). As previously described, P_S cells possess abundant cytoplasm with a flattened morphology and become more flattened and spread out with differentiation (Figure 4.5.4A and B). P_S+P_N cells grow in a similar manner to P_S cells whilst P_S+D_N cells and D_S+D_N cells grow in a similar manner to D_S cells (Figure 4.5.4A, B and C).

Compared to P_S cells, in D_S cells there was a 37% increase in total Ca^{2+} store release ($P<0.0001$) and total SOCE was reduced by 83% (Figure 4.5.5A and B). Consistent with this, there was a 21% increase in maximal Ca^{2+} store ($P<0.0001$) and maximal SOCE was down-regulated by 79% (Figure 4.5.6A). There was an 18% increase in rate of Ca^{2+} store release ($P=0.003$) and a 20% decrease in rate of SOCE ($P=0.003$, Figure 4.5.6.B). There was no change in Ca^{2+} store release decline rate ($P=0.863$), a decrease in total and late SOCE decline rate (15% and 80%, respectively) and a 67% increase in initial SOCE decline rate (all $P<0.0001$, Figure 4.5.6C). These results confirm an uncoupling of Ca^{2+} store release and SOCE in D_S populations as described previously (Results 4.2).

Total Ca^{2+} store release in P_S+P_N cells was 37% higher than that of P_S cells ($P<0.00001$) and there was a 42% decrease in total SOCE (Figure 4.5.5A and B). Maximal Ca^{2+} store release was increased (21% $P<0.001$) and maximal SOCE was down-regulated (33%, Figure 4.5.6A). There was a 41% increase in rate of Ca^{2+} store release ($P<0.0001$) and 55% decrease in rate of SOCE ($P<0.0001$, Figure 4.5.6B). There was a reduction in Ca^{2+} store release decline rate (9%, $P=0.037$), total (21%) and late (76%) SOCE decline rate whilst initial SOCE decline was increased by 50% (all $P<0.0001$, Figure 4.5.6C). These results show that treatment of P_S cells with P_N media induces an uncoupling of Ca^{2+} store release and SOCE similar to that seen in D_S cells, although SOCE down-regulation occurred to a much lesser extent.

Compared to P_S cells, there was no difference in total Ca^{2+} store release of P_S+D_N cells and total SOCE was reduced by 49% (P<0.0001, Figure 4.5.5A and B). There was no difference in maximal Ca^{2+} store release (P=0.789) and maximal SOCE was reduced by 98% (P<0.0001, Figure 4.5.6A). There was no difference in rate of Ca^{2+} store release (P=0.404) or rate of SOCE (P=0.071, Figure 4.5.6B). There was a reduction in Ca^{2+} store release decline rate (12%, P=0.0006), total (9%, P=0.042) and late (52%, P<0.0001) SOCE decline rate whilst initial SOCE decline rate was increased by 56% (P<0.0001, Figure 4.5.6C). Treating P_S cells with D_N media therefore does not affect store size or sensitivity to TG like P_N media however, it does induce changes in the SOCE response similar to that of P_N media, thereby causing an uncoupling of store release and SOCE to a lesser extent than in D_S cells.

There was a 28% reduction in total Ca^{2+} store release in P_S+D_N cells compared to D_S cells (P<0.0001) and a two-fold increase in total SOCE (Figure 4.5.5A and B). There was a reduction in maximal Ca^{2+} store release (22%, P<0.0001) and maximal SOCE (90%, Figure 4.5.6A). There was no difference in rate of Ca^{2+} store release (P=0.143) and a 41% increase in rate of SOCE (P<0.0001, Figure 4.5.6B). Ca^{2+} store release decline rate was reduced by 9% (P=0.021), late SOCE decline rate was increased by 1.5 fold (P<0.0001) and here was no difference in total (P=0.134) or initial (P=0.425) SOCE decline rate (Figure 4.5.6C). This confirms that effect of D_N media on P_S cells does not induce a fully differentiating Ca^{2+} response, largely influenced by an increase in rate of SOCE activation and late deactivation.

Compared to P_S cells, there was no difference in total Ca^{2+} store release in D_S+D_N cells (P=0.775) and total SOCE was reduced by 63% (p<0.0001, Figure 4.5.5A and B). There was no difference in maximal Ca^{2+} store release whilst maximal SOCE was reduced by 52% (P<0.0008, Figure 4.5.6.A). There was an increase in rate of Ca^{2+} store release (16%, P=0.017) and SOCE (23%, P=0.0004, Figure 4.5.6.B). Ca^{2+} store release decline rate, total and late SOCE decline rate were reduced (26%, 27% and 70% respectively, all P<0.0001) whilst initial SOCE decline rate was increased by (26%, P=0.003, Figure 4.5.6C). These results show that differentiating S-type cells alongside D_N media

application induces a differentiation response similar to that seen in P_S+D_N cells, with a greater extent of SOCE down-regulation.

Total Ca^{2+} store release was reduced by 28% in D_S+D_N cells compared to D_S cells ($P<0.0001$) and total SOCE was 1 fold greater (Figure 4.5.5A and B). Maximal Ca^{2+} store release was reduced by 21% ($P<0.0001$) and maximal SOCE was increased by 1.5 fold (Figure 4.5.6A). There was no difference in rate of Ca^{2+} store release ($P=0.986$) or rate of SOCE ($P=0.981$, Figure 4.5.6B). Ca^{2+} store release decline rate, total and initial SOCE decline rate were reduced (23%, $P<0.0001$, 14%, $P=0.004$ and 24%, $P<0.0001$, respectively) whilst late SOCE decline rate was increased by 51% ($P=0.021$, Figure 4.5.6C). This confirms that differentiating S-type cells alongside D_N media application does not induce a fully differentiating response but brings the cells closer to a differentiating response than that seen in P_S+D_N cells.

All of this data confirms that the Ca^{2+} signals of S-type populations can be influenced by N-type conditioned media (Table 4.5.2).

Compared to	P_S	D_S
D_S	Ca^{2+} release: increased SOCE: decreased	- -
$P_S + P_N$	Ca^{2+} release: increased SOCE: decreased	- -
$P_S + D_N$	Ca^{2+} release: no change SOCE: decreased	Ca^{2+} release: decreased SOCE: increased
$D_S + D_N$	Ca^{2+} release: no change SOCE: decreased	Ca^{2+} release: decreased SOCE: increased

Table 4.5.2. Summary of S-type population single cell Ca^{2+} signals determined by N-type conditioned media

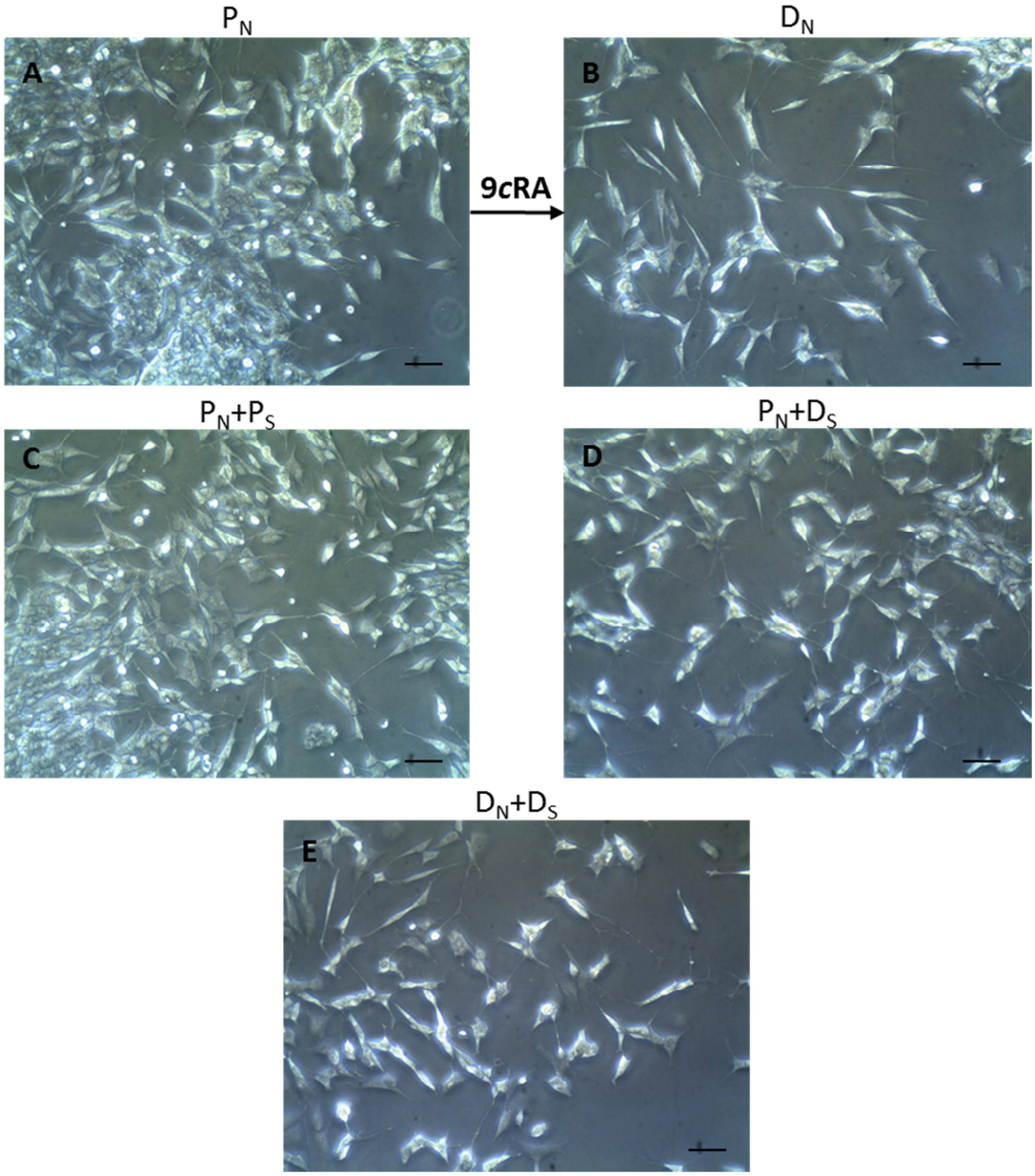

Figure 4.5.1. Effect of S media on N-type populations morphology

N-type populations were treated for 7 days with EtOH (P_N, proliferating), 1 µM 9cRA (D_N, differentiating), media from proliferating S-type populations (P_N+P_S), media from differentiating S-type populations (P_N+D_S) or with 1 µM 9cRA plus media from differentiating S-type populations (D_N+D_S). **(A)** P cells possess short neurite-like processes and **(B)** upon differentiation, neurites become elongated and cell numbers decrease. **(C)** P_N+P_S cells grow in a similar aggregated fashion to P_N cells and possess short neurite-like processes. **(D)** P_N+D_S cells and **(E)** D_N+D_S cells grow in a similar manner to D_N cells and possess elongated neurite-like processes. Scale bar represents of phase contrast images represents 20 µm.

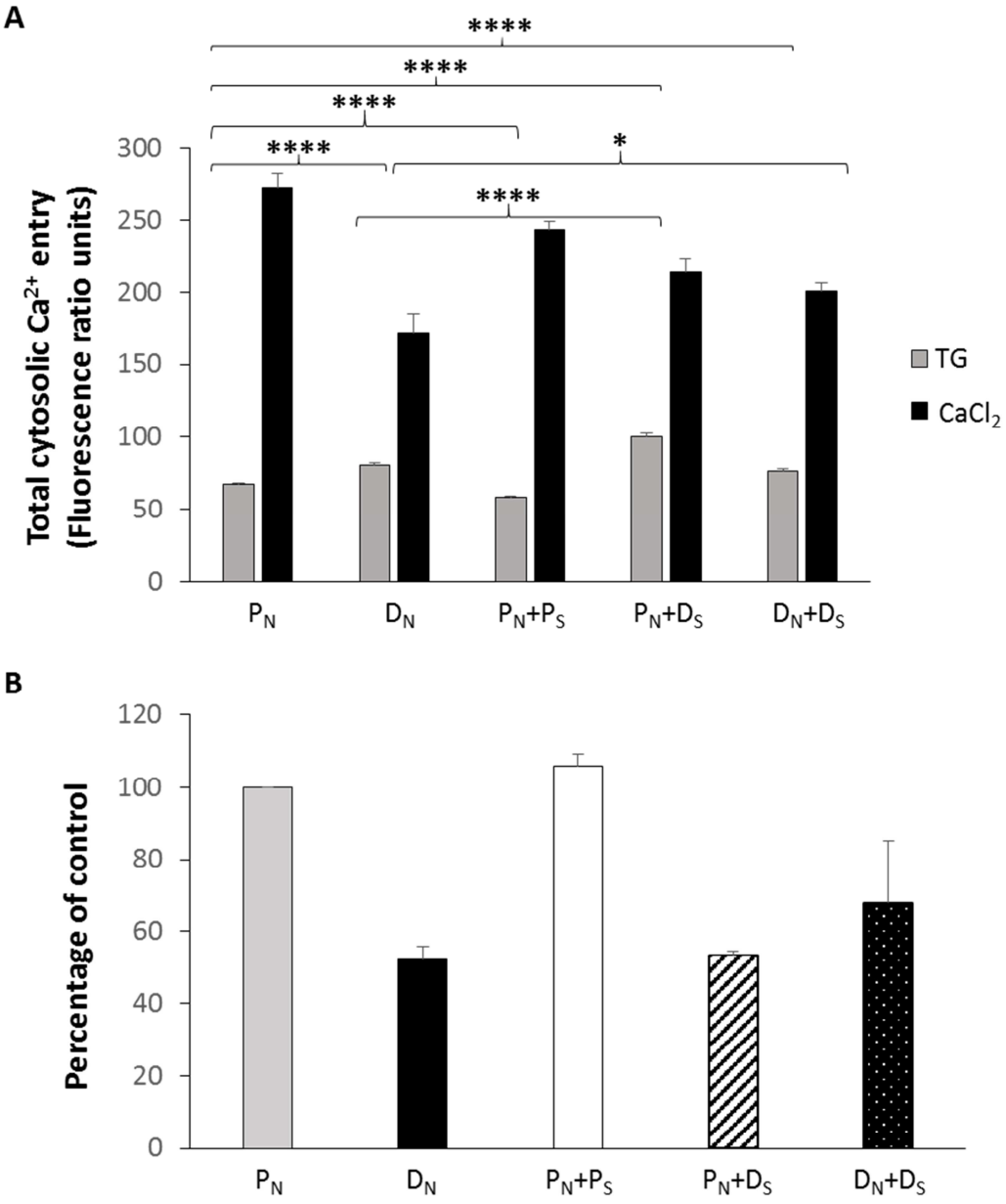

Figure 4.5.2. Effect of S media on Ca^{2+} responses of N-type populations

N-type populations were treated for 7 days with EtOH (P_N, proliferating), 1 µM 9cRA (D_N, differentiating), media from proliferating S-type populations (P_N+P_S), media from differentiating S-type populations (P_N+D_S) or with 1 µM 9cRA plus media from differentiating S-type populations (D_N+D_S). Changes in fluorescence ratio units (FRUs) are reflective of changes in $[Ca^{2+}]_i$ following addition of thapsigargin (TG) indicating Ca^{2+} store release and subsequent Ca^{2+}-addback ($CaCl_2$) indicating SOCE to replenish depleted stores. **(A)** Compared to P_N cells, in D_N cells there was a 19.75% increase in total Ca^{2+} store release (67.11 ± 1.17 and 80.37 ± 1.50 FRUs, respectively,

P<0.0001****) and, taking this change into account, total SOCE was reduced by 52.79% (271.87 ± 10.65 and 171.87 ± 13.22 FRUs, respectively). Total Ca^{2+} store release in P_N+P_S cells (58.15 ± 1.20 FRUs) was 13.36% lower than that of P_N cells (P<0.00001****) and there was no change in total SOCE (243.60 ± 5.99 FRUs). Compared to P_N cells, total Ca^{2+} store release of P_N+D_S cells was increased by 49.88% (100.59 ± 2.43 FRUs, P<0.0001****) and total SOCE was reduced by 47.55% (213.72 ± 9.18 FRUs). There was a 25.16% increase in total Ca^{2+} store release in P_N+D_S cells compared to D_N cells (P<0.0001****) but no difference in total SOCE. Compared to P_N cells, total Ca^{2+} store release in D_N+D_S cells (76.66 ± 1.43 FRUs) was increased by 14.22% (P<0.0001****) and total SOCE (200.57 ± 6.05 FRUs) was reduced by 35.41%. Total Ca^{2+} store release in D_N+D_S cells was no different to that of D_N cells (P=0.084) and total SOCE was increased by 16.70% (P=0.028*). **(B)** When taking into account any changes in total Ca^{2+} store release, compared to P_N cells, all other treatments caused a down-regulation of total SOCE, except P_N+P_S. P_N: n=597, D_N: n=311, P_N+P_S: n=456, P_N+D_S: n=386, D_N+D_S: n=476. N=3.

A

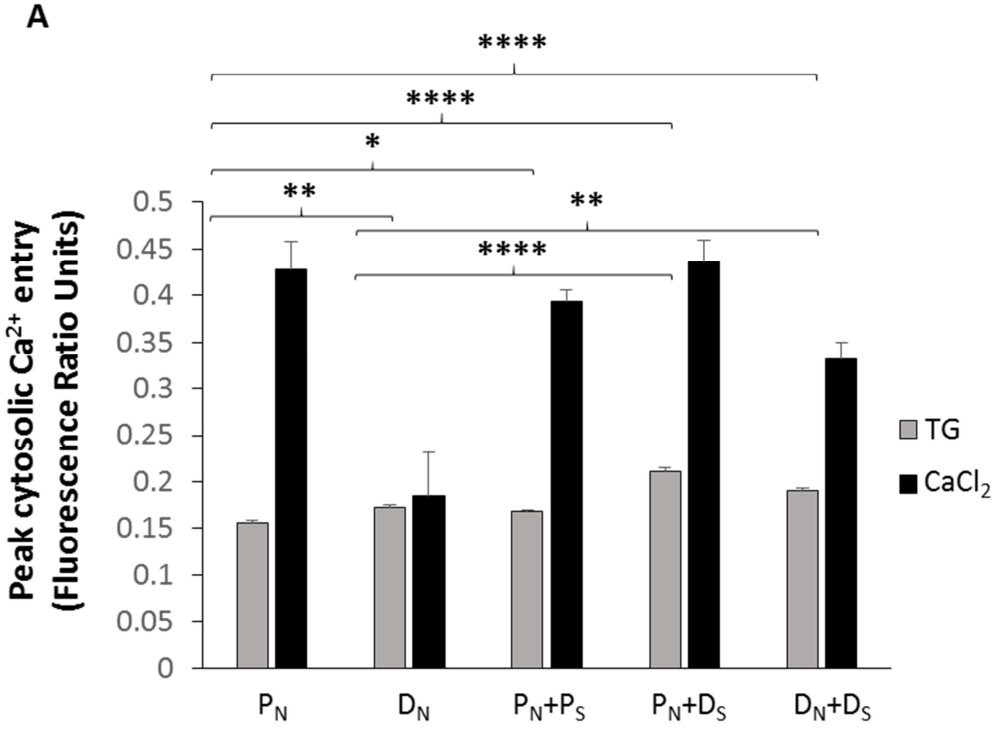

B

	Rate of rise (FRU x 10^{-4})				
	P	D	P+SP	P+SD	D+SD
TG	7.47 ± 0.11	8.32 ± 0.17	11.10 ± 0.18	9.60 ± 0.16	12.48 ± 0.18
$CaCl_2$	67.91 ± 5.00	63.30 ± 6.13	36.86 ± 1.93	68.59 ± 4.64	36.28 ± 1.78

C

	Rate of decline (FRU x 10^{-4})				
	P	D	P+SP	P+SD	D+SD
TG	2.36 ± 0.03	2.37 ± 0.04	2.73 ± 0.03	2.65 ± 0.04	2.13 ± 0.05
$CaCl_2$ (Total)	3.69 ± 0.10	3.46 ± 0.13	2.65 ± 0.08	3.97 ± 0.14	2.83 ± 0.05
$CaCl_2$ (Initial)	4.45 ± 0.27	5.34 ± 0.37	3.89 ± 0.24	8.75 ± 0.30	6.54 ± 0.20
$CaCl_2$ (Late)	3.35 ±0.09	2.71 ± 0.11	2.12 ± 0.08	2.06 ± 0.13	1.47 ± 0.06

Figure 4.5.3. Effect of S media on Ca^{2+} response dynamics of N-type populations

N-type populations were treated for 7 days with EtOH (P_N, proliferating), 1 µM 9cRA (D_N, differentiating), media from proliferating S-type populations (P_N+P_S), media from differentiating S-type populations (P_N+D_S) or with 1 µM 9cRA plus media from differentiating S-type populations (D_N+D_S). Changes in fluorescence ratio units (FRUs) are reflective of changes in $[Ca^{2+}]_i$ following addition of thapsigargin (TG) indicating Ca2+ store release and subsequent Ca^{2+}-addback ($CaCl^2$) indicating SOCE to replenish depleted stores. **(A)** DMSO (TG control) measurements were deducted from the experimental data. There was a 10.30% increase in maximal Ca^{2+} store release in D_N cells (0.17 ± 0.003 FRUs) compared to P_N cells (0.16 ± 0.003 FRUs, P=0.004**). Taking

this change in Ca^{2+} store release into account, maximal SOCE was down-regulated by 60.72% in D_N cells (0.19 ± 0.05 FRUs) compared to P_N cells (0.43 ± 0.03 FRUs). There was a 7.39% increase in maximal Ca^{2+} store release in P_N+P_S cells (0.17 ± 0.002 FRUs) compared to P_N cells (P=0.034*) . Taking this change in Ca^{2+} store release into account, maximal SOCE was down-regulated by 14.39% in P_N+P_S cells (0.39 ± 0.01 FRUs) compared to P_N cells. Maximal Ca^{2+} store release was increased by 34.68% in P_N+D_S cells (0.21 ± 0.01 FRUs) compared to P_N cells (P<0.0001****). Taking this change in Ca^{2+} store release into account, maximal SOCE was down-regulated by 24.36% in P_N+D_S (0.44 ± 0.02 FRUs) compared to P_N cells. Compared to D_N cells, there was a 22.10% increase in maximal Ca^{2+} store release in P_N+D_S cells (P<0.0001****) and, taking this change in Ca^{2+} store release into account, maximal SOCE was increased by 92.58%. Compared to P_N cells, maximal Ca^{2+} store release in D_N+D_S cells (0.19 ± 0.003 FRUs) was increased by 21.58% (P<0.0001****) and, taking this this change in Ca^{2+} store release into account, maximal SOCE (0.33 ± 0.02 FRUs) was reduced by 36.25%. Maximal Ca^{2+} store release in D_N+D_S cells was increased by 10.23% compared to that of D_N cells (P=0.004**) and taking this this change in Ca^{2+} store release into account, maximal SOCE was increased by 62.31%. **(B)** There was an 11.41% increase in rate of Ca^{2+} store release (P=0.003) and but no difference in rate of SOCE (P=0.948) in D_N cells compared to P_N cells. There was a 48.66% increase in rate of Ca^{2+} store release (P<0.0001) and 45.72% down-regulation of SOCE (P<0.0001) in P_N+P_S cells compared to P_N cells. There was a 28.59% increase in rate of Ca^{2+} store release (P<0.0001) but no difference in rate of SOCE (P>0.999) in P_N+D_S cells compared to P_N cells. There was a 15.41% increase in rate of Ca^{2+} store release (P<0.0001) and 8.36% increase in rate of SOCE (P<0.0001) in P_N+D_S cells compared to D_N cells. There was a 67.04% increase in rate of Ca^{2+} store release (P<0.0001) and 46.57% decrease in rate of SOCE (P<0.0001) in D_N+D_S cells compared to P_N cells. There was a 49.93% increase in rate of Ca^{2+} store release (P=0.0001) and 57.32% decrease in rate of SOCE (P=0.0008) in D_N+D_S cells compared to D_N cells. **(C)** There was no change in Ca^{2+} store release decline rate (P=0.997) between P_N cells and D_N cells or total SOCE decline rate (P=0.579). There was no difference in initial SOCE decline rate (P=0.166) whilst late SOCE decline rate was reduced by 19.25% in D_N cells compared to P_N cells (P<0.0001). Ca^{2+} store release decline rate was increased by 15.69% and total SOCE decline rate was reduced by 27.99% in P_N+P_S cells

compared to P_N cells (both P<0.0001). There was no difference in the initial SOCE decline rate (P=0.517) and late SOCE decline rate was reduced by 36.83% in P_N+P_S cells compared to P cells (P=0.072). Ca^{2+} store release decline rate was increased by 12.63% in P_N+D_S cells compared to P_N cells (P<0.0001) but there was no difference in total SOCE decline rate (P=0.268). The initial SOCE decline rate was increased by 96.76% in P_N+D_S cells compared to P_N cells (P<0.0001) whilst late SOCE decline rate was significantly reduced by 38.58% (P<0.0001). Ca^{2+} store release decline rate and total SOCE decline rate were significantly increased in P_N+D_S cells compared to D_N cells (by 12.11%, P<0.0001 and 14.65% P=0.019, respectively). The initial SOCE decline rate was increased by 63.84% in P_N+D_S cells compared to D_N cells (P<0.0001) whilst late SOCE decline rate was reduced by 23.94% (P<0.0001). Ca^{2+} store release decline rate and total SOCE decline rate were significantly reduced in D_N+D_S cells compared to P_N cells (9.58% and 23.28%, respectively, both P<0.0001). The initial SOCE decline rate was increased by 47.06% in D_N+D_S cells compared to P_N cells (P<0.0001) whilst late SOCE decline rate was reduced by 56.23% (P<0.0001). Ca^{2+} store release decline rate and total SOCE decline rate were significantly reduced in D_N+D_S cells compared to D_N cells (by 9.99%, P=0.0008 and 18.32%, P=0.0014, respectively). The initial SOCE decline rate was increased by 22.45% in D_N+D_S cells compared to D_N cells (P=0.033) whilst late SOCE decline rate was reduced 45.80% (P<0.0001). P_N: n=597, D_N: n=311, P_N+P_S: n=456, P_N+D_S: n=386, D_N+D_S: n=476. N=3.

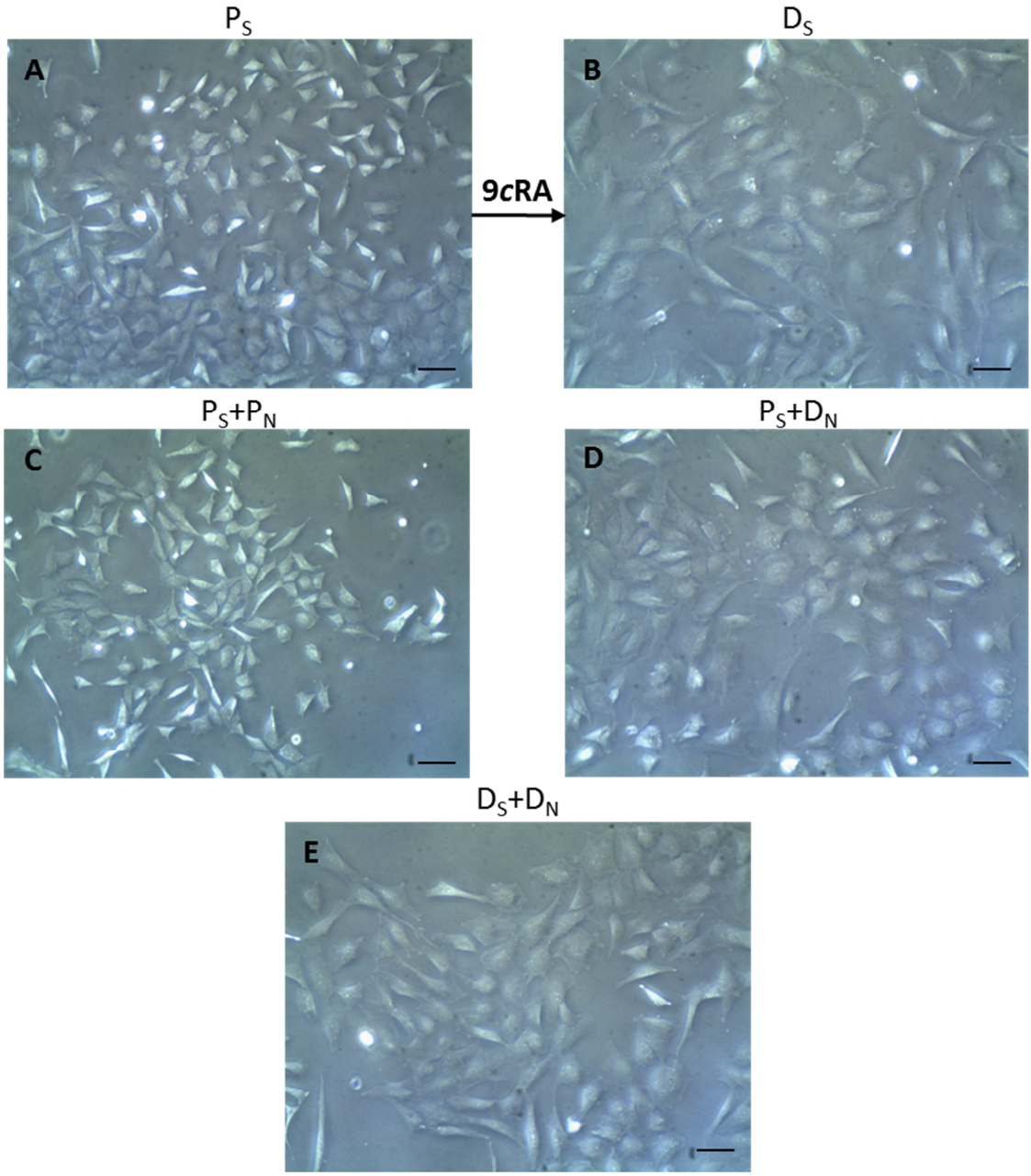

Figure 4.5.4. There is an effect of N-type media on S-type populations morphology

S-type populations were treated for 7 days with EtOH (P_S, proliferating), 1 µM 9cRA (D_S, differentiating), media from proliferating N-type populations (P_S+P_N), media from differentiating N-type populations (P_S+D_N) or with 1 µM 9cRA plus media from differentiating N-type populations (D_S+D_N). **(A)** P_S cells possess abundant cytoplasm with a flattened morphology and **(B)** upon differentiation, cells become more flattened and spread out. **(C)** P_S+P_N cells grow in a similar manner to P_S cells whilst **(D)** P_S+D_N cells and **(E)** D_S+D_N cells grow in a similar manner to D_S cells. Scale bar represents of phase contrast images represents 20 µm.

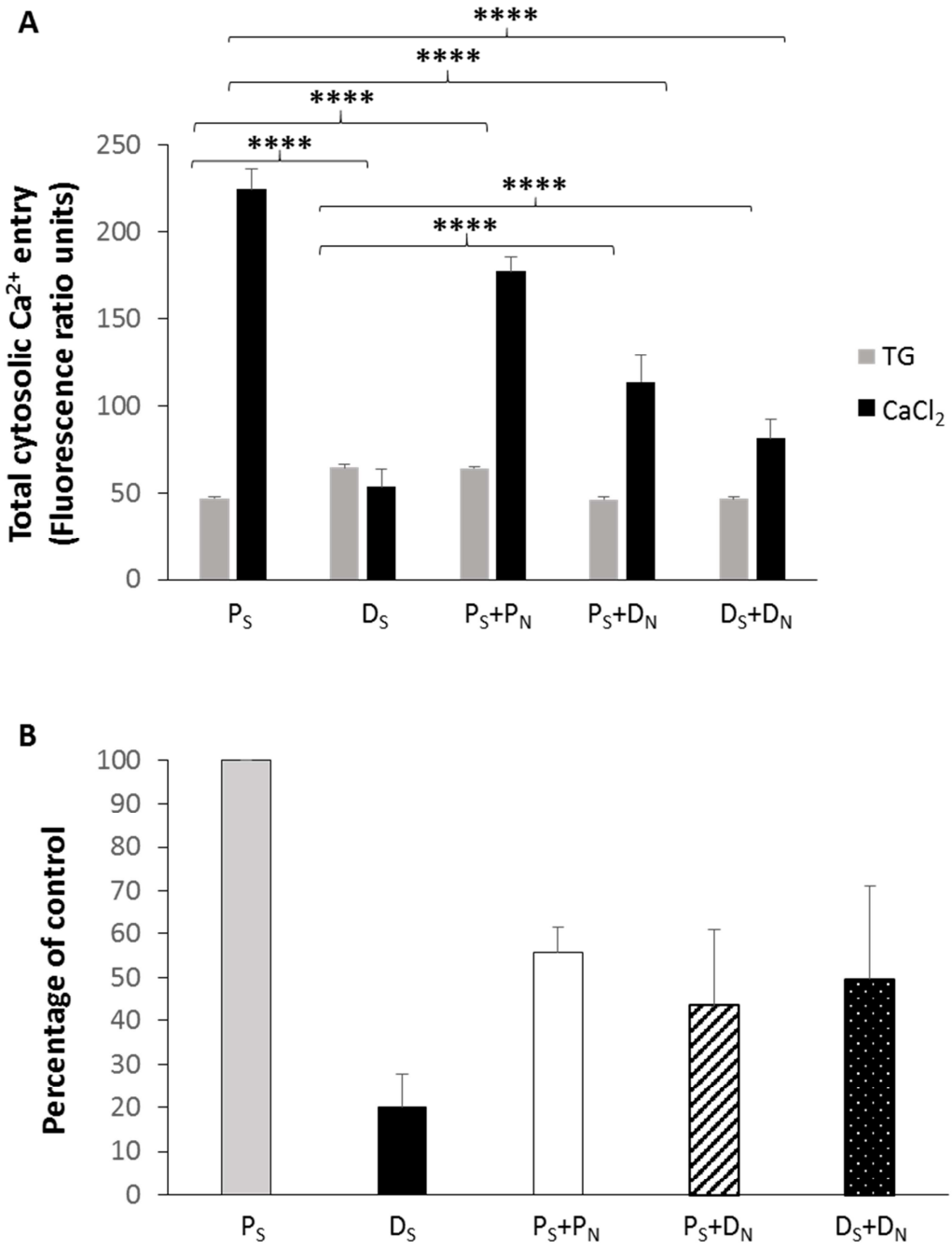

Figure 4.5.5. There is an effect of N-type media on Ca^{2+} responses of S-type populations

S-type populations were treated for 7 days with EtOH (P_S, proliferating), 1 µM 9cRA (D_S, differentiating), media from proliferating N-type populations (P_S+P_N), media from differentiating N-type populations (P_S+D_N) or with 1 µM 9cRA plus media from differentiating N-type populations (D_S+D_N). Changes in fluorescence ratio units (FRUs) are reflective of changes in $[Ca^{2+}]_i$ following addition of thapsigargin (TG) indicating

Ca^{2+} store release and subsequent Ca^{2+}-addback ($CaCl_2$) indicating SOCE to replenish depleted stores. **(A)** Compared to P_S cells, in D_S cells there was a 37.01% increase in total Ca^{2+} store release (46.92 ± 1.04 and 64.29 ± 1.73, respectively, P<0.0001****) and, taking this change into account, total SOCE was reduced by 82.59% (224.17 ± 12.23 and 53.47 ± 10.08, respectively). Total Ca^{2+} store release in P_S+P_N cells (64.09 ± 1.02) was 36.61% higher than that of P_S cells (P<0.00001****) and, taking this change into account, there was a 42.25% decrease in total SOCE (176.85 ± 8.66). Compared to P_S cells, there was no difference in total Ca^{2+} store release of P_S+D_N cells (46.21 ± 1.22, P=0.692) and total SOCE was reduced by 48.55% (113.58 ± 15.11, P<0.0001****). There was a 28.12% reduction in total Ca^{2+} store release in P_S+D_N cells compared to D_S cells (P<0.0001****) and, taking this change into account, a two-fold increase in total SOCE. Compared to P_S cells, there was no difference in total Ca^{2+} store release in D_S+D_N cells (46.41 ± 1.44, P=0.775) and total SOCE (81.61 ± 10.69) was reduced by 63.19% (p<0.0001****). Total Ca^{2+} store release was reduced by 27.81% in D_S+D_N cells compared to D_S cells (P<0.0001****) and, taking this change into account, total SOCE was 1 fold greater. **(B)** When taking into account any changes in total Ca^{2+} store release, compared to P_S cells, all other treatments caused a down-regulation of total SOCE. P_S: n=345, D_S: n=379, P_S+P_N: n=682, P_S+D_N: n=605, D_S+D_N: n=373. N=3.

A

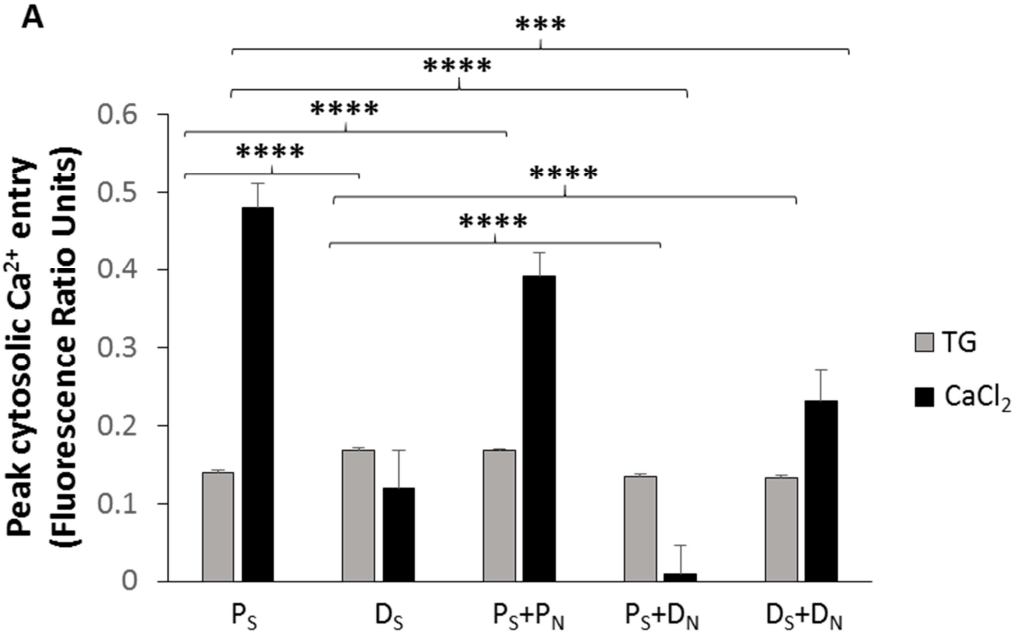

B

	Rate of rise (FRU x 10^{-4})				
	P	**D**	**P+NP**	**P+ND**	**D+ND**
TG	8.55 ± 0.29	10.11 ± 0.31	12.09 ± 0.13	9.24 ± 0.22	9.89 ± 0.47
$CaCl_2$	221.42 ± 9.18	177.80 ± 8.45	99.37 ± 3.70	250.23 ± 8.75	171.10 ± 8.33

C

	Rate of decline (FRU x 10^{-4})				
	P	**D**	**P+NP**	**P+ND**	**D+ND**
TG	2.51 ± 0.05	2.42 ± 0.06	2.29 ± 0.03	2.20 ± 0.06	1.86 ± 0.06
$CaCl_2$ (Total)	5.97 ± 0.11	5.05 ± 0.16	4.69 ± 0.10	5.46 ± 0.12	4.36 ± 0.13
$CaCl_2$ (Initial)	9.15 ± 0.39	15.25 ± 0.48	13.75 ± 0.32	14.25 ± 0.41	11.55 ± 0.47
$CaCl_2$ (Late)	5.06 ± 0.18	1.00 ± 0.07	1.22 ± 0.07	2.44 ± 0.12	1.51 ± 0.10

Figure 4.5.6. There is an effect of N-type media on Ca^{2+} response dynamics of S-type populations

S-type populations were treated for 7 days with EtOH (P_S, proliferating), 1 µM 9cRA (D_S, differentiating), media from proliferating N-type populations (P_S+P_N), media from differentiating N-type populations (P_S+D_N) or with 1 µM 9cRA plus media from differentiating N-type populations (D_S+D_N). Changes in fluorescence ratio units (FRUs) are reflective of changes in $[Ca^{2+}]_i$ following addition of thapsigargin (TG) indicating Ca^{2+} store release and subsequent Ca^{2+}-addback ($CaCl_2$) indicating SOCE to replenish depleted stores. **(A)** DMSO (TG control) measurements were deducted from the experimental data. There was a 20.50% increase in maximal Ca^{2+} store release in D_S cells (0.17 ± 0.002 FRUs) compared to P_S cells (0.14 ± 0.003 FRUs, P<0.0001****).

Taking this change in Ca^{2+} store release into account, maximal SOCE was down-regulated by 79.31% in D_S cells (0.12 ± 0.05 FRUs) compared to P_S cells (0.48 ± 0.03 FRUs). There was a 21.09% increase in maximal Ca^{2+} store release in P_S+P_N cells (0.17 ± 0.002 FRUs) compared to P_S cells (P<0.001****). Taking this change in Ca^{2+} store release into account, maximal SOCE was down-regulated by 32.68% in P_S+P_N cells (0.39 ± 0.03 FRUs) compared to P_S cells. There was no difference in maximal Ca^{2+} store release between P_S and P_S+D_N cells (0.13 ± 0.004 FRUs, P=0.789) and maximal SOCE was reduced by 98.04% in P_S+D_N cells (0.01 ± 0.04 FRUs) compared to P_S cells (P<0.0001****). Compared to D_S cells, there was a 21.51% decrease in maximal Ca^{2+} store release in P_S+D_N cells (P<0.0001****) and, taking this change in Ca^{2+} store release into account, maximal SOCE was reduced by 90.13%. There was no difference in maximal Ca^{2+} store release in D_S+D_N cells (0.13 ± 0.005 FRUs) compared to P_S cells and maximal SOCE was reduced by 51.74% in D_S+D_N cells (0.23 ± 0.04 FRUs, P<0.0008***). Maximal Ca^{2+} store release in D_S+D_N cells was reduced by 21.43% compared to that of D_S cells (P<0.0001****) and, taking this this change in Ca^{2+} store release into account, maximal SOCE was increased by 1.5 fold. **(B)** There was an 18.18% increase in rate of Ca^{2+} store release (P=0.003) and a 19.70% decrease in rate of SOCE (P=0.003) in D_S cells compared to P_S cells. There was a 41.29% increase in rate of Ca^{2+} store release (P<0.0001) and 55.12% decrease in rate of SOCE (P<0.0001) in P_S+P_N cells compared to P_S cells. There was no difference in rate of Ca^{2+} store release (P=0.404) or rate of SOCE (P=0.071) in P_S+D_N cells compared to P_S cells. There was no difference in rate of Ca^{2+} store release (P=0.143) and a 40.74% increase in rate of SOCE (P<0.0001) in P_S+D_N cells compared to D_S cells. There was a 15.66% increase in rate of Ca^{2+} store release (P=0.017) and 22.73% increase in rate of SOCE (P=0.0004) in D_S+D_N cells compared to P_S cells. There was no difference in rate of Ca^{2+} store release (P=0.986) or rate of SOCE (P=0.981) in D_S+D_N cells compared to D_S cells. **(C)** There was no change in Ca^{2+} store release decline rate (P=0.863) between P_S cells and D_S cells. There was a decrease in total and late SOCE decline rate (by 15.42% and 80.29%, respectively) and a 66.64% increase in initial SOCE decline rate in D_S cells compared to P_S cells (all P<0.0001). Ca^{2+} store release decline rate was reduced by 8.53% in P_S+P_N cells compared to P_S cells (P=0.037). Total and late SOCE decline rate were reduced by 21.34% and 75.88% respectively whilst initial SOCE decline was increased by 50.18% in P_S+P_N cells

compared to P_S cells (all P<0.0001). Ca^{2+} store release decline rate was reduced by 12.39% in P_S+D_N cells compared to P_S cells (P=0.0006). Total and late SOCE decline rate were reduced by 8.51% (P=0.042) and 51.84% (P<0.0001) respectively whilst initial SOCE decline rate was increased by 55.72% (P<0.0001) in P_S+D_N cells compared to P_S cells. Ca^{2+} store release decline rate was reduced by 9.37% (P=0.021) and late SOCE decline rate was increased by 1.5 fold (P<0.0001) in P_S+D_N cells compared to D_S cells. There was no difference in total or initial SOCE decline rate (P=0.134 and P=0.425) between P_S+D_N cells and D_S cells. Ca^{2+} store release decline rate and total SOCE decline rate were significantly reduced in D_S+D_N cells compared to P_S cells (25.74% and 26.95%, respectively, both P<0.0001). The initial SOCE decline rate was increased by 26.19% in D_S+D_N cells compared to P_S cells (P=0.003) whilst late SOCE decline rate was reduced by 70.17% (P<0.0001). Ca^{2+} store release decline rate, total and initial SOCE decline rate were significantly reduced in D_S+D_N cells compared to D_S cells (by 23.18%, P<0.0001, 13.63%, P=0.004 and 24.27%, P<0.0001, respectively). The late SOCE decline rate was increased by 51.34% (P=0.021) in D_S+D_N cells compared to D_S cells.
P_S: n=345, D_S: n=379, P_S+P_N: n=682, P_S+D_N: n=605, D_S+D_N: n=373. N=3.

Chapter 4: Discussion

It has previously been shown that 9*c*RA-induced differentiation of N-type populations induces down-regulation of SOCE which does not occur in S-type populations (N. Bell 2013). The aim of this chapter was to investigate the Ca^{2+} signalling responses of the cell phenotypes underlying these populations and determine the effects of the predominant cell environment on minority cell responses using single cell Ca^{2+} analysis to study relative changes in the extent and dynamics of the Ca^{2+} store release and SOCE response.

An uncoupling of Ca^{2+} store release and SOCE occurred in differentiating N-type populations, correlating with previous findings (Brown 2005; N. Bell 2013). N-type cells differentiate towards a neuronal phenotype and it has been shown that the SOCE response that is present in proliferating cells is dampened with neuronal differentiation. SOCE was found to be necessary for adult neural progenitor cell proliferation (Li 2012) and there was a reduction in voltage-independent Ca^{2+} entry and an increase in TG-sensitive Ca^{2+} ATPase activity in differentiating neurons compared to proliferating progenitors isolated from embryonic rat cortex (Maric 2000). Similarly, differentiation of neural stem cells of the neuroepithelium to neuronal cells involves a down-regulation of SOCE, which is replaced with voltage-operated channel activity (Yamashita 2013). Voltage-operated channel activity was also shown to increase as SOCE decreased in neurons derived from mouse embryonic stem cells (Hao 2014). These results show that SOCE is present in proliferating neural progenitors and is dampened with differentiation towards a neuronal phenotype, as has been shown in this study. However, there is some evidence to suggest that an increase in SOCE is associated with the initial differentiation response (Wu 2004; Shin 2010; Hao 2014) and this will be investigated in a subsequent chapter (Chapter 6: Differentiation time-course).

An uncoupling of Ca^{2+} store release and SOCE also occurred with differentiation of S-type populations, and actually to a greater extent than that seen in N-type populations, in contrast to previous findings that uncoupling does not occur in S-type populations (N. Bell 2013). The reasons for this contrast with previous findings are

unclear. One possibility is that the variability seen in S-type responses has affected the overall population response between investigations. Indeed, the Ca signals observed in S_O, S_A and S_E cells demonstrate the extent of variability underlying the Ca^{2+} signals observed at the population level. Of course, these results also raise the possibility that the current S-type populations are simply behaving in a different manner to that previously observed. An important point to note, however, is that SOC protein expression is consistent with the SOCE responses of both the N-type and S-type population, as will be discussed in a later chapter (Chapter 5: SOCE machinery).

It is noteworthy that there was a slight decrease in Ca^{2+} store release in differentiating N-type populations whereas in S-type populations, Ca^{2+} store release was significantly increased with differentiation. Previously, Ca^{2+} store release was unchanged with N-type and S-type differentiation (N. Bell 2013). The changes observed in this study suggest that the capacity of the Ca^{2+} store may be altered or there might be a change in sensitivity to TG with differentiation. Bcl-2 expression has previously been associated with changes in Ca^{2+} store release. Bcl-2 is able to bind to IP_3Rs, enhancing sensitivity, so that resting levels of $InsP_3$ induced channel opening and thereby increased release of Ca^{2+} from internal stores at rest (Li 2007; Eckenrode 2010). This lead to a reduction in TG-stimulated Ca^{2+} store size and was associated with apoptotic resistance (Li 2007; Eckenrode 2010), consistent with the increase in Bcl-2 expression (Results 3.3) and reduction in Ca^{2+} store release in differentiating N-type populations observed in this study. Bcl-2 up-regulation with differentiation of N-type populations has previously been associated with lability of caffeine-sensitive ER Ca^{2+} store depletion (Riddoch 2007). Bcl-2 expression has also been shown to decrease activity of the SERCA pump (Dremina 2004) and increase ER membrane Ca^{2+} permeability leading to a reduction in TG-stimulated Ca^{2+} store release (Foyouzi-Youssefi 2000; Pinton 2000). Therefore the increase in Bcl-2 expression in differentiating N-type populations may explain the reduced Ca^{2+} store release observed in this study and down-regulated Bcl-2 expression in differentiating S-type populations may explain the increased Ca^{2+} store release observed. Additionally, up-regulation of Bcl-2 expression causes a down-regulation in SOCE activity in HeLa cells and prostate cancer epithelial cells (Pinton 2000; Abeele 2002). Bcl-2 expression was up-regulated with differentiation of N-type

populations but slightly down-regulated with differentiation of S-type populations, yet SOCE was down-regulated in both cases, suggesting that, potentially, the mechanisms underlying the down-regulation of SOCE with differentiation may not be the same in N-type and S-type populations.

Within N-type and S-type populations, there are always N-type, S-type and I-type cells present, regardless of extent of enrichment (Introduction 1.3 and Methods 2.3), and these cells are known to transdifferentiate in culture, both of which are important points to consider when examining cell population responses. A major benefit of adopting the single cell imaging technique is that specific Ca^{2+} responses can by identified and attributed to each cell phenotype within a population, therefore the Ca^{2+} responses of the cell phenotypes underlying the population responses were extracted and analysed from the previous population data. It was clear that an uncoupling of Ca^{2+} store release and SOCE occurred in all cell types grown within an N-type or an S-type population yet there were distinct differences in the Ca^{2+} signalling responses and extent of SOCE down-regulation between the two environments.

Within an N-type population, the Ca^{2+} signalling profile of N-type cells reflect that which was observed at overall N-type population level. The extent of Ca^{2+} store release was slightly reduced with differentiation and SOCE was down-regulated by 53%, with an increase in SOCE activation and deactivation rate, leading to a dampened and shortened SOCE response with differentiation. However, N-type cells within an S-type population exhibited Ca^{2+} store release that was significantly increased by 65% and SOCE was down-regulated by 68% with differentiation, reflecting that which was seen at the S-type population level. This indicates that N-type Ca^{2+} signalling responses are either influenced by the surrounding cell population or that N-type cells influence the population level response, regardless of whether they are the minority phenotype. By resolving the responses of the S-type and I-type cells, the explanation for these results becomes clearer.

S-type cells grown within both an N-type population and an S-type population maintain the same extent of Ca^{2+} store release with differentiation and SOCE is down-

regulated by a slighter greater extent in differentiating S-type populations (68%) compared to differentiating N-type populations (60%). The rate of SOCE activation is unaltered whilst rate of SOCE deactivation is reduced by a greater extent in differentiating S-type populations (23%) compared to differentiating N-type populations (15%). The S-type cell SOCE response is therefore dampened but deactivated at a slower rate with differentiation in both N-type and S-type predominant environments. These results indicate that the S-type cell response is not greatly influenced by the surrounding cell population like that seen in N-type cells. These responses also suggest that the N-type cell response is influenced by the surrounding cell population and has driven the increase in Ca^{2+} store release observed at the S-type population level.

I-type cells in an N-type population exhibit significantly increased Ca^{2+} store release (51%) with differentiation with an increase in rate of activation and emptying which is different to that seen in both N-type and S-type cells and at the N-type population level. SOCE was down-regulated by a greater extent (63%) than that observed at the N-type population level (54%) and rate of SOCE activation and deactivation were increased (by 50% and 40%, respectively) to a greater extent than that of N-type and S-type cells within a differentiating N-type population, indicating that the I-type SOCE response is much faster and shorter with differentiation of N-type populations. In contrast, however, I-type cells grown in an S-type predominant environment have no change in Ca^{2+} store release with differentiation and, whilst the extent of SOCE down-regulation was similar to that in differentiating S-type populations, the extent of the increase in rate of SOCE activation was less (32%) and rate of SOCE deactivation was reduced (by 22%), indicating a dampened but extended I-type SOCE response in differentiating S-type populations.

Taken together, these results indicate that N-type and I-type cells, but not S-type cells, exhibit a plasticity in their Ca^{2+} signal responses with differentiation that is influenced by the predominant cell phenotype in the surrounding environment. Given that spontaneous transdifferentiation occurs in these cells in culture (Biedler 1975; Ross 1983; Ciccarone 1989), this Ca^{2+} signal plasticity may be indicative of events associated

with phenotypic interconversion that are induced by the surrounding predominant cell phenotype. This conclusion is in line with the speculation that I-type cells represent a stem cell population within SH-SY5Y cell line (Ciccarone 1989; Ross 1995) and therefore may be more flexible in changing their differentiation response according to environmental influence. The dependency of phenotype-specific differentiation responses on the surrounding cellular environment may represent an intrinsic change in a particular phenotypic behaviour to cause it to differentiate towards the phenotype of the predominant cell type. This could be caused by factors released extracellularly by the predominant phenotype or through local cell-cell interactions and influences.

The S-phenotype consists of three sub-phenotypes (S_O, S_A and S_E) that may be indicative of S-type sub-populations (Chapter 1: Introduction). The Ca^{2+} responses of these sub-phenotypes were therefore extracted and analysed from the previous N-type and S-type population data. Within an S-type population, the overall S-type cell response with differentiation involves no change in extent or rate of Ca^{2+} store release and a down-regulation of SOCE by 68%, with a 23% decrease in deactivation rate but no change in SOCE activation rate. There were subtle differences in rates of activation and deactivation of Ca^{2+} store release and SOCE in S_O, S_A and S_E cells, however the overall maintenance of Ca^{2+} store release extents SOCE down-regulation were similar in all three sub-phenotypes and reflected that seen in S-type compartment of the S-type population response, with S_A cells exhibiting a greater extent of SOCE down-regulation (73%). The extent of change in the S-type cell differentiation response is similar when grown in N-type populations, however, the underlying S_O S_A and S_E cells exhibit more variability in their responses. Specifically, S_A cells and S_E show a reduction in Ca^{2+} store release (by 22% and 42%, respectively) whilst S_O show a 17% increase, driving the overall response to exhibit unchanged Ca^{2+} store release with differentiation. All three sub-phenotypes exhibit SOCE down-regulation but the S_A cells exhibit the least extent of down-regulation (53%) in a differentiating N-type population in contrast to that seen in S-type populations. Also, S_E cells show a considerable decrease in rate of SOCE deactivation compared to S_O and S_A cells. This shows that S-type cells also exhibit plasticity in their Ca^{2+} signal response with differentiation dependent on the environment in which they are grown and that this plasticity is

masked when considering the overall S-type compartment. S-type sub-populations grown within N-type predominant environments also exhibit more variability in their responses. Collectively, these results further highlight the variability in Ca^{2+} signal responses underlying those seen at the population level, and may therefore explain the differing observations from S-type populations in Bell et al (2013), and reinforce the notion that the surrounding cell environment can affect the differentiation response of minority phenotypes.

The possibility that the predominant cell phenotype in a population could release factors extracellularly that can influence the differentiation response of minority phenotypes was therefore investigated through experiments involving media from proliferating and differentiating S-type populations being applied to N-type populations whilst media from proliferating or differentiating N-type populations was applied to S-type populations.

In N-type populations, uncoupling of store release and SOCE occurred with differentiation, confirming previous findings (Results 4.2). Proliferating S-type media partly maintained the proliferating N-type response whilst applying differentiating S-type media to proliferating N-type populations induced a response similar to that of differentiating N-type populations. Differentiating N-type populations alongside application of differentiating S-type media resulted in a dampened differentiating response and dampened the effect of just applying differentiating S-type media.

In S-type populations, uncoupling of store release and SOCE occurred with differentiation, confirming previous findings (Results 4.2). Both proliferating N-type media and differentiating N-type media induced a dampened differentiating response in proliferating S-type, although SOCE down-regulation occurred to a lesser extent than what was observed in differentiating S-type populations. Differentiating S-type populations alongside application of differentiating N-type media did not induce a fully differentiating response but brought the cells closer to a differentiating response than that seen with just differentiating N-type media application.

Taken together, these results confirm that there is an effect of media application on the Ca^{2+} response of the other phenotype, suggesting that the predominant phenotype within the cell environment may be releasing factors that can influence the Ca^{2+} responses associated with differentiation and, potentially, transdifferentiation.

It is currently unclear whether the down-regulation of SOCE in all differentiating environments is caused by partial SOCE down-regulation and reduced function in all differentiating cells or if differentiating cells fully suppress their SOCE response and the observed SOCE that remains is caused by proliferating cell that are unresponsive to the differentiating agent. Although out of the scope of this study, this can now be investigated in our laboratory through re-analysis of the single cell data that has been collected, by pairing of individual cell SOCE responses with the extent of N-type cell neurite outgrowth or S-type cell diameter as morphological markers of differentiation (Final Discussion 7.2).

A likely explanation for the down-regulation of SOCE observed here is a change in expression or function of, or a lack of, SOCE machinery components. It was previously observed that N-type differentiation-induced down-regulation of SOCE is accompanied by reduced expression of both the Ca^{2+} sensing protein, STIM1 and the CRAC channel protein Orai1, both of which were expressed in proliferating N-type cells with a robust SOCE response (N. Bell 2013). It was also shown that both proliferating and differentiating S-type cells expressed STIM1 and Orai1 alongside a robust SOCE response (N. Bell 2013). To confirm that the differentiation-associated SOCE down-regulation observed in this study could be attributed to a potential alteration in Orai1, the effect of treatment with the CRAC inhibitor BTP2 was investigated (Appendix I). Treatment of proliferating N-type populations with varying concentrations (100 nM – 20 μM) of BTP2 for 24 hours induced a drastically significant down-regulation of SOCE activity, confirming that the SOCE-downregulation observed here could in fact be due to potential dampening of Orai1 function (Appendix). The expression and localisation of the SOCE-associated proteins STIM1 and Orai1 has therefore been investigated further in this study (Chapter 5: SOCE machinery and Chapter 6: Differentiation time-course).

Additionally, RNAseq analysis was performed in proliferating and differentiating N-type populations under a collaboration with Professor Caroline Austin and Lauren Harkin. The preliminary data for overall gene expression, genes of interest that include markers discussed in chapter 3 and those associated with Ca^{2+} signalling and the SOCE response discussed in this chapter and chapter 5 as well as calcium signalling pathway analysis are presented in Appendix II.

Chapter 5: SOCE machinery

Chapter 5 -Introduction

The proteins STIM1, Orai1 and TRPC1 have been shown to be involved in SOCE (Introduction). Dampened SOCE activity was associated with differentiation of N-type and S-type populations in this study (Chapter 4) therefore this chapter aimed to investigate the expression of SOCE associated proteins in the 9*c*RA-induced differentiation response.

All experiments in this chapter were performed on N-type or S-type populations that had been treated for 7 days with 1 µM 9*c*RA (differentiating) or an equivalent volume of EtOH as a control (proliferating). Proliferating N-type and S-type populations will be referred to as P_N and P_S, respectively, whilst differentiating N-type and S-type populations will be referred to as D_N and D_S, respectively.

Chapter 5 – Results

5.1 Expression of three key SOCE proteins; STIM1, Orai1 and TRPC1, is altered with differentiation of N-type and S-type populations

The Ca^{2+} sensing protein STIM1 alters gating of SOCs at the PM to induce Ca^{2+} entry and replenish depleted ER Ca^{2+} stores (Hoover 2011; Sauc 2015). STIM1 was expressed by both proliferating and differentiating N-type and S-type populations (Figure 5.1.1A). Expression of STIM1 was 36% higher in P_S populations than P_N populations (P=0.045, Figure 5.1.1B). Overall STIM1 expression was down-regulated by 18% in D_N populations and D_S populations compared to P_N and P_S populations but quantitatively, this was not significant (P=0.211 and P=0.232, respectively, Figure 5.1.1B). However, two scenarios of STIM1 expression were observed in D_N and D_S populations. In some cases, there was a down-regulation of STIM1 expression (Figure 5.1.1Ai) and in others, STIM1 was expressed at a slightly higher molecular weight, as detected by a slight upward band shift (Figure 5.1.1Aii). This shift in molecular weight could be indicative of the presence of a different isoform of STIM1 or of phosphorylation events or some other post-translational modification that could alter STIM1 function. Both scenarios could contribute to the dampened SOCE activity observed in D_N and D_S populations and

indicate that STIM1 is involved in SOCE in N-type and S-type populations. Occasionally, STIM1 expression could be observed as a double band (Figure 5.1.1Aiii), though this was not always present and could not be associated solely with proliferation or differentiation or with either either phenotype. This further indicates that STIM1 may exist in multiple states that could affect its function and thereby SOCE activity.

Orai1 is a PM protein that forms the SOC channel pore and is gated by STIM1 for SOCE regulation (Demuro 2011; Hoover 2011; Mignen 2008). Orai1 was expressed by both proliferating and differentiating N-type and S-type populations (Figure 5.1.2A) and was significantly down-regulated by 44% in D_N populations compared to P_N populations (P=0.037) and by 69% in D_S populations compared to P_S populations (P=0.003, Figure 5.1.2B). This down-regulation would likely contribute to the dampened SOCE observed in D_N and D_S populations. The extent of SOCE down-regulation was 54% in N-type populations and 66% in S-type populations (Section 4.2), which is consistent with the extent of Orai1 down-regulation and indicates that Orai1 is involved in SOCE in N-type and S-type populations. Orai1 expression was 26% lower in P_S populations than P_N populations (P=0.252) which may, at least in part, explain the lower Ca^{2+} permeability found in S-type predominant populations (Results 4.2).

TRPC1 channels are Ca^{2+} permeable and, through STIM1 interactions, may function as a SOCs (Alicia 2008; Jardin 2008; Yuan 2007). TRPC1 was expressed in both proliferating and differentiating N-type and S-type populations but there was no significant difference in TRPC1 expression between P_N and P_S populations (P=0.823, Figure 5.1.3A and B). TRPC1 was down-regulated by 36% in D_N populations compared to P_N populations (P=0.451) and by 27% in D_S populations compared to P_S populations (P=0.702) though non-significantly (Figure 5.1.3B). TRPC1 expression was however, highly variable and unfortunately, the TRPC1 antibody was unreliable.

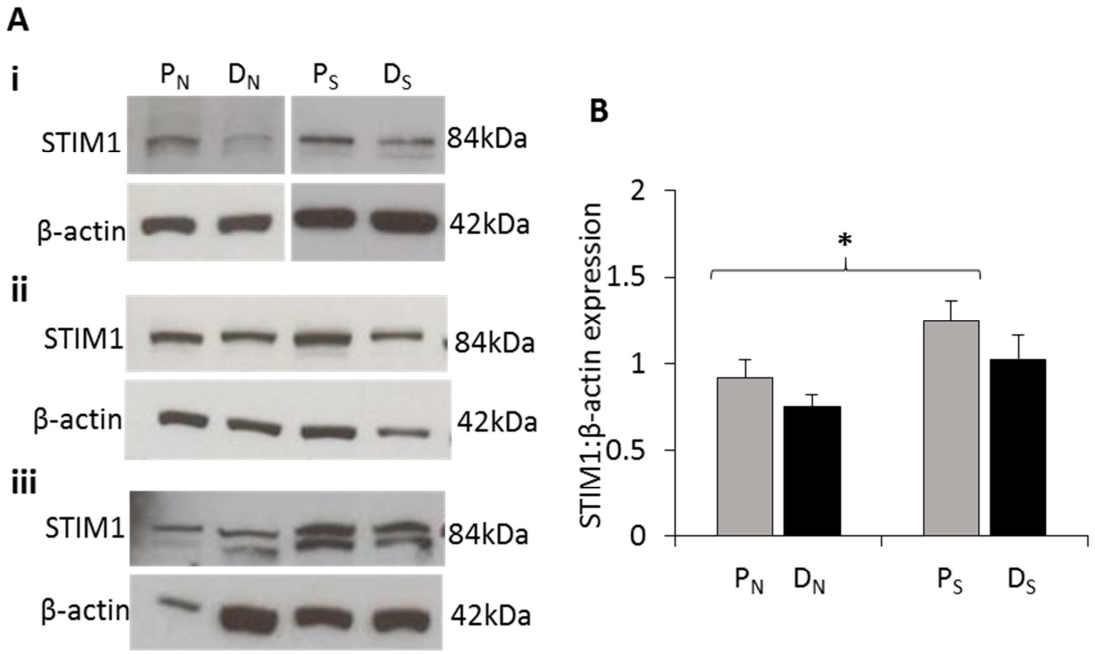

Figure 5.1.1. STIM1 expression is down-regulated or modified with differentiation of N-type and S-type populations

Western blots were performed on protein samples from N-type and S-type populations that were treated for 7 days with 1 µM 9*c*RA (D_N and D_S respectively, differentiating) or an equivalent volume of EtOH (P_N and P_S respectively, proliferating). Blots were probed with anti-STIM1 antibody which detected a band at 84 kDa and β-actin antibody which was used as a loading control and detected a band at 42 kDa. Quantitative band measurements were performed using densitometry in ImageJ. **(A)** STIM1 was expressed in both proliferating and differentiating N-type and S-type populations. STIM1 expression was **(A.i)** down-regulated in some D_N and D_S populations compared to P_N and P_S populations or **(A.ii)** was expressed at a slightly higher molecular weight isoform in other D_N and D_S populations compared to P_N and P_S populations. **(A.iii)** STIM1 expression was occasionally observed as a double band though this was not associated solely with differentiation or phenotype. **(B)** STIM1 expression was down-regulated by 18% in D_N populations and D_S populations compared to P_N and P_S populations, but this was not significant (P=0.211 and P=0.232, respectively). STIM1 expression was 36.16% higher in P_S populations compared to P_N populations (P=0.045*). For N-type populations N=14, for S-type populations N=12.

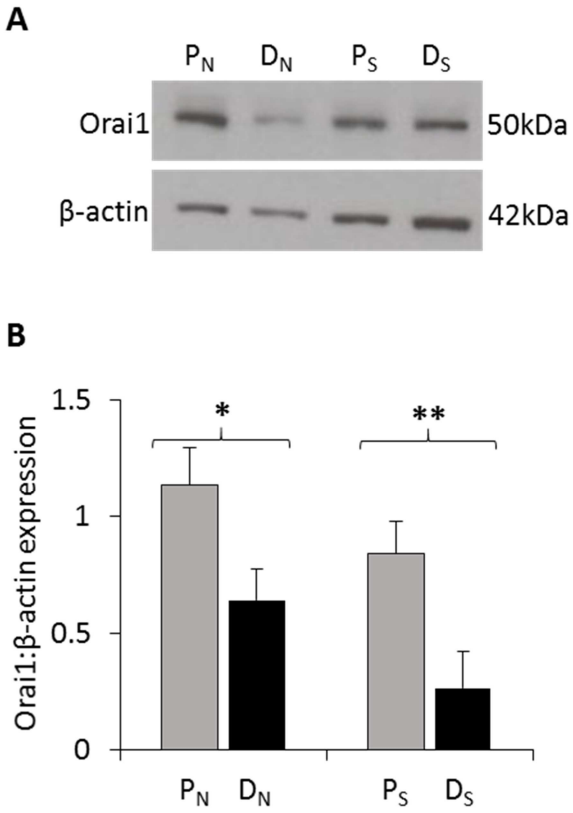

Figure 5.1.2 Orai1 expression is down-regulated with differentiation of N-type and S-type populations

Western blots were performed on protein samples from N-type and S-type populations that were treated for 7 days with 1 µM 9*c*RA (D_N and D_S respectively, differentiating) or an equivalent volume of EtOH (P_N and P_S respectively, proliferating). Blots were probed with anti-Orai1 antibody which detected a band at 50 kDa and β-actin antibody which was used as a loading control and detected a band at 42 kDa. Quantitative band measurements were performed using densitometry in ImageJ. **(A)** Orai1 was expressed in both proliferating and differentiating N-type and S-type populations. Orai1 band intensity was reduced in D_N and D_S populations compared to P_N and P_S populations. **(B)** Orai1 expression was significantly down-regulated by 43.50% in D_N populations compared to P_N populations (P=0.037*) and by 68.90% in D_S populations compared to P_S populations (P=0.003**). Orai1 expression was 25.84% higher in P_N populations than P_S populations, though this was not significant (P=0.252). For N-type populations N=7, for S-type populations N=4.

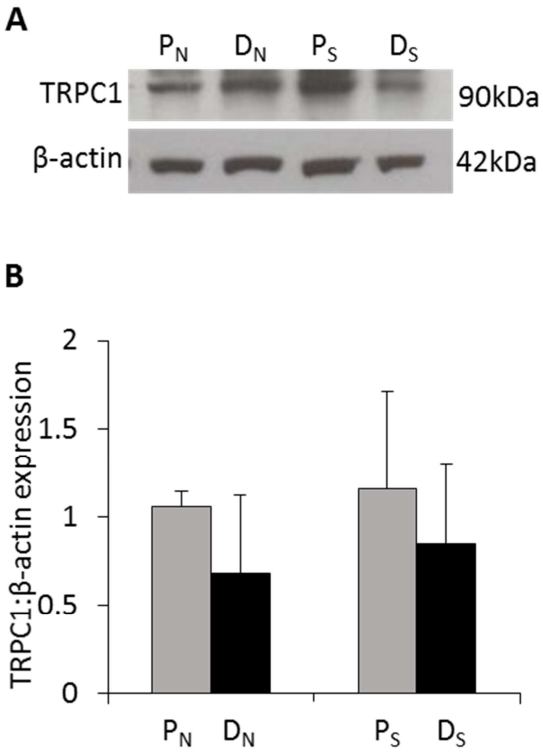

Figure 5.1.3 TRPC1 expression is variable with differentiation of N-type and S-type populations

Western blots were performed on protein samples from N-type and S-type populations that were treated for 7 days with 1 µM 9*c*RA (D_N and D_S respectively, differentiating) or an equivalent volume of EtOH (P_N and P_S respectively, proliferating). Blots were probed with anti-TRPC1 antibody which detected a band at 90 kDa and β-actin antibody which was used as a loading control and detected a band at 42 kDa. Quantitative band measurements were performed using densitometry in ImageJ. **(A)** TRPC1 was expressed in both proliferating and differentiating N-type and S-type populations. **(B)** TRPC1 expression was down-regulated, although not significantly, by 35.92% in D_N populations compared to P_N populations (P=0.451) and by 26.96% in D_S populations compared to P_S populations (P=0.702). There was no significant difference in the level of TRPC1 expression between P_N and P_S populations (P=0.823). For N-type populations N=3, for S-type populations N=2.

5.2. Localisation of STIM1 and Orai1 is altered with differentiation of N-type and S-type populations

Since the expression of STIM1 and Orai1 were altered with differentiation of N-type and S-type populations, localisation of these SOCE proteins in the differentiation response were investigated.

There was widespread expression of STIM1 throughout the cytoplasm and neurites of P_N cells and there was evidence of localisation into foci (Figure 5.2.1A). There was a similar expression pattern in D_N cells although there appeared to be an increased occurrence of STIM1 clustering (Figure 5.2.1B). STIM1 was present throughout P_S cells and D_S cells, with no apparent areas of clustering, however there were clear examples of D_S cells with an accumulation of STIM1 at the cell membrane (Figure 5.2.1C and D). There was no obvious change in the overall intensity of fluorescence of STIM1 between proliferating and differentiating cells, consistent with the extent of expression (Results 5.1). Clearly, these changes in localisation of STIM1 with differentiation of N-type and S-type populations may affect STIM1 function and its ability to contribute to SOCE activity.

Orai1 was expressed throughout the cytoplasm and neurites of P_N and D_N cells and formed foci in P_N cells and, seemingly less frequently, in D_N cells (Figure 5.2.2A and B). There was diffuse expression of Orai1 in P_S and D_S cells and Orai1 formed foci in P_S cells that were more dispersed and granular in D_S cells (Figure 5.2.2C and D). Although these changes in Orai1 localisation with differentiation are subtle, they may affect the extent of SOCE activity.

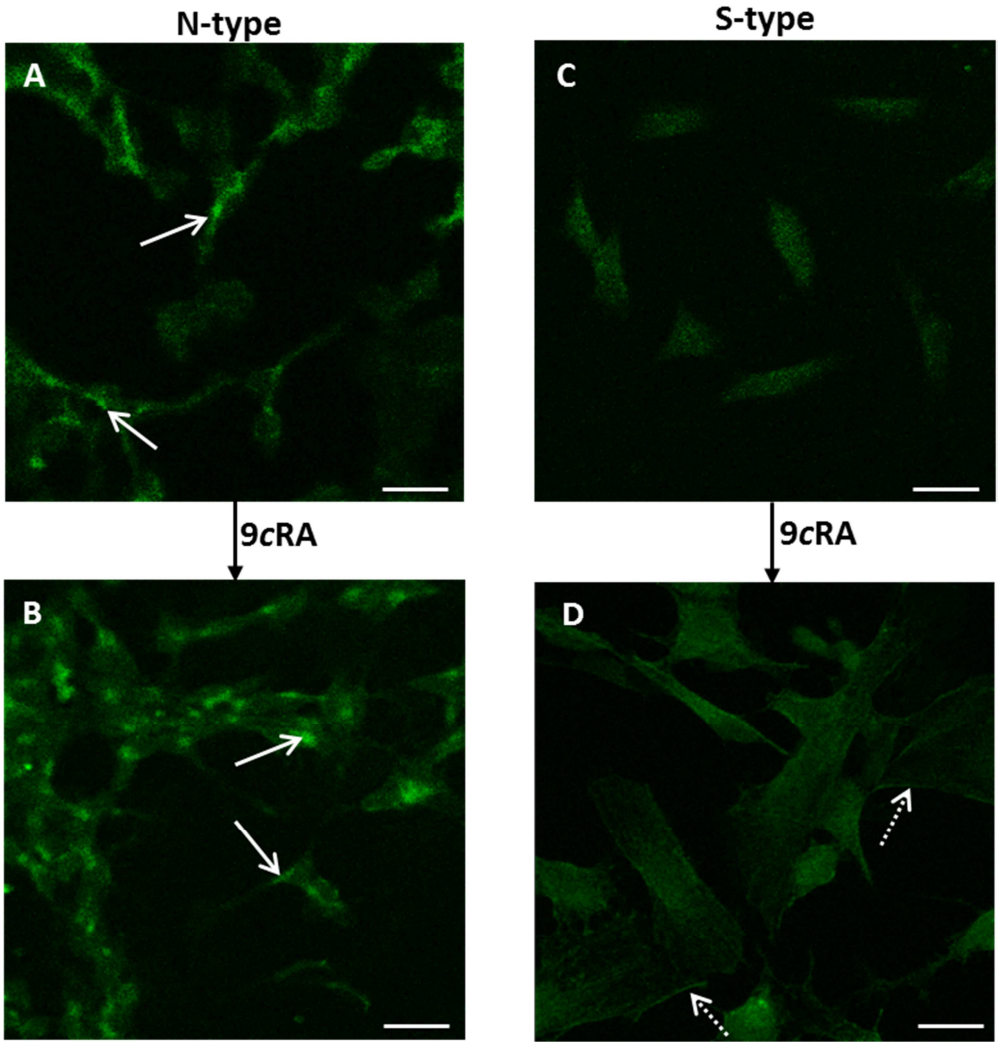

Figure 5.2.1. STIM1 expression is diffuse in proliferating N-type and S-type cells and localises into clusters in differentiating N-type cells and at the membrane of S-type cells

N-type and S-type populations were treated for 7 days with 1 µM 9*c*RA (D_N and D_S, respectively) or an equivalent volume of EtOH (P_N and P_S, respectively) and cells were stained with anti-STIM1 primary antibody followed by FITC-conjugated secondary antibody. Images were captured using laser scanning confocal microscopy. **(A)** In P_N cells, STIM1 was present throughout the cell and neurite like processes and there were some examples of localisation into foci (white arrows) and in **(B)** D_N cells there appeared to be a higher occurrence of STIM1 clustering (white arrows). **(C)** In P_S cells, STIM1 was present throughout the cell, with no apparent areas of clustering and in **(D)** D_S cells STIM1 was present throughout the cell however, there were clear examples of cells that expressed higher levels of STIM1 at the cell membrane (dashed arrows).

Scale bars represent 20 µm. Images are representative of >20 images and taken using a x63 objective. N=5.

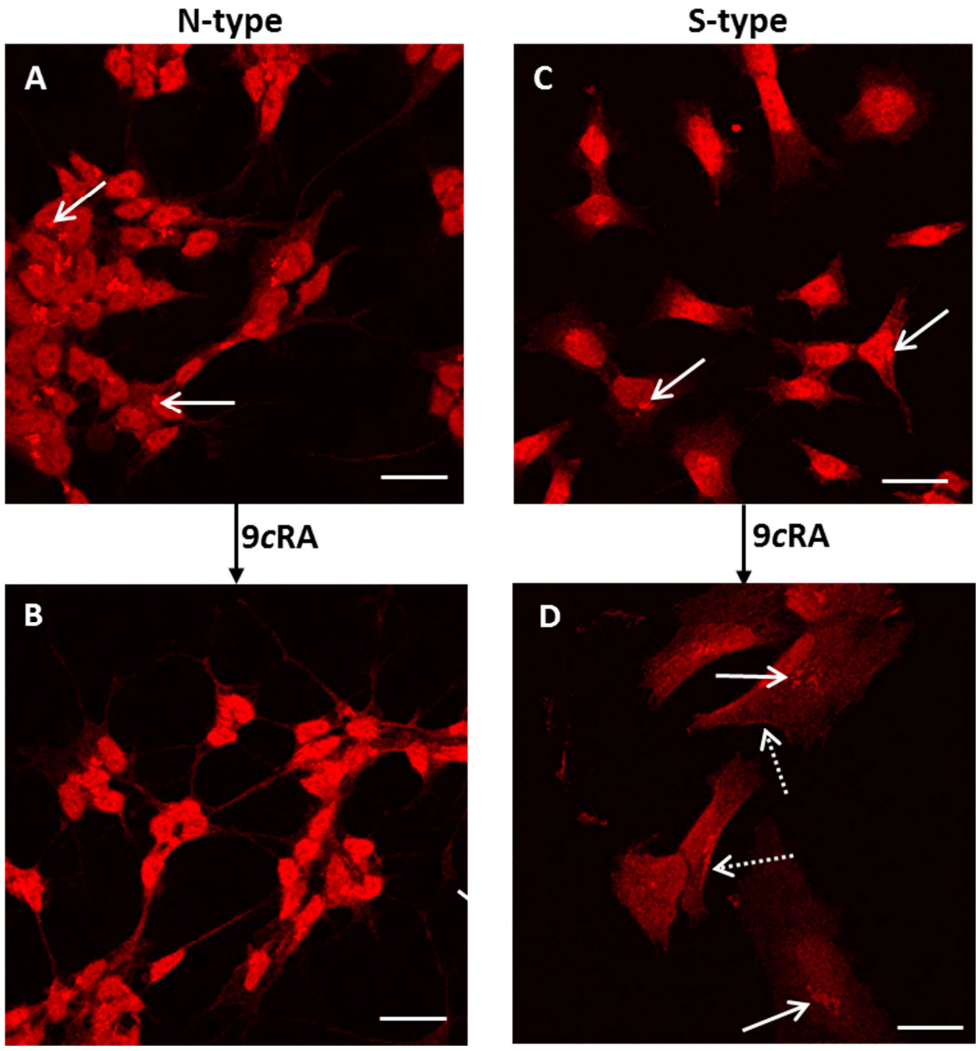

Figure 5.2.2. Orai1 localisation is altered with differentiation of N-type and S-type cells

N-type and S-type populations were treated for 7 days with 1 µM 9*c*RA (D_N and D_S, respectively) or an equivalent volume of EtOH (P_N and P_S, respectively) and cells were stained with anti-Orai1 primary antibody followed by TRITC-conjugated secondary antibody. Images were captured using laser scanning confocal microscopy. **(A)** In P_N cells, Orai1 was present throughout the cell and there were some examples of localisation into foci (white arrows) and in **(B)** D_N cells there appeared to be a less occurrence of Orai1 clustering (white arrows). **(C)** In P_S cells, there was some localisation of Orai1 into clusters arranged close to the cell nucleus (white arrows) and in **(D)** D_S cells some Orai1 clustering was present but this appeared more dispersed (white arrow) than in proliferating S-type cells. Some cells were observed to have an accumulation of Orai1 at the cell membrane (dashed arrow). Scale bars represent 20

µm. Images are representative of >20 confocal images and taken using a x63 objective. N=5.

5.3. Localisation of STIM1 is altered following Ca^{2+} store depletion and SOCE in N-type cells but not S-type cells

STIM1 localisation was altered with differentiation of N-type and S-type cells (Results 5.2). Given the role of STIM1 in regulating SOCE, that SOCE activity was dampened in differentiating N-type and S-type cells (Results 4.2) and that expression as well as localisation of STIM1 were altered with differentiation of N-type and S-type cells, localisation of STIM1 over the Ca^{2+}-addback time-course was investigated.

At a resting state, there was widespread expression of STIM1 throughout the cytoplasm and neurites of P_N cells and there was evidence of localisation into foci (Figure 5.3.1A). Following TG exposure there was a similar distribution of STIM1 expression and occurrence of STIM1 clustering (Figure 5.3.1B and C) whilst upon Ca^{2+}-addback, STIM1 expression became more diffuse, with minimal clustering (Figure 5.3.1 D and E), indicating that there may be a redistribution of STIM1 following SOCE and Ca^{2+} store replenishment. In D_N cells at rest, STIM1 was expressed throughout the cell and neurites and there were many examples of STIM1 clustering (Figure 5.3.2A). Following TG exposure and Ca^{2+}-addback, there was a similar occurrence of STIM1 clustering (Figure 5.3.2B-E), suggesting that differentiation of N-type cells may prevent STIM1 redistribution following Ca^{2+} store replenishment.

At rest, STIM1 was expressed diffusely throughout P_S cells (Figure 5.3.3A). Following TG exposure and Ca^{2+}-addback, there was a similar diffuse expression of STIM1 with some evidence of STIM1 localisation at the cell membrane, though this was minimal (Figure 5.3.3B-E). In D_S cells, STIM1 was present throughout the cell and there were examples STIM1 accumulation at the membrane that remained following TG and $CaCl_2$ exposure (Figure 5.3.4). These results indicate that the distribution of STIM1 is not altered during Ca^{2+} store release and SOCE in S-type cells.

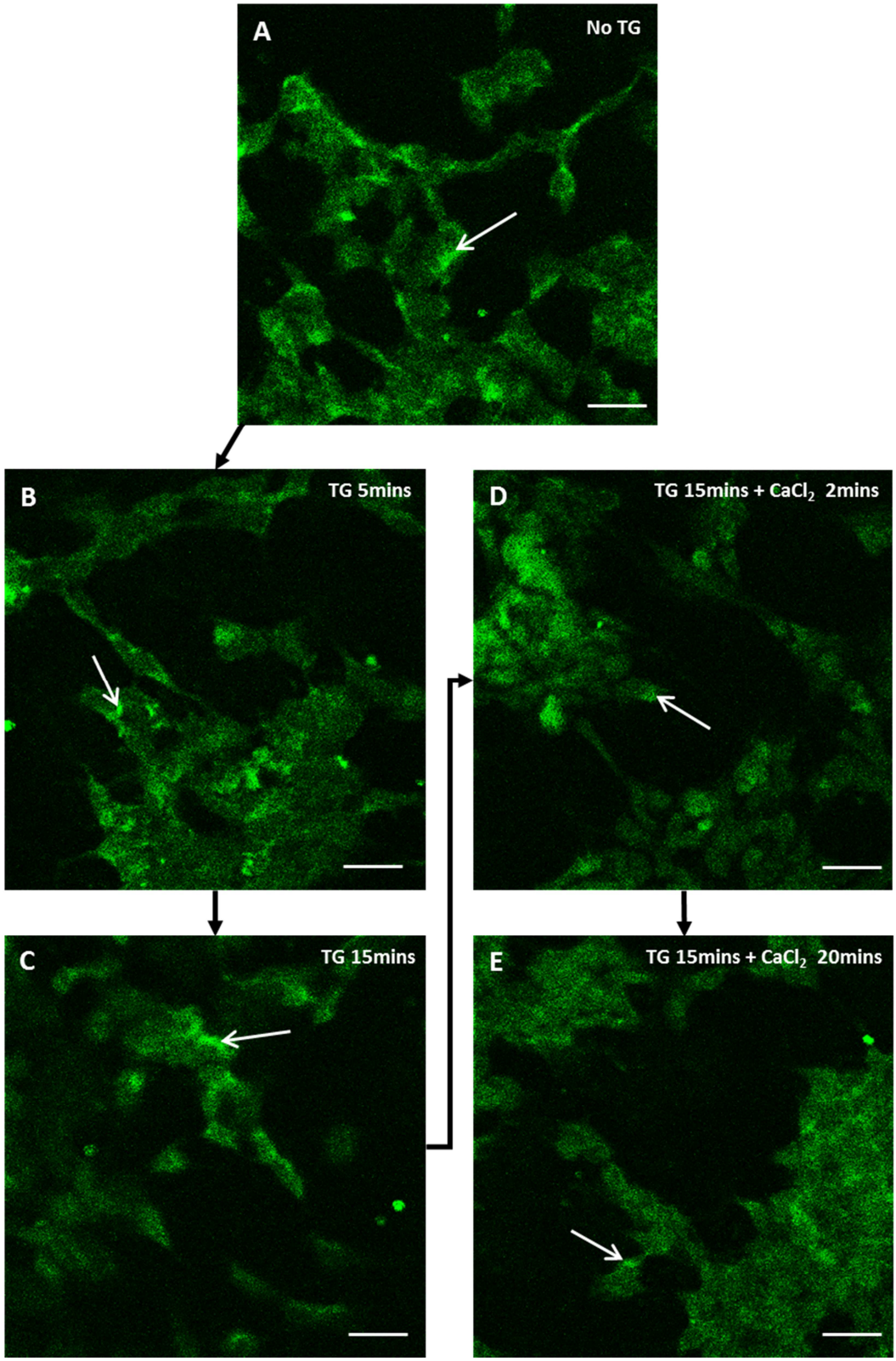

Figure 5.3.1. STIM1 becomes more diffuse in proliferating N-type cells over the Ca^{2+} add-back time-course

Proliferating N-type populations (P_N, EtOH treated for 7 days) were exposed to 200 nM thapsigargin (TG) for 15 minutes to induce Ca^{2+} store release followed by exposure to 2

mM $CaCl_2$ for 20 minutes to induce SOCE. Cells were fixed at various time-points throughout and stained with anti-STIM1 primary antibody followed by FITC-conjugated secondary antibody. Images were captured using laser scanning confocal microscopy. **(A)** In P_N cells, STIM1 was present throughout the cell and there were some examples of localisation into foci (white arrows). Following TG exposure for **(B)** 5 minutes and **(C)** 15 minutes, there was a similar occurrence of STIM1 clustering (white arrows). Following $CaCl_2$ exposure for **(D)** 2 minutes and **(E)** 20 mins, STIM1 expression became more diffuse, with minimal clustering (white arrows). Scale bars represent 20 μm. Images are representative of >15 images and taken using a x63 objective. N=3.

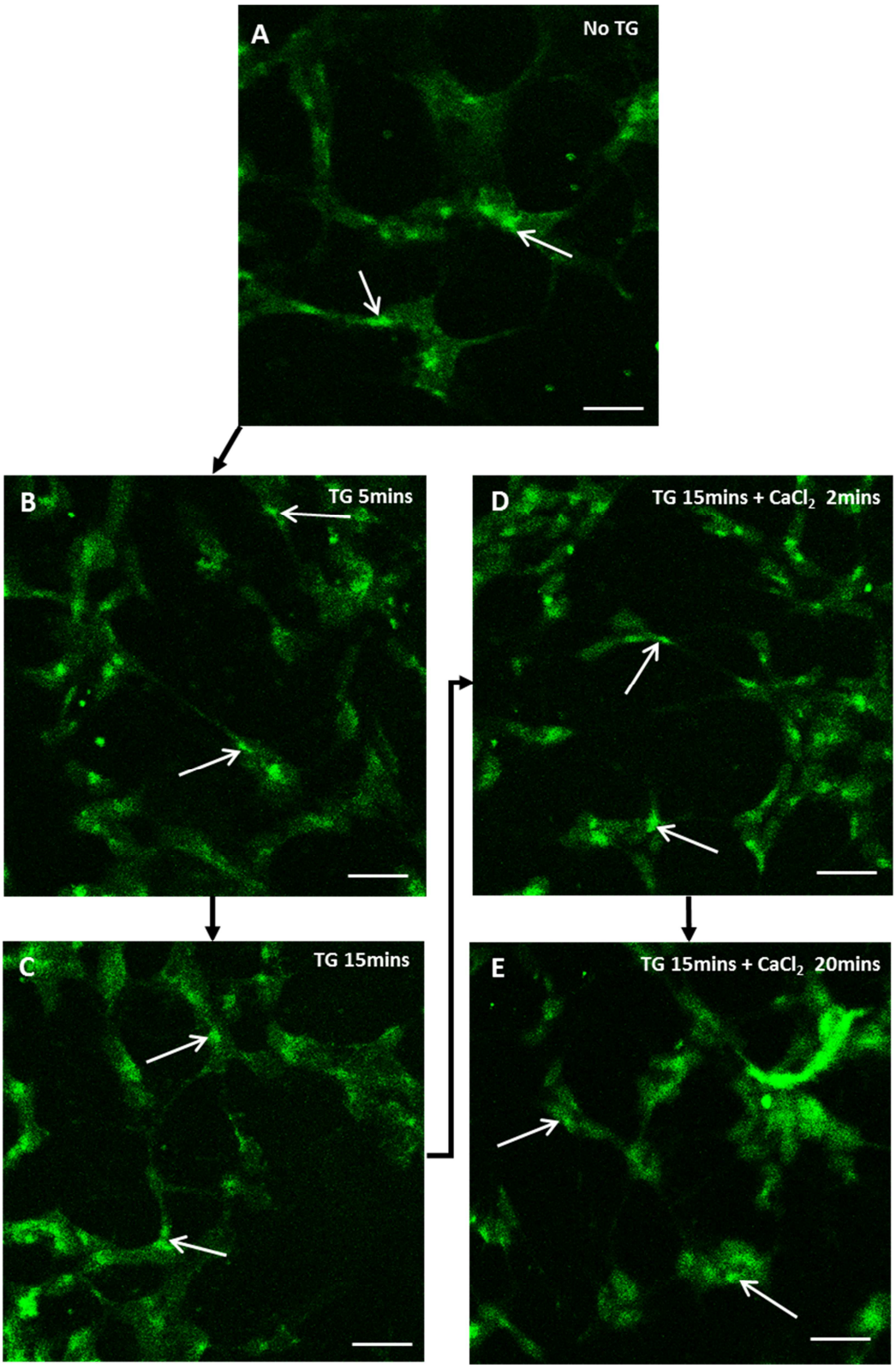

Figure 5.3.2. STIM1 is localised into clusters in differentiating N-type cells throughout the Ca^{2+} add-back time-course

Differentiating N-type populations (D_N, 1 µM 9*c*RA treated for 7 days) were exposed to 200 nM thapsigargin (TG) for 15 minutes to induce Ca^{2+} store release followed by

exposure to 2 mM $CaCl_2$ for 20 minutes to induce SOCE. Cells were fixed at various time-points throughout and stained with anti-STIM1 primary antibody followed by FITC-conjugated secondary antibody. Images were captured using laser scanning confocal microscopy. **(A)** In D_N cells, STIM1 was present throughout the cell and there were many examples STIM1 clustering (white arrows). Following TG exposure for **(B)** 5 minutes and **(C)** 15 minutes, there was a similar occurrence of STIM1 clustering (white arrows). Following $CaCl_2$ exposure for **(D)** 2 minutes and **(E)** 20 mins, there was a similar occurrence of STIM1 clustering (white arrows). Scale bars represent 20 μm. Images are representative of >15 images and taken using a x63 objective. N=3.

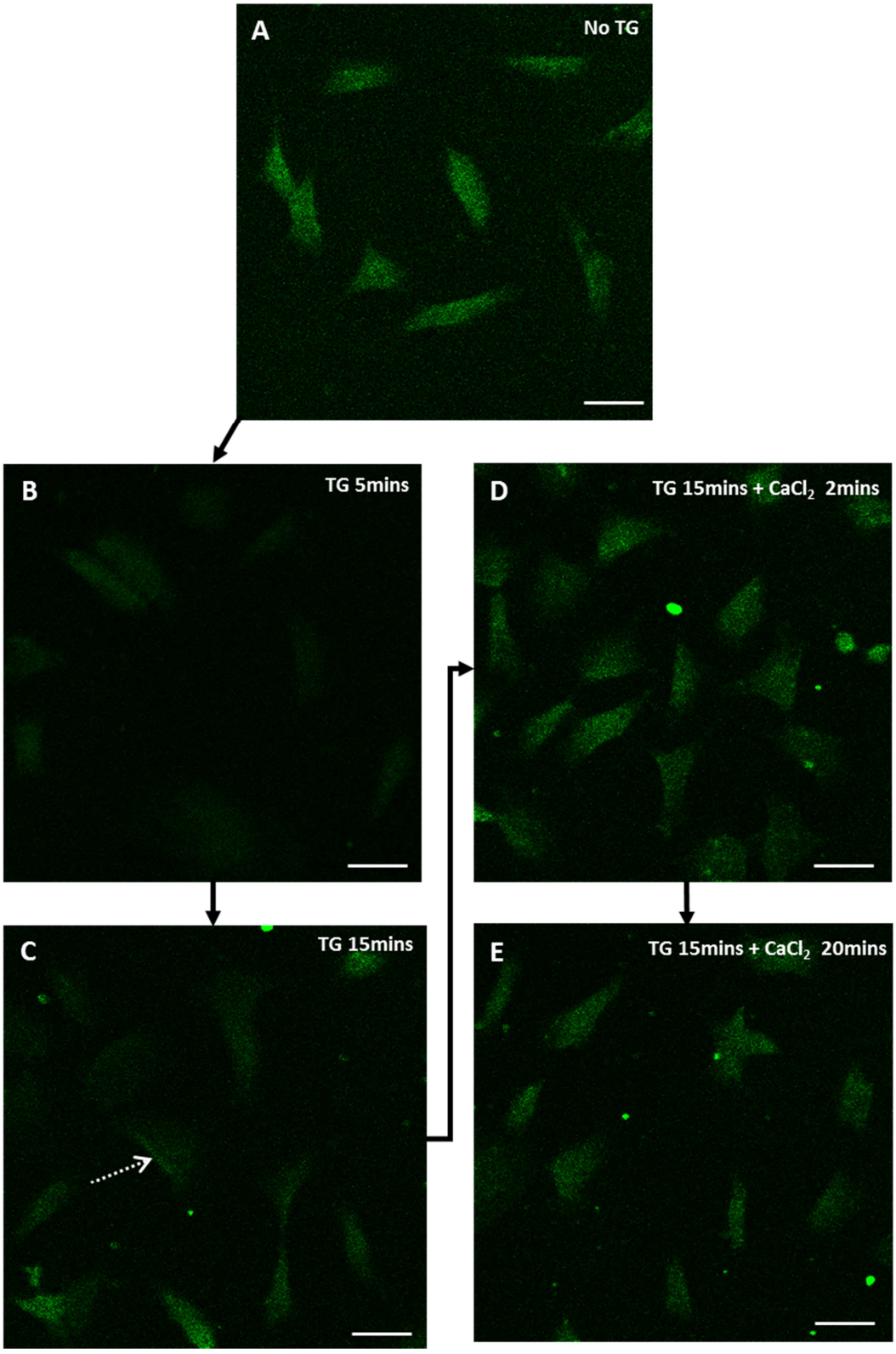

Figure 5.3.3. STIM1 localisation is relatively unchanged in proliferating S-type cells over the Ca^{2+} add-back time-course

Proliferating S-type populations (P_S, EtOH treated for 7 days) were exposed to 200 nM thapsigargin (TG) for 15 minutes to induce Ca^{2+} store release followed by exposure to 2

mM $CaCl_2$ for 20 minutes to induce SOCE. Cells were fixed at various time-points throughout and stained with anti-STIM1 primary antibody followed by FITC-conjugated secondary antibody. Images were captured using laser scanning confocal microscopy. **(A)** In P_S cells, STIM1 was present throughout the cell. Following TG exposure for **(B)** 5 minutes and **(C)** 15 minutes, there was a similar diffuse expression of STIM1 with a few examples STIM1 localisation at the cell membrane (white arrow). Following $CaCl_2$ exposure for **(D)** 2 minutes and **(E)** 20 mins, there was a similar diffuse pattern of STIM1 expression. Scale bars represent 20 µm. Images are representative of >15 images and taken using a x63 objective. N=3.

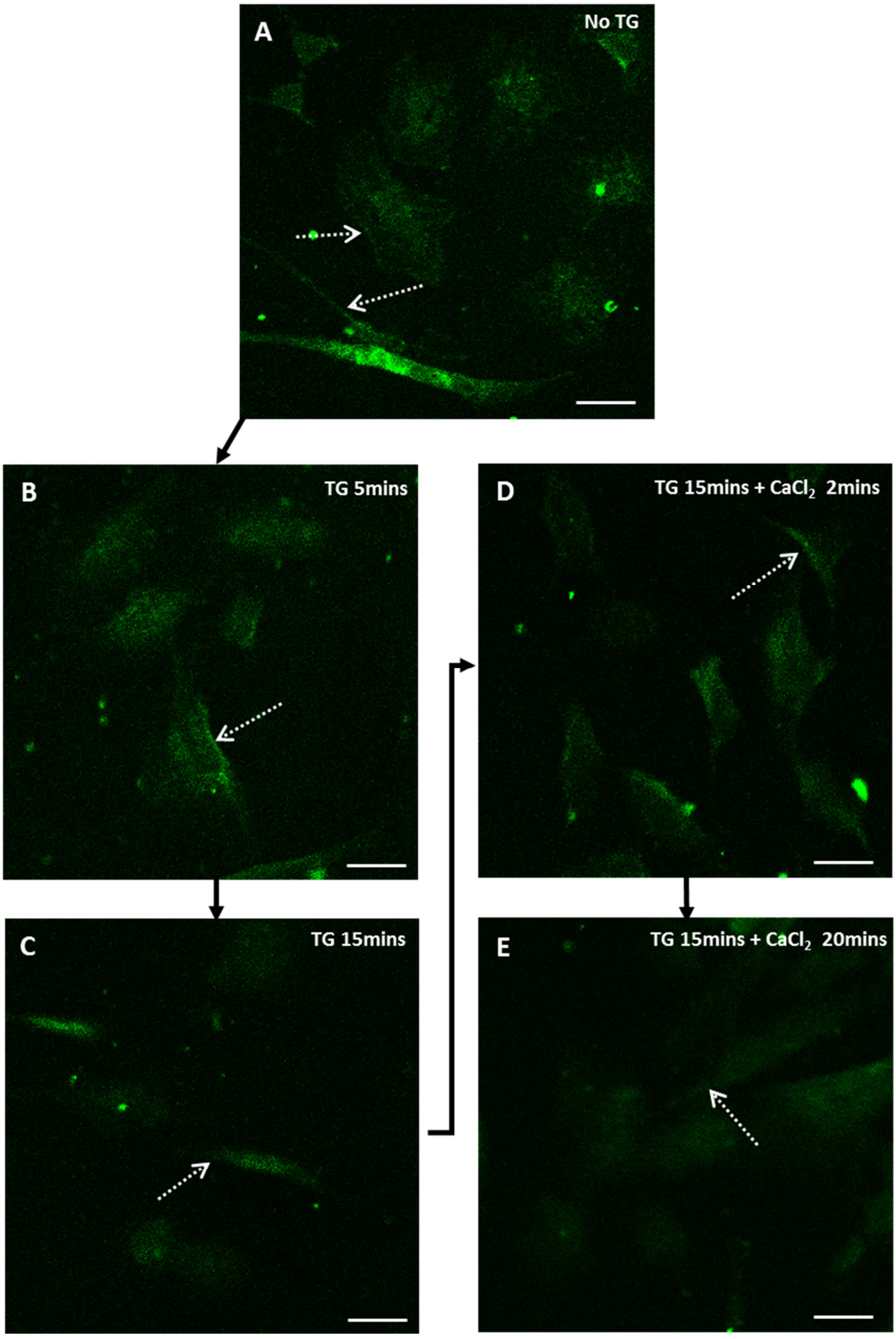

Figure 5.3.4. STIM1 expression is relatively unchanged in differentiating S-type cells over the Ca^{2+} add-back time-course

Differentiating S-type populations (D_S, 1 µM 9*c*RA treated for 7 days) were exposed to 200 nM thapsigargin (TG) for 15 minutes to induce Ca^{2+} store release followed by

exposure to 2 mM $CaCl_2$ for 20 minutes to induce SOCE. Cells were fixed at various time-points throughout and stained with anti-STIM1 primary antibody followed by FITC-conjugated secondary antibody. Images were captured using laser scanning confocal microscopy. **(A)** In D_S cells, STIM1 was present throughout the cell and there were examples STIM1 accumulation at the membrane (white arrows). Following TG exposure for **(B)** 5 minutes and **(C)** 15 minutes, there was a similar extent of diffuse STIM1 expression with some examples of accumulation at the membrane that remained following $CaCl_2$ exposure for **(D)** 2 minutes and **(E)** 20 mins (white arrows). Scale bars represent 20 µm. Images are representative of >15 images and taken using a x63 objective. N=3.

5.4. Localisation of Orai1 is not altered following Ca^{2+} store depletion and SOCE in N-type and S-type cells

Orai1 localisation was altered with differentiation of N-type and S-type cells (Results 5.2). Given the role of Orai1 as a SOC channel, that SOCE activity was dampened in differentiating N-type and S-type cells (Results 4.2) and that expression as well as localisation of Orai1 were altered with differentiation of N-type and S-type cells, localisation of STIM1 over the Ca^{2+}-addback time-course was investigated.

In P_N cells at rest, Orai1 was expressed throughout the cell and there were some examples of localisation into foci, which remained following TG exposure and Ca^{2+}-addback (Figure 5.4.1). In resting D_N cells, Orai1 was expressed throughout the cell with minimal examples of Orai1 foci and this expression pattern remained following TG exposure and Ca^{2+}-addback (Figure 5.4.2). This suggests that there is no detectable redistribution of Orai1 with Ca^{2+} store release or SOCE in N-type cells.

In resting P_S cells, Orai1 was expressed throughout the cell and the majority of cells exhibited localisation into foci whilst cells with a more flattened morphology could be observed that exhibited dispersed clusters of Orai1 (Figure 5.4.3A). This expression pattern for Orai1 remained the same following TG exposure and Ca^{2+}-addback (Figure 5.4.3B-E). In D_S cells at rest, Orai1 was expressed throughout the cell and there were examples of localisation into dispersed clusters and accumulation of Orai1 at the cell membrane (Figure 5.4.4A). This expression pattern remained similar following TG exposure and Ca^{2+}-addback (Figure 5.4.4B-E). These results indicate that there is no detectable redistribution of Orai1 with Ca^{2+} store release or SOCE in N-type cells.

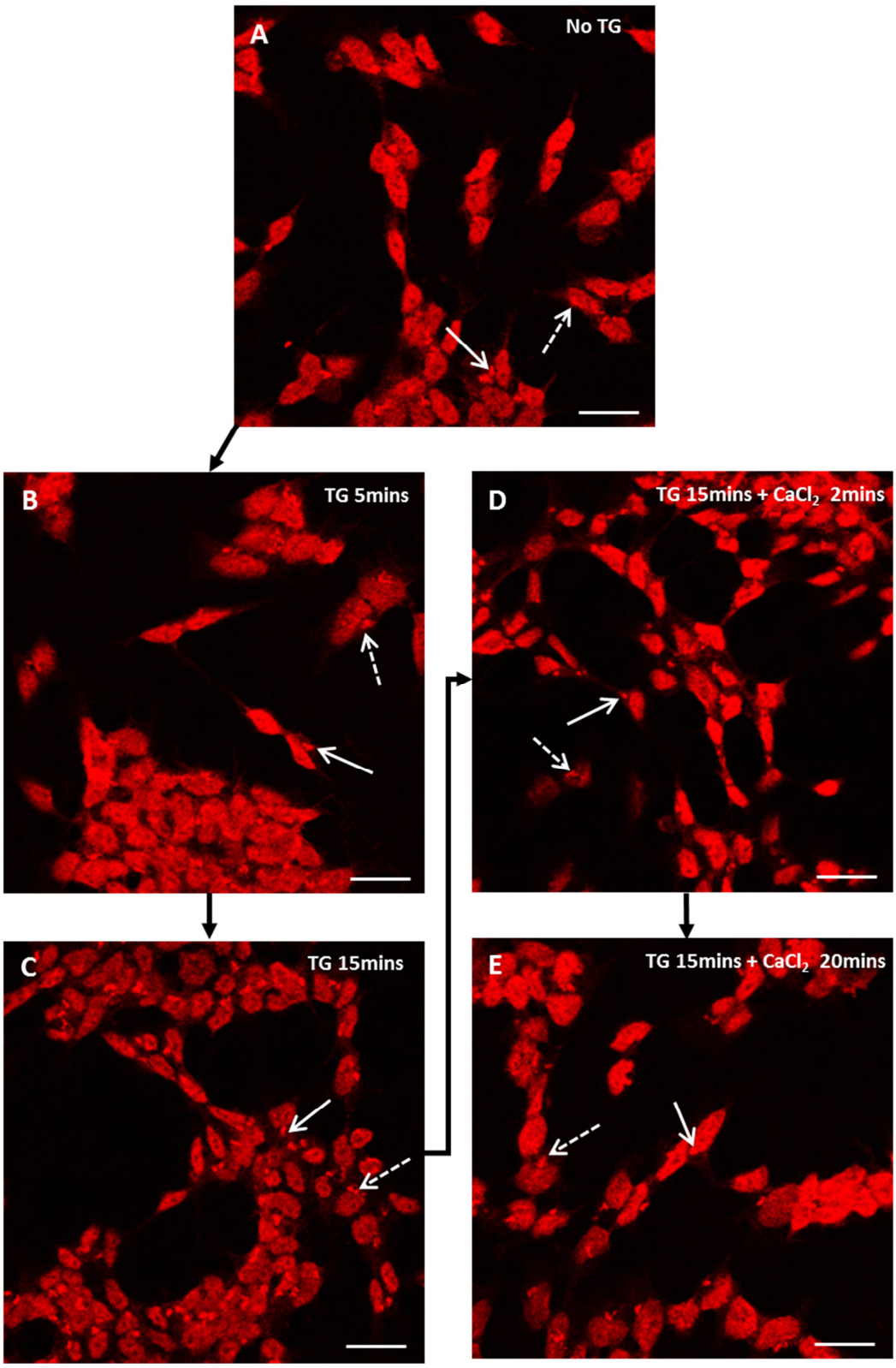

Figure 5.4.1. Orai1 localisation is not altered in proliferating N-type cells over the Ca^{2+} add-back time-course

Proliferating N-type populations (P_N, EtOH treated for 7 days) were exposed to 200 nM thapsigargin (TG) for 15 minutes to induce Ca^{2+} store release followed by exposure to

2 mM $CaCl_2$ for 20 minutes to induce SOCE. Cells were fixed at various time-points throughout and stained with anti-Orai1 primary antibody followed by TRITC-conjugated secondary antibody. Images were captured using laser scanning confocal microscopy. **(A)** In P_N cells, Orai1 was expressed throughout the cell and there were some examples of localisation into foci (white arrows). S-type cells could be observed with similar Orai1 localisation to N-type cells (dashed arrows). This expression pattern remained following TG exposure for **(B)** 5 minutes and **(C)** 15 minutes and following $CaCl_2$ exposure for **(D)** 2 minutes and **(E)** 20 mins. Scale bars represent 20 μm. Images are representative of >15 images and taken using a x63 objective. N=3.

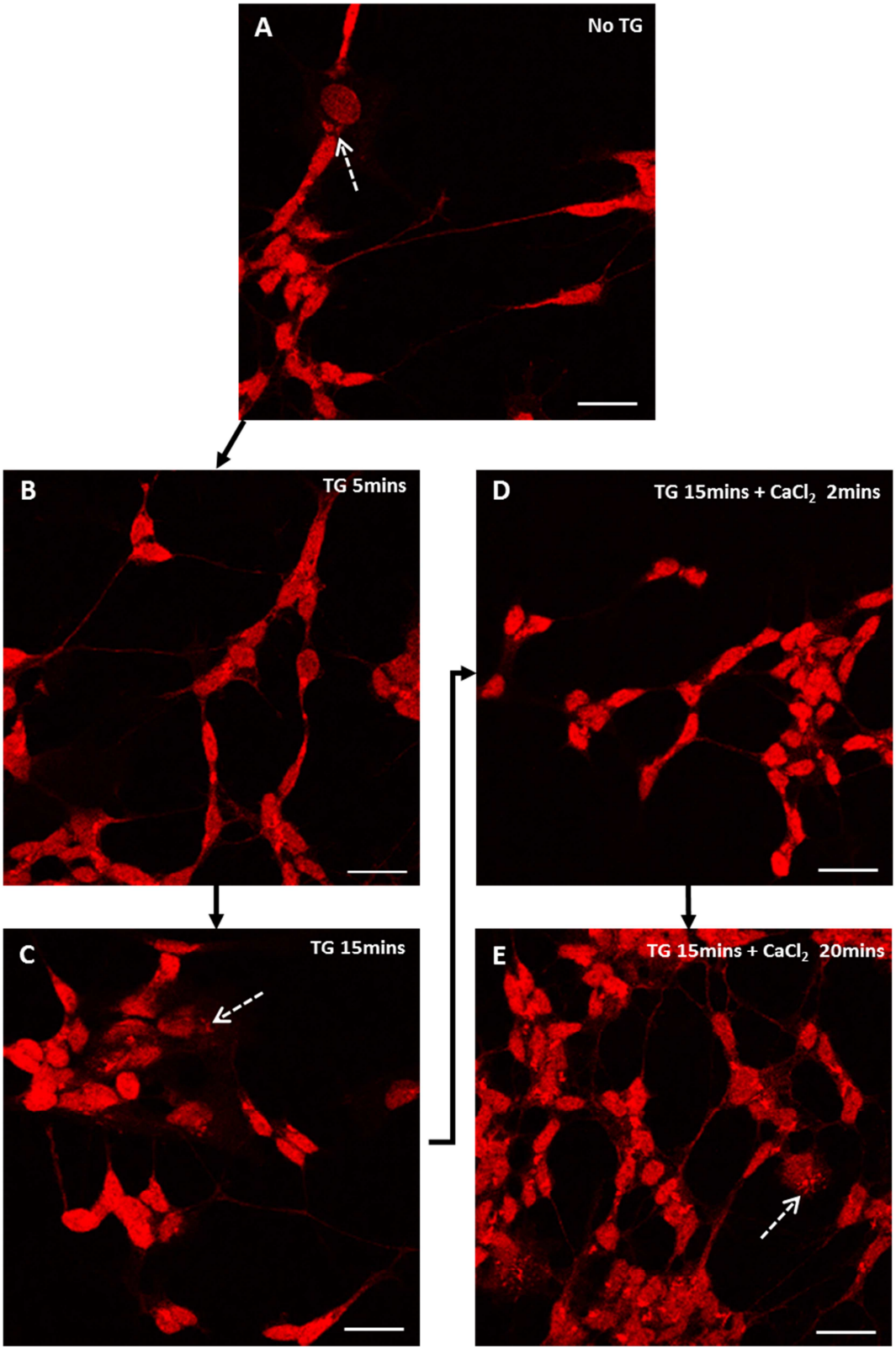

Figure 5.4.2 Orai1 localisation is not altered in differentiating N-type cells over the Ca^{2+} add-back time-course

Differentiating N-type populations (D_N, 1 µM treated for 7 days) were exposed to 200 nM thapsigargin (TG) for 15 minutes to induce Ca^{2+} store release followed by exposure

to 2 mM $CaCl_2$ for 20 minutes to induce SOCE. Cells were fixed at various time-points throughout and stained with anti-Orai1 primary antibody followed by TRITC-conjugated secondary antibody. Images were captured using laser scanning confocal microscopy. **(A)** In D_N cells, Orai1 was expressed throughout the cell. S-type cells could be observed with dispersed clusters of Orai1 (dashed arrows). This expression pattern remained following TG exposure for **(B)** 5 minutes and **(C)** 15 minutes and following $CaCl_2$ exposure for **(D)** 2 minutes and **(E)** 20 mins. Scale bars represent 20 μm. Images are representative of >15 images and taken using a x63 objective. N=3.

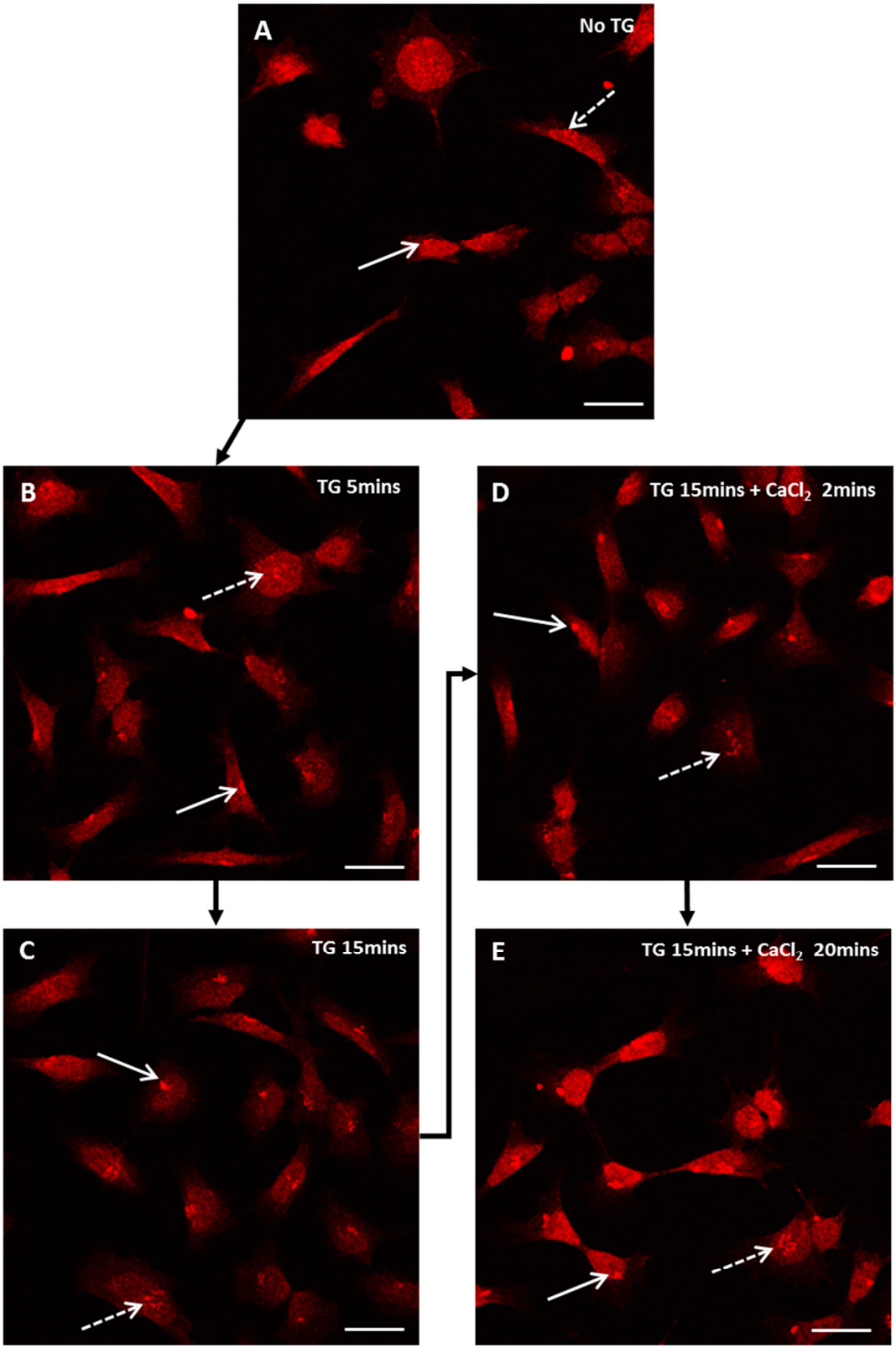

Figure 5.4.3. Orai1 localisation is not altered in proliferating S-type cells over the Ca^{2+} add-back time-course

Proliferating S-type populations (P_S, EtOH treated for 7 days) were exposed to 200 nM thapsigargin (TG) for 15 minutes to induce Ca^{2+} store release followed by exposure to 2

mM $CaCl_2$ for 20 minutes to induce SOCE. Cells were fixed at various time-points throughout and stained with anti-Orai1 primary antibody followed by TRITC-conjugated secondary antibody. Images were captured using laser scanning confocal microscopy. **(A)** In P_S cells, Orai1 was expressed throughout the cell and there were some examples of localisation into foci (white arrows). S-type cells with a more flattened morphology could be observed that exhibited dispersed clusters of Orai1 (dashed arrows) This expression pattern remained following TG exposure for **(B)** 5 minutes and **(C)** 15 minutes and following $CaCl_2$ exposure for **(D)** 2 minutes and **(E)** 20 mins. Scale bars represent 20 µm. Images are representative of >15 images and taken using a x63 objective. N=3.

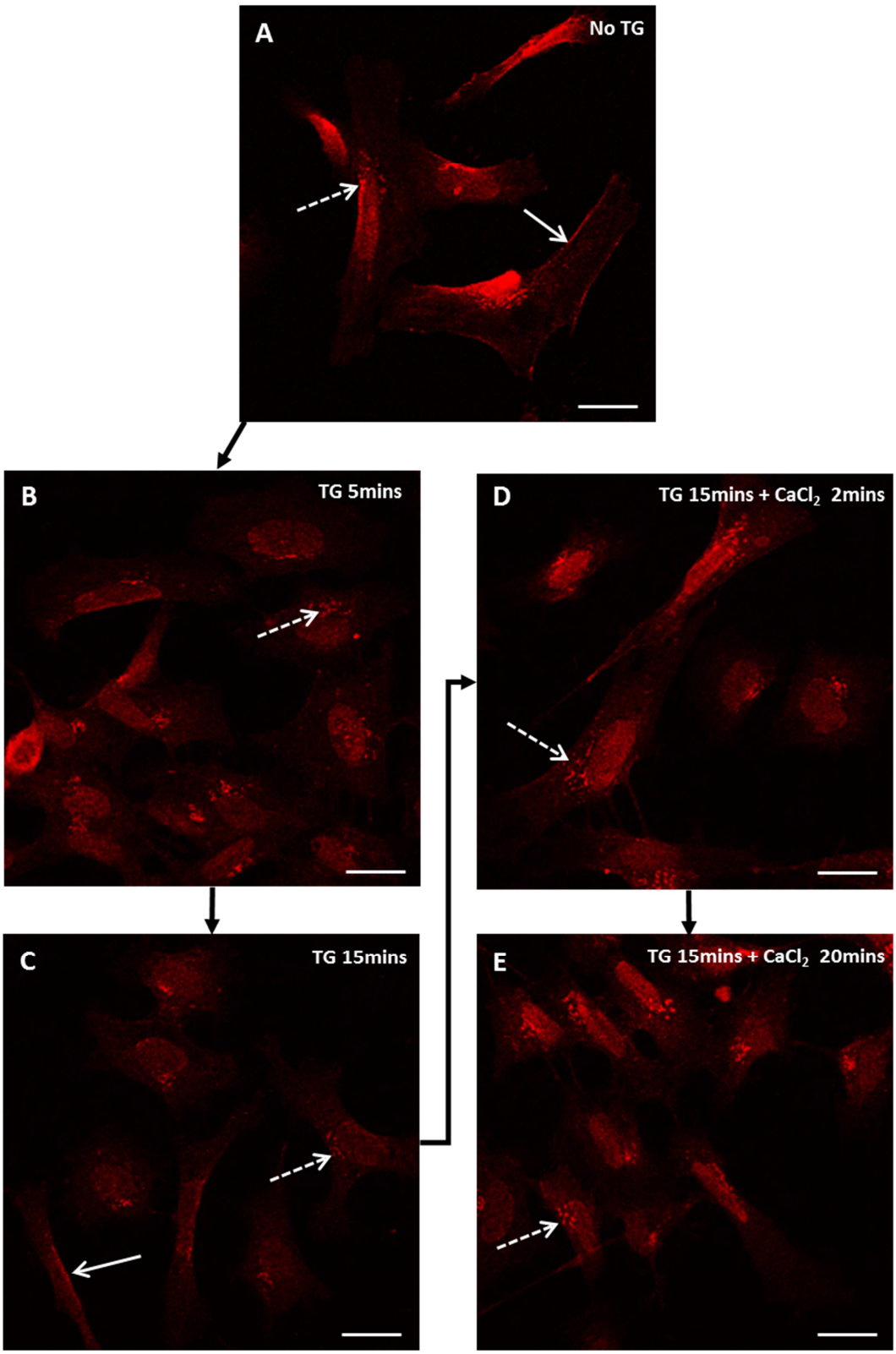

Figure 5.4.4 Orai1 localisation is not altered in differentiating S-type cells over the Ca^{2+} add-back time-course

Differentiating S-type populations (D_S, 1 µM 9*c*RA treated for 7 days) were exposed to 200 nM thapsigargin (TG) for 15 minutes to induce Ca^{2+} store release followed by

exposure to 2 mM $CaCl_2$ for 20 minutes to induce SOCE. Cells were fixed at various time-points throughout and stained with anti-Orai1 primary antibody followed by TRITC-conjugated secondary antibody. Images were captured using laser scanning confocal microscopy. **(A)** In D_S cells, Orai1 was expressed throughout the cell and there were examples of localisation into dispersed clusters (dashed arrows) and accumulation at the cell membrane (white arrows). This expression pattern remained following TG exposure for **(B)** 5 minutes and **(C)** 15 minutes and following $CaCl_2$ exposure for **(D)** 2 minutes and **(E)** 20 mins. Scale bars represent 20 μm. Images are representative of >15 images and taken using a x63 objective. N=3.

5.5. Conditioned media from proliferating and differentiating N-type and S-type populations alters the expression of STIM1 and Orai1

There was an uncoupling of SOCE with differentiation of N-type and S-type populations (Results 4.2). Conditioned media from S-type populations affected SOCE activity of N-type populations and conditioned media from N-type populations affected SOCE activity of S-type populations (Results 4.5). Media from P_S populations did not alter the P_N population SOCE response whilst media from D_S populations induced down-regulation of SOCE in P_N populations. Media from D_S populations dampened the SOCE down-regulation observed in D_N populations. In P_S populations, media from P_N and D_N populations induced partial down-regulation of SOCE whilst media from D_N populations also dampened the extent of SOCE down-regulation seen in D_S populations. Given the effect of conditioned media on SOCE activity and the involvement of STIM1 and Orai1 in SOCE, the expression of STIM1 and Orai1 in cells grown in a conditioned media environment was investigated.

N-type populations were treated for 7 days with EtOH (P_N, proliferating), 1 µM 9cRA (D_N, differentiating), media from proliferating S-type populations (P_N+P_S), media from differentiating S-type populations (P_N+D_S) or with 1 µM 9cRA plus media from differentiating S-type populations (D_N+D_S). There was no significant difference in the level of expression of STIM1 between P_N and D_N populations (P=0.999) however there was a slight increase in molecular weight of STIM1 in D_N populations (Figure 5.5.1). This is consistent with previously observed STIM1 expression in N-type populations (Results 5.1) and involvement of STIM1 in SOCE since SOCE was down-regulated in D_N populations (Results 4.2 and 4.5). There was a ~40% increase in STIM1 expression in P_N+P_S populations compared to P_N cells (Figure 5.5.1), although this was not significant (P=0.384), consistent with the previous finding that SOCE activity in P_N populations was not affected by P_S conditioned media (Results 4.5). There was no significant difference in the level of expression of STIM1 between P_N and P_N+D_S populations (P=0.275) and no change in STIM1 molecular weight (Figure 5.5.1), therefore the previously observed down-regulation of SOCE induced in P_N populations by D_S conditioned media (Results 4.5) is not attributed to a change in STIM1 expression. There was a ~40% increase in STIM1 expression in D_N+D_S populations compared to P_N populations, but this was not

significant (P=0.300), however there was a slight increase in STIM1 molecular weight, similar to that of D_N populations (Figure 5.5.1). This is consistent with the previous finding that SOCE activity was down-regulated in D_N populations treated with D_S conditioned media (Results 4.5) and a role for STIM1 in SOCE in N-type populations. There was a 51% increase in STIM1 expression in D_N+D_S populations compared to D_N populations, although this was not significant (P=0.214) but given that there was a similar increase in STIM1 molecular weight (Figure 5.5.1), this is consistent with the previous finding that there was no difference in SOCE activity between D_N+D_S populations and D_N populations (Results 4.5).

There was a slight but non-significant 9% decrease in Orai1 expression in D_N compared to P_N populations (P>0.999, Figure 5.5.2) whilst Orai1 expression and SOCE was previously observed to be significantly down-regulated in D_N populations (Results 4.2, 4.5 and 5.1). There was a ~150% increase in Orai1 expression in P_N+P_S populations compared to P_N cells (Figure 5.5.2), although this was not significant (P=0.333), consistent with the previous finding that SOCE activity in P_N populations was not down-regulated by P_S conditioned media (Results 4.5). There was a slight but non-significant 9% decrease in the level of expression of Orai1 in P_N+D_S compared to P_N populations (P>0.999, Figure 5.5.2), therefore the previously observed down-regulation of SOCE induced in P_N populations by D_S conditioned media (Results 4.5) may not be attributed to a change in Orai1 expression. There was a 32% decrease in Orai1 expression in D_N+D_S populations compared to P_N populations, but this was not significant (P=0.989, Figure 5.5.2), however this is consistent with the previous finding that SOCE activity was down-regulated in D_N populations treated with D_S conditioned media (Results 4.5) and a role for Orai1 in SOCE in N-type populations. There was a 26% decrease in Orai1 expression in D_N+D_S populations compared to D_N populations, although this was not significant (P=0.997, Figure 5.5.2), yet there was no difference in SOCE activity between D_N+D_S populations and D_N populations (Results 4.5) indicating that a decrease in Orai1 expression did not induce further SOCE down-regulation.

S-type populations were treated for 7 days with EtOH (P_S, proliferating), 1 µM 9cRA (D_S, differentiating), media from proliferating N-type populations (P_S+P_N), media from

differentiating N-type populations (P_S+D_N) or with 1 µM 9cRA plus media from differentiating N-type populations (D_S+D_N). The level of expression of STIM1 was down-regulated by 40% in D_S populations compared to P_S populations, although quantitatively this was not significant (P=0.459), and there was a slight increase in STIM1 molecular weight (Figure 5.5.3). This is consistent with previously observed STIM1 expression in S-type populations (Results 5.1) and involvement of STIM1 in SOCE since SOCE was down-regulated in D_S populations (Results 4.2 and 4.5). STIM1 expression was up-regulated by 38% in P_S+P_N populations compared to P_S populations (Figure 5.5.3), but non-significantly (P=0.499), therefore the previously observed down-regulation of SOCE induced in P_S populations by P_N conditioned media (Results 4.5) is not attributed to a change in STIM1 expression. There was no significant difference in the level of STIM1 expression in P_S+D_N populations and D_S+D_N populations compared to P_S populations (P=0.989 and P=0.829, respectively) however, an increase in the molecular weight was observed in both P_S+D_N populations and D_S+D_N populations (Figure 5.5.3). This is consistent with the previous finding that SOCE activity is down-regulated in P_S and D_S populations treated with D_N conditioned media (Results 4.5) and a role for STIM1 in SOCE in S-type populations. STIM1 expression in D_S+D_N populations was up-regulated by 28%, although not significantly, compared to D_S populations (P=0.930, Figure 5.5.3) consistent with a slight increase in SOCE activity (Results 4.5).

The level of expression of Orai1 was down-regulated by 39% in D_S populations compared to P_S populations, although quantitatively this was not significant (P=0.583, Figure 5.5.4). This is consistent with previously observed Orai1 expression in S-type populations (Results 5.1) and involvement of Orai1 in SOCE since SOCE was down-regulated in D_S populations (Results 4.2 and 4.5). Orai1 expression was up-regulated by 60% in P_S+P_N populations compared to P_S populations (Figure 5.5.4), but non-significantly (P=0.258), therefore the previously observed down-regulation of SOCE induced in P_S populations by P_N conditioned media (Results 4.5) is not attributed to a decrease in Orai1 expression. There was a 41% decrease in Orai1 expression in P_S+D_N compared to P_S populations (Figure 5.5.4) but this was not significant (P=0.537). This is consistent with the previous finding that SOCE activity is down-regulated in P_S

populations treated with D_N conditioned media (Results 4.5) and a role for Orai1 in SOCE in S-type populations. There was no significant change in Orai1 expression in D_S+D_N populations compared to P_S populations (P>0.999, Figure 5.5.4), which indicates that the previous finding of SOCE down-regulation in D_S populations treated with D_N conditioned media (Results 4.5) is not attributed to a change in Orai1 expression. Orai1 expression in D_S+D_N populations was up-regulated by 61%, although not significantly, compared to D_S populations (P=0.606, Figure 5.5.4) consistent with the apparent slight increase in SOCE activity (Results 4.5).

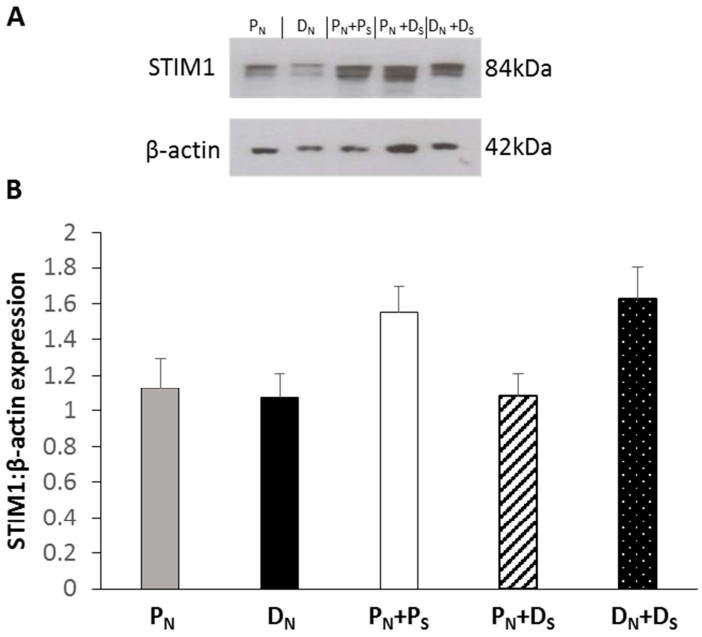

Figure 5.5.1. S-type conditioned media alters STIM1 expression in proliferating and differentiating N-type populations

Western blots were performed on protein samples from N-type populations that were treated for 7 days with EtOH (P_N, proliferating), 1 µM 9cRA (D_N, differentiating), media from proliferating S-type populations (P_N+P_S), media from differentiating S-type populations (P_N+D_S) or with 1 µM 9cRA plus media from differentiating S-type populations (D_N+D_S). Blots were probed with anti-STIM1 antibody which detected a band at 84 kDa and β-actin antibody which was used as a loading control and detected a band at 42 kDa. Quantitative band measurements were performed using densitometry in ImageJ. **(A)** All cell conditions expressed STIM1. There was reduced band intensity and a slight increase in molecular weight in D_N cells compared to P_N populations. Band intensity of P_N+P_S, P_N+D_S and D_N+D_S populations was similar to that of P_N populations. There was a slight band shift in D_N+D_S populations, similar to that of D_N cells. **(B)** There was no significant effect of growth condition on the level of STIM1 expression (P=0.115). There was no significant difference in the level of expression of STIM1 between P_N and D_N populations (P=0.999) or P_N+D_S populations (P=0.275). There was a ~40% increase in STIM1 expression in P_N+P_S populations and D_N+D_S populations compared to P_N populations, but this was not significant (P=0.384 and P=0.300, respectively). There was a 51.53% increase in STIM1 expression in D_N+D_S populations compared to D_N populations, but this was not significant (P=0.214). N=2.

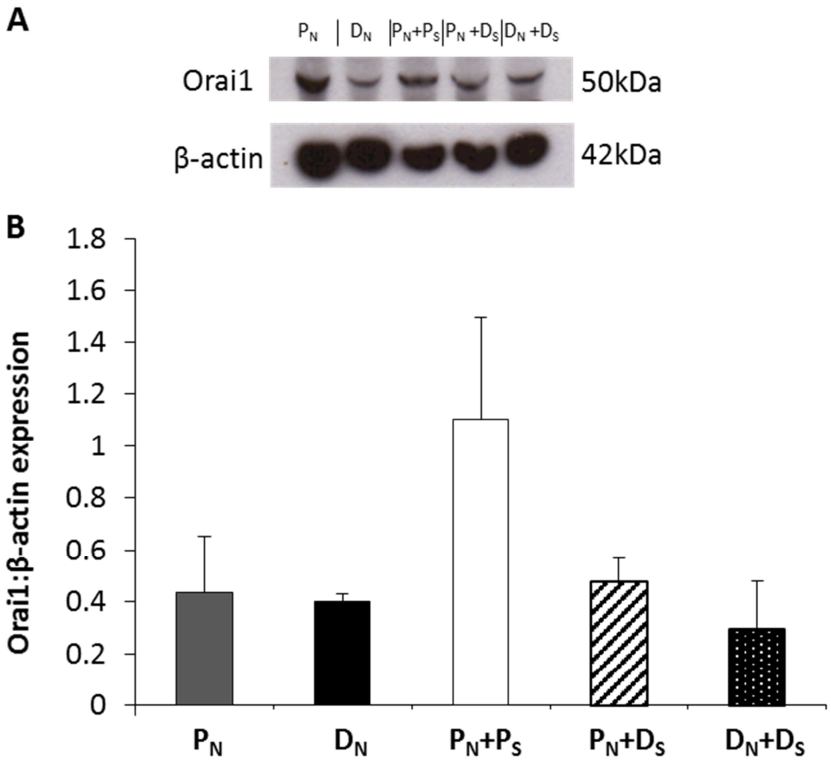

Figure 5.5.2. S-type conditioned media alters Orai1 expression in proliferating and differentiating N-type populations

Western blots were performed on protein samples from N-type populations that were treated for 7 days with EtOH (P_N, proliferating), 1 µM 9cRA (D_N, differentiating), media from proliferating S-type populations (P_N+P_S), media from differentiating S-type populations (P_N+D_S) or with 1 µM 9cRA plus media from differentiating S-type populations (D_N+D_S). Blots were probed with anti-Orai1 antibody which detected a band at 50 kDa and β-actin antibody which was used as a loading control and detected a band at 42 kDa. Quantitative band measurements were performed using densitometry in ImageJ. **(A)** All cell conditions expressed Orai1. There was an apparent reduced band intensity in D_N, P_N+D_S, and D_N+D_S populations compared to P_N populations. **(B)** There was no significant effect of growth condition on the level of Orai1 expression (P>0.999). Orai1 expression was down-regulated by 8.89% in D_N compared to P_N populations but this was not significant (P>0.999). There was a non-significant ~152% increase in Orai1 expression in P_N+P_S populations compared to P_N populations (P=0.333). There was a non-significant 9.22% increase in Orai1 expression in P_N+D_S compared to P_N populations (P>0.999). Orai1 expression was down-regulated

by 32.09% in D_N+D_S compared to P_S populations and by 25.47% in D_N+D_S populations compared to D_N populations, but this was not significant (P=989 and P=0.997, respectively). N=2.

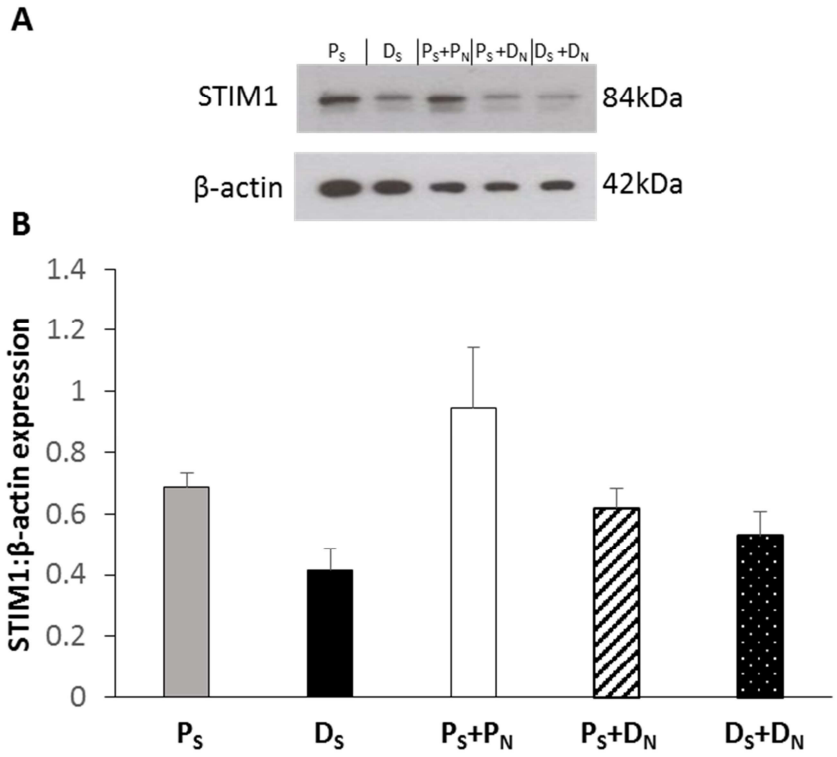

Figure 5.5.3. N-type conditioned media alters STIM1 expression in proliferating and differentiating S-type populations

Western blots were performed on protein samples from S-type populations that were treated for 7 days with EtOH (P_S, proliferating), 1 µM 9cRA (D_S, differentiating), media from proliferating N-type populations (P_S+P_N), media from differentiating N-type populations (P_S+D_N) or with 1 µM 9cRA plus media from differentiating N-type populations (D_S+D_N). Blots were probed with anti-STIM1 antibody which detected a band at 84 kDa and β-actin antibody which was used as a loading control and detected a band at 42 kDa. Quantitative band measurements were performed using densitometry in ImageJ. **(A)** All cell conditions exhibited expression of STIM1. There was reduced band intensity in D_S populations compared to P_S populations. Band intensity of P_S+P_N populations was similar to that of P_S populations. There was reduced band intensity in P_S+D_N and D_S+D_N populations similar to that of D_S populations and there was a slight increase in molecular weight compared to all other conditions. **(B)** There was no significant effect of growth conditions on the level of STIM1 expression (P=0.101). The level of expression of STIM1 was down-regulated by 39.72% in D_S populations compared to P_S populations, although this was not significant (P=0.459).

STIM1 expression was up-regulated by 37.72% in P_S+P_N populations compared to P_S populations, but non-significantly (P=0.499). There was no significant difference in STIM1 expression in P_S+D_N populations (P=0.989). STIM1 expression in D_S+D_N populations was down-regulated by 22.82% compared to P_S populations and up-regulated by 28.03% compared to D_S populations (P=0.829 and P=0.930, respectively). N=2.

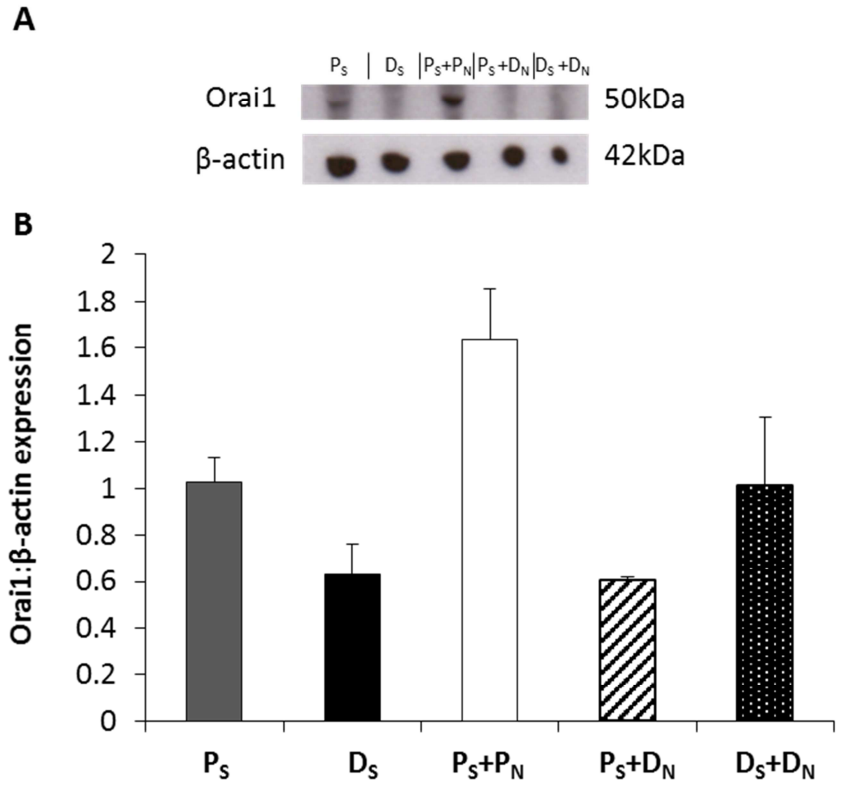

Figure 5.5.4. N-type conditioned media alters Orai1 expression in proliferating and differentiating S-type populations

Western blots were performed on protein samples from S-type populations that were treated for 7 days with EtOH (P_S, proliferating), 1 µM 9cRA (D_S, differentiating), media from proliferating N-type populations (P_S+P_N), media from differentiating N-type populations (P_S+D_N) or with 1 µM 9cRA plus media from differentiating N-type populations (D_S+D_N). Blots were probed with anti-Orai1 antibody which detected a band at 50 kDa and β-actin antibody which was used as a loading control and detected a band at 42 kDa. Quantitative band measurements were performed using densitometry in ImageJ. **(A)** There was reduced band intensity in D_S, P_S+D_N and D_S+D_N populations compared to P_S populations. Band intensity of P_S+P_N populations was similar to that of P_S populations. **(B)** There was no significant effect of growth conditions on the level of Orai1 expression (P>0.999). The level of expression of Orai1 was down-regulated by 38.53% in D_S populations compared to P_S populations, although this was not significant (P=0.583). Orai1 expression was up-regulated by 59.60% in P_S+P_N populations compared to P_S populations, but non-significantly (P=0.258). Orai1 expression was non-significantly down-regulated by 40.90% in P_S+D_N

compared to P_S populations (P=0.537). There was no significant change in Orai1 expression in D_S+D_N compared to P_S populations and Orai1 was non-significantly up-regulated by 60.78% in D_S+D_N compared to D_S populations (P>0.999 and P=0.606, respectively). N=2.

5.6. Conditioned media from proliferating and differentiating N-type and S-type populations alters the expression of a neuronal and a non-neuronal marker

Due to the interesting changes induced by conditioned media that were observed in morphology, SOCE activity (Results 4.6) and STIM1 (Results 5.5), expression of the neuronal marker β-tubulin III and the non-neuronal marker vimentin were also investigated in cells grown in a conditioned media environment.

N-type populations were treated for 7 days with EtOH (P_N, proliferating), 1 μM 9cRA (D_N, differentiating), media from proliferating S-type populations (P_N+P_S), media from differentiating S-type populations (P_N+D_S) or with 1 μM 9cRA plus media from differentiating S-type populations (D_N+D_S).

There was a ~20% increase in β-tubulin III expression in D_N and D_N+D_S populations compared to P_N populations (Figure 5.6.1A and B), although this was not significant (P=0.923 and P=0.891,respectively). This indicates that differentiation of N-type cells may induce a transition towards a neuronal phenotype, as expected, and that this is not an affected by D_S conditioned media. There was a non-significant ~20% increase in β-tubulin III expression in P_N+P_S populations compared to P_N populations (Figure 5.6.1A and B), although this was not significant (P=0.927). There was no significant difference in β-tubulin III expression between P_N+D_S and P_N populations (P=0.995, Figure 5.6.1A and B). This suggests that D_S conditioned media does not induce the same effect as P_S conditioned media, perhaps since D_S populations are moving towards a non-neuronal phenotype and that D_S conditioned media does not induce a more neuronal-like phenotype in P_N populations. There was no significant difference in in β-tubulin III expression between D_N+D_S and D_N populations (P>0.999, Figure 5.6.1A and B), indicating that D_S conditioned media does not affect the ability of N-type populations to differentiate towards a neuronal phenotype.

Vimentin expression was increased ~20-fold in D_N populations compared to P_N populations (Figure 5.6.1A and C), although this was not significant (P=0.414), consistent with previous findings (Results 3.3). There was no significant difference in vimentin expression between P_N populations and P_N+P_S populations (P>0.999, Figure

5.6.1A and C), implying that P_S conditioned media does not induce a non-neuronal phenotype or differentiation of P_N populations. There was a ~6-fold increase in vimentin expression in P_N+D_S populations and a ~10-fold increase in D_N+D_S populations compared to P_N populations (Figure 5.6.1A and C). There was a 48% decrease in vimentin expression in D_N+D_S populations compared to D_N populations. However, since these changes were not significant, further studies will be required to determine whether D_S conditioned media induces a non-neuronal or differentiating phenotype in P_N populations while dampening differentiation of N-type populations

S-type populations were treated for 7 days with EtOH (P_S, proliferating), 1 µM 9cRA (D_S, differentiating), media from proliferating N-type populations (P_S+P_N), media from differentiating N-type populations (P_S+D_N) or with 1 µM 9cRA plus media from differentiating N-type populations (D_S+D_N).

There was no significant difference in β-tubulin III expression in D_S populations compared to P_S populations (P=0.973, Figure 5.6.2A and B), confirming that S-type populations do not become more neuronal-like with differentiation. There was a 65% increase in β-tubulin III expression in P_S+P_N populations and a 52% increase in P_S+D_N populations compared to P_S populations (Figure 5.6.2A and B), but this was non-significant (P=0.199 and P=0.352, respectively). Therefore further investigation is needed to determine whether P_N and D_N conditioned media may induce a shift towards a neuronal phenotype in P_S populations. There was no significant difference in β-tubulin III expression between D_S+D_N populations and P_S populations (P>0.999) and a slight but non-significant decrease in β-tubulin III compared to D_S populations (P=0.967, Figure 5.6.2A and B). Also, β-tubulin III was down-regulated by 35% in D_S+D_N populations compared to P_S+D_N populations, but this was non-significant (P=0.341, Figure 5.6.2A and B). These results indicate that D_S populations are committed to a non-neuronal lineage that is not dampened by D_N conditioned media.

Vimentin expression was increased by 67% in D_S populations compared to P_S populations (Figure 5.6.2A and C) but this was non-significant (P=0.106), indicating that further investigation is needed to ensure S-type differentiation towards a more non-

neuronal phenotype. There was no significant difference in vimentin expression between P_S+P_N populations and P_S populations (P=0.924), implying that P_N conditioned media does not affect the non-neuronal phenotype of P_S populations. There was a significant ~2-fold increase in vimentin expression in P_S+D_N populations compared to P_S populations (P=0.014) and D_S+D_N populations compared to P_S populations (P=0.034) and a slight but non-significant increase in vimentin expression in D_S+D_N populations compared to D_S populations (P=0.761 Figure 5.6.2A and C), suggesting that D_N conditioned media can induce differentiation in P_S populations but only slightly enhances this effect in D_S populations.

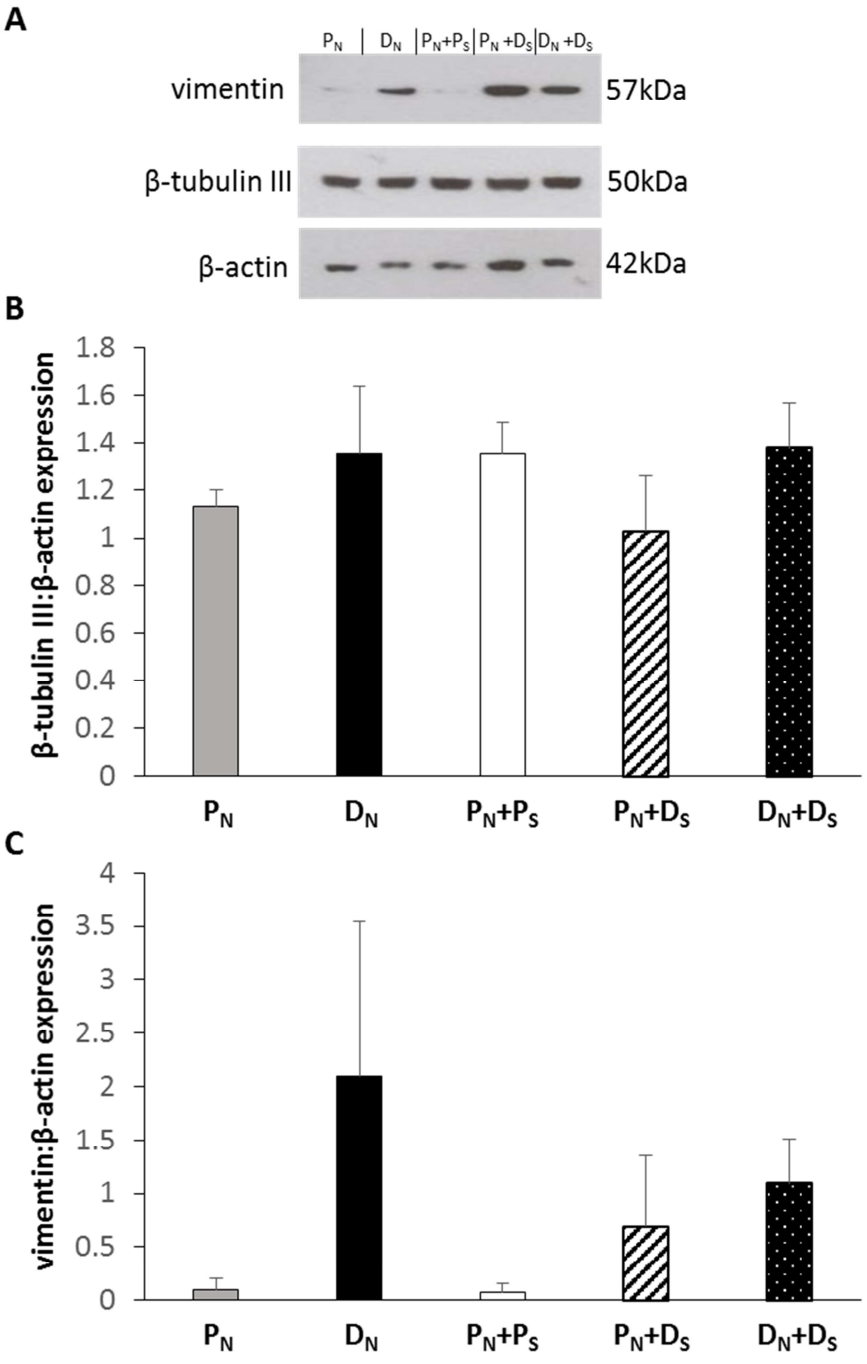

Figure 5.6.1. S-type conditioned media alters the expression of a neuronal and a non-neuronal marker in N-type populations

Western blots were performed on protein samples from N-type populations that were treated for 7 days with EtOH (P_N, proliferating), 1 µM 9cRA (D_N, differentiating), media from proliferating S-type populations (P_N+P_S), media from differentiating S-type populations (P_N+D_S) or with 1 µM 9cRA plus media from differentiating S-type populations (D_N+D_S). Blots were probed with anti-β-tubulin III antibody which detected

a band at 50 kDa, anti-vimentin antibody which detected a band at 57 kDa and β-actin antibody which was used as a loading control and detected a band at 42 kDa. Quantitative band measurements were performed using densitometry in ImageJ. **(A)** All cell conditions exhibited expression of β-tubulin III to a similar extent. All cell conditions exhibited vimentin expression though band intensity was minimal in P_N populations and P_N+P_S populations. **(B)** There was no significant effect of growth condition on expression of β-tubulin III (P=0.657). There was a ~20% increase in β-tubulin III expression in D_N, P_N+P_S and D_N+D_S populations compared to P_N populations but this was not significant (P=0.923, P=0.927 and P=0.891,respectively). There was no significant difference in β-tubulin III expression between P_N+D_S and P_N populations (P=0.995). There was no significant difference in in β-tubulin III expression between D_N+D_S and D_N populations (P>0.999). N=2. **(C)** There was no significant effect of growth condition on expression of vimentin (P=0.387). There was 20-fold increase in vimentin expression in D_N populations compared to P_N populations, though this was not significant (P=0.414). There was no significant difference in vimentin expression between P_N populations and P_N+P_S populations (P>0.999). There was a 6-fold increase in vimentin expression in P_N+D_S populations compared to P_N populations, but this was not significant (P=0.975). There was a 10-fold increase in vimentin expression in D_N+D_S populations compared to P_N populations, but this was not significant (P=0.866). There was a 47.75% decrease in vimentin expression in D_N+D_S populations compared to D_N populations, but this was not significant (P=0.862). N=2.

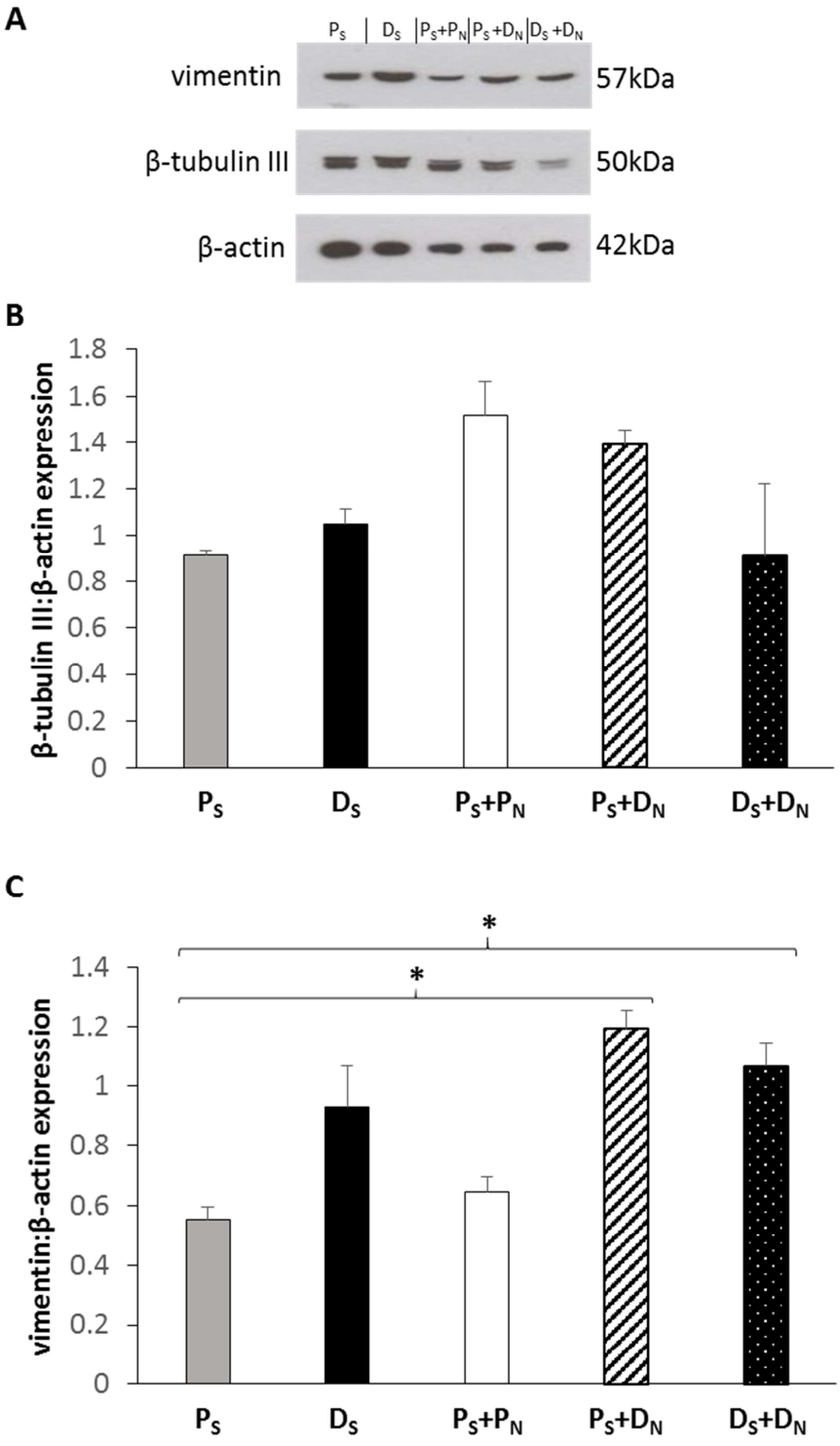

Figure 5.6.2. N-type conditioned media alters expression of a neuronal and a non-neuronal marker in S-type populations

Western blots were performed on protein samples from S-type populations that were treated for 7 days with EtOH (P_S, proliferating), 1 µM 9cRA (D_S, differentiating), media from proliferating N-type populations (P_S+P_N), media from differentiating N-type

populations (P_S+D_N) or with 1 µM 9cRA plus media from differentiating N-type populations (D_S+D_N). Blots were probed with anti-β-tubulin III antibody which detected a band at 50 kDa, anti-vimentin antibody which detected a band at 57 kDa and β-actin antibody which was used as a loading control and detected a band at 42 kDa. Quantitative band measurements were performed using densitometry in ImageJ. **(A)** All cell conditions exhibited expression of β-tubulin III to a similar extent except D_S+D_N populations, where band intensity was reduced. All cell conditions exhibited expression of vimentin. There was an increase in vimentin band intensity in D_S populations compared to P_S populations. Vimentin band intensity in P_S+P_N populations was reduced to that of D_S populations. P_S+D_N and D_S+D_N populations expressed vimentin to a similar extent. **(B)** There was no significant effect of growth condition on expression of β-tubulin III (P=0.128). There was a 14.37% increase in β-tubulin III expression in D_S populations compared to P_S populations, though this was non-significant (P=0.973). There was a 65.28% increase in β-tubulin III expression in P_S+P_N populations compared to P_S populations, but this was non-significant (P=0.199). There was a 51.56% increase in β-tubulin III expression in P_S+D_N populations compared to P_S populations, but this was non-significant (P=0.352). There was no significant difference in β-tubulin III expression between D_S+D_N populations and P_S populations (P>0.999). There was a 13.25% decrease in β-tubulin III in D_S+D_N populations compared to D_S populations, but this was non-significant (P=0.967). β-tubulin III was down-regulated by 34.54% in D_S+D_N populations compared to P_S+D_N populations, but this was non-significant (P=0.341). N=2. **(C)** There was a significant effect of growth condition on vimentin expression (P=0.011). There was a 67.44% increase in vimentin expression in D_S populations compared to P_S populations, though this was non-significant (P=0.106). There was a 16.40% increase in vimentin expression in P_S+P_N populations compared to P_S populations, but this was non-significant (P=0.924). There was a significant ~2-fold increase in vimentin expression in P_S+D_N populations compared to P_S populations (P=0.014*) and D_S+D_N populations compared to P_S populations (P=0.034*). There was a 14.72% increase in vimentin expression in D_S+D_N populations compared to D_S populations (P=0.761), although this was not significant. N=2.

Chapter 5: Discussion

The proteins STIM1 and Orai1 have been shown to be involved in SOCE (Introduction). The Ca^{2+} sensing protein STIM1 is able to detect ER Ca^{2+} store depletion and localise to ER/PM junctions where it gates PM SOCs to induce Ca^{2+} entry and replenish the depleted ER Ca^{2+} stores (Liou 2005; Hoover 2011; Sauc 2015). Orai1 is a PM protein that forms the SOC channel pore and is gated by STIM1 for SOCE regulation (Mignen 2008; Demuro 2011; Hoover 2011). Dampened SOCE activity was observed with differentiation of N-type and S-type populations (Chapter 4). This SOCE down-regulation was accompanied by either a modification or a down-regulation of STIM1 expression alongside a down-regulation of Orai1 expression in N-type and S-type populations, consistent with their role in SOCE.

The level of STIM1 expression has been extensively associated with extent of SOCE activity. Previous findings in this laboratory have shown knockdown of STIM1 to cause a down-regulation of SOCE in proliferating N-type populations whilst overexpression of STIM1 in differentiating N-type populations restores previously dampened SOCE (Bell 2011). STIM1 expression in other cell types has a common role in SOCE as knockdown of STIM1 in SH-SY5Y cells, HEK293 cells, Jurkat T cells and Drosophila S2 cells (Roos 2005), as well as endothelial cells (Abdullaev 2008), HeLa cells (Liou 2005), endothelial progenitor cells (Kuang 2010) and vascular smooth muscle cells (Takahashi 2007; Aubart 2009; Potier 2009) causes a reduction in SOCE. STIM1 expression also affects the extent of differentiation. Our laboratory has previously shown that whilst knockdown of STIM1 in N-type cells does not induce morphological differentiation, overexpression of STIM1 in differentiating N-type populations restores previously dampened SOCE and reduces morphological differentiation (Bell 2011). STIM1 knockdown reduced SOCE and prevented proliferation of neural progenitor cells derived from mouse embryonic cells (Hao 2014) and endothelial cells (Abdullaev 2008). STIM1 is up-regulated in proliferating vascular smooth muscle cells and STIM1 knockdown inhibits proliferation and SOCE (Takahashi 2007; Aubart 2009; Potier 2009). Knockdown of STIM1 also prevents endothelial progenitor cell proliferation (Kuang 2010) and, similarly, it was also found that hepatocyte growth factor induces endothelial progenitor cell differentiation with an in increase in SOCE alongside STIM1

expression whilst knockdown of STIM1 expression inhibits this effect (Shi 2010). Taken together, this indicates that STIM1 does not have a direct role in the switch from proliferation to differentiation but may be involved in promoting the proliferative cell state.

The observed changes in STIM1 expression could be a direct effect of RA treatment. However, it has been shown that the promoter region or upstream enhancer region of the STIM1 gene does not contain a consensus motif for RAR/RXR binding therefore a lack of RA regulatory elements in the STIM1 gene demonstrates that STIM1 expression is not altered by RA directly but by an indirect effect of RA on cellular differentiation processes (Zhang 2007).

An increase in the molecular weight of STIM1 found in this study suggests that there may some sort of modification, such as phosphorylation, that could affect STIM1 function which is likely to impact on SOCE. STIM1 phosphorylation at multiple serine residues has recently been identified and extensively investigated (Manji 2000; Smyth 2009; Sundivakkam 2012; Pozo-Guisado 2013; Sundivakkam 2013). STIM1 phosphorylation has been shown to have a role in STIM1 activation during ER Ca^{2+} store depletion (Lopez 2012; Pozo-guisado 2013) but can also inhibit SOCE by preventing puncta formation (Smyth 2009; Sundivakkam 2013). This demonstrates that STIM1 phosphorylation can greatly affect STIM1 function and therefore may play a role in the observed change of expression and SOCE activity in this study. STIM1 can also be glycosylated (Manji 2000; Dziadek 2007), which can affect localisation of STIM1 to the PM (Williams 2002). Potentially, the shift in molecular weight of STIM1 could indicate the presence of an alternative isoform of STIM1 that serves different function. The existence of a higher molecular weight isoform of STIM1, coined STIM1L as opposed to the more extensively studied STIM1S isoform, has recently been identified (Darbellay 2011) and is able to activate SOCE in cells lacking STIM1 (Sauc 2015). STIM1L has been shown to induce SOCE quicker than STIM1S, attributable to its association with Orai1 at rest rather than needing to migrate to bind Orai1 following store depletion like that of STIM1S (Darbellay 2011; Horinouchi 2012).

Consistent with the possibility of a STIM1 modification, STIM1 localisation was altered with differentiation of N-type and S-type cells. In N-type cells, there was increased clustering STIM1 with differentiation whilst in S-type cells, STIM1 accumulated at the PM. This varied distribution of STIM1 was altered in N-type cells following induction of SOCE, whereby STIM1 expression became more diffuse in P_N cells and remained clustered in D_N cells but was not altered in P_S or D_S cells. These differences in STIM1 localisation with differentiation and between N-type and S-type cells highlight a potential differences in STIM1 modification and/or function between phenotypes. STIM1 has been shown to redistribute to the PM and co-localise with Orai1 upon Ca^{2+} store depletion in sinoatrial node cells (Liu 2015), *Xenopus* oocytes (Courjaret 2014) and HEK293 cells (Fukushima 2012). Similarly, STIM1 association with the ER and redistribution of STIM1 into punctate structures forming within 100 nm of the PM following TG stimulation has been observed in HeLa cells whilst a STIM1 mutant lacking an EF-hand binding domain failed to reorganise into puncta following TG addition (Liou 2005). Phosphorylation of STIM1 is required for associated with PM channels and SOCE activation in platelets (Lopez 2012) and therefore may affect localisation patterns. N-linked glycosylation within the SAM domain of STIM1 is important for STIM1 cell surface trafficking (Williams 2002) and may have a role in expression patterns observed here in N-type and S-type cells.

As well as a role for STIM1 in SOCE, the level of Orai1 expression has been associated with SOCE. In this study, Orai1 down-regulation was associated with differentiation of N-type and S-type cells and a reduction in SOCE. Our laboratory has previously shown that Orai1 knockdown causes dampened SOCE in N-type populations and that overexpression of Orai1 restores SOCE in differentiating N-type populations (Bell 2011). Orai1 has a role in SOCE in other cell types, as knockdown of Orai1 induced a down-regulation of SOCE activity in neural progenitor cells (Hao 2014), acinar cells (Hong 2011), osteoclasts (Zhou 2011), endothelial cells (Abdullaev 2008), Jurkat T cells (Gwack 2007) and HEK293 cells (Gwack 2007; Kawasaki 2010). Orai1 overexpression causes an increase in SOCE in HEK293 cells (Fukushima 2012) and restores SOCE in SCID T cells and fibroblasts (Gwack 2007). Orai1 down-regulation was associated with differentiation of N-type and S-type cells in this study and our laboratory has

previously shown that overexpression of Orai1 in differentiating N-type populations restores SOCE activity and reduces morphological differentiation (Bell 2011), suggesting that Orai1 expression drives cells towards a proliferative state. Similarly, earlier studies have demonstrated that Orai1 knockdown inhibited proliferation of vascular smooth muscle cells (Potier 2009)and endothelial cells (Abdullaev 2008). Orai1 expression is suppressed in mitotic HeLa and HEK293 cells, coinciding with a down-regulation of SOCE (Smyth 2009). Orai1 also has a known role in the switch from proliferation to differentiation as knockdown of Orai1 was sufficient to induce differentiation of N-type populations and enhance morphological differentiation of 9*c*RA-treated N-type populations (Bell 2011). Conversely, neural differentiation of mouse embryonic stem cells is not affected by Orai1 knockdown (Hao 2014) whilst Orai1 down-regulation dampens SOCE but suppresses osteoclast differentiation (Zhou 2011; Hwang 2012). Therefore evidence suggests that Orai1 may be a negative regulator of differentiation in some cell types and promote differentiation in others but nevertheless has a direct role in the switch from proliferation to differentiation.

In this study, Orai1 localisation was altered with differentiation of N-type and S-type populations. In N-type cells, there was a reduction in Orai1 foci with differentiation whilst in S-type cells, there was a dispersion of Orai1 clusters, indicating that there may be a modification of Orai1 or a change in function between phenotypes. Indeed, two isoforms of Orai1 have been identified in a range of cell types; a longer isoform Orai1α and short isoform Orai1β which localise similarly at the PM and interact with STIM1 but Orai1β is more motile in the PM (Fukushima 2012). Both Orai1 isoforms are capable of supporting SOCE in HEK293 cells (Fukushima 2012). Another potential explanation for the observed differences in localisation is that Orai1 is heavily post-translationally glycosylated, however in HEK293 cells, inhibition of glycosylation had no effect on Orai1 localisation or SOCE activity (Gwack 2007) and extra bands that would indicate glycosylation on western blots were not observed. Alternatively, Orai1 can be phosphorylated by protein kinase C, causing inactivation of SOCE however it is unclear how Orai1 function is altered by this modification (Kawasaki 2010).

TRPC1 channels are Ca^{2+} permeable and, through STIM1 interactions (Yuan 2007; Alicia 2008; Jardin 2008), as well as other mechanisms (Putney 2007), may function as a SOCs. Indeed, it has been shown that STIM1 is able to bind TRPC1 and induce SOC channel functionality (Yuan 2007) and induce SOC rather than ROC function through insertion of TRPC1 into lipid raft domains (Alicia 2008). In this study, levels of TRPC1 expression indicated a down-regulation with differentiation of N-type and S-type populations, however this was variable and lack of availability of a reliable TRPC1 antibody hindered this particular investigation. Previously this laboratory has shown TRPC1 expression to be up-regulated with differentiation of N-type populations (N. Bell 2013), as has been demonstrated in myoblast differentiation (Louis 2008; Zanou 2012) and hippocampal neuronal cell differentiation (Wu 2004). Knockdown of TRPC1 did not affect SOCE or induce morphological differentiation in proliferating N-type populations whilst TRPC1 knockdown prevented SOCE down-regulation and reduced morphological differentiation caused by 9*c*RA treatment (Bell 2011), therefore TRPC1 could have a role in SOCE such as compensating for a lack of Orai1. However, inhibition of TRPC1 was found to suppress proliferation of A549 lung cancer cells whereas overexpression of TRPC1 enhanced proliferation (Jiang 2013). Similarly, knockdown of TRPC1 in keratinocytes caused a reduction in SOCE and inhibited differentiation (Cai 2006) indicating that TRPC1 is involved in keratinocyte differentiation by promoting SOCE activity. This conflicting evidence supports that there is a role for TRPC1 in SOCE but TRPC1 function in SOCE activity and the differentiation response in neuroblastoma cells warrants further investigation.

Conditioned media had an effect on SOCE in N-type and S-type populations (Results 4.5) and was found to alter the expression of STIM1, Orai1, β-tubulin III and vimentin. P_S conditioned media did not significantly alter β-tubulin III expression or vimentin expression in P_N populations. Since vimentin expression was not affected, and a non-significant increase in vimentin expression was associated with N-type differentiation (Results 3.3), and cells retained a P_N phenotype (Results 4.5), P_S conditioned media does not induce differentiation of P_N populations. This is consistent with the finding that P_S conditioned media caused an apparent increase in STIM1 and Orai1 expression

in P_N populations and did not alter SOCE activity (Results 4.5). P_S conditioned media was therefore not sufficient to influence the P_N phenotype.

D_S conditioned media did not affect β-tubulin III expression but caused a 6-fold increase in vimentin expression in P_N populations, indicating that D_S conditioned media may induce a non-neuronal phenotype or a differentiating phenotype in P_N populations. A non-significant up-regulation of vimentin expression was associated with N-type differentiation (Results 3.3) and the morphology of P_N populations treated with D_S conditioned media was similar to that of D_N populations, indicating that the observed increase in vimentin expression was likely due to D_S conditioned media inducing P_N differentiation towards a neuronal phenotype. Since D_S conditioned media also induced SOCE down-regulation in P_N cells (Results 4.5), consistent with the discussed induction of neuronal differentiation, but did not affect STIM1 or Orai1 expression, another mechanism for SOCE (e.g. TRPC1 or Orai3) may be induced by D_S conditioned media. Taken together these results indicate D_S conditioned media, at least in part, induces some characteristics of neuronal differentiation in P_N populations.

D_S conditioned media did not affect the expression of β-tubulin III in D_N populations, suggesting that D_S conditioned media does not affect the ability of N-type populations to differentiate towards a neuronal phenotype. There was a 10-fold increase in vimentin expression in D_N populations treated with D_S conditioned media however, this was dampened compared to D_N population vimentin expression implying that D_S conditioned media may dampen some aspects of the differentiation of N-type populations. There was an increase in STIM1 molecular weight and a down-regulation of Orai1 expression in D_N+D_S populations, similar to that of D_N populations, and SOCE activity was down-regulated compared to P_N populations but similar to D_N populations (Results 4.5). Taken together, these results indicate that D_S conditioned media did not drastically affect differentiation or the role of STIM1 or Orai1 in SOCE in N-type populations but may have subtle differentiation dampening effects.

P_N conditioned media up-regulated β-tubulin III expression in P_S populations but did not affect vimentin expression, suggesting that P_N conditioned media may induce a biochemical shift towards a neuronal phenotype in P_S populations but does not drastically affect the non-neuronal phenotype of P_S populations. P_N conditioned media caused an apparent up-regulation of STIM1 and Orai1 expression in P_S populations, therefore the previously observed down-regulation of SOCE induced by P_N conditioned media was not attributed to a change in STIM1 or Orai1 expression, suggesting a possible change in the mechanism of SOCE (e.g. TRPC1 or Orai3). These results indicate that P_N conditioned media may influence the phenotype of S-type populations to become more N-type-like.

D_N conditioned media up-regulated β-tubulin III and vimentin expression in P_S populations suggesting that D_N conditioned media may induce a shift towards a neuronal phenotype in P_S populations, since this expression pattern is characteristic of N-type differentiation (Results 3.3)(N. Bell 2013), however morphologically, S-type cells were differentiating (Results 4.5). D_N conditioned media caused an increase in the molecular weight of STIM1 and an apparent down-regulation of Orai1 in P_S populations, consistent with the previous finding that SOCE activity is down-regulated in P_S populations treated with D_N conditioned media (Results 4.5). These results demonstrate that D_N conditioned media may induce a differentiating phenotype in P_S populations.

D_N conditioned media did not alter β-tubulin III expression in D_S populations but expression was down-regulated compared to P_S+D_N populations, indicating that differentiation of S-type populations commits S-type cells to a non-neuronal lineage that is not affected by D_N conditioned media. There was a 2-fold increase in vimentin expression in D_S populations treated with D_N conditioned media that was slightly higher than that observed in D_S populations but lower than that of P_S+D_N suggesting that D_N conditioned media does not affect differentiation of S-type populations. There was no change in Orai1 expression but there was an increase in the molecular weight of STIM1 in D_S populations treated with D_N conditioned media was still present, indicating that the previous finding that SOCE activity was also down-regulated

(Results 4.5) was attributed to changes in STIM1 expression. The expression of Orai1 and increase in molecular weight of STIM1 in D_S+D_N populations was similar to that of D_S populations but the level of STIM1 and Orai1 expression was up-regulated compared to D_S populations consistent with a slight increase in SOCE activity (Results 4.6). This suggests that differentiating S-type populations are committed to a non-neuronal lineage that may be slightly dampened by D_N conditioned media.

Taken together, these results demonstrate that conditioned media from proliferating S-type populations does not drastically influence N-type population characteristics whilst differentiating S-type populations may influence the phenotype of N-type populations by promoting differentiation of N-type populations slightly dampening 9*c*RA-induced differentiation of N-type populations. Conditioned media from proliferating N-type populations can influence the S-type populations to exhibit more N-type-like characteristics, suggesting that N-type cells may exert this influence to ensure the neuroblastoma populations remain predominantly N-type in order to thrive. Differentiation of S-type populations appears to commit them to a non-neuronal cell fate that can be slightly dampened by conditioned media from differentiating N-type populations.

It is plausible that the effects of D_N and D_S conditioned media could, at least in part, be due to residual 9*c*RA in the media. However, the observed results do indicate that the conditioned media effect is caused by phenotype rather than a direct influence of 9*c*RA. For example, D_S conditioned media alone did not alter STIM1 molecular weight in P_N cells, and D_N conditioned media caused an increase in β-tubulin III expression that was not observed to the same extent in D_S populations. Similarly, the application of 9*c*RA together with D_S and D_N condition media as a control identified that the down-regulation in the level of STIM1 expression seen with N-type differentiation was dampened by D_S media and that the increase in β-tubulin III expression caused by D_N conditioned media was not present when S-type populations were differentiated alongside treatment. This also suggests that the observed effects were caused by phenotype rather than direct effect of residual 9*c*RA.

Alterations in STIM1 and Orai1 expression were found to underlie the down-regulation of SOCE associated with 7 day 9*c*RA-induced differentiation of N-type and S-type populations (Chapter 4). The relationship and sequence of these changes were further investigated over the time-course of the differentiation response.

Chapter 6: Differentiation time-course

Chapter 6 – Introduction

As previously discussed, treatment of N-type and S-type populations with 1 µM 9*c*RA for 7 days induces morphological and biochemical differentiation. For N-type cells, this involves an elongation of neurite-like processes, up-regulation of Bcl-2, uncoupling of Ca^{2+} store release and SOCE and a down-regulation of the SOCE proteins STIM1 and Orai1. For S-type cells, this involves cell margin spreading with an increase in cell diameter, down-regulation of Bcl-2, uncoupling of Ca^{2+} store release and SOCE and a down-regulation of the SOCE proteins STIM1 and Orai1.

The sequence of these differentiation-associated events is unclear therefore this chapter aimed to investigate the differentiation time-course in N-type and S-type populations through study of the relationship between these markers of differentiation over the 7 days of differentiation induction. The effect of differentiation agent withdrawal was also explored to determine the possibility of differentiation reversal.

Throughout this chapter, proliferating N-type and S-type populations (EtOH treated) will be referred to as P_N and P_S, respectively, whilst differentiating N-type and S-type populations (9*c*RA treated) will be referred to as D_N and D_S, respectively. The day of treatment will be referred to between days 1-7 of each condition. After 7 days, treatment was withdrawn and cells were grown in standard culture media alone for a further 5 days (day 12).

Chapter 6 – Results

6.1. Morphological differentiation is induced early in the 9cRA treatment time-course

9*c*RA-induced differentiation of N-type cells for 7 days causes elongation of neurite-like processes and an increase in percentage of differentiated cells, as determined by the number of cells with at least one neurite >50 µm in length (Results 3.1). In S-type cells, 9*c*RA-induced differentiation for 7 days causes cell margin spreading and an increase in diameter of S_O and S_A cells and an increase in length of S_E cells (Results 3.1). Morphological differentiation was observed over the 7 day time-course of 9*c*RA treatment to determine the onset and progression of morphological differentiation.

As described previously, neurite length was used to classify N-type cells as morphologically proliferating or differentiated and cells possessing one or more neurites >50 µm in length were classed as differentiated. From the first day of treatment, elongation of neurites could observed in D_N cells compared to the short neurites of P_N cells and elongation was seen to progress over the treatment time-course (Figure 6.1.1). Over the treatment time-course, there was a significant increase in percentage differentiation and average neurite length of D_N cells (both $P<0.0001$) that were not significantly altered in P_N cells ($P=0.607$ and $P=0.263$, respectively, Figure 6.1.2A and B). There was a significant increase in percentage differentiation and average neurite length in D_N cells compared to P_N cells over the treatment time-course (both $P<0.0001$ Figure 6.1.2A and B).

From day 1 of treatment, the percentage of differentiated cells and average neurite length was significantly higher in D_N cells (12% and 40 µm, respectively) compared to P_N cells (3%, $P=0.018$ and 25 µm, $P=0.0002$, respectively, Figure 6.1.2A and B). Percentage differentiation and average neurite length progressively increased over the treatment time-course, peaking at day 5 of treatment, where percentage differentiation and average neurite length in D_N cells (25% and 49 µm, respectively) were significantly higher than that of P_N cells (4%, $P<0.0001$ and 29 µm, $P=0.002$, respectively, Figure 6.1.2A and B). There was no significant change in percentage differentiation between D_N cells at day 5 and day 7 ($P=0.997$ and $P=0.719$, respectively, Figure 6.1.2A and B). Following treatment withdrawal, percentage differentiation and

average neurite length were significantly reduced in D_N cells (4% and 31 µm) compared to D_N cells at day 7 (both P<0.0001) and were not significantly different to that of P_N cells at day 12 (1%, P>0.999 and 23 µm, P=0.417, respectively, Figure 6.1.2A and B).

As described previously, diameter of S_O and S_A cells and length of S_E cells were used to classify S-type cells as morphologically proliferating or differentiating. From the first day of treatment, there was no noticeable difference in cell margin spreading in D_S cells compared to P_S cells however cell margin spreading can be observed from day 3 of treatment in D_S cells and progresses up to day 7 of treatment (Figure 6.1.3). Over the treatment time-course, there was a significant increase in D_S S_O and D_S S_A cell diameter and D_S S_E cell length (all P<0.0001, Figure 6.1.4A, B and C) but no significant change in P_S S_E cell length (P=0.075, Figure 6.1.4 C). There was a slight but significant change in P_S S_O and P_S S_A cell diameter over the treatment time-course (P=0.0031 and P=0.004, respectively) but this was attributed to a small decrease in cell diameter at day 4 (Figure 6.1.4A and B). D_S S_O and D_S S_A cell diameter and D_S S_E cell length were significantly higher than that of P_S S_O, P_S S_A and P_S S_E cells, respectively over the treatment time-course (all P<0.0001, Figure 6.1.4A, B and C).

There was no significant difference between the diameter of P_S S_O cells (35 µm) and D_S S_O cells (32 µm), P_S S_A cells (29 µm) and D_S S_A cells (30 µm) and the length of P_S S_E cells (46 µm) and D_S S_E cells (46 µm) from day 1 of treatment (all P>0.999, Figure 6.1.4A, B and C). By day 4 of treatment the diameter of D_S S_O cells (39 µm) was significantly higher than that of P_S S_O cells (28 µm, P=0.0032, Figure 6.1.4A). At day 4 of treatment, the diameter of D_S S_A cells (38 µm) and length of D_S S_E cells (61 µm) were increased compared to that of P_S S_A cells (28 µm) and P_S S_E cells (41 µm), however this was non-significant (P=0.167 and P=0.372, respectively, Figure 6.1.4B and C). By day 5 of treatment, there was a peak in the diameter of D_S S_O cells (52 µm) and D_S S_A cells (46 µm) whilst the length of D_S S_E cells continued to increase up to day 7 of treatment (90 µm). Following treatment withdrawal, compared to day 7 D_S cells, there was no significant change in cell diameter of D_S S_O cells (45 µm, P=0.533) or D_S S_A cells (46 µm, P=0.999) and cell diameter remained significantly greater than that of day 12 P_S S_O cells (34 µm, P=0.0005) and P_S S_A cells (31 µm, P=0.0003), respectively (Figure 6.1.4A and B).

Length of P_S S_A cells was slightly increased at day 12 (31 µm) compared to day 7 (27 µm) but this was not significant (P=0.183). Following treatment withdrawal, there was a significant reduction in cell length of D_S S_E cells (60 µm) compared to day 7 D_S S_E cells (90 µm, P=0.0018) and this was not significantly different to that of day 12 P_S S_E cells (56 µm, P>0.999). Length of P_S S_E cells was slightly increased at day 12 (56 µm) compared to day 7 (48 µm) but this was not significant (P=0.713).

Taken together, these results indicate that morphological differentiation progressed in a multi-step manner in N-type populations that was initiated within the first day of 9*c*RA treatment in N-type populations, with a further increase in differentiation and peak at day 5 of treatment. For S-type populations, morphological differentiation was induced gradually from the third day of treatment, peaking at day 5 for S_O and S_A cells but at day 7 for S_E cells. Following 5 days of treatment withdrawal, D_N populations seem to revert back to a P_N phenotype indicating that N-type cells may lose their differentiating characteristics following removal of the differentiation stimulus. D_S S_E cells show a potential reversion to a P_S phenotype whilst D_S S_O and D_S S_A cells retain a D_S morphology. Given that P_S S_E cells seem to become more morphologically differentiated over time in culture, based on the increase in length between day 7 and 12, it may be that 9*c*RA withdrawal does not cause D_S S_E cells to completely lose their differentiating characteristics. This therefore suggests that S-type cells may remain a fully differentiating phenotype following removal of the differentiation stimulus.

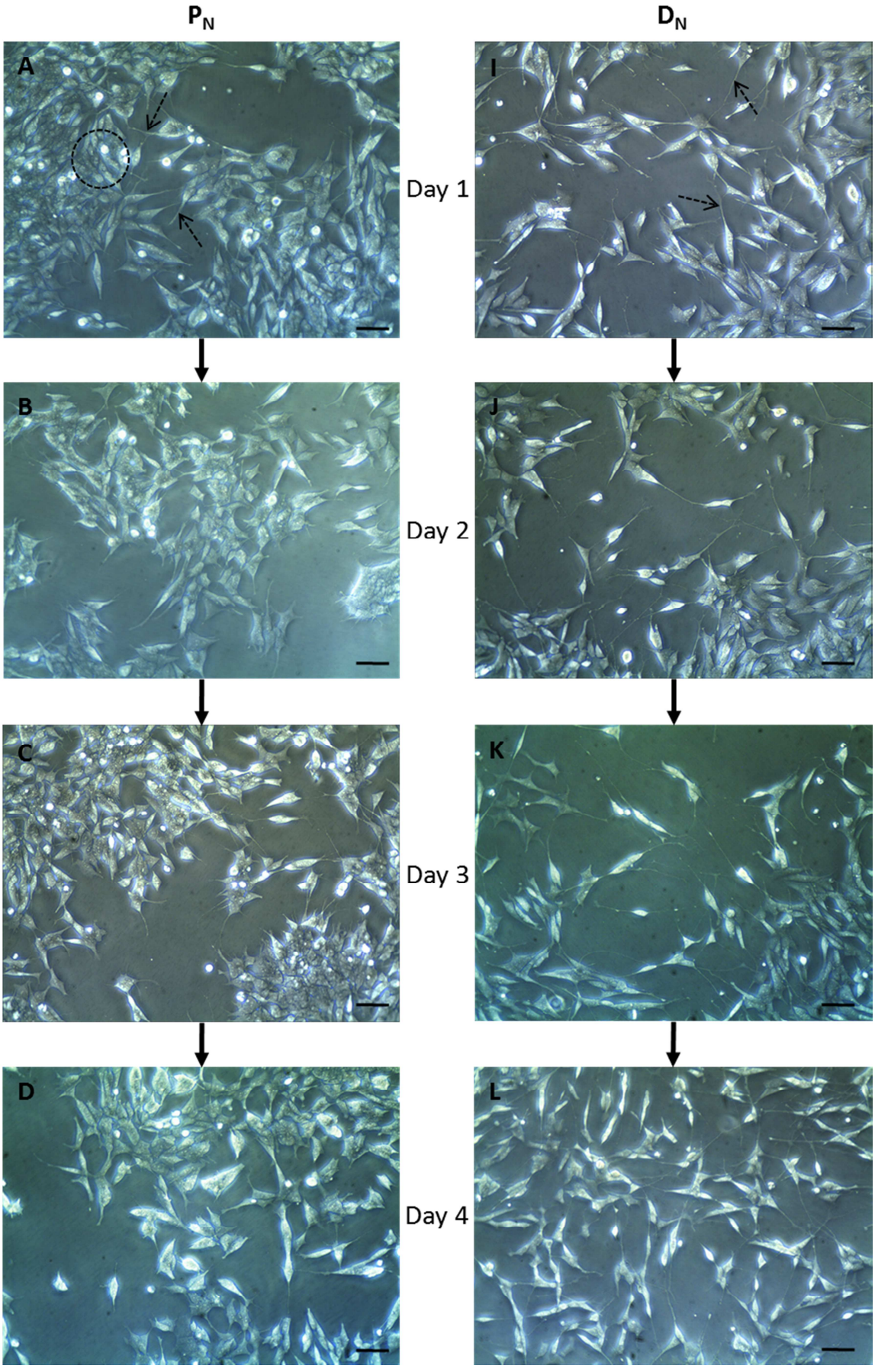
P_N
D_N
A
I
Day 1
B
J
Day 2
C
K
Day 3
D
L
Day 4

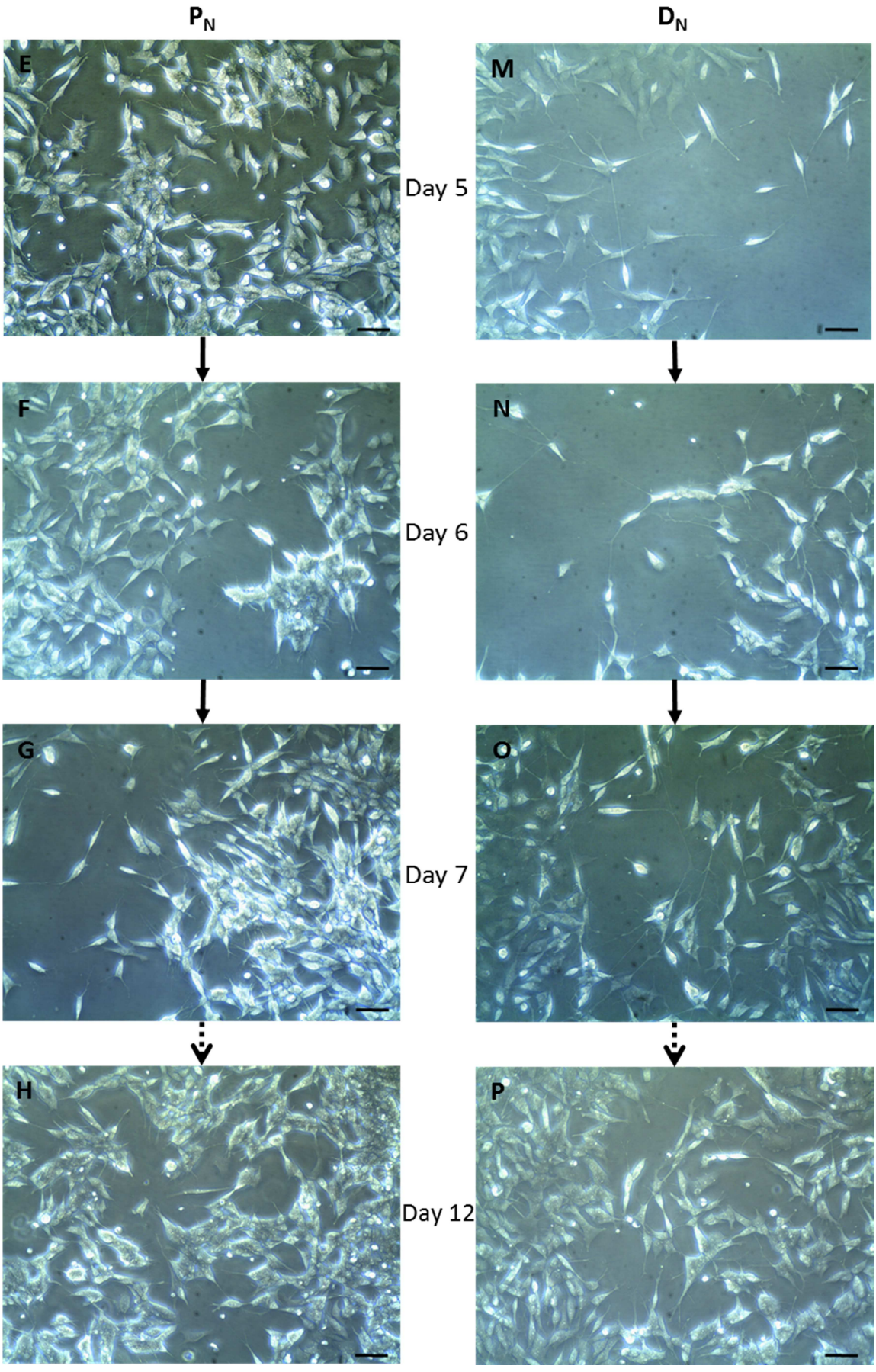
P_N
D_N
E
M
Day 5
F
N
Day 6
G
O
Day 7
H
P
Day 12

Figure 6.1.1. Neurite elongation in N-type cells can be observed from the first day of 9*c*RA treatment

N-type populations were treated for 7 days (1-7) with 1 µM 9*c*RA (D_N) or an equivalent volume of EtOH (P_N). After 7 days, treatment was withdrawn from both P_N and D_N cells, which were grown in standard culture media alone for a further 5 days (12). **(A-G)** P_N cells possess short neurite-like processes (as demonstrated by dashed arrows in A) and grow in aggregates (demonstrated by dashed circle in A). **(I-O)** D_N cells exhibit elongated neurites (as demonstrated by dashed arrows in I) and decreased growth. This neurite elongation can be observed from **(I)** the first day of 9*c*RA treatment and is seen to progress **(J-O)** over the treatment time-course. Five days following treatment withdrawal, **(P)** D_N cells exhibit a similar morphology to **(H)** P_N cells. Scale bars of phase contrast images represents 50 µm.

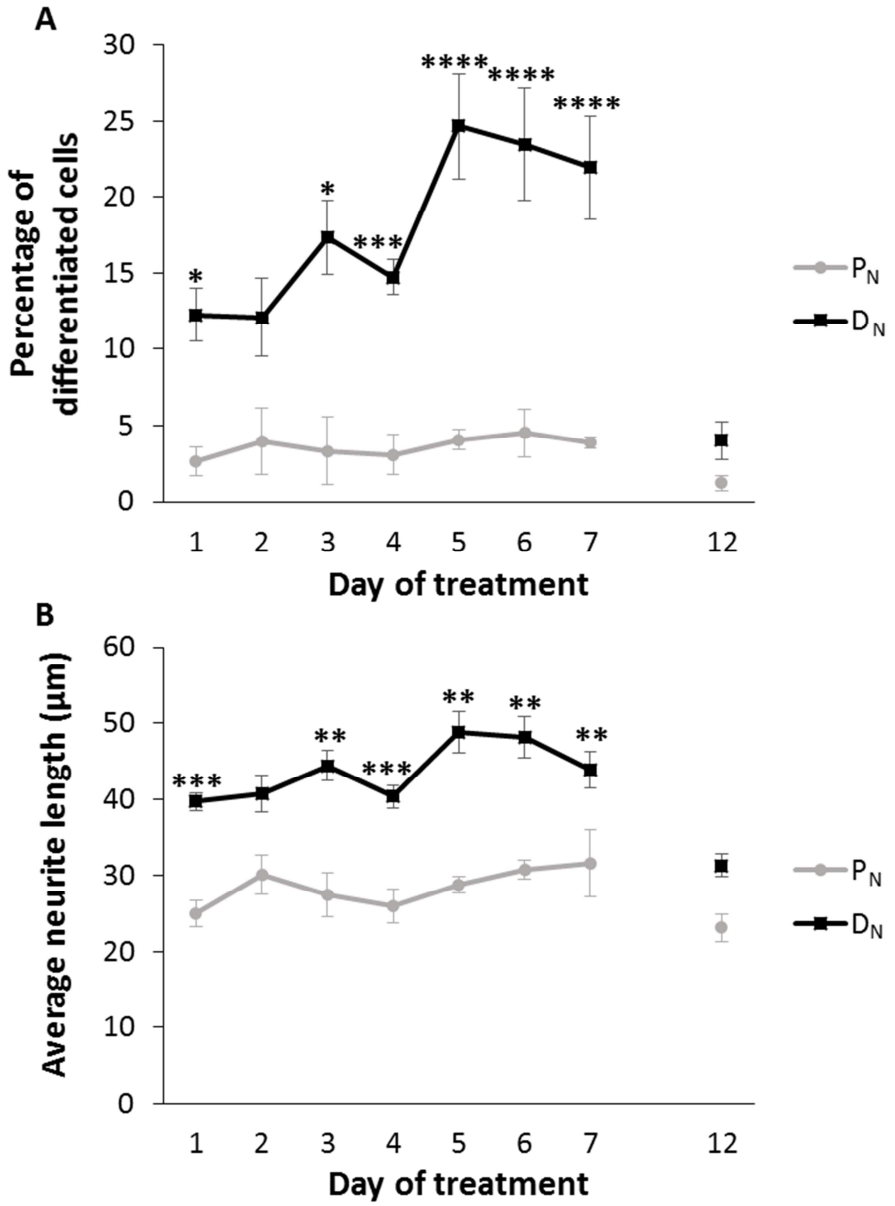

Figure 6.1.2. 9*c*RA-induced morphological differentiation of N-type populations is induced from the first day of treatment

N-type populations were treated over 7 days (1-7) with 1 µM 9*c*RA (D_N) or an equivalent volume of EtOH (P_N). After 7 days, treatment was withdrawn from both P_N and D_N cells, which were grown in standard culture media alone for a further 5 days (12). Phase contrast were used for neurite measurements using Metamorph software. **(A)** Neurite length was used to classify N-type cells as morphologically proliferating or differentiated. Cells possessing one or more neurites >50 µm in length were classed as differentiated. Over the treatment time-course, there was a significant increase in percentage differentiation of D_N cells ($P<0.0001$) but was not significantly altered in P_N

cells (P=0.607). There was a significant increase in percentage differentiation in D_N cells compared to P_N cells over the treatment time-course (P<0.0001). From day 1 of treatment, the percentage of differentiated cells was significantly higher in D_N cells (12.26%) compared to P_N cells (2.67%, P=0.018*). At day 2, percentage differentiation was higher in D_N cells (12.08%) compared to P_N cells (3.97%) but this was not significant (P=0.560). Percentage differentiation was further increased in D_N cells compared to P_N cells at day 3 (17.34% and 3.33% respectively, P=0.011*) and day 4 (14.74% and 3.07% respectively, P=0.0002***). There was a further significant increase in percentage differentiation in D_N cells at day 5 (24.66%) compared to D_N cells at day 1 (P=0.0042) and compared to P_N cells at day 5 (4.06%, P<0.0001****). Percentage differentiation remained significantly higher in D_N cells compared to P_N cells at day 6 (23.48% and 4.51% respectively, P<0.0001****) and day 7 (21.95% and 3.90% respectively, P<0.0001****). Following treatment withdrawal, percentage differentiation was significantly reduced in D_N cells (4.02%) compared to D_N cells at day 7 (P<0.0001****) and was not significantly different to that of P_N cells at 12 (1.22%, P>0.999). **(B)** Over the treatment time-course, there was a significant increase in the neurite length of D_N cells (P<0.0001) whilst neurite length was not significantly altered in P_N cells (P=0.263). There was a significant increase in neurite length in D_N cells compared to P_N cells over the treatment time-course (P<0.0001). From day 1 of treatment, the average neurite length of D_N cells (39.63 µm) was significantly longer than that of P_N cells (24.96 µm, P=0.0002***). At day 2, average neurite length was higher in D_N cells (40.69 µm) compared to P_N cells (30.12 µm) but this was not significant (P=0.404). Neurite length was further increased in D_N cells compared to P_N cells at day 3 (44.38 µm and 27.45 µm respectively, P=0.0099**), day 4 (40.29 µm and 25.96 µm respectively, P=0.0001***), day 5 (48.83 µm and 28.75 µm respectively, P=0.0016**) and day 6 (48.16 µm and 30.74 µm respectively, P=0.0099**) and day 7 (43.76 µm, and 31.55 µm respectively, P=0.0032**). Following treatment withdrawal, neurite length was significantly reduced in D_N cells (31.28 µm) compared to that of day 7 D_N cells (P<0.0001****) and was not significantly different to that of day 12 P_N cells (23.10 µm, P=0.417). P_N: 1 n=1084, 2 n=515, 3 n=493, 4 n=1015, 5 n=398, 6 n=515, 7 n=1043, 12 n=919. D_N: 1 n=889, 2 n=611, 3 n=488, 4 n=1192, 5 n=514, 6 n=654, 7 n=1131, 12 n=926.

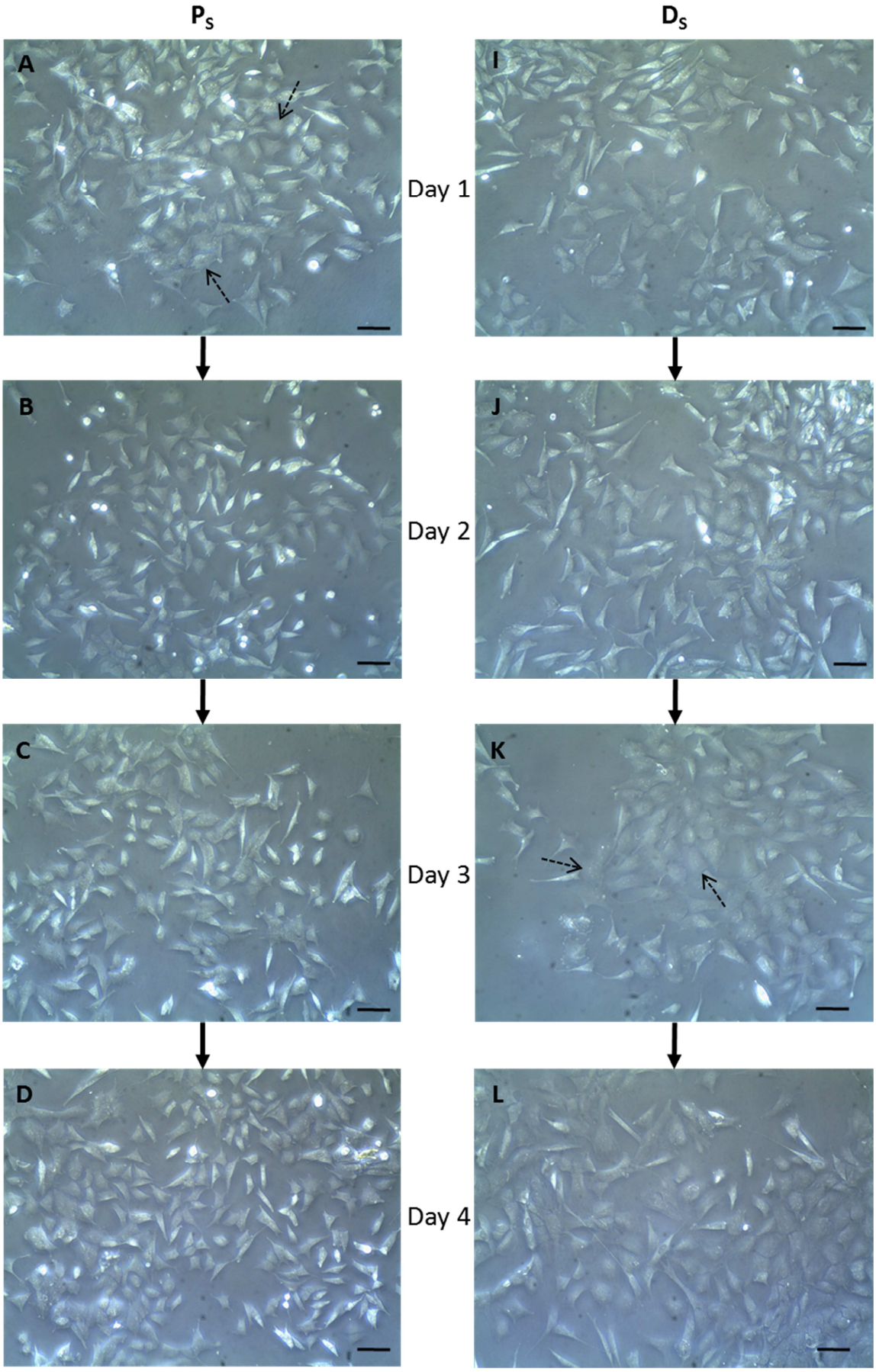
P_S
D_S
A
I
Day 1
B
J
Day 2
C
K
Day 3
D
L
Day 4

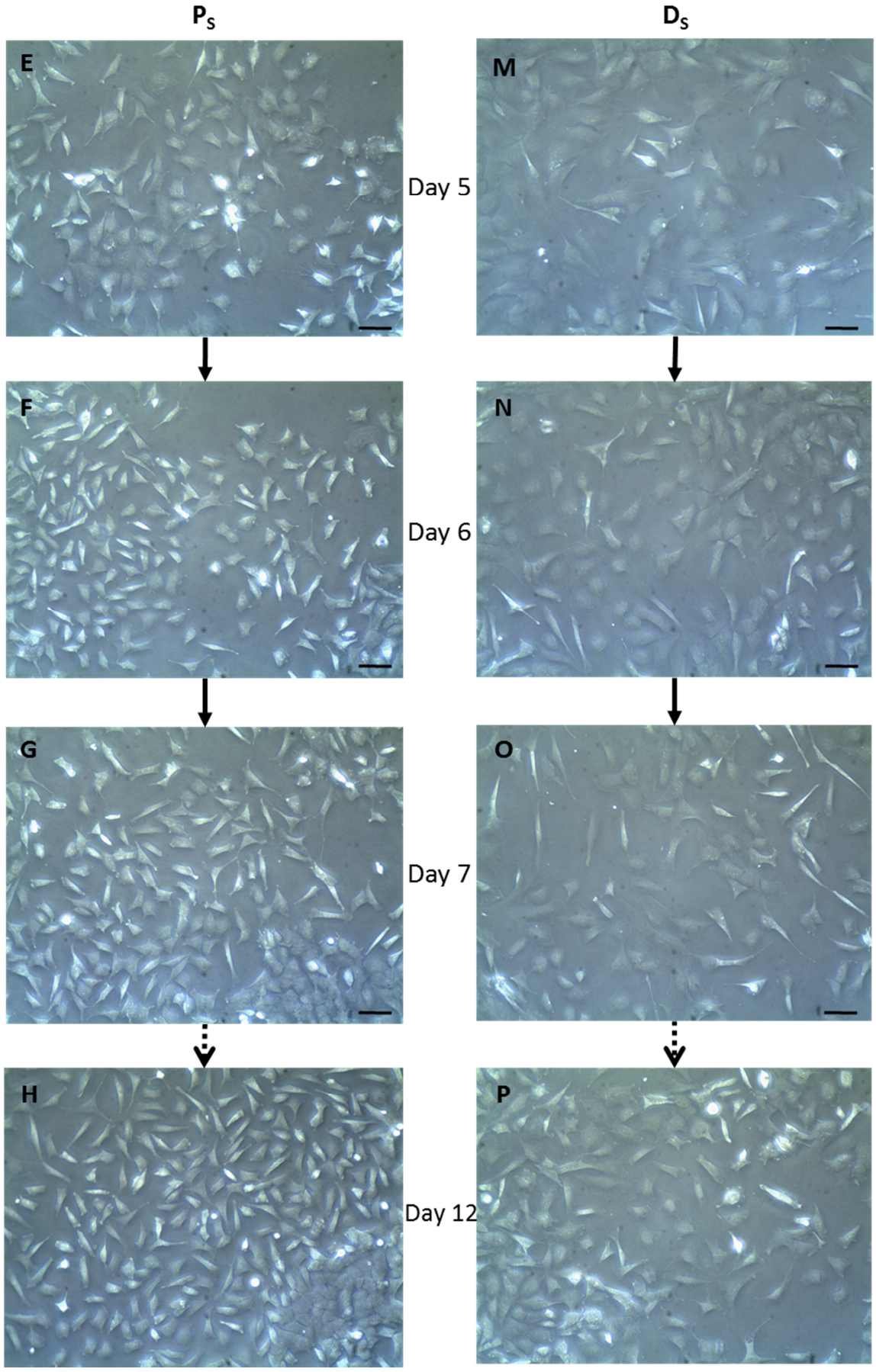
P_S
D_S
E
M
Day 5
F
N
Day 6
G
O
Day 7
H
P
Day 12

Figure 6.1.3. Cell margin spreading in S-type cells can be observed from the third day of 9*c*RA treatment

S-type populations were treated for 7 days (1-7) with 1 µM 9*c*RA (D_S) or an equivalent volume of EtOH (P_S). After 7 days, treatment was withdrawn from both P_S and D_S cells, which were grown in standard culture media alone for a further 5 days (12). **(A-H)** P_S cells possess abundant cytoplasm and a flattened morphology (as demonstrated by dashed arrows in A). At day 1 and 2 of treatment **(I-J)**, D_S cells resemble P_S cells and from day 3 of treatment, **(K-P)** D_S cells are more flattened with spread cell margins (as demonstrated by dashed arrows in K). **(H and P)** Five days following treatment withdrawal, **(P)** D_S cells appear to retain a differentiating morphology but less so than at **(O)** day 7 of treatment. Scale bars of phase contrast images represents 50 µm.

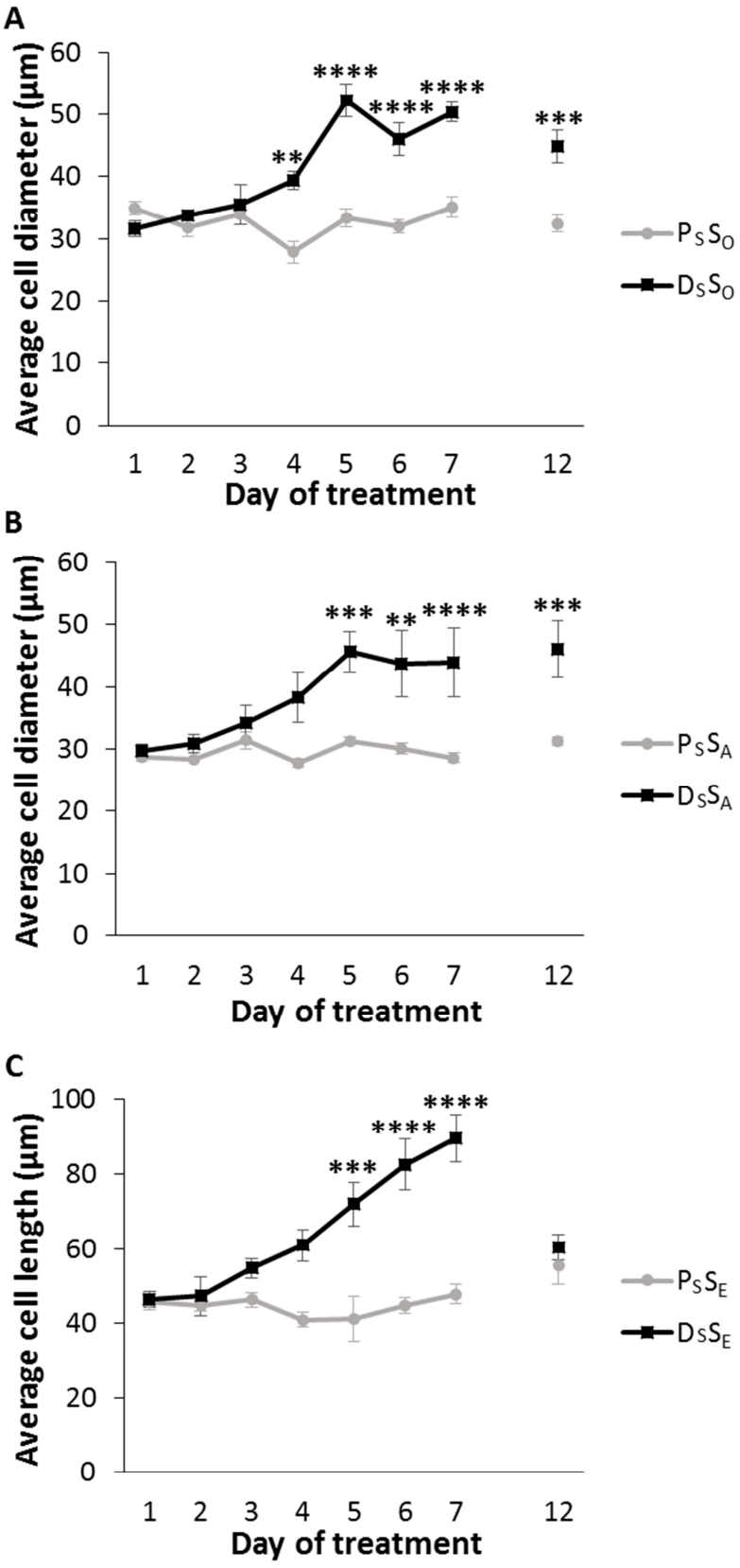
A
Average cell diameter (µm)
60
50
40
30
20
10
0
**
****
****
****
***
1 2 3 4 5 6 7 12
Day of treatment
PSSO
DSSO
B
Average cell diameter (µm)
60
50
40
30
20
10
0
***
**
****
***
1 2 3 4 5 6 7 12
Day of treatment
PSSA
DSSA
C
Average cell length (µm)
100
80
60
40
20
0
***
****
****
1 2 3 4 5 6 7 12
Day of treatment
PSSE
DSSE

Figure 6.1.4. 9*c*RA-induced morphological differentiation of S-type populations is induced from the fourth day of treatment

S-type populations were treated over 7 days (1-7) with 1 µM 9*c*RA (D_S) or an equivalent volume of EtOH (P_S). After 7 days, treatment was withdrawn from both P_S and D_S cells, which were grown in standard culture media alone for a further 5 days (12). Phase contrast were used for cell measurements using Metamorph software. The diameter of S_O and S_A cells and the length of S_E cells was used to determine the extent of morphological differentiation. **(A)** There was a slight but significant change in P_S S_O cell diameter over the treatment time-course (P=0.0031) that was attributed to a decrease in cell diameter at day 4. There was a significant increase D_S S_O cell diameter over the treatment time-course (P<0.0001). D_S S_O cell diameter was significantly higher than that of P_S S_O cells over the treatment time-course (P<0.0001). At day 1, 2 and 3, there was no significant difference between the diameter of P_S S_O cells (34.95 µm, 31.85 µm and 34.04 µm respectively) and D_S S_O cells (31.63 µm, 33.79 µm and 35.48 µm respectively, all P>0.999). At day 4, the diameter of D_S S_O cells (39.40 µm) was significantly higher than that of P_S S_O cells (27.83 µm, P=0.0032**). At day 5, the diameter of D_S S_O cells (52.27 µm) was significantly higher than that of P_S S_O cells (33.36 µm, P<0.0001****) and day 4 D_S S_O cells (P=0.0019). At day 6, the diameter of D_S S_O cells (46.04 µm) was significantly increased compared to P_S S_O cells (32.07 µm, P<0.0001****). At day 7, the diameter of D_S S_O cells (50.41 µm) was significantly increased compared to P_S S_O cells (35.12 µm, P<0.0001****) and day 4 D_S S_O cells (P=0.006). Treatment withdrawal led to a slight reduction in cell diameter in D_S S_O cells (44.84 µm) but this was still greater than that of P_S S_O cells (32.48 µm, P=0.0005***) and was not significantly different to that of day 7 D_S S_O cells (P=0.533). P_S S_O: 1 n=121, 2 n=97, 3 n=180, 4 n=226, 5 n=156, 6 n=189, 7 n=194, 12 n=226. D_S S_O: 1 n=304, 2 n=194, 3 n=272, 4 n=262, 5 n=235, 6 n=272, 7 n=328, 12 n=297. **(B)** There was a slight but significant change in P_S S_A cell diameter over the treatment time-course (P=0.004) that was attributed to a slight decrease in cell diameter at day 4. There was a significant increase D_S S_A cell diameter over the treatment time-course (P<0.0001). D_S S_A cell diameter was significantly higher than that of P_S S_A cells over the treatment time-course (P<0.0001). At day 1, 2 and 3, there was no significant difference between the diameter of P_S S_A cells (28.78 µm, 28.39 µm and 31.44 µm respectively) and D_S S_A

cells (29.73 µm, 30.89 µm and 34.27 µm respectively, all P>0.999). At day 4, the diameter of D_S S_A cells (38.36 µm) was higher than that of P_S S_A cells (27.77 µm) but non-significantly (P=0.167). At day 5, there was a significant increase in the diameter in D_S S_A cells (45.67 µm) compared to P_S S_A cells (31.36 µm, P=0.0003***) and day 2 D_S S_A cells (P=0.032). The diameter of D_S S_A cells at day 6 (43.72 µm) was significantly higher than that of P_S S_A cells (30.11 µm, P=0.003**). At day 7, the diameter of D_S S_A cells (43.90 µm) was significantly higher than that of P_S S_A cells (28.64 µm, P<0.0001****) and day 1 D_S S_A cells (P=0.007). Treatment withdrawal led to a further increase in cell diameter in D_S S_A cells (46.09 µm) that was significantly higher than that of day 2 D_S S_A cells (P=0.038) and day 12 P_S S_A cells (31.34 µm, P=0.0003***). P_S S_A: 1 n=194, 2 n=243, 3 n=202, 4 n=176, 5 n=307, 6 n=489, 7 n=304, 12 n=354. D_S S_A: 1 n=453, 2 n=230, 3 n=172, 4 n=166, 5 n=185, 6 n=127, 7 n=215, 12 n=157. **(C)** There was no significant change in P_S S_E cell length over the treatment time-course (P=0.075) and a significant increase D_S S_E cell length over the treatment time-course (P<0.0001). D_S S_E cell length was significantly higher than that of P_S S_E cells over the treatment time-course (P<0.0001). At day 1, 2 and 3, there was no significant difference between the length of P_S S_E cells (45.85 µm, 44.66 µm and 46.26 µm respectively) and D_S S_E cells (46.32 µm, P>0.999, 47.22 µm, P>0.999 and 54.72 µm, P=0.997, respectively). At day 4, the length of D_S S_E cells (60.93 µm) was increased compared to P_S S_E cells (40.99 µm) but this was not significant (P=0.372). At day 5, the length of D_S S_E cells (71.99 µm) was significantly increased compared to P_S S_E cells (41.32 µm, P=0.0002***) and day 2 D_S S_E cells (P=0.03). At day 6, there was a further increase in length of D_S S_E cells (82.51 µm) compared to P_S S_E cells (44.69 µm, P<0.0001****) and compared to day 3 D_S S_E cells (P=0.006). At day 7, length of D_S S_E cells (89.51 µm) was significantly greater than that of P_S S_E cells (47.86 µm, P<0.0001****) and that of day 4 D_S S_E cells (P=0.003). Treatment withdrawal caused a significant reduction in cell length in D_S S_E cells (60.33 µm) compared to day 7 D_S S_E cells (P=0.0018) that was not significantly different to that of day 12 P_S S_E cells (55.51 µm, P>0.999). Length of P_S S_E cells was slightly increased at day 12 compared to day 7 but this was not significant (P=0.713). P_S S_E: 1 n=26, 2 n=33, 3 n=36, 4 n=27, 5 n=36, 6 n=65, 7 n=44, 12 n=59. D_S S_E: 1 n=41, 2 n=31, 3 n=43, 4 n=37, 5 n=61, 6 n=44, 7 n=55, 12 n=40.

6.2. Expression of differentiation markers is altered before day 7 of 9cRA-induced differentiation

As previously described (Chapter 1 and 3), 9*c*RA-induced differentiation of N-type populations for 7 days does not alter β-tubulin III expression but induces up-regulation of vimentin and Bcl-2 and a slight increase in levels of CD133 expression whilst 9*c*RA-induced differentiation of S-type populations for 7 days does not alter β-tubulin III expression but induces up-regulation of vimentin, and apparent down-regulation of Bcl-2 and a slight decrease in levels of CD133 expression. The expression of the biochemical markers of differentiation; β-tubulin III, vimentin, Bcl-2 and CD133, were therefore investigated over the time-course of 9cRA treatment.

β-tubulin III is a microtubule protein expressed in neuronal cells (Katsetos 2003; Dráberová 2008) previously used as a marker of N-type population differentiation (Bell 2011) and was used to determine the neuronal-like nature of N-type and S-type populations. Both P_N and D_N populations expressed β-tubulin III throughout the treatment time-course and there was little variation in band intensity (Figure 6.2.1A). There was no significant difference in β-tubulin III expression over the treatment time-course of P_N (P=0.908), D_N populations (P=0.978) or between P_N and D_N populations (P=0.994, Figure 6.2.1B) indicating that whilst β-tubulin III expression is a marker for the neuronal lineage of N-type cells, it does not distinguish between proliferating and differentiating N-type cells. Following 5 days of treatment withdrawal, β-tubulin III expression was reduced by 35% in D_N cells compared to P_N cells (Figure 6.2.1B). β-tubulin III was also expressed in both P_S and D_S populations over the treatment time-course (Figure 6.2.2A and B), though to a lesser extent than that of P_N and D_N populations, likely due to S-type cells being of non-neuronal lineage. Following treatment withdrawal, β-tubulin III expression was slightly reduced D_S cell compared to P_S cells (Figure 6.2.2B).

The intermediate filament protein vimentin is expressed in non-neuronal neural crest cells such as Schwann and glial cells (Ciccarone 1989) and was used to determine the non-neuronal nature of N-type and S-type populations. Vimentin was weakly expressed by D_N populations and P_N populations throughout the treatment time-

course though there was an increase in band intensity in D_N populations from day 3 (Figure 6.2.1A). There was no significant change in vimentin expression over the treatment time-course by P_N populations (P=0.998), D_N populations (P=0.965) or between P_N and D_N populations (P=0.934), however vimentin expression was increased over 2-fold from day 3 (P=0.181) to day 7 (P=0.319) of treatment in D_N populations compared to P_N populations (Figure 6.2.1C). Vimentin was expressed by both D_S and P_S populations (Figure 6.2.2A) and to a greater extent than that of P_N (P=0.0002) and D_N populations (P=0.0025). There was a slight but non-significant increase in vimentin expression in both P_S populations (P=0.414) and D_S populations (P=0.101) over the treatment time-course (Figure 6.2.2C). There was no significant difference in vimentin expression between D_S and P_S populations over the treatment time-course (P=0.131, Figure 6.2.2C). Following 5 days of treatment withdrawal, vimentin expression was 3-fold higher in D_S populations compared to P_S populations (Figure 6.2.2C), suggesting that D_S populations continue to move toward a non-neuronal phenotype despite removal of the differentiation stimulus.

These results confirm that, as expected, the neuronal marker β-tubulin III was expressed to a greater extent in N-type populations than S-type populations and the non-neuronal marker vimentin was expressed to a greater extent in S-type populations than N-type populations. The expression of β-tubulin III does not change over the differentiation time-course of D_N or D_S populations, indicating that the level of β-tubulin III expression is unaffected by the differentiation response of N-type and S-type populations. Vimentin expression was slightly higher in D_N populations than P_N populations early in the treatment time-course, correlating with the previous finding that vimentin is temporarily up-regulated with neurite outgrowth (Shea 1993).
A slight increase in vimentin expression in P_S populations early in the treatment time-course implies that these cells may move towards a more non-neuronal phenotype over time in culture. Vimentin expression was slightly higher in D_S than P_S populations at day 6 and 7. Although not significant, this could be indicative of S-type populations becoming more non-neuronal-like with differentiation.

Following treatment withdrawal, potentially, N-type populations move away from a neuronal phenotype and possibly revert back to a P_N phenotype whilst S-type populations seem to retain a differentiating non-neuronal phenotype.

The anti-apoptotic protein Bcl-2 has been used as a marker of differentiation in SH-SY5Y cells as it is up-regulated with 9*c*RA-induced differentiation (Riddoch 2007; Bell 2011). Bcl-2 was clearly expressed from day 2 of treatment of P_N and D_N populations (Figure 6.2.3A). Over the treatment time-course, Bcl-2 expression was increased in P_N populations ($P<0.0001$) and D_N populations ($P=0.0019$) and Bcl-2 expression was significantly higher in D_N than P_N populations ($P<0.0001$, Figure 6.2.3B). Bcl-2 expression is up-regulated by 51% from day 2 of treatment ($P=0.366$) and significantly by more than 3-fold by day 4 ($P<0.0001$). By day 7 of treatment, Bcl-2 expression was significantly 74% higher in D_N populations than P_N populations ($P=0.002$) however, following 5 days of treatment withdrawal, there was no difference in Bcl-2 expression between P_N and D_N populations, perhaps suggesting that N-type populations move away from a neuronal phenotype after removal of the differentiation stimulus (Figure 6.2.3B). Bcl-2 was expressed by both P_S and D_S populations over the treatment time-course and following treatment withdrawal (Figure 6.2.4A). Over the treatment time-course, there was no significant difference in Bcl-2 expression in P_S populations ($P=0.762$) or D_S populations ($P=0.246$) or between P_S and D_S populations ($P=0.472$, Figure 6.2.4B). By day 7 of treatment, Bcl-2 expression was slightly reduced in D_S populations compared to P_S populations, though this was non-significant (34%, $P=0.121$, Figure 6.2.4B). Following 5 days of treatment withdrawal, Bcl-2 expression was 76% lower in D_S populations compared to P_S populations (Figure 6.2.4B). These results suggest that Bcl-2 is an effective marker for differentiation in N-type populations as an increase of expression coincides with the differentiation response of N-type populations but not S-type populations.

CD133 is a cell surface glycoprotein that is associated with stem cells (Mizrak 2008) and was non-significantly up-regulated in D_N populations compared to P_N populations (Results 3.4). CD133 was expressed in both P_N and D_N populations over the treatment time-course (Figure 6.2.5.A). Over the treatment time-course there was a non-

significant decrease in CD133 expression in P_N populations (P=0.712) and a non-significant increase in expression in D_N populations (P=0.074). However, in D_N populations, CD133 expression was increased by 84% from day 3 of treatment (P=0.219), and was over 4-fold higher by day 7 of treatment (P=0.117) compared to P_N populations (Figure 6.2.5B). It may be that with differentiation, N-type populations may retain stem-cell like properties from the early stages in the differentiation response but this remains to be tested. Given the timing of these experiments, unfortunately, CD133 expression was not determined over the S-type population differentiation response or following treatment withdrawal as there was a lack of antibody stock.

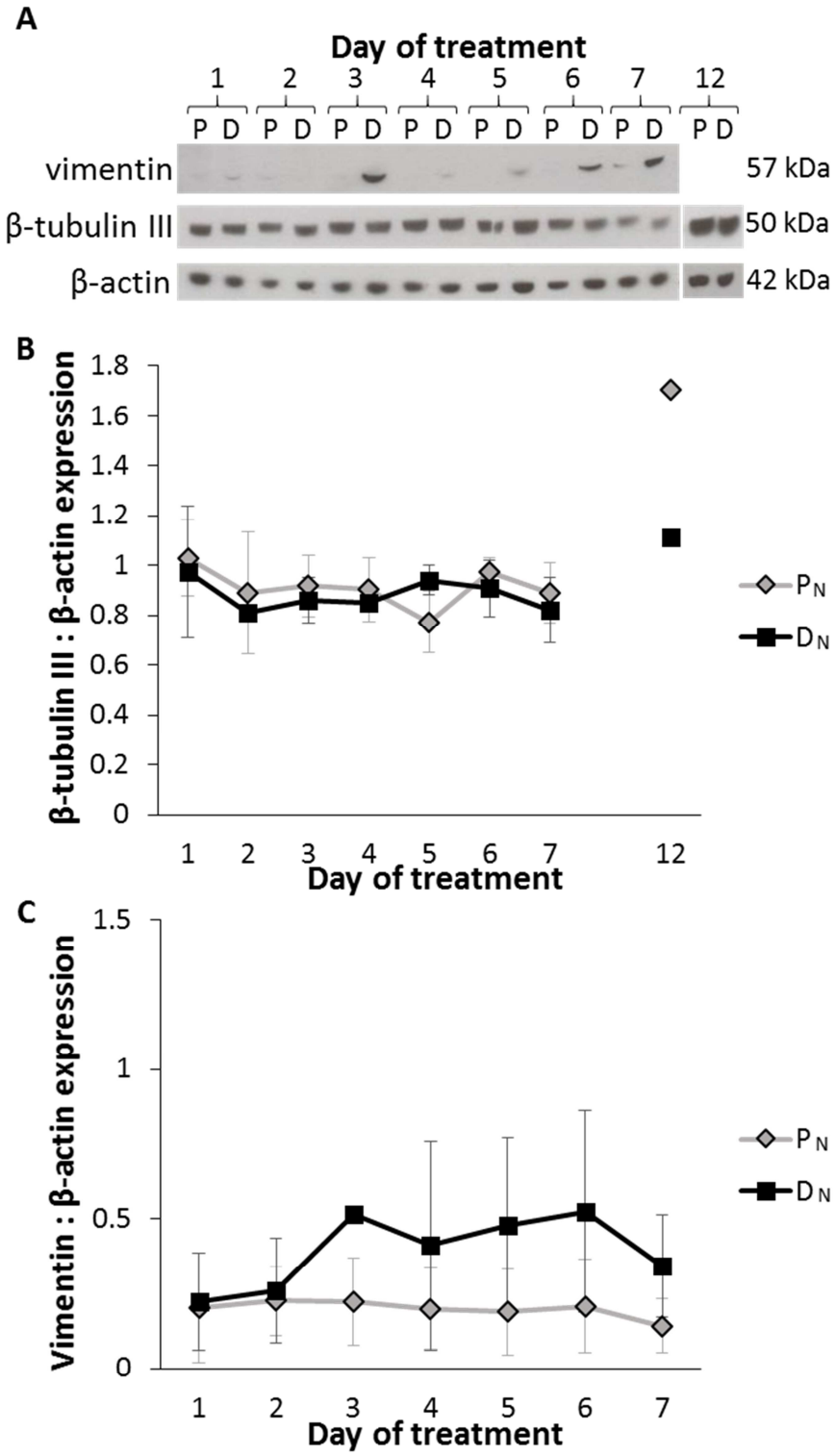

Figure 6.2.1. Expression of vimentin is altered early in differentiating N-type populations whilst β-tubulin III expression remains constant

Western blots were performed on protein samples from N-type populations that were treated over 7 days (1-7) with 1 µM 9*c*RA (D_N) or an equivalent volume of EtOH (P_N).

After 7 days, treatment was withdrawn from both P_N and D_N populations, which were grown in standard culture media alone for a further 5 days (12). Blots were probed with anti-β-tubulin III antibody which detected a band at 50 kDa, anti-vimentin antibody which detected a band at 57 kDa or β-actin antibody which was used as a loading control and detected a band at 42 kDa. **(A)** β-tubulin III was expressed at a similar level by both P_N and D_N populations with little variation in band intensity over the treatment time-course. β-tubulin III expression was also detected in both P_N and D_N populations following 5 days of treatment withdrawal. Vimentin was barely detected in P_N populations and D_N populations however there was an increase in band intensity from day 3 of treatment in D_N populations. **(B)** There was no change in expression of β-tubulin III over the treatment time-course in P_N populations (P=0.908) or D_N populations (P=0.978). Throughout the differentiation time-course, there was no significant difference in β-tubulin III expression between P_N and D_N populations (P=0.994) though there was a 22% increase in expression at day 5 (P=0.344). After 5 days of treatment withdrawal, β-tubulin III expression was 35% lower in D_N populations compared to P_N populations. All N≥2 except 12 N=1. **(C)** There was no change in expression of vimentin over the treatment time-course in P_N populations (P=0.998) or D_N populations (P=0.965). Throughout the differentiation time-course, there was no significant difference in vimentin expression between P_N and D_N populations (P=0.934), although vimentin expression was 2-fold higher in D_N populations from day 3 of treatment (P=0.181) and over 2-fold higher by day 7 of treatment (P=0.319). All N≥2.

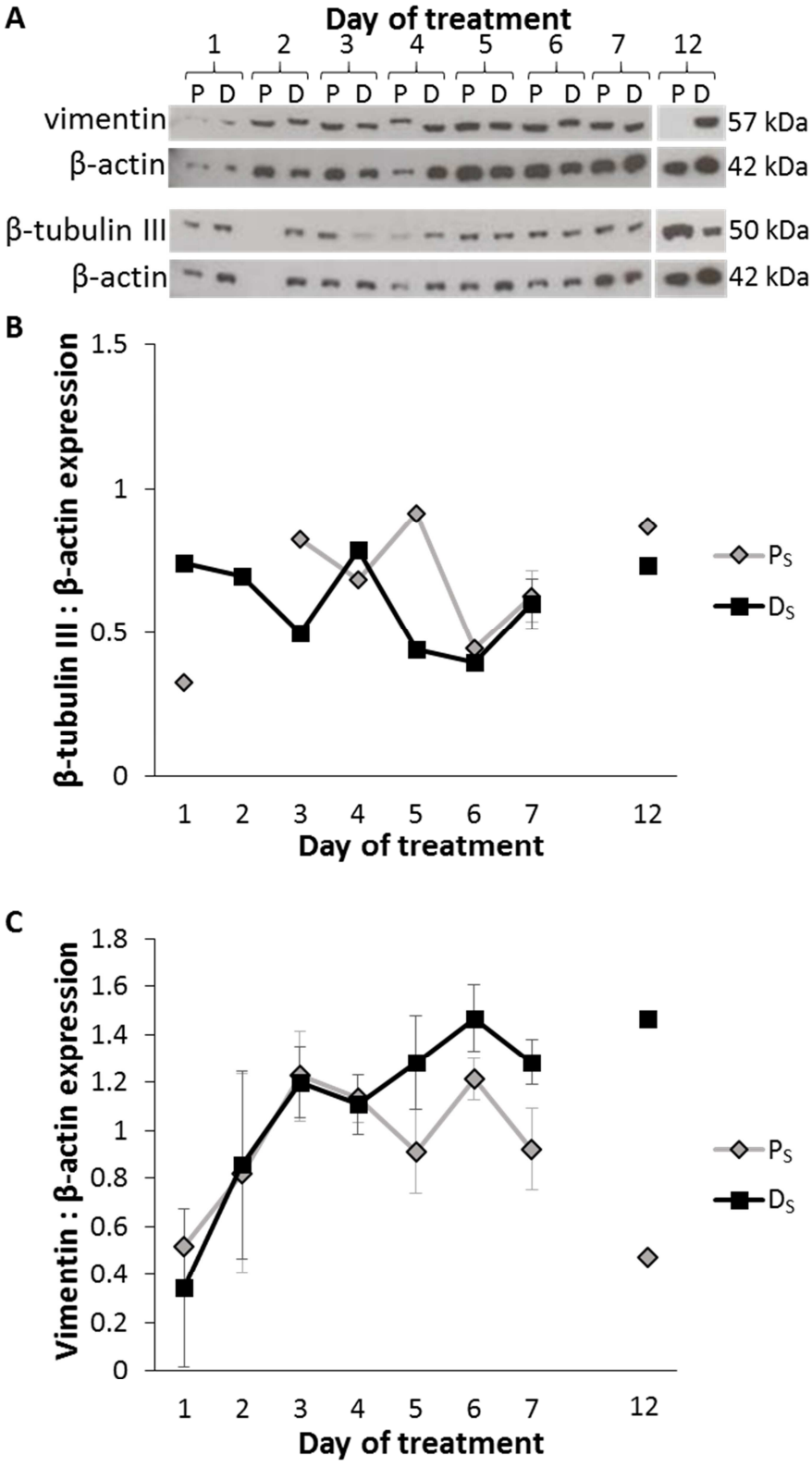
A
Day of treatment
1 2 3 4 5 6 7 12
P D P D P D P D P D P D P D P D
vimentin
β-actin
β-tubulin III
β-actin
57 kDa
42 kDa
50 kDa
42 kDa
B
β-tubulin III : β-actin expression
1.5
1
0.5
0
1 2 3 4 5 6 7 12
Day of treatment
PS
DS
C
Vimentin : β-actin expression
1.8
1.6
1.4
1.2
1
0.8
0.6
0.4
0.2
0
1 2 3 4 5 6 7 12
Day of treatment
PS
DS

Figure 6.2.2. Expression of β-tubulin III and vimentin in differentiating S-type populations

Western blots were performed on protein samples from S-type populations that were treated over 7 days (1-7) with 1 µM 9*c*RA (D_S) or an equivalent volume of EtOH (P_S). After 7 days, treatment was withdrawn from both P_S and D_S populations, which were grown in standard culture media alone for a further 5 days (12). Blots were probed with anti-β-tubulin III antibody which detected a band at 50 kDa, anti-vimentin antibody which detected a band at 57 kDa or β-actin antibody which was used as a loading control and detected a band at 42 kDa. **(A)** β-tubulin III was expressed by both P_S and D_S populations and was also detected in both P_S and D_S populations following 5 days of treatment withdrawal. Vimentin was detected in both P_S populations and D_S populations with a steady increase in band over the treatment time-course. Following 5 days of treatment withdrawal, vimentin was detected in D_S populations but not P_S populations. **(B)** From day 3 of treatment β-tubulin III expression was reduced by 39% in D_S populations and following treatment withdrawal, expression was reduced by 16%. N≥1. **(C)** Over the treatment time-course, there was a steady but non-significant increase in vimentin expression in both P_S populations (P=0.414) and D_S populations (P=0.101). There was no significant difference in vimentin expression between D_S and P_S populations (P=0.131), although there was a 41% increase in vimentin expression at day 5 (P=0.231), 21% increase at day 6 (P=0.197) and 39% increase at day 7 (P=0.134) of treatment in D_S compared to P_S cells. Following 5 days of treatment withdrawal, vimentin expression remained over 3-fold higher in D_S populations compared to P_S populations. N≥2 except 12 N=1.

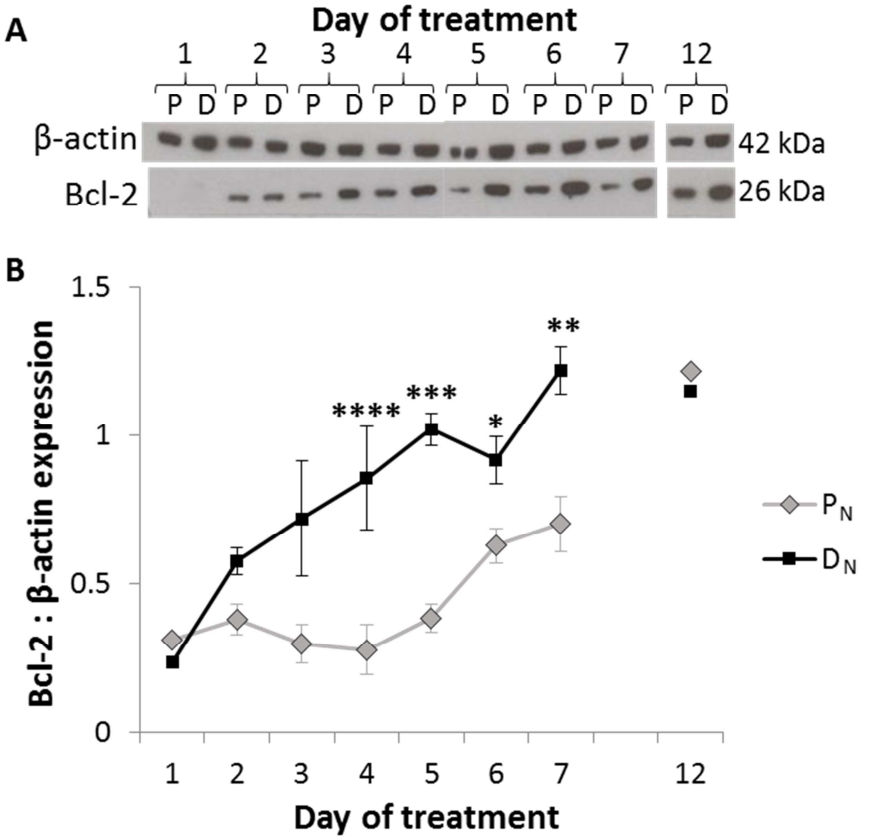

Figure 6.2.3 Expression of Bcl-2 is altered early in differentiating N-type populations

Western blots were performed on protein samples from N-type populations treated over 7 days (1-7) with 1 µM 9*c*RA (D_N) or an equivalent volume of EtOH (P_N). After 7 days, treatment was withdrawn and cells were grown in standard culture media for a further 5 days (12). Blots were probed with anti-Bcl-2 antibody which detected a band at 27 kDa or β-actin antibody which was used as a loading control and detected a band at 42 kDa. **(A)** Bcl-2 was expressed by both P_N and D_N populations over the treatment time-course and following treatment withdrawal, with little to no expression at day 1. Band intensity was greater in D_N populations compared to P_N populations and increased over the treatment time-course. **(B)** Bcl-2 expression increased significantly over the treatment time-course in P_N populations ($P<0.0001$) and D_N populations ($P=0.0019$). Over the treatment time-course, Bcl-2 expression was significantly higher in D_N than P_N populations ($P<0.0001$). Bcl-2 expression was increased in D_N populations compared to P_N populations by 51% at day 2 ($P=0.366$), over 2-fold at day 3 ($P=0.060$), 3-fold at day 4 ($P<0.0001$****), over 2-fold at day 5 ($P=0.0002$***), 46% at day 6

(P=0.045*) and 74% at day 7 (P=0.002**). Following treatment withdrawal, there was no difference in Bcl-2 expression between D_N and P_N populations. N≥4 except 12 N=1.

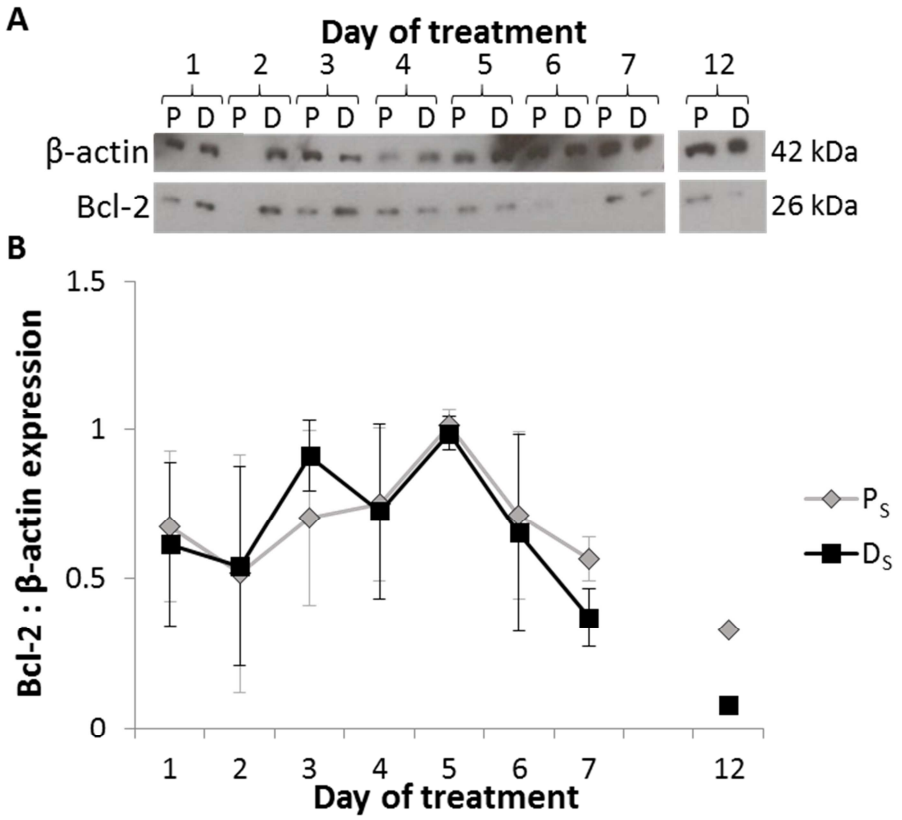

Figure 6.2.4 Expression of Bcl-2 is not altered in differentiating S-type populations

Western blots were performed on protein samples from S-type populations that were treated over 7 days (1-7) with 1 µM 9*c*RA (D_S) or an equivalent volume of EtOH (P_S). After 7 days, treatment was withdrawn and cells were grown in standard culture media alone for a further 5 days (12). Blots were probed with anti-Bcl-2 antibody which detected a band at 27 kDa or β-actin antibody which was used as a loading control and detected a band at 42 kDa. **(A)** Bcl-2 was expressed by both P_S and D_S populations over the treatment time-course and following treatment withdrawal. **(B)** There was no significant difference in Bcl-2 expression over the treatment time-course in P_S populations (P=0.762) or D_S populations (P=0.246). There was no significant difference in Bcl-2 expression between P_S and D_S populations over the treatment time-course (P=0.472), though Bcl-2 was down-regulated by 34% at day 7 (P=0.121) in D_S populations compared to P_S populations. Following treatment withdrawal for 5 days, Bcl-2 expression was 76% lower in D_S populations compared to P_S populations. N≥3 except 12 N=1.

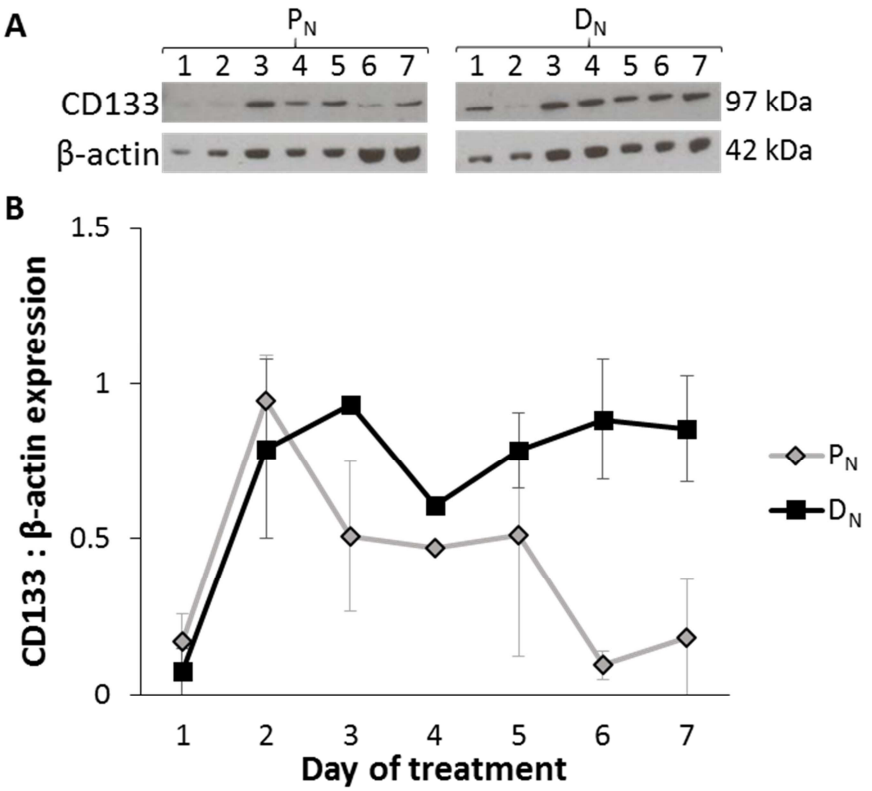

Figure 6.2.5. CD133 expression is altered early in differentiating N-type populations
Western blots were performed on protein samples from N-type populations that were treated over 7 days (1-7) with 1 µM 9*c*RA (D_N) or an equivalent volume of EtOH (P_N). Blots were probed with anti-CD133 antibody which detected a band at 97 kDa or β-actin antibody which was used as a loading control and detected a band at 42 kDa. **(A)** CD133 was expressed in both P_N and D_N populations over the treatment time-course. **(B)** There was a non-significant decrease in CD133 expression over the treatment time-course in P_N populations (P=0.712). There was a non-significant increase in CD133 expression over the treatment time-course in D_N populations (P=0.074). From day 3 of treatment, CD133 expression was increased by 84% (P=0.219) in D_N populations compared to P_N populations and by over 4-fold by day 7 (P=0.117)). N≥1.

6.3. Changes in SOCE activity occur from the first day of 9cRA treatment

As previously described (Chapter 4), there was an uncoupling of Ca^{2+} store release and SOCE in day 7 9*c*RA-differentiated N-type and S-type populations with the extent of SOCE down-regulation greater in S-type than N-type populations. In this section, Ca^{2+} signals associated differentiation responses were observed over the 7 day time-course of 9cRA treatment.

In D_N populations compared to P_N populations, from the first day of 9*c*RA treatment, total SOCE was down-regulated by 39% ($P<0.0001$, Figure 6.3.1A and B). Total Ca^{2+} store release was reduced at day 2 by 15% ($P=0.007$) and day 3 by 26% ($P<0.0001$) whilst the extent of total SOCE down-regulation remained at ~30% (Figure 6.3.1A and B). The extent of total SOCE down-regulation peaked to 61% at day 4 ($P<0.0001$) of treatment and remained down-regulated by ~60% until day 6 of treatment and by day 7, total SOCE was down-regulated by 39% ($P=0.012$, Figure 6.3.1A and B). Following 5 days of treatment withdrawal, total Ca^{2+} store release was increased by 38% ($P<0.0001$) and total SOCE remained down-regulated by 40% (Figure 6.3.1A and B). These results suggest that 9*c*RA-induced differentiation of N-type populations induces an uncoupling of Ca^{2+} store release and SOCE in a multi-step manner, causing uncoupling from the first day of treatment, the extent of which is exaggerated from the fourth day of treatment. This data reveals that the previously observed Ca^{2+} signalling profile seen at day 7 (Chapter 4) is present in D_N populations from the fourth day of exposure to 9*c*RA. Following treatment withdrawal, the extent of uncoupling of Ca^{2+} store release and SOCE remains similar to that seen at day 7 of treatment, indicating that SOCE uncoupling is at least partially maintained following removal of the differentiating stimulus.

In D_N populations compared to P_N populations, there was some reduction in maximal Ca^{2+} store release but there was no significant difference over the treatment time-course ($P>0.997$, Figure 6.3.2A). Maximal SOCE trended towards a down-regulation over the treatment time-course ($P<0.0001$), however this was only significant at day 1 ($P<0.0001$) and day 5 ($P=0.032$) of treatment (Figure 6.3.2A). This implies that maximal

Ca^{2+} entry is not significantly altered over the differentiation response of N-type populations of following the withdrawal of the differentiation stimulus.

In D_N populations compared to P_N populations, rate of Ca^{2+} store release was significantly reduced at day 1 (P=0.006), day 6 (P=0.05), day 7 and day 12 (P<0.0001, Figure 6.3.2B). Rate of SOCE showed an increase over the treatment time-course (P<0.0001), however this was only significant at day 7 and 12 (both P<0.0001, Figure 6.3.2B). This observation suggests that alterations in the speed and/or efficiency of Ca^{2+} entry are confined to the later phase of the differentiation response rather than in the initiation of differentiation in N-type populations and are maintained following removal of the differentiation stimulus.

In D_N populations compared to P_N populations, rate of decline of Ca^{2+} store release was reduced over the treatment time-course (P<0.0001) and from the first day of treatment (P=0.009, Figure 6.3.2C). Rate of decline was reduced up to day 5 and increased from day 6, however this was only significant at day 12 (P<0.0001, Figure 6.3.2C). Rate of initial SOCE decline was increased throughout the treatment time-course (P<0.0001) except at day 6 (P=0.630) whilst rate of late SOCE decline was reduced throughout the treatment time-course (P<0.0001) except and day 12 (P=0.448) and an increase at day 6 (P=0.018, Figure 6.3.2C). These results indicate that alterations in speed and/or efficiency of Ca^{2+} entry inhibition occur early in the differentiation response of N-type populations and are maintained following removal of the differentiation stimulus.

In D_S populations compared to P_S populations, from the first day of 9*c*RA treatment, total Ca^{2+} store release was reduced by 20% (P<0.0001) and total SOCE was down-regulated by 21% (Figure 6.3.3A and B). The extent of SOCE down-regulation shows a steady increase over the treatment time-course, peaking at 71% SOCE down-regulation by day 5 (P<0.0001). SOCE remains down-regulated at day 7 (P<0.0001, Figure 6.3.3A and B). This suggests that 9*c*RA-induced differentiation of S-type populations causes an uncoupling of Ca^{2+} store release and SOCE in a gradually increasing manner from the first day of treatment. These data reveal that the previously observed Ca^{2+} signalling

profile seen at day 7 (Chapter 4) is present in D_S populations from the fifth day of exposure to 9*c*RA. Interestingly, following treatment withdrawal, Ca^{2+} store release is reduced by 34% (P=0.005) and SOCE is restored to that seen in P_S populations (Figure 6.3.3A and B). This suggests that following treatment withdrawal, there is no longer an uncoupling of Ca^{2+} store release and SOCE, indicating that D_S populations may either revert back to a coupled SOCE response like that of P_S populations or that SOCE uncoupling is involved in the initiation of the early differentiation response but not in maintaining the differentiated state of S-type populations.

In D_S populations compared to P_S populations, there is a reduction in maximal Ca^{2+} store release early in the differentiation response day 1 (P=0.002), day 2 (P=0.0005) and day 3 (P<0.0001) which becomes unaltered at day 4 (P>0.999) and 5 (P=0.701) then increases at day 6 (P<0.0001, Figure 6.3.4A), suggesting a varied effect on Ca^{2+} store size or TG sensitivity between the early and late differentiation response of S-type populations. Maximal SOCE is down-regulated throughout the treatment time-course (P<0.0001) except following treatment withdrawal (P>0.999, Figure 6.3.4A), indicating maximal Ca^{2+} entry to be altered early in the differentiation response of S-type populations which is either lost following the removal of the differentiation stimulus or not needed to maintain the differentiation response.

In D_S populations compared to P_S populations, rate of Ca^{2+} store release was reduced from day 2 (P<0.0001) to day 5 (P=0.012) of treatment but was increased from day 6 (P=0.0001) and following treatment removal (P=0.028, Figure 6.3.4B), again suggesting a varied effect on the speed of Ca^{2+} store release rate or on TG sensitivity between the early and late differentiation response of S-type populations. Rate of SOCE was reduced at day 1 (P<0.0001) and day 2 (P=0.004) of treatment but was increased from day 4 (P<0.0001) of treatment and following treatment withdrawal (P=0.028, Figure 6.3.4B), indicating that the speed and/or efficiency of Ca^{2+} entry is altered early in the differentiation response of S-type populations but is altered in a different manner during the differentiation response.

In D_S populations compared to P_S populations, rate of decline of Ca^{2+} store release was reduced from day 1 to 4 ($P<0.0001$) and was increased at day 6 ($P<0.0001$) of treatment whilst rate of total SOCE decline was also reduced early in the differentiation response (Figure 6.3.4C). Rate of initial SOCE decline was increased throughout the treatment time-course and following treatment withdrawal ($P<0.0001$) but was increased at day 7 ($P=0.016$) whilst rate of late SOCE decline was reduced up to day 5 ($P<0.0001$) and non-significantly increased at day 6 and 7 ($P>0.999$). These results suggest that rate of deactivation of Ca^{2+} entry is altered early in the differentiation response of S-type populations and in a different manner to that observed late in the differentiation response.

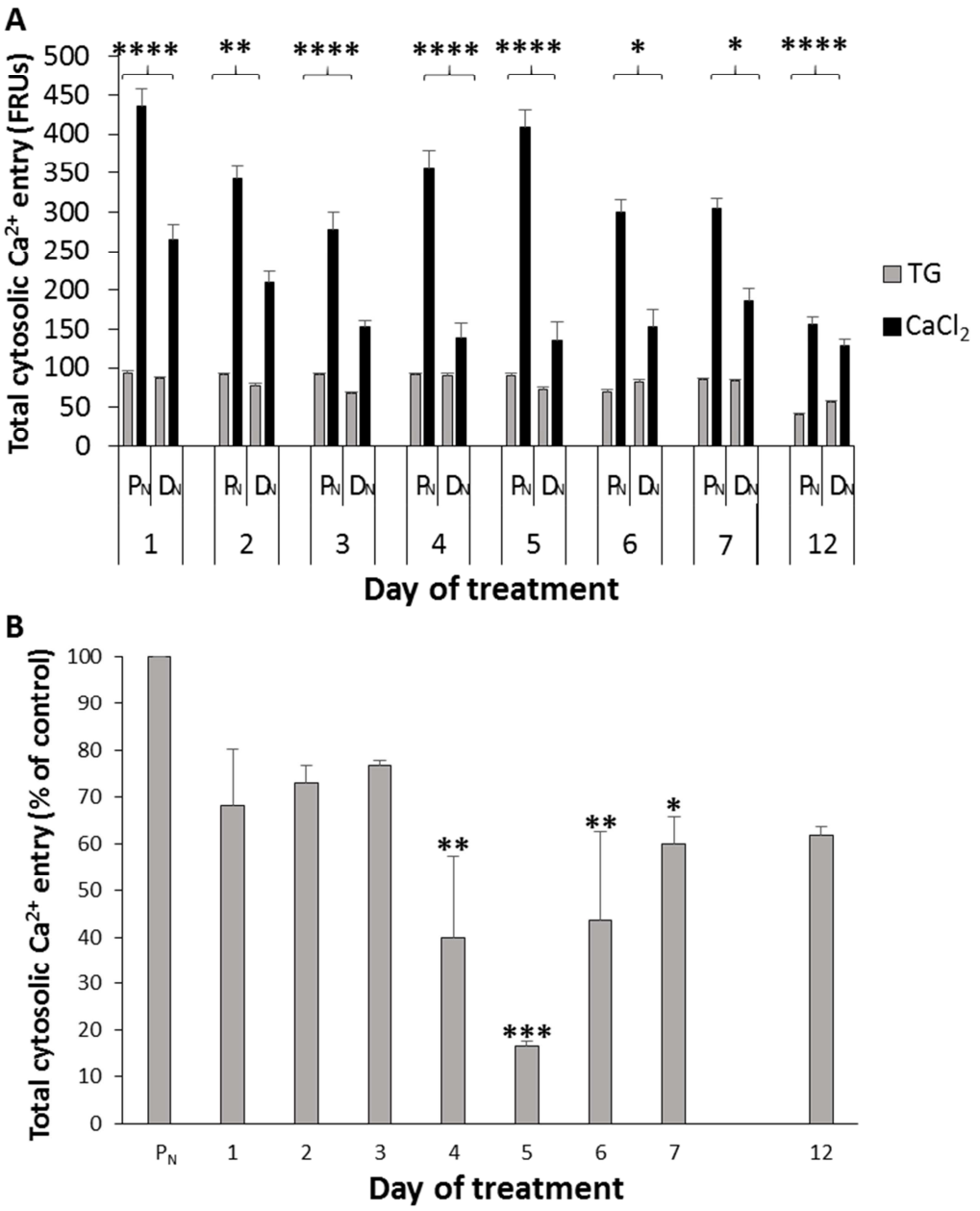

Figure 6.3.1. 9*c*RA-induced differentiation of N-type populations induces SOCE changes in a multi-step manner

N-type populations were treated over 7 days (1-7) with 1 µM 9*c*RA (D_N) or an equivalent volume of EtOH (P_N). After 7 days, treatment was withdrawn from both P_N and D_N cells, which were grown in media alone for a further 5 days (12). Changes in fluorescence ratio units (FRUs) are reflective of changes in $[Ca^{2+}]_i$. Following addition of thapsigargin (TG) there was increase in FR in P_N and D_N populations indicating Ca^{2+} store release. Subsequent Ca^{2+}-addback ($CaCl_2$) caused an increase in FR in P_N and D_N

populations, indicating SOCE to replenish depleted stores. **(A)** At day 1, there was no significant difference in total Ca^{2+} store release between D_N populations (86.16 ± 2.11 FRUs) and P_N populations (93.66 ± 1.83 FRUs, P=0.349) and total SOCE was down-regulated by 39.23% in D_N populations (264.94 ± 18.51 FRUs) compared to P_N populations (436.01 ± 21.83 FRUs, P<0.0001****). At day 2, there was a 14.78% reduction in total Ca^{2+} store release in D_N populations (77.50 ± 3.10 FRUs) compared to P_N populations (90.94 ± 2.14 FRUs, P=0.007**) and total SOCE was down-regulated by 27.87% in D_N populations (210.53 ± 12.81 FRUs) compared to P_N populations (342.47 ± 15.52 FRUs). At day 3, there was a 26.42% reduction in total Ca^{2+} store release in D_N populations (67.13 ± 2.14 FRUs) compared to P_N populations (91.25 ± 2.36 FRUs, P<0.0001****) and total SOCE was down-regulated by 25.52% in D_N populations (152.36 ± 9.10 FRUs) compared to P_N populations (278.06 ± 21.49 FRUs). At day 4, there was no difference in total Ca^{2+} store release between P_N populations (90.85 ± 2.10 FRUs) and D_N populations (90.19 ± 2.53 FRUs, P>0.999) and total SOCE was down-regulated by 60.85% in D_N populations (138.75 ± 19.11 FRUs) compared to P_N populations (354.41 ± 23.99 FRUs, P<0.0001****). At day 5, there was an 18.43% reduction in total Ca^{2+} store release in D_N populations (73.24 ± 2.17 FRUs) compared to P_N populations (89.79 ± 3.01 FRUs, P<0.0001****) and total SOCE was down-regulated by 59.33% in D_N populations (135.59 ± 23.71 FRUs) compared to P_N populations (408.68 ± 22.62 FRUs). At day 6, there was an 18.28% increase in total Ca^{2+} store release in D_N populations (82.24 ± 2.83 FRUs) compared to P_N populations (69.53 ± 2.36 FRUs, P=0.020*) and total SOCE was down-regulated by 57.12% in D_N populations (152.43 ± 23.15 FRUs) compared to P_N populations (300.52 ± 14.59 FRUs). At day 7, there was no significant difference in total Ca^{2+} store release between D_N populations (83.59 ± 2.08 FRUs) and P_N populations (84.66 ± 2.10 FRUs, P>0.999) and total SOCE was down-regulated by 38.86% in D_N populations (186.22 ± 15.61 FRUs) compared to P_N populations (3004.57 ± 12.82 FRUs, P=0.011*). Following 5 days of treatment withdrawal, Ca^{2+} store release was increased by 37.72% in D_N populations (56.26 ± 1.53 FRUs) compared to P_N populations (40.85 ± 0.98 FRUs, P<0.0001) and SOCE was down-regulated by 40.5% in D_N populations (127.77 ± 9.75 FRUs) compared to P_N populations (155.93 ± 10.25 FRUs). **(B)** The following percentages compare the average total SOCE of D_N populations with corresponding P_N populations from each day taken

to be 100%. Total SOCE was down-regulated by 31.88% at day 1 (P=0.081), 26.74% at day 2 (P=0.253) and 23.23% at day 3 (P=0.276) of treatment. There was a greater extent of down-regulation at 4 by 60.07% (P=0.003**) and further down-regulation at day 5 by 83.33% (P=0.0002***). By day 6, there was some recovery with total SOCE down-regulated by 56.50% (P=0.005**) and further still at day 7 with total SOCE down-regulated by 40.06% (P=0.045*). Following treatment withdrawal for 5 days, SOCE remained down-regulated by 38.08% (P=0.0506). P_N: 1 n=335, 2 n=242, 3 n=254, 4 n=283, 5 n=228, 6 n=253, 7 n=329, 12=282. D_N: 1 n=355, 2 n=236, 3 n=390, 4 n=286, 5 n=279, 6 n=211, 7 n=253, 12=278. N≥2.

A

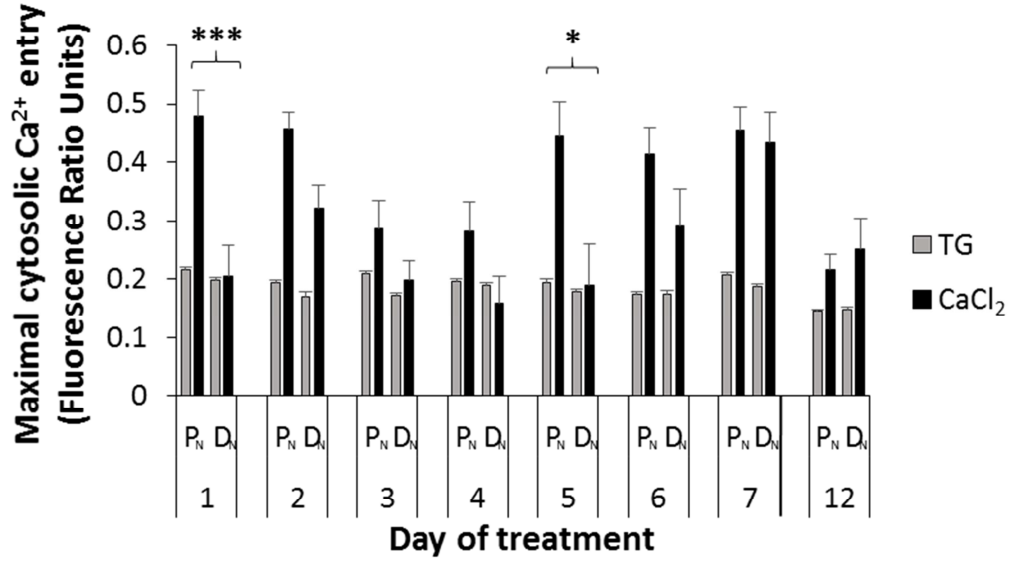

B

P_N Rate of Rise (FRUs x 10^{-4})								
	Day 1	Day 2	Day 3	Day 4	Day 5	Day 6	Day 7	Day 12
TG	12.35 ± 0.24	10.14 ± 5.34	11.33 ± 0.22	9.71 ± 0.16	10.00 ± 0.23	10.73 ± 0.18	12.09 ± 0.25	12.83 ± 0.20
$CaCl_2$	66.23 ± 6.30	33.09 ± 5.34	41.06 ± 4.40	48.35 ± 5.31	71.57 ± 6.69	26.63 ± 2.78	52.98 ± 4.59	34.53 ± 3.05

D_N Rate of Rise (FRUs x 10^{-4})								
	Day 1	Day 2	Day 3	Day 4	Day 5	Day 6	Day 7	Day 12
TG	11.26 ± 0.23	10.48 ± 0.23	11.00 ± 0.81	10.34 ± 0.21	10.91 ± 0.19	9.38 ± 0.24	10.34 ± 0.22	9.57 ± 0.20
$CaCl_2$	62.39 ± 5.99	40.44 ± 6.30	49.28 ± 4.08	57.14 ± 4.19	108.72 ± 10.30	91.38 ± 7.34	115.14 ± 10.35	131.67 ± 7.85

C

P_N Rate of Decline (FRUs x 10^{-4})								
	Day 1	Day 2	Day 3	Day 4	Day 5	Day 6	Day 7	Day 12
TG	2.83 ± 0.05	2.37 ± 0.05	2.66 ± 0.05	2.64 ± 0.05	2.54 ± 0.06	2.43 ± 0.04	2.88 ± 0.05	2.04 ± 0.03
Total $CaCl_2$	4.07 ± 0.12	3.09 ± 0.10	3.57 ± 0.14	3.67 ± 0.12	4.47 ± 0.16	3.06 ± 0.14	4.50 ± 0.13	1.99 ± 0.08
Initial $CaCl_2$	4.76 ± 0.36	1.90 ± 0.17	1.99 ± 0.24	3.39 ± 0.33	5.23 ± 0.50	10.85 ± 0.96	3.42 ± 0.41	3.46 ± 0.21
Late $CaCl_2$	3.88 ± 0.14	3.54 ± 0.13	4.16 ± 0.17	3.81 ± 0.12	4.05 ± 0.14	2.33 ± 0.15	4.90 ± 0.14	1.39 ± 0.08

D_N Rate of Decline (FRUs x 10^{-4})								
	Day 1	Day 2	Day 3	Day 4	Day 5	Day 6	Day 7	Day 12
TG	2.61 ± 0.04	2.47 ± 0.05	2.44 ± 0.03	2.34 ± 0.05	2.51 ± 0.04	2.15 ± 0.05	2.43 ± 0.05	1.98 ± 0.05
Total $CaCl_2$	3.69 ± 0.12	3.16 ± 0.15	3.01 ± 0.11	3.25 ± 0.11	4.23 ± 0.19	4.92 ± 0.26	4.75 ± 0.26	4.73 ± 0.19
Initial $CaCl_2$	7.33 ± 0.43	6.97 ± 0.43	5.76 ± 0.32	6.82 ± 0.37	8.05 ± 0.59	9.16 ± 0.64	10.48 ± 0.77	13.47 ± 0.59
Late $CaCl_2$	2.48 ± 0.14	1.79 ± 0.14	1.97 ± 0.08	1.92 ± 0.11	2.54 ± 0.10	3.06 ± 0.18	2.43 ± 0.15	0.94 ± 0.05

Figure 6.3.2. 9*c*RA-induced differentiation of N-type populations induces changes in SOCE dynamics from the first day of treatment

N-type populations were treated over 7 days (1-7) with 1 µM 9*c*RA (D_N) or an equivalent volume of EtOH (P_N). After 7 days, treatment was withdrawn from both P_N and D_N cells, which were grown in media alone for a further 5 days (12). All calculations are for D_N cells compared to P_N cells. Changes in fluorescence ratio units (FRUs) are reflective of changes in $[Ca^{2+}]_i$. Following addition of thapsigargin (TG) there was

increase in FRU in P_N and D_N populations indicating Ca^{2+} store release. Subsequent Ca^{2+}-addback ($CaCl_2$) caused an increase in FR in P_N and D_N populations, indicating SOCE to replenish depleted stores. **(A)** At day 1, there was no significant difference in maximal Ca^{2+} store release (P>0.999) and maximal SOCE was down-regulated by 57.23% (P=0.0009***). At day 2, there was no significant difference in maximal Ca^{2+} store release (P>0.999) and maximal SOCE was down-regulated by 29.88%, though this was non-significant (P=0.895). At day 3, there was no significant difference in maximal Ca^{2+} store release (P>0.999) and maximal SOCE was down-regulated by 30.54%, though this was non-significant (P=0.994). At day 4, there was no significant difference in maximal Ca^{2+} store release (P>0.999) and maximal SOCE was down-regulated by 43.81%, though this was non-significant (P=0.904). At day 5, there was no significant difference in maximal Ca^{2+} store release (P>0.999) and maximal SOCE was down-regulated by 57.61% (P=0.032*). At day 6, there was no significant difference in maximal Ca^{2+} store release (P>0.999) and maximal SOCE was down-regulated by 29.68%, though this was non-significant (P=0.961). At day 7, there was no difference in maximal Ca^{2+} store release (P>0.999) or maximal SOCE (P>0.999). Following treatment withdrawal for 5 days, there was no significant difference in maximal Ca^{2+} store release (P>0.999) or maximal SOCE (P>0.999). **(B)** Rate of Ca^{2+} store release was significantly reduced at day 1 (P=0.006), day 6 (P=0.005) and day 7 (P<0.0001). Rate of SOCE was significantly increased at day 7 (P<0.0001). All other rates were not significantly altered. **(C)** Rate of decline of Ca^{2+} store release was decreased at day 1 (P=0.009), day 3 (P=0.020), day 4 (P=0.0001), day 6 (P=0.003) and day 7 (P=0.029). Rate of total SOCE decline was significantly increased at day 12 (P<0.0001). Rate of initial SOCE decline was significantly increased at day 1 (P=0.002), day 2, 3, 4, 7 and 12 (all P<0.0001) and day 5 (P=0.007). Rate of late SOCE decline rate was decreased at day 1-5 and day 7 (all P<0.0001) and was increased at day 6 (P=0.018). All other rates were not significantly altered. P_N: 1 n=335, 2 n=242, 3 n=254, 4 n=283, 5 n=228, 6 n=253, 7 n=329, 12=282. D_N: 1 n=355, 2 n=236, 3 n=390, 4 n=286, 5 n=279, 6 n=211, 7 n=253, 12=278. N≥2.

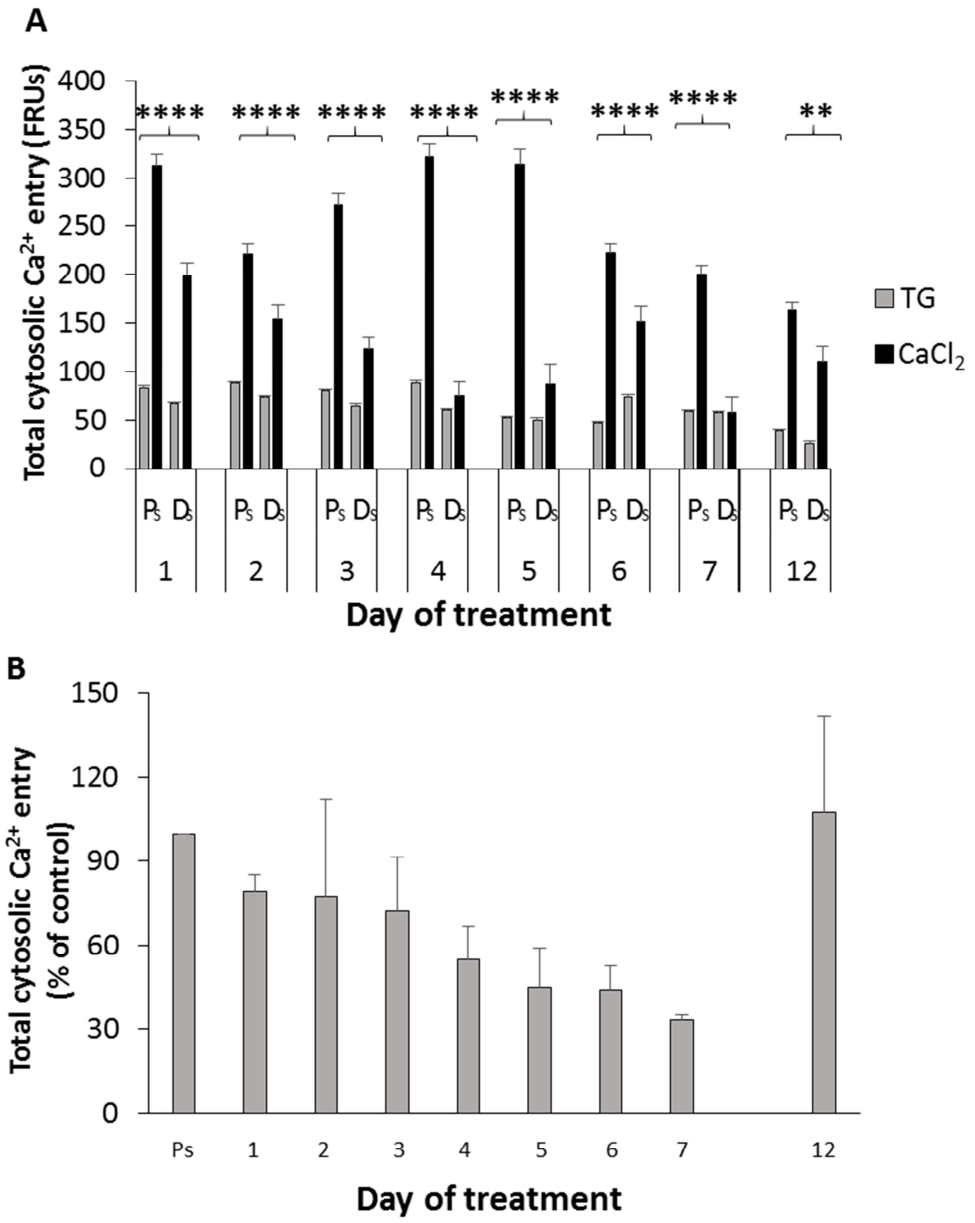

Figure 6.3.3. 9*c*RA-induced differentiation of S-type populations induces SOCE changes in a gradual manner

S-type populations were treated over 7 days (1-7) with 1 µM 9*c*RA (D_S) or an equivalent volume of EtOH (P_S). After 7 days, treatment was withdrawn from both P_S and D_S cells, which were grown in media alone for a further 5 days (12). Changes in fluorescence ratio units (FRUs) are reflective of changes in $[Ca^{2+}]_i$. Following addition of thapsigargin (TG) there was increase in FRU in P_N and D_N populations indicating Ca^{2+} store release. Subsequent Ca^{2+}-addback ($CaCl_2$) caused an increase in FR in P_S and D_S populations, indicating SOCE to replenish depleted stores. **(A)** At day 1, there was a

20.33% reduction in total Ca^{2+} store release in D_S populations (66.30 ± 1.27 FRUs) compared to P_S populations (83.22 ± 1.54 FRUs, P<0.0001****) and total SOCE was down-regulated by 20.25% in D_S populations (198.42 ± 14.12 FRUs) compared to P_S populations (312.29 ± 12.20 FRUs). At day 2, there was a 16.88% reduction in total Ca^{2+} store release in D_S populations (73.03 ± 1.96 FRUs) compared to P_S populations (87.85 ± 1.87 FRUs, P<0.0001****) and total SOCE was down-regulated by 16.41% in D_S populations (153.48 ± 15.39 FRUs) compared to P_S populations (220.9 ± 11.38 FRUs). At day 3, there was a 19.22% reduction in total Ca^{2+} store release in D_S populations (64.37 ± 1.92 FRUs) compared to P_S populations (79.69 ± 1.69 FRUs, P<0.0001****) and total SOCE was down-regulated by 43.29% in D_S populations (124.21 ± 10.98 FRUs) compared to P_S populations (271.16 ± 12.94 FRUs). At day 4, there was a 32.37% reduction in total Ca^{2+} store release in D_S populations (59.83 ± 1.92 FRUs) compared to P_S populations (88.47 ± 2.39 FRUs, P<0.0001****) and total SOCE was down-regulated by 65.48% in D_S populations (75.01 ± 14.35 FRUs) compared to P_S populations (321.32 ± 13.48 FRUs). At day 5, there was no significant difference in total Ca^{2+} store release between P_S populations (52.08 ± 1.23 FRUs) and D_S populations (49.82 ± 1.87 FRUs, P=0.9997) and total SOCE was down-regulated by 71.09% in D_S populations (86.99 ± 20.48 FRUs) compared to P_S populations (314.49 ± 15.57 FRUs, P<0.0001****). At day 6, there was a 54.22% increase in total Ca^{2+} store release in D_S populations (73.40 ± 2.44 FRUs) compared to P_S populations (47.59 ± 1.21 FRUs, P<0.0001****) and total SOCE was down-regulated by 55.82% in D_S populations (151.77 ± 15.56 FRUs) compared to P_S populations (222.72 ± 9.57 FRUs). At day 7, there was no significant difference in total Ca^{2+} store release between P_S populations (59.13 ± 1.27 FRUs) and D_S populations (57.52 ± 1.96 FRUs, P>0.999) and total SOCE was down-regulated by 70.36% in D_S populations (57.82 ± 15.79 FRUs) compared to P_S populations (200.52 ± 9.11 FRUs, P<0.0001****). Following 5 days of treatment withdrawal, Ca^{2+} store release was reduced by 34.26% in D_S populations (25.91 ± 2.20 FRUs) compared to P_S populations (39.41 ± 0.85 FRUs, P=0.005**) and there was no change in SOCE between P_S populations (162.88 ± 8.05 FRUs) and D_S populations (110.55 ± 16.46 FRUs). **(B)** The following percentages compare the average total SOCE of D_S populations with corresponding P_S populations from each day taken to be 100%. At day 1 and 2 of treatment, total SOCE is down-regulated by 20.90% and 22.61% respectively. There is a

gradual greater extent of total SOCE down-regulation with subsequent days of treatment, with down-regulation by 27.62% at day 3, 44.94% at day 4, 55.02% at day 5, 56.11% at day 6 and 66.59% at day 7. Following treatment withdrawal for 5 days, there was no difference in SOCE. P_S: 1 n=453, 2 n=361, 3 n=442, 4 n=334, 5 n=513, 6 n=584, 7 n=260, 12 n=401. D_S: 1 n=487, 2 n=407, 3 n=379, 4 n=280, 5 n=317, 6 n=420, 7 n=263, 12 n=135. N≥2.

A

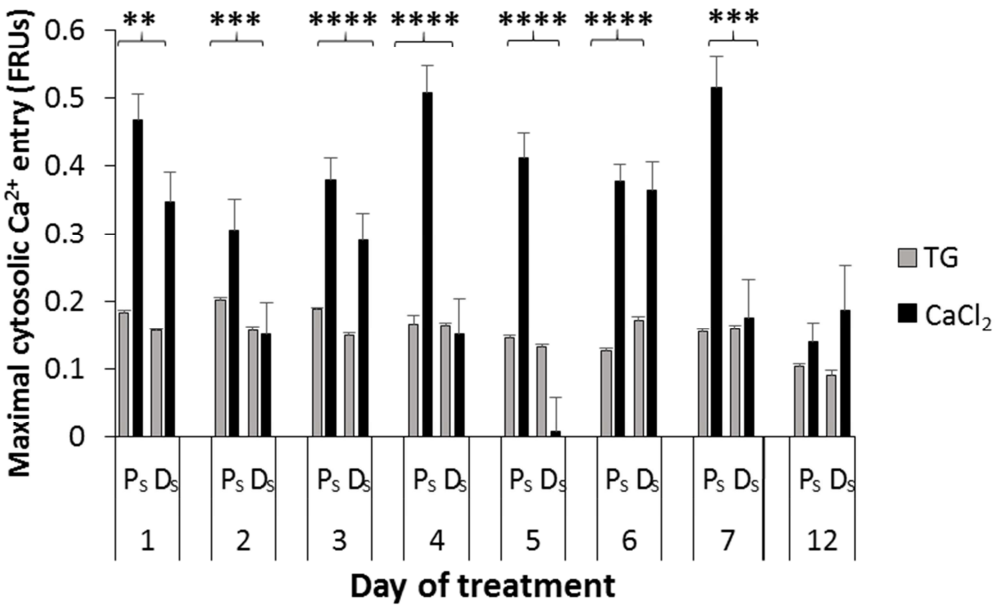

B

P_S Rate of Rise (FRUs x 10^{-4})								
	Day 1	Day 2	Day 3	Day 4	Day 5	Day 6	Day 7	Day 12
TG	8.77 ± 0.15	11.94 ± 0.24	10.88 ± 0.17	12.49 ± 0.29	10.30 ± 0.21	8.80 ± 0.19	9.77 ± 0.19	7.60 ± 0.20
$CaCl_2$	79.00 ± 5.38	89.20 ± 5.52	67.27 ± 2.48	60.49 ± 2.12	71.46 ± 3.44	92.89 ± 4.69	195.55 ± 14.82	63.45 ± 4.11

D_S Rate of Rise (FRUs x 10^{-4})								
	Day 1	Day 2	Day 3	Day 4	Day 5	Day 6	Day 7	Day 12
TG	9.99 ± 0.17	8.95 ± 0.24	9.76 ± 0.18	11.10 ± 0.25	9.07 ± 0.25	10.19 ± 0.22	10.15 ± 0.39	9.20 ± 0.75
$CaCl_2$	163.89 ± 10.88	48.07 ± 5.14	83.45 ± 4.34	129.25 ± 8.22	102.91 ± 6.66	179.58 ± 8.13	180.96 ± 10.40	111.43 ± 14.57

C

P_S Rate of Decline (FRUs x 10^{-4})								
	Day 1	Day 2	Day 3	Day 4	Day 5	Day 6	Day 7	Day 12
TG	2.35 ± 0.04	2.44 ± 0.04	2.44 ± 0.04	2.71 ± 0.06	1.91 ± 0.03	1.76± 0.03	2.08 ± 0.04	1.41 ± 0.04
Total $CaCl_2$	4.55 ± 0.12	4.50 ± 0.10	4.26 ± 0.08	4.73 ± 0.10	4.91 ± 0.12	4.03 ± 0.09	5.41 ± 0.25	2.42 ± 0.08
Initial $CaCl_2$	10.72 ± 0.40	9.51 ± 0.37	8.31 ± 0.25	7.51 ± 0.27	6.40 ± 0.27	7.94 ± 0.25	13.84 ± 0.68	5.71 ± 0.23
Late $CaCl_2$	2.19 ± 0.09	2.62 ± 0.10	2.79 ± 0.08	3.72 ± 0.13	4.35 ± 0.13	2.52 ± 0.08	2.25 ± 0.16	1.07 ± 0.06

D_S Rate of Decline (FRUs x 10^{-4})								
	Day 1	Day 2	Day 3	Day 4	Day 5	Day 6	Day 7	Day 12
TG	1.97 ± 0.04	1.98 ± 0.05	1.87 ± 0.04	2.17 ± 0.05	1.92 ± 0.11	2.19 ± 0.08	2.03 ± 0.07	1.27 ± 0.09
Total $CaCl_2$	4.75 ± 0.16	2.63 ± 0.05	3.73 ± 0.10	4.23 ± 0.14	3.83 ± 0.15	5.55 ± 0.17	4.95 ± 0.19	3.24 ± 0.26
Initial $CaCl_2$	11.09 ± 0.52	10.19 ± 0.40	9.20 ± 0.35	10.91 ± 0.45	9.71 ± 0.42	13.11 ± 0.42	11.31 ± 0.57	9.94 ± 0.78
Late $CaCl_2$	2.23 ± 0.08	1.04 ± 0.10	1.61 ± 0.07	1.65 ± 0.08	1.48 ± 0.11	2.68 ± 0.13	2.45 ± 0.12	0.85 ± 0.13

Figure 6.3.4. 9*c*RA-induced differentiation of S-type populations induces changes in SOCE dynamics from the first day of treatment

S-type populations were treated over 7 days (1-7) with 1 µM 9*c*RA (D_S) or an equivalent volume of EtOH (P_S). After 7 days, treatment was withdrawn from both P_S and D_S cells, which were grown in media alone for a further 5 days (12). All calculations

are for D_S cells compared to P_S cells. Changes in fluorescence ratio units (FRUs) are reflective of changes in $[Ca^{2+}]_i$. Following addition of thapsigargin (TG) there was increase in FRU in P_S and D_S populations indicating Ca^{2+} store release. Subsequent Ca^{2+}-addback ($CaCl_2$) caused an increase in FR in P_N and D_N populations, indicating SOCE to replenish depleted stores. **(A)** At day 1, there was a 14.27% reduction in maximal Ca^{2+} store release (P=0.002**) and maximal SOCE was down-regulated by 13.72%. At day 2, there was a 21.72% reduction in maximal Ca^{2+} store release (P=0.0005***) and maximal SOCE was down-regulated by 36.65%. At day 3, there was a 20.30% reduction in maximal Ca^{2+} store release (P<0.0001****) and maximal SOCE was down-regulated by 3.51%. At day 4, there was no difference in maximal Ca^{2+} store release (P>0.999) and maximal SOCE was down-regulated by 70.14% (P<0.0001****). At day 5, there was no difference in maximal Ca^{2+} store release (P=0.701) and maximal SOCE was down-regulated by 97.92% (P<0.0001****). At day 6, there was a 35.83% increase in maximal Ca^{2+} store release (P<0.0001****) and maximal SOCE was down-regulated by 29.01%. At day 7, there was no difference in maximal Ca^{2+} store release (P>0.999) and maximal SOCE was down-regulated by 66.95% (P=0.0001***). Following treatment withdrawal, there was no significant difference in maximal Ca^{2+} store release and SOCE was up-regulated by 33.54%, though this was non-significant (P>0.999). **(B)** The rate of Ca^{2+} store release was significantly increased at day 1 (P=0.003), day 6 (P=0.0001) and day 12 (P=0.028) and was significantly decreased at day 2 (P<0.0001), day 3 (P=0.028), day 4 (P=0.011) and day 5 (P=0.012). The rate of SOCE was significantly reduced at day 1 (P<0.0001) and day 2 (P=0.004) and significantly increased at day 4 and 6 (both P<0.0001) and day 12 (P=0.028). All other rates were not significantly altered. **(C)** Rate of Ca^{2+} store release was significantly reduced at day 1-4 (all P<0.0001) and was significantly increased at day 6 (P<0.0001). Rate of total SOCE decline was significantly reduced at day 2 and 5 (both P<0.0001) and was significantly increased at day 6 (P<0.0001). Rate of initial SOCE decline was significantly increased at day 4-6 and day 12 (all P<0.0001) and significantly reduced at day 7 (P=0.016). Rate of late SOCE decline was significantly reduced at day 2-5 (all P<0.0001). All other rates were not significantly altered. P_S: 1 n=453, 2 n=361, 3 n=442, 4 n=334, 5 n=513, 6 n=584, 7 n=260, 12 n=401. D_S: 1 n=487, 2 n=407, 3 n=379, 4 n=280, 5 n=317, 6 n=420, 7 n=263, 12 n=135. N≥2.

6.4. Changes in SOCE machinery expression are induced from the first day of 9cRA treatment

SOCE becomes down-regulated in a multi-step manner in N-type populations, being down-regulated from the first day of 9*c*RA treatment, the extent of which is increased from day 4 of treatment and is retained following treatment withdrawal. SOCE is also down-regulated from the first day of 9*c*RA treatment in S-type populations, the extent of which increases in a gradual manner over the treatment time-course and is lost following treatment withdrawal. This suggests that there may be underlying difference in the expression of SOCE proteins between N-type and S-type populations over the time-course of the differentiation response. Therefore expression of the SOCE proteins STIM1 and Orai1 were investigated over the time-course of 9cRA treatment and following treatment withdrawal in N-type and S-type populations to determine any changes in expression that may be associated with the observed changes in SOCE.

STIM1 was expressed in P_N and D_N populations over the treatment time-course (Figure 6.4.1A). The total level of STIM1 expression was unchanged over the treatment time-course in both P_N populations (P=0.741) and D_N populations (P=0.387, Figure 6.4.1B). Also, total STIM1 was expressed to a slightly less extent in D_N populations compared to P_N populations over the treatment time-course (P=0.078), although this was not significant. STIM1 was down-regulated by 40% from the first day of treatment (P=0.088). However, expression of total STIM1 levels masks the observation that a band of less intensity or a slight increase in molecular weight was often observed in D_N populations. This became particularly clear from the third day of treatment (Figure 6.4.1A). Following treatment withdrawal, there was a 16% down-regulation in the level of STIM1 expression in D_N populations compared to P_N populations (Figure 6.4.1B) and, importantly, the increased molecular weight form of STIM1 normally associated with D_N cells was no longer observed (Figure 6.4.1A).

Orai1 was expressed in P_N populations and to much a lesser extent or was absent in D_N populations over the treatment time-course (Figure 6.4.1A). There was no significant change in the level of Orai1 expression over the treatment time-course by P_N populations (P=0.127) or D_N populations (P=0.116). Orai1 was expressed to a lesser

extent in D_N populations compared to P_N populations over the treatment time-course (P=0.0007). There was down-regulation of Orai1 expression in D_N populations compared to P_N populations by 80% at day 1 (P=0.008) and Orai1 remained down-regulated by 75% at day 5 (P=0.095, Figure 6.4.1C). However, the extent of Orai down-regulation recovered somewhat by day 6 (31%, P=0.602) and remained down-regulated by 40% at day 7 (P=0.046, Figure 6.4.1C). Following treatment withdrawal, Orai1 expression remained 41% lower in D_N populations compared to P_N populations (Figure 6.4.1A and C).

Taken together, these results are consistent with a down-regulation of both STIM1 and Orai1 underlying the initial down-regulation of SOCE observed from the first day of 9*c*RA treatment in N-type populations. It may be that an initial down-regulation of STIM1 and Orai1 coupled with a potential modification of STIM1, such as phosphorylation, drives the initial down-regulation of SOCE. The later 'step' of SOCE down-regulation could potentially be due to a further drop in expression of STIM1. Following treatment withdrawal, the change in STIM1 molecular weight is lost and total levels of STIM1 remain slightly dampened whilst Orai1 down-regulation is maintained. The observed reduction in SOCE activity could therefore result from a combination of dampened Orai1 expression plus dampened STIM1 expression, even though the form of STIM1 present may be functional.

STIM1 was expressed in P_S and D_S populations over the treatment time-course, generally with less band intensity in D_S populations (Figure 6.4.2A). However, there was no significant difference in the level of STIM1 expression in P_S populations compared to D_S populations over the treatment time-course (P=0.948, Figure 6.4.2B). Also, the level of STIM1 expression was not significantly altered over the treatment time-course in P_S populations (P=0.900) or D_S populations (P=0.714, Figure 6.4.2A and B). Following treatment withdrawal, STIM1 expression was up-regulated over 3-fold in D_N populations compared to P_N populations (Figure 6.4.2B) and a clear increase in STIM1 molecular weight could be observed in D_S populations (Figure 6.4.2A).

Orai1 was expressed in P_S populations and to a lesser extent in D_S populations, with expression diminishing from day 3 of treatment in D_S populations (Figure 6.4.2A). Over the treatment time-course, there was no significant change in the level of Orai1 expression in P_S populations (P=0.460) and a slight but non-significant decline in the level of Orai1 expression in D_S populations (P=0.816, Figure 6.4.2A and C). Orai1 was generally expressed to a lesser extent in D_S populations compared to P_N populations throughout the treatment time-course, though this was non-significant (P=0.684, Figure 6.4.2A and C). Orai1 expression was down-regulated by ~20% from day 2 (P=0.271) of treatment, increasing to a down-regulation of ~30% by day 6 (P=0.402) and by ~40% by day 7 (P=0.073, Figure 6.4.2C). Following treatment withdrawal, Orai1 expression was reduced by 95% in D_S populations compared to P_S populations (Figure 6.4.2A and C).

Taken together, these results suggest that the reduction in SOCE activity during the differentiation response of S-type populations could be driven predominantly by Orai1 down-regulation as the expression of STIM1 is only slightly altered. By day 6 and 7 of treatment dampened Orai1 expression coincides with the observed peak in dampened SOCE activity. Following treatment withdrawal, there is an increase in the level of STIM1 expression however an increase in STIM1 molecular weight can be observed. This is accompanied by a further increase in the extent of Orai1 down-regulation. Given that SOCE activity is seen to recover after treatment withdrawal, this implies that perhaps another SOC channel (e.g.TRPC1) by which SOCE can occur may either be up-regulated or undergo a modification in its function in order to compensate for the lack of Orai1 following removal of the differentiation stimulus from S-type populations.

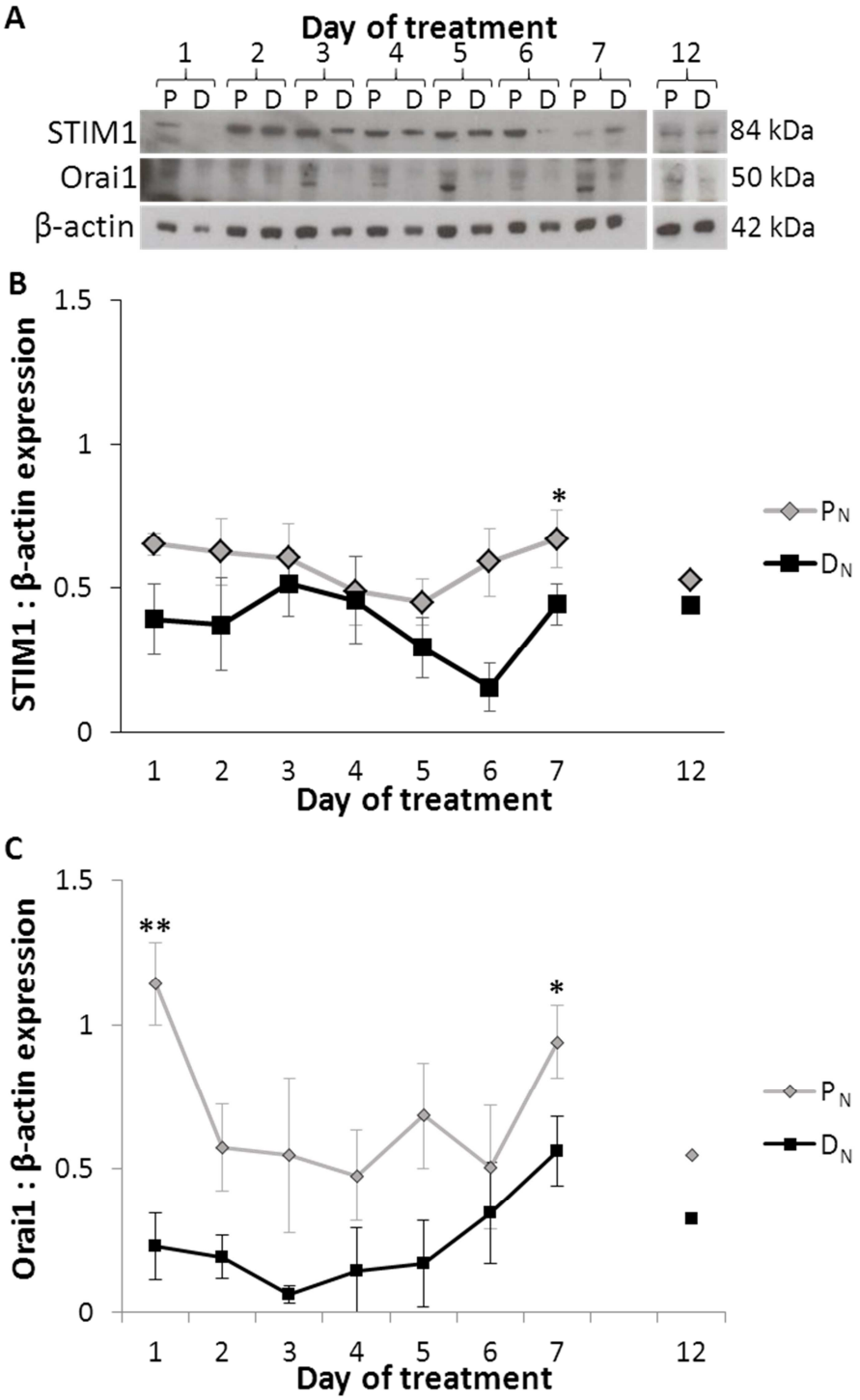

Figure 6.4.1. STIM1 and Orai1 expression are altered early in differentiating N-type populations

Western blots were performed on protein samples from N-type populations that were treated over 7 days (1-7) with 1 µM 9*c*RA (D_N) or an equivalent volume of EtOH (P_N). After 7 days, treatment was withdrawn from both P_N and D_N cells, which were grown

in standard culture media alone for a further 5 days (12). Blots were probed with anti-STIM1 antibody which detected a band at 84 kDa, anti-Orai1 antibody which detected a band at 50 kDa or β-actin antibody which was used as a loading control and detected a band at 42 kDa. **(A)** STIM1 was expressed in both P_N and D_N populations over the treatment time-course, sometimes with lesser band intensity or a slight increase in molecular weight in D_N populations, which becomes clear from day 3 of treatment. Following treatment withdrawal, this increase in STIM1 molecular weight was also observed. Orai1 was expressed in P_N populations and to much a lesser extent or was absent in D_N populations over the treatment time-course and following treatment withdrawal. **(B)** There was no significant change in the level of STIM1 expression over the treatment time-course by P_N populations (P=0.741) or D_N populations (P=0.387). D_N populations expressed STIM1 to a slightly lesser extent, though non-significantly, compared to P_N populations over the treatment time-course (P=0.078). In D_N populations compared to P_N populations, STIM1 was down-regulated by 40% at day 1 (P=0.088) and day 2 (P=0.253). The extent of down-regulation was reduced at day 3 (by 14%, P=0.612) and day 4 (7%, P=0.870). However, by day 5, the extent of STIM1 down-regulation had increased to 35% (P=0.275) then was significantly down-regulated by 74% at day 6 (P=0.017*) and by 34% at day 7 (P=0.134). Following treatment withdrawal, there was a 16% reduction in level of STIM1 expression of D_N populations compared to P_N populations. N≥3 except 12 N=1. **(C)** There was no significant change in the level of Orai1 expression over the treatment time-course by P_N populations (P=0.127) or D_N populations (P=0.116). Orai1 was expressed to a lesser extent in D_N populations compared to P_N populations over the treatment time-course (P=0.0007). There was a down-regulation of Orai1 expression in D_N populations compared to P_N populations by 80% at day 1 (P=0.008**), 66% at day 2 (P=0.086), 89% at day 3 (P=0.147), 69% at day 4 (P=0.198), 75% at day 5 (P=0.095), 31% at day 6 (0.602) and 40% at day 7 (P=0.046*). Following treatment withdrawal, Orai1 expression was 41% lower in P_N populations compared to D_N populations. N≥3 except 12 N=1.

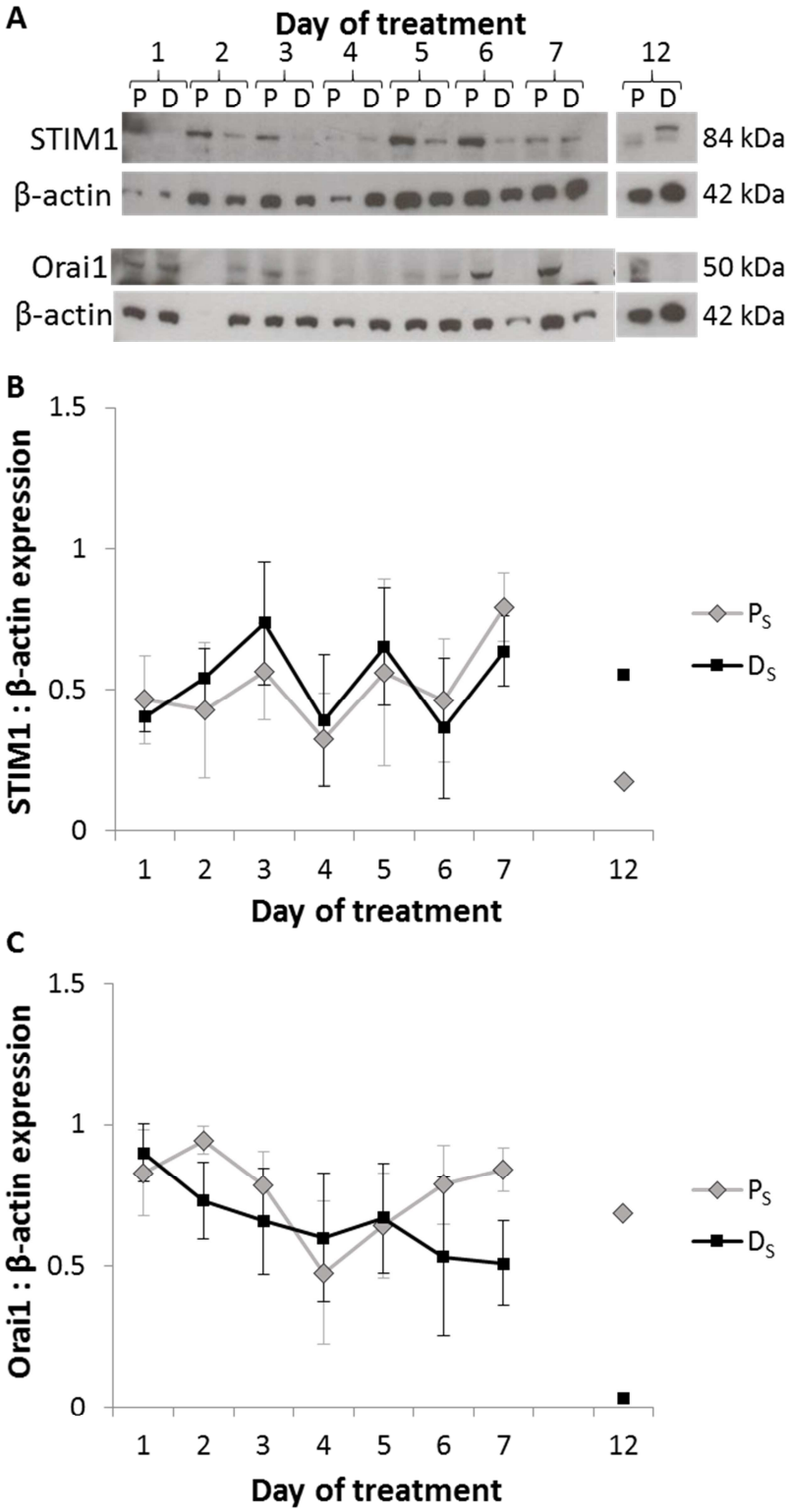

Figure 6.4.2. STIM1 and Orai1 expression are altered gradually in differentiating S-type populations

Western blots were performed on protein samples from S-type populations that were treated over 7 days (1-7) with 1 µM 9*c*RA (D_S) or an equivalent volume of EtOH (P_S).

After 7 days, treatment was withdrawn from both P_S and D_S cells, which were grown in standard culture media alone for a further 5 days (12). Blots were probed with anti-STIM1 antibody which detected a band at 84 kDa, anti-Orai1 antibody which detected a band at 50 kDa or β-actin antibody which was used as a loading control and detected a band at 42 kDa. **(A)** STIM1 was expressed in both P_S and D_S populations over the treatment time-course, sometimes with less band intensity as can be observed at day 2, or a slight increase in molecular weight. Following treatment withdrawal, a clear increase in STIM1 molecular weight could be observed in D_S populations. Orai1 was expressed in P_S populations and to a lesser extent in D_S populations, with expression diminishing from day 3 of treatment in D_S populations and being absent at day 6 and 7 and following treatment withdrawal. **(B)** The level of STIM1 expression was not significantly altered over the treatment time-course in P_S populations (P=0.900) or D_S populations (P=0.714). There was no significant difference in the level of STIM1 expression in P_S populations compared to D_S populations over the treatment time-course (P=0.948). In D_S compared to P_S populations, STIM1 expression was down-regulated by 13% at day 1 (P=0.716), by 21% at day 6 (P=0.775) and by 20% at day 7 (P=0.422) and was up-regulated by 27% at day 2 (P=0.670), 31% at day 3 (P=0.549), 20% at day 4 (P=0.826) and 16% at day 5 (P=0.824). Following treatment withdrawal, STIM1 expression was up-regulated over 3-fold in D_N populations compared to P_N populations. N≥3 except 12 N=1. **(C)** There was no significant change in the level of Orai1 expression in P_S populations (P=0.460) and a slight but non-significant decline in the level of Orai1 expression in D_S populations (P=0.816) over the treatment time-course. Orai1 was generally expressed to a lesser extent in D_S populations compared to P_N populations over the treatment time-course, but this was non-significant (P=0.684). Orai1 expression was down-regulated by 23% at day 2 (P=0.271), by 16% at day 3 (P=0.660), by 32% at day 6 (P=0.402) and by 39% at day 7 (P=0.073) and was up-regulated by 27% at day 4 (P=0.730). Following treatment withdrawal, Orai1 expression was down-regulated by 95% in D_S populations compared to P_S populations. N≥2 except 12 N=1.

Chapter 6 – Discussion

As previously explored (Chapter 3-5), treatment of N-type and S-type neuroblastoma populations with 1 µM 9*c*RA for 7 days induces morphological and biochemical differentiation. For N-type cells, this includes elongation of neurite-like processes, up-regulation of Bcl-2, uncoupling of Ca^{2+} store release and SOCE and a down-regulation of the SOCE proteins STIM1 and Orai1. For S-type cells, differentiation involves cell margin spreading with increased cell dimensions, a slight down-regulation of Bcl-2, uncoupling of Ca^{2+} store release and SOCE and a down-regulation of the SOCE proteins STIM1 and Orai1. The aim of this chapter was to investigate the relationship between these characteristic biochemical changes and their association with the time-course of morphological the differentiation response.

Morphological differentiation progressed in a multi-step manner in N-type cells and was initiated within the first day of 9*c*RA treatment in N-type populations, as has previously been shown (Cheung 2009; N. Bell 2013). There was further increase and a peak in differentiation at the fifth day of treatment, suggesting that there may a differentiation 'step' for N-type cells mid-way through the treatment time-course that defines their progression towards a neuronal phenotype. For S-type cells, however, morphological differentiation was induced gradually from the third day of treatment, peaking at day 5 for S_O and S_A cells but at day 7 for S_E cells, highlighting a subtle variability between the sub-populations response to 9*c*RA-induced differentiation. These results also indicate that morphological 9*c*RA–induced differentiation is initiated earlier in N-type populations than S-type populations. RA can induce changes in gene expression just hours after exposure (LaRosa 1988) which is consistent with the changes observed at day 1 of treatment in N-type populations. Over the treatment time-course, the extent of differentiation does not exceed 30% in N-type cells, indicating that either cells respond to varying degrees in the given time or that not all cells respond to RA treatment, which could have implications for neuroblastoma treatment using RA in patients (Discussion 7.1).

Following 5 days of treatment withdrawal, D_N populations seem to revert back to a P_N phenotype indicating that N-type cells may lose their differentiating characteristics

following removal of the differentiation stimulus. However, for S-type cells, D_S S_E cells show a potential reversion to a P_S phenotype whilst D_S S_O and D_S S_A cells retain a D_S morphology. P_S S_E cells seem to become more morphologically differentiated over time in culture, based on the increase in length between day 7 and 12, therefore it may be possible that 9*c*RA withdrawal does not cause D_S S_E cells to completely lose their differentiating characteristics, suggesting that, overall, S-type morphological differentiation may be mostly retained following removal of the differentiation stimulus. It is possible that N-type cells need longer exposure to 9*c*RA than S-type cells to reach an irreversible differentiating cell fate. Alternatively, given that N-type cells are known to be more tumourigenic than S-type cells in culture and *in vivo* (Ciccarone 1989; Picacentini 1996; Walton 2004), N-type cells may be more capable of phenotypic interconversion and, in this case, favour a proliferating phenotype and this could potentially explain the poor retinoic acid response seen in patients.

Over the differentiation time-course, as expected, the neuronal marker β-tubulin III was expressed to a greater extent in N-type populations than S-type populations. Since β-tubulin III expression was not altered over the differentiation time-course of D_N or D_S populations, this suggests that the level of β-tubulin III expression was unaffected by the differentiation response of N-type and S-type populations. It was expected that β-tubulin III expression would increase over the differentiation time-course in N-type populations as they progress towards a neuronal phenotype, similar to other neuron specific proteins such as NeuN (Cheung 2009; Agholme 2010) and neurofilament-68 (Messi 2008), and decrease over the differentiation time-course in S-type populations as they move towards a non-neuronal phenotype. However, as observed here, it has previously been shown that expression of other neuronal markers, such as neurofilaments and dopamine transporters, do not change with RA-induced differentiation (Encinas 2000; Cheung 2009) and that S-type cells can express other neuronal markers, such as NF-68 (Messi 2008; Acosta 2009). Following treatment withdrawal, β-tubulin III expression was reduced in D_N compared to P_N populations, and there was no difference in expression between P_S and D_S populations. This suggests that there may be some reversion away from a neuronal phenotype with removal of the differentiation stimulus in N-type populations that does not occur in S-

type populations, which corresponds to the morphological response observed, perhaps due to the non-neuronal nature of S-type cells.

The non-neuronal marker vimentin was expressed to a greater extent in S-type populations than N-type populations throughout the treatment time-course. A slight increase in vimentin expression in P_S populations early in the treatment time-course implies that these cells may move towards a more non-neuronal phenotype over time in culture. Vimentin expression also increased in D_S populations over the treatment time-course and was slightly higher than P_S populations at day 6 and 7, indicative of S-type populations becoming more non-neuronal-like with differentiation. Following treatment withdrawal, vimentin expression remained higher in D_S compared to P_S populations, suggesting that S-type cells remain committed to a non-neuronal lineage despite removal of the differentiation stimulus, corresponding with the previously discussed morphological response and β-tubulin III expression. Vimentin was expressed very weakly in P_N populations and expression was slightly higher in D_N populations early in the treatment time-course, which corresponds with the previous finding that vimentin is temporarily up-regulated with neurite outgrowth (Shea 1993; Whitworth 2012; N. Bell 2013). Vimentin is known to have a role in initial neuritogenesis then becomes down-regulated through phosphorylation by Rho-kinase (Y. Nakamura 2000) and replaced by neurofilaments, coinciding with dampened neurite outgrowth or retraction (Shea 1993; Boyne 1996; Yabe 2003; Dubey 2004).

Bcl-2 expression increased over the differentiation response of N-type populations but is slightly reduced with differentiation of S-type populations. This suggests that Bcl-2 is an effective marker for differentiation in N-type populations as an increase of expression coincides with the differentiation response of N-type populations but not S-type populations, as previously shown (Bell 2011). Bcl-2 expression was up-regulated early in the differentiation process and in D_N populations progressively increased from the first day of treatment. Bcl-2 expression is associated with neural differentiation (Zhang 1996; Middleton 1998; Suzuki 1998) and given that the up-regulation observed in this study begins shortly after initial neurite elongation occurs, Bcl-2 may be involved in enhancing neurite outgrowth and establishing a differentiating phenotype

rather than initiating the neurite elongation seen on the first day of 9*c*RA treatment. Following treatment withdrawal, this up-regulation of Bcl-2 expression in D_N populations is lost, indicating that N-type cells may revert away from a differentiating phenotype following the removal of the differentiation stimulus, correlating with the previous morphological and β-tubulin III findings and consistent with the role of Bcl-2 in neural differentiation (Zhang 1996; Middleton 1998; Suzuki 1998). Bcl-2 expression is slightly reduced in D_S populations compared to P_S populations following treatment withdrawal, indicating that S-type cells may retain their non-neuronal-like differentiating phenotype, correlating with the previous morphological, β-tubulin III and vimentin results.

Expression of the stem cell marker CD133 was slightly up-regulated in D_N populations compared to P_N populations, implying that with differentiation, N-type populations may retain stem-cell like properties throughout the differentiation response. These findings are in contrast to those which have shown CD133 expression to repress cell differentiation and promote proliferation in neuroblastoma (Takenobu 2011) and brain tumours (Singh 2003). One possible explanation for this difference is that the increase in CD133 expression observed in differentiating cells here actually promotes the N-type reversion from a differentiating to a proliferating phenotype following removal of 9*c*RA, as seen in the morphological response and change in β-tubulin III and Bcl-2 expression. However, this possibility requires further investigation.

9*c*RA-induced differentiation of N-type populations was found to induce an uncoupling of Ca^{2+} store release and SOCE in a multi-step manner, with down-regulation of SOCE occurring from the first day of treatment and the extent of which is exaggerated from the fourth day of treatment. These data extend the previous findings by revealing that the previously observed Ca^{2+} signalling profile seen at day 7 (Chapter 4) was present in D_N populations from the fourth day of exposure to 9*c*RA. Furthermore, down-regulation of SOCE was confined to the total SOCE response since maximal SOCE was not significantly altered over the differentiation response. This suggests that the SOCE response was of a shortened duration either through accelerated or more efficient Ca^{2+} entry and store replenishment or an increased efficiency of inactivation. Changes

in the rate or efficiency of Ca^{2+} entry were confined to the later phase of the differentiation response rather than during the initial differentiation of N-type populations whilst alterations in speed and/or efficiency of Ca^{2+} entry deactivation occurred early in the differentiation response of N-type populations, indicating that the various phases of the differentiation response may induce changes in the dynamics of SOCE activity in a different manner.

These overall changes in SOCE activity can be explained by the expression patterns of the Ca^{2+} sensing protein STIM1 and the SOC channel Orai1. Down-regulation of both STIM1 and Orai1 occurred early in the differentiation response of N-type populations, thereby potentially driving the initial down-regulation of SOCE observed from the first day of 9*c*RA treatment. By day 3 and 4 of treatment, down-regulated SOCE activity seemed to be predominantly driven by a down-regulation of Orai1 given that STIM1 expression recovered. However, there was an increase in the molecular weight of STIM1 suggesting that there may be a modification, such as phosphorylation, taking place that could affect STIM1 function thereby contributing to dampened SOCE activity, or presence of an alternative isoform of STIM1 that serves a slightly altered function. Indeed, as previously discussed (Discussion 5). STIM1 phosphorylation at multiple serine residues has been identified (Manji 2000; Smyth 2009; Sundivakkam 2012; Pozo-Guisado 2013; Sundivakkam 2013) and was found to have multiple roles in STIM1 function (Smyth 2009; Pozo-Guisado 2013; Sundivakkam 2013) and the existence of the STIM1L isoform has also been identified (Darbellay 2011; Sauc 2015). STIM1L has been shown to induce SOCE quicker than STIM1S, attributable to its association with Orai1 at rest rather than needing to migrate to bind Orai1 following store depletion like that of STIM1S (Darbellay 2011; Horinouchi 2012). The observed changes in rate of Ca^{2+} entry over the differentiation response may therefore be associated with shifts in the contribution of these STIM1 isoforms to SOCE activity and the presence of STIM1L may also explain the observed changes in STIM1 molecular weight as STIM1L has a higher molecular weight than STIM1S (Darbellay 2011).

By day 5 of treatment, STIM1 down-regulation was reinstated, perhaps triggered by a potential modification as discussed that was observed in the previous days, whilst

Orai1 remained extensively down-regulated and perhaps drives the second 'step' in dampened SOCE activity in the N-type differentiation response. There was a peak in STIM1 down-regulation at day 6 of treatment alongside some recovery of Orai1 expression that perhaps indicates that Orai1 is contributing less to the maintenance of the differentiation response at this stage. These findings correspond with that of the previously discussed markers of differentiation and provide further evidence to support a multi-step differentiation response in N-type populations.

Following treatment withdrawal from N-type populations, the extent of uncoupling of Ca^{2+} store release and SOCE remained similar to that seen at day 7 of treatment, both in total and maximal Ca^{2+} entry as well as the rates of Ca^{2+} entry and deactivation, indicating that SOCE uncoupling is maintained following removal of the differentiating stimulus. This result is in contrast to the previously discussed data that has indicated that N-type cells revert back to a proliferating phenotype but can be explained by the expression of the underlying SOCE proteins. There was minimal down-regulation of STIM1 and the change in STIM1 molecular weight seen with differentiation was lost but Orai1 down-regulation was maintained, indicating that the observed reduction in SOCE activity is driven solely by dampened Orai1 expression following removal of the differentiation stimulus. The restoration of STIM1 expression correlates with the previously discussed morphological and β-tubulin III, Bcl-2 and CD133 expression findings that N-type cells revert from a differentiating to a proliferating phenotype following removal of the differentiation stimulus. Therefore all of the differentiation markers used in this study point to N-type cells moving away from a neuronal phenotype and losing the characteristics of a differentiating phenotype when exposure to 9*c*RA is stopped, except that of Orai1 expression and SOCE activity. Orai1 expression may take longer to recover, leaving SOCE activity dampened. Alternatively, loss of Orai1 may represent an irreversible change, perhaps because its place has been taken by up-regulation of an alternative SOC such as TRPC1 (Bell et al. 2013). It is important to emphasise that, given time restrictions, the protein expression results are made up just one time point, therefore the conclusions drawn are speculative and must not be over-extrapolated. It will be interesting to determine whether the current hypotheses hold true when the analysis is concluded (Discussion 7.2).

The ratio of STIM1:Orai1 is known to play an important role in the extent of SOCE activity (Hoover 2011; Hodeify 2015). SOCE activation occurs via a diffusion-trap mechanism by which ER Ca^{2+} store depletion induces STIM1 accumulation at plasma membrane junctions, where STIM1 is able to bind and trap Orai1 dimers and trigger the formation of tetrameric Orai1 channels that cause SOCE (Mignen 2008; Penna 2008; Hoover 2011; Hodeify 2015). This process has been shown to induce peak SOCE activity with a ratio of 2 STIM1:Orai1 and therefore binding of 8 STIM1 per Orai1 channel (Hoover 2011). In the observed scenario whereby STIM1 expressed and functional, there is enough STIM1 to gate all available channels, but since Orai1 remains depleted, SOCE activity cannot be increased with more STIM1 as the capacity for SOCE to occur has been reached.

9*c*RA-induced differentiation of S-type populations caused an uncoupling of Ca^{2+} store release and SOCE in a gradually increasing manner from the first day of treatment and the previously observed Ca^{2+} signalling profile seen at day 7 (Chapter 4) is present in D_S populations from the fifth day of exposure to 9*c*RA, both in total and maximal Ca^{2+} entry. These findings correspond with the previously discussed markers of differentiation and provide further evidence to support a gradual differentiation response in S-type populations. Similar to N-type populations, there was a varied effect on Ca^{2+} store size or TG sensitivity, as well as changes in the speed and/or efficiency of Ca^{2+} entry and deactivation, between the early and late differentiation response of S-type populations, indicating that the various phases of the differentiation response may induce changes in Ca^{2+} entry in a different manner. During the differentiation response of S-type populations, the observed reduction in SOCE activity appears to be driven predominantly by Orai1 down-regulation as the expression of STIM1 was only slightly altered. By day 6 and 7 of treatment, a slight down-regulation of STIM1 and dampened Orai1 expression coincides with, and is likely to cause, the observed peak in dampened SOCE activity.

Following treatment withdrawal, the Ca^{2+} store release and SOCE uncoupling seen in differentiating S-type populations was lost and both total and maximal SOCE activity

was restored, indicating that differentiating S-type populations may either revert back to a coupled SOCE response like that of proliferating S-type populations or that SOCE uncoupling is involved in the initiation of the early differentiation response but is not needed to maintain the differentiated state of S-type populations. Alongside this restoration of SOCE activity, there was an increase in the level of STIM1 expression, however, an increase in STIM1 molecular weight could be observed alongside a further increase in the extent of Orai1 down-regulation. Given that SOCE activity recovered following treatment withdrawal, this implies that potentially there is a SOC channel other than Orai1, such as TRPC1, by which SOCE can occur in S-type cells. Indeed, it has been shown that STIM1 is able to bind TRPC1 and induce SOC channel functionality (Yuan 2007) and induce SOC rather than ROC function through insertion of TRPC1 into lipid raft domains (Alicia 2008). This channel may be up-regulated or undergo a functional modification to compensate for the lack of Orai1 following removal of the differentiation stimulus, thereby inferring that SOCE down-regulation may play a role in driving differentiation but is not required to maintain the differentiation response in S-type populations, since all other differentiation markers are retained. Again, it must be noted that the protein expression results observed are made up just one time point, therefore further analysis will test our current hypotheses (Discussion 7.2).

In summary, these results imply that the differentiation response of N-type populations occurs in a multi-step manner whilst the S-type cell differentiation response occurs gradually. Following the removal of the differentiating stimulus, N-type populations seem able to revert away from a differentiating neuronal-like phenotype whilst S-type populations seem to maintain a differentiating non-neuronal-like phenotype. This demonstrates that, potentially, N-type cells have a greater capacity for therapy evasion, are less sensitive to the differentiating effects of RA or that it takes longer exposure to RA to induce irreversible commitment to a neuronal fate.

Chapter 7: Final Discussion

7.1. Summary of findings

The aim of this study was to investigate the morphological, biochemical (immunofluorescence) and functional (Ca^{2+} signalling) markers in proliferating and 9cRA-induced differentiating N-type and S-type neuroblastoma populations at the single cell level to establish a phenotype-specific profile of the differentiation process.

The results presented in this thesis provide clear evidence for a multi-step N-type morphological and biochemical differentiation response towards a neuronal phenotype that coincided with multi-step SOCE down-regulation and a gradual S-type morphological and biochemical differentiation towards a non-neuronal phenotype that coincided with gradual SOCE down-regulation (summarised in Table 7.1.1).

An uncoupling of Ca^{2+} store release and SOCE in 9*c*RA-differentiated N-type populations correlates with previous findings (Brown 2005; N. Bell 2013). The predominant mechanisms by which Ca^{2+} entry occurs is dependent on cell type (Berridge 2000; Bootman 2001). Whilst SOCE is a ubiquitous Ca^{2+} entry pathway, excitable cells are more reliant on VOC-mediated Ca^{2+} entry (Berridge 1998) and, since N-type cells differentiate towards a neuronal phenotype, this may explain the observed dampened SOCE response with N-type differentiation. Indeed, our laboratory has previously found that voltage-operated Ca^{2+} entry remains active in 9*c*RA differentiated SH-SY5Y cells (Brown 2005).

An uncoupling of Ca^{2+} store release and SOCE also occurred with differentiation of S-type populations which is in contrast to that shown previously (N. Bell 2013). Given the differences in S-type sub-population responses (Table 4.4), this may be due to variability in the S-type responses. It is important to note that Ca^{2+} store size was slightly reduced in N-type populations over the differentiation response and was reduced early but increased late in the differentiation response of S-type populations. This change in Ca^{2+} store size was not previously observed (N. Bell 2013) and may contribute to this disparity since SOCE is governed by the extent of store depletion.

Another noteworthy point is that the changes in SOCE activity with differentiation were consistent with the expression of the SOCE proteins STIM1 and Orai1 in both studies (Table 7.1.1).

Dampened SOCE in differentiating S-type populations was unexpected since non-excitable cells tend to rely on SOCE as a predominant Ca^{2+} entry pathway. The identity of the S-type population phenotype has yet to be discerned, a feat that becomes more complex when considering the variability within this cell compartment both in the morphology (i.e. S_O, S_A and S_E cells) and the Ca^{2+} signal profiles attributed to them (Table 4.4). This non-neuronal lineage is thought to consist of glial cells, Schwann cells and melanocytes, since markers of these cell types have been observed in S-type cells (Ross 1985; Ciccarone 1989; Whitworth 2012; N. Bell 2013). Uncovering the identity of S-type cells may therefore explain the reduced reliance on SOCE as a Ca^{2+} entry pathway with 9*c*RA-induced differentiation. For example, as well as SOCE, voltage-operated Ca^{2+} entry has been observed in melanocytes (Wiesner 2002; Bogeski 2012) and VOCs are expressed in astrocytes (Carmignoto 1998). Therefore it is also plausible that S-type differentiation towards a non-neuronal phenotype brings about changes in the predominant Ca^{2+} entry pathway and this may contribute to the observed dampened SOCE response.

N-type and S-type populations exhibit phenotype-specific Ca^{2+} signals in their differentiation response (Table 4.3). Differentiation of N-type populations caused a slight reduction in Ca^{2+} store release and drastically smaller, shortened SOCE responses. This Ca^{2+} signal profile differed from that of differentiating S-type populations which had increased Ca^{2+} store release and rate of store depletion, indicating a potential increase in the size of the ER Ca^{2+} store capacity and/or an increased sensitivity to TG and the SOCE was dampened but maintained for longer. These differences highlight the possibility of targeting the differentiated SOCE pathway as a means of neuroblastoma treatment to be specific to cell phenotype. For example, S-type cells are less tumourigenic than N-type cells in culture and *in vivo* therefore manipulation of N-type differentiation-associated Ca^{2+} signals to induce a more S-type

response may pose an interesting route for the development of more effective treatment.

This potential for altering phenotype-specific Ca^{2+} signals has applicability in the process of phenotypic transdifferentiation. Within N-type and S-type predominant populations, N-type, S-type and I-type cells are always present, regardless of extent of enrichment (Introduction 1.3 and Methods 2.3). This may be explained by the fact that these cells are known to transdifferentiate in culture (Ciccarone 1989). Both of these points are important to consider when investigating cell population responses. A major benefit of adopting the single cell approach to Ca^{2+} signal studies is that specific Ca^{2+} responses can by identified and attributed to each cell phenotype within a population thereby allowing the Ca^{2+} responses of the cell phenotypes underlying the population responses to be studied. An uncoupling of Ca^{2+} store release and SOCE occurred in all cell types grown in either an N-type or an S-type population yet there were distinct differences in the Ca^{2+} signalling responses and extent of SOCE down-regulation between the two environments (Table 4.3 and 4.4).

N-type cells within an N-type population exhibited Ca^{2+} signals that reflected those observed at the N-type population level however N-type cells within an S-type population showed an increase in Ca^{2+} store release reflective of either an increase in store size or sensitivity to TG and SOCE was down-regulated to a greater extent. This indicates that N-type cells may display plasticity in Ca^{2+} signals that are influenced by the surrounding predominant phenotype. S-type cells in an N-type or an S-type population exhibited similar Ca^{2+} signals however the observed response was made up of variable responses at the sub-population level. Indeed, the Ca^{2+} signals in S_O, S_A and S_E cells were altered dependent on the predominant phenotype of the population in which they were grown but were consistently down-regulated SOCE with differentiation (Table 4.4). This sub-population analysis has revealed that S-type cells may in fact exhibit plasticity in Ca^{2+} signals that are influenced by the surrounding predominant phenotype which were previously masked by observing Ca^{2+} signals at the population level. I-type cells in an N-type population showed an increase in Ca^{2+} store release reflective of either an increase in store size or sensitivity to TG but in an

S-type population Ca^{2+} store release was not altered. SOCE was down-regulated in I-type cells to a similar extent in each population but SOCE was shorted in N-type populations and of longer duration in S-type populations. This indicates that I-type cells may also display plasticity in Ca^{2+} signals that are influenced by the surrounding predominant phenotype.

Additionally, conditioned media from proliferating and differentiating N-type and S-type populations affected phenotypic characteristics of morphology, protein expression and SOCE activity (summarised in Table 7.1.2). This provides evidence for an effect of the surrounding phenotypic environment due to the release of factors by the predominant population affecting the minority phenotypes characteristics. These findings also seemed to indicate that S-type population characteristics were influenced by N-type conditioned media, more so than N-type populations characteristics were by S-type conditioned media. This could suggest that S-type cells may be more likely to transdifferentiate than N-type cells due to the influence of the surrounding predominant phenotypic environment. It would be very interesting to determine if this influence contributes phenotypic transdifferentiation (Discussion 7.2) as this process is currently poorly understood and may play an important in the context of disease progression in neuroblastoma patients.

Taken together, these results have revealed the variability Ca^{2+} signals with differentiation, between cell phenotypes and as influenced by the predominant surrounding cell population, thus highlighting the advantage of using single cell analysis to uncover these differences that may be masked in responses at the population level. This heterogeneity within the SH-SY5Y neuroblastoma cell line may be reflective of tumour heterogeneity in patients, which could have implications in disease progression and/or treatment failure. For example, response to RA treatment in neuroblastoma patients is often poor (Matthay 2009; Navalkele 2011). This may be attributed to just one compartment of the tumour population, for sake of example, the highly tumourigenic putative I-type cells. These I-type cells, which are actually the minority cell phenotype, may be less responsive to RA treatment than other phenotypes within the population and perhaps actually come into existence through

transdifferentiation from another phenotype, to which phenotype-specific Ca^{2+} signals may contribute. The characteristics that I-type cells fundamentally possess or acquire through transdifferentiation therefore gives them the ability to continue to proliferate and evade treatment. Perhaps they even transdifferentiate back into other phenotypes along the way due to influence from other cells, giving rise to a perpetual supply of mixed phenotypes and, ultimately, leading to aggressive and unresponsive tumour growth. However, if the phenotypic characteristics of these highly tumourigenic I-type cells could be identified and remodelled, perhaps through manipulation of underlying SOCE-specific components, they could potentially be pushed towards a less tumourigenic phenotype or forced to transdifferentiate to another phenotype and become responsive to RA treatment. Identification of these phenotype-specific responses is the first step to this process and this thesis has addressed this problem directly.

On a similar note, withdrawal of 9*c*RA treatment appeared to induce partial reversion of N-type populations from a differentiating phenotype to a phenotype similar to that of proliferating N-type cells whilst S-type populations seemed to retain a differentiating phenotype (summarised in Table 7.1.3). This suggests that 9*c*RA-induced differentiation of S-type cells induces commitment to a non-neuronal lineage despite removal of the differentiation stimulus. Moreover, given the low tumourigenic characteristics of S-type cells in culture and *in vivo* (Ciccarone 1989; Picacentini 1996; Walton 2004), it seems that S-type cells may be less likely than N-type cells to contribute to RA resistance. Despite the apparent maintenance of the differentiating S-type state, and prevailing Orai1 down-regulation, SOCE activity was restored upon removal of the differentiating stimulus. This suggests that in S-type cells, Orai1 may drive the differentiation response and another channel, such as TRPC1, may compensate to restore SOCE activity and maintain the differentiated state of S-type cells. This notion would be consistent with the predominance of SOCE as a Ca^{2+} entry pathway in non-neuronal cells.

These findings also suggest that 9*c*RA-induced differentiation of N-type cells potentially induces a transient shift towards a neuronal phenotype that is reversible,

with maintenance of the differentiating phenotype dependent on the presence of the differentiating stimulus. It may instead be that N-type cells are less sensitive to 9*c*RA or that they require prolonged exposure to 9*c*RA compared to S-type cells to reach an irreversible differentiating cell fate. On the other hand, N-type cells may acquire some form of resistance to 9*c*RA treatment that could enable them to be more adept at evading a fully differentiated phenotype. Alternatively, since N-type cells are more tumourigenic than S-type cells in culture and *in vivo* (Ciccarone 1989; Picacentini 1996; Walton 2004), N-type cells may be intrinsically more capable of phenotypic interconversion and, in this case, favour a proliferating phenotype. Clearly any of these scenarios could have dramatic impact on tumour progression and, the ability of just one compartment of the neuroblastoma population to outsmart the differentiation-inducing effects of RA treatment could potentially explain the poor response to RA that is observed in neuroblastoma patients (Matthay 2009; Navalkele 2011).

Overall, this thesis has revealed the extent of variability in the differentiation responses attributed to heterogeneity within the SH-SY5Y neuroblastoma cell line. The SOCE pathway in the different cell types and, in the case of S-type cells, sub-populations, may represent potential targets for novel therapeutics of neuroblastoma disease.

	P_N		D_N		P_S		D_S	
	Early	Late	Early	Late	Early	Late	Early	Late
Morphology	-	-	↑	↑↑	-	-	-	↑↑
β-tubulin III	-	-	-	-	-	-	-	-
Vimentin	X or ↓↓	X or ↓↓	↑	↑	-	↑	-	↑↑
Bcl-2	-	-	↑	↑↑	-	-	-	↓
CD133	-	-	-	↑	U	-	U	↓
MiTF	U	-	U	-	U	-	U	-
STIM1	-	-	- or ↓	↓ ↑ MW	-	-	-	↓ ↑ MW
Orai1	-	-	↓↓	↓	-	-	- or ↓	↓ or ↓↓
TRPC1	U	-	U	↓	U	-	U	↓
SOCE	-	-	↓	↓↓	-	-	↓ to ↓↓	↓↓

Table 7.1.1. Summary of findings over the 9*c*RA-induced differentiation response in N-type and S-type populations

Each population response is defined by the early differentiation response (Days 1-4) and late differentiation response (Days 5-7). For N-type populations (P_N and D_N) morphology represents a change in neurite length whilst for S-type populations (P_S and D_S) this represents a change in cell dimensions (sub-type diameter or length). – represents general expression. X represents no expression. ↑ represents an increase. ↑↑ represents a large increase. ↓ represents a decrease. ↓↓ represents a large decrease. U represents an unknown that was not investigated. MW represents a change in the molecular weight of STIM1.

	P_N		D_N	P_S		D_S
	+ P_S	+ D_S	+ D_S	+ P_N	+ D_N	+ D_N
Morphology	X	↑	↑	X	↑	↑
β-tubulin III	↑	-	↑	↑↑	↑	-
Vimentin	-	↑↑	↑↑	-	↑↑	↑
STIM1	↑	-	↑MW	↑	↓MW	↓MW
Orai1	↑↑	-	↓	↑	↓	-
SOCE	-	↓↓	↓	↓	↓	↓

Table 7.1.2. Summary of findings with the application of conditioned media to N-type and S-type populations

Each population response is defined by the addition of P_S, D_S, P_N or D_N conditioned media. For N-type populations (P_N and D_N) morphology represents a change in neurite length whilst for S-type populations (P_S and D_S) this represents a change in cell dimensions (sub-type diameter or length). – represents general expression. X represents no expression. ↑ represents an increase. ↑↑ represents a large increase. ↓ represents a decrease. ↓↓ represents a large decrease. MW represents a change in the molecular weight of STIM1.

	D_N	D_S
Morphology	-	↑
β-tubulin III	↓	↓
Vimentin	U	↑↑
Bcl-2	-	↓↓
STIM1	-	↑↑↑ MW
Orai1	↓	↓↓
SOCE	↓↓	-

Table 7.1.3. Summary of findings following 9*c*RA treatment withdrawal for 5 days

For N-type populations (D_N) morphology represents a change in neurite length whilst for S-type populations (D_S) this represents a change in cell dimensions (sub-type diameter or length). – represents general expression. X represents no expression. ↑ represents an increase. ↑↑ represents a large increase. ↓ represents a decrease. ↓↓ represents a large decrease. U represents an unknown that was not investigated. MW represents a change in the molecular weight of STIM1.

7.2. Future investigations

This study investigated the sequence of changes in expression of STIM1 and Orai1 over the differentiation response however, since the reliability of TRPC1 antibody was poor, further investigation is needed to determine whether TRPC1 plays a role in SOCE in N-type and S-type populations. Determining whether any changes in TRPC1 expression occur with differentiation and the relationship with changes in expression of STIM1 and Orai1 over the 9*c*RA-induced differentiation response is crucial for understanding the proliferation-differentiation switch. Similarly, manipulating TRPC1 expression may affect the STIM1-Orai1 relationship with SOCE activity in the differentiation response.

A potential STIM1 modification was found to precede down-regulation in N-type populations and was present in differentiating S-type populations. This modification could represent phosphorylation or glycosylation events or perhaps an increase in expression of an alternative isoform, all of which have been previously established in STIM1 characterisation (Discussion 5). It would be interesting to investigate this further since protein modification may affect function and contribute to dampened SOCE.

This thesis has suggested that following withdrawal of 9*c*RA treatment, N-type cells potentially revert back to a proliferating morphology whilst S-type cells may retain characteristics of non-neuronal differentiation. Since these conclusions are speculative due to one time-point being assessed, this may be confirmed through experimental repeats and raises the question as to how N-type cells are able to revert whilst S-type cells do not. N-type cells are known to be more tumourigenic than S-type cells in culture and *in vivo* and therefore may be less sensitive to 9*c*RA-induced differentiation. The heterogeneity in the responses observed has implications for the interpretation of this data. At present, we assume that the D_N cells that exhibit SOCE down-regulation and the D_S cells that fully recover the SOCE response following treatment withdrawal are the same cells that have SOCE down-regulation in the presence of 9*c*RA, however this is not known for certain. This has the potential to be investigated by mapping the morphological changes in specific cells over the differentiation time-course and attributing Ca^{2+} signals to each specific cell. Determining the relationship between the morphological and Ca^{2+} signalling differentiation responses over time may provide

clues as to the nature of the changes associated with removal of the differentiating stimulus.

Around half of neuroblastoma patients relapse despite RA therapy (Armstrong 2012) which may be due to variable cellular RA responses associated with heterogeneity. As shown in this study, not all cells were morphologically differentiated following 9*c*RA treatment (Results 3.1). This may be due to some cells exhibiting slower responses to 9*c*RA, complete insensitivity to RA or perhaps differential expression of the RARs and RXRs through which 9*c*RA exerts its effects. Whether all cells within N-type and S-type populations down-regulate SOCE activity with 9*c*RA-induced differentiation or whether SOCE is completely is abolished in some cells and fully intact in other has yet to be determined. The single cell technique and data collected in this thesis have given indication that the former is more likely and this is currently being quantified. Not all N-type cells were morphologically differentiated in response to 9*c*RA therefore the extent of differentiation may correlate with the extent of SOCE activity, which can now be examined through determination of the relationship between morphology and the Ca^{2+} response of individual cells. Some cells may have a delayed respond to RA or may be completely RA insensitive. RA acts via binding of RARs and RXRs, which may be differentially expressed between cells and therefore bring about variability in the RA response (Schug 2007). It is important that the mechanism of action of RA is further investigated at the single cell level to understand therapeutic resistance.

This thesis suggests that the predominant phenotype in a population may influence the responses of minority cell populations, perhaps as an effect of release of factors that affect the local signalling environment. It will be interesting to assess these findings further through experimental repeats to reach more solid conclusions. Unfortunately, given time constraints, Orai1 expression was not determined but it seems likely that it could be down-regulated given the observed changes in SOCE activity observed and will be useful to investigate. Also tracking specific cellular changes in individual cells, for example determining the incidence of transdifferentiation may provide clues as to the phenotypic influence on the differentiation response.

7.3. Conclusions

Understanding the mechanistic changes that underlie the differentiation response of neuroblastoma cells is a valuable strategy to elucidate novel drug targets and improve disease treatment. This strategy has applications in tumour cell differentiation towards a benign phenotype, which may improve understanding of retinoid resistance in neuroblastoma disease, as well as in neurobiology, since the ability to control neuronal precursor differentiation to a fully neuronal phenotype has implications for treatment of neurodegenerative disorders.

This study has utilised a system for detection and analysis of Ca^{2+} signals at the single cell level to identify phenotype-specific alterations in the differentiation response or neuroblastoma cells. Whilst uncoupling of a SOCE was a universal feature of differentiation there were extensive differences in Ca^{2+} signal profiles and underlying protein expression. There was also plasticity in Ca^{2+} signalling that was influenced by the predominant phenotype in the population and cell phenotypes could also be altered.

The results presented in this thesis have revealed variability in the differentiation responses attributed to heterogeneity within the SHSY5Y neuroblastoma cell line. These findings contribute to the understanding of the changes in SOCE responses with differentiation, which may be a valuable tool for manipulation in the context of treatment for neuroblastoma disease.

Appendix

I: BTP2

Introduction

Dampened SOCE activity was associated with differentiation of N-type and S-type populations in this study (Chapter 4) indicating that there may be changes occurring in SOCE associated proteins with differentiation. Ca^{2+} entry via the PM can occur via ROC or SOC channels (Introduction) and, since there is crosstalk between these pathways and association of the proteins involved (Yuan 2007; Jardin 2008; Hong 2011), it is important to distinguish that the apparent SOCE changes observed are attributable to only SOCE and no other Ca^{2+} entry pathways. Therefore this chapter investigated the effects of BTP2; a cell permeable 3,5-bis(trifluoromethyl)pyrazole derivative that inhibits CRAC channels, on N-type populations.

Results

BTP2 inhibits SOCE in N-type populations in a dose-dependent manner

Treatment of N-type populations with 100 nM - 5 µM BTP2 for 24 hours did not alter N-type cell morphology, which possessed small, rounded cell bodies with short neurite-like processes and grew to form cell aggregates (Figure Ai.A-D). Treatment with ≥10 µM BTP2 reduced cell viability and induced cell death (Figure Ai.E and F).

BTP2 caused a significant increase in Ca^{2+} store release ($P<0.0001$) and a substantial down-regulation of SOCE ($P<0.0001$) in N-type populations, even at low concentrations (Figure Aii). Changes in relative cytosolic Ca^{2+} entry are expressed as fluorescence ratio units (FRUs) and compared to DMSO treated cells unless stated otherwise. Treating cells for 24 hours with 100 nM BTP caused a 37% increase in total Ca^{2+} store release (85.86 ± 1.82 FRUs) compared to DMSO treated cells (62.87 ± 1.77 FRUs, $P<0.0001$) and total SOCE was reduced by 69% (143.41 ± 9.82 and 337.57 ± 14.60 FRUs, respectively, Figure Aii). SOCE was down-regulated by BTP2 in a dose-dependent manner and the maximum uncoupling of Ca^{2+} store release and SOCE was achieved at 1 µM BTP2, where SOCE was almost completely abolished (10.11 ± 10.36 FRUs, $P<0.0001$ Figure Aii). There was a second phase of SOCE down-regulation and BTP2

dose dependency from 2 μM BTP2 whereby SOCE (78.34 ± 13.87 FRUs) was almost 9-fold higher compared to cells treated with 1 μM BTP2, when taking the change in Ca^{2+} store size into account (Figure Aii). Ca^{2+} store release and SOCE uncoupling was then heightened with greater concentrations of BTP2 (Figure Aii) but was deemed toxic to cells treated with 10 μM BTP2 or more (Figure Ai.E and F and Figure Aii).

BTP2 also affected Ca^{2+} store release and SOCE dynamics. Maximal SOCE was affected in a dose dependent manner with an inverse correlation and maximal SOCE was significantly reduced with 200 nM – 10 μM BTP2 treatment (all $P<0.0001$, Figure Aiii.A). Maximal SOCE was almost completely abolished with 1 μM BTP2 treatment and was restored at 2 μM BTP2 before a second phase of inverse correlation (Figure Aiii A). Maximal Ca^{2+} store release was only marginally affected by BTP2 concentration (Figure Aiii.A). Rate of Ca^{2+} store release was significantly reduced with all concentrations of BTP2 below 1 μM ($P<0.0001$) and non-significantly reduced with 2 μM and 5 μM BTP2 (Figure Aiii.B) whilst rate of Ca^{2+} store release deactivation was reduced with all concentrations of BTP2 (Figure Aiii.C). Rate of SOCE and rate of SOCE deactivation were reduced with 200 nM - 10 μM BTP2 (Figure Aiii.B and C). Rate of initial SOCE deactivation was increased with all concentrations of BTP2 except 1 and 5 μM BTP2 which exhibited a decrease (Figure Aiii.C). Rate of late SOCE deactivation was also significantly reduced with all concentrations of BTP2 (all $P<0.0001$ except 20 μM $P=0.0003$, Figure Aiii.C).

Taken together, these results demonstrate a dose-dependent uncoupling of Ca^{2+} store release and SOCE with an inverse correlation between BTP2 concentration and extent of SOCE down-regulation made up of two phases; increasing concentrations from 100 nM BTP2 and increasing concentrations from 2 μM BTP2. Maximal SOCE inhibition was achieved at 1 μM BTP2 treatment. BTP2 caused an increase in total Ca^{2+} store release that was driven by a slight increase in maximal Ca^{2+} store release and reduced rates of activation and deactivation, increasing the duration of Ca^{2+} store release. Substantial down-regulation of total SOCE that was driven by large decreases in maximal SOCE and rate of activation with increases in initial rate of deactivation and decreases in late rate of deactivation, indicating a dampened SOCE response that was of shortened duration.

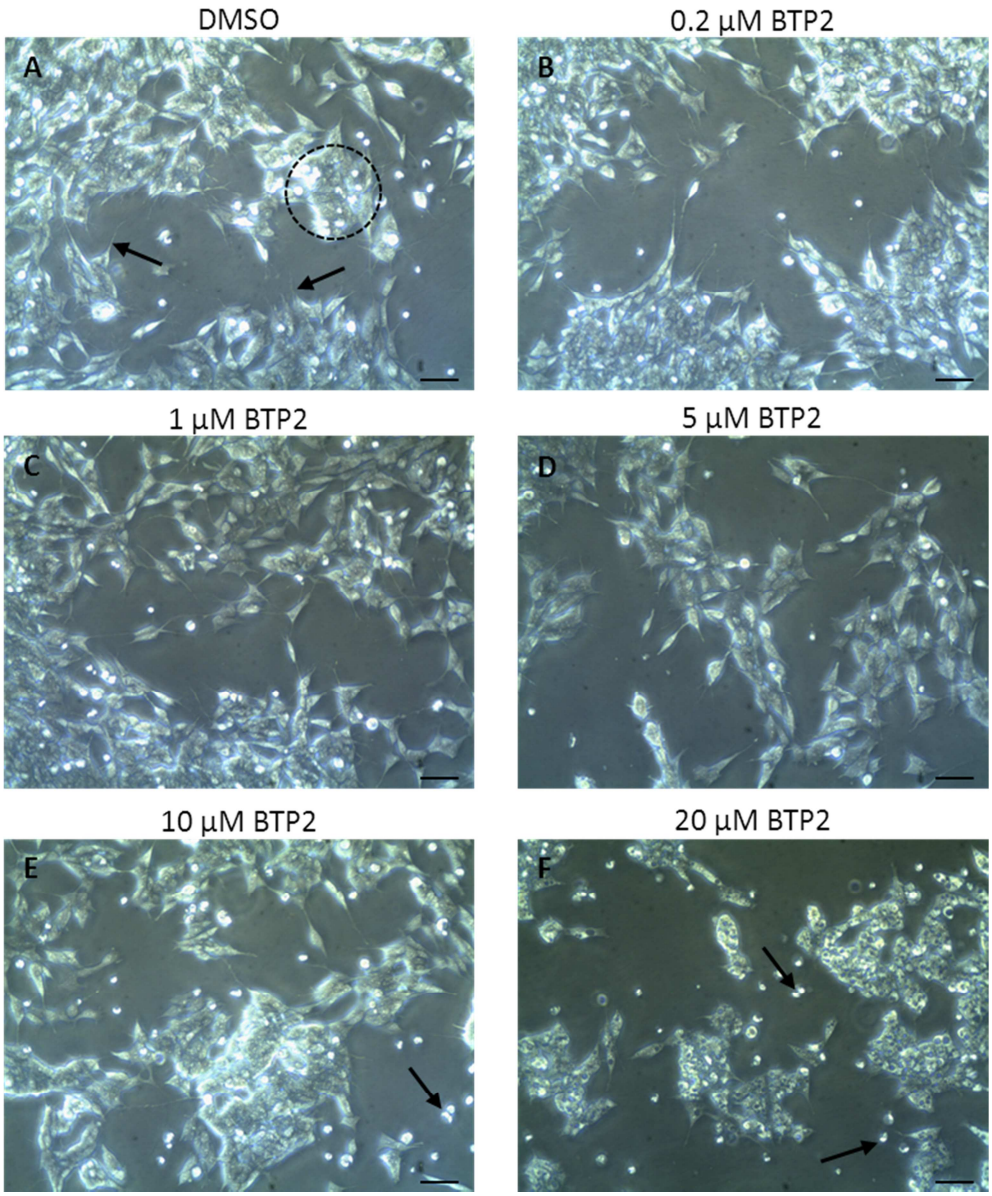

Figure A.i. BTP2 does not affect N-type population morphology at low concentrations but induces cell death at higher concentrations

N-type populations were treated for 24 hours with various concentrations of BTP2 (0.1-20µM) or DMSO as a loading control. **(A)** DMSO treated N-type cells possess short neurite-like processes (arrows), and can grow to form aggregates (dashed circle). **(B-D)** N-type cells treated with 0.1 - 5 µM BTP2 grow in a similar manner to DMSO treated cells. **(E)** At a concentration of 10 µM BTP2, N-type cells show reduced cellular integrity and increased cell death as observed by an increase in floating cell debris (black arrows). **(F)** At a concentration of 20 µM BTP2, all cells are dead (arrows) or dying.

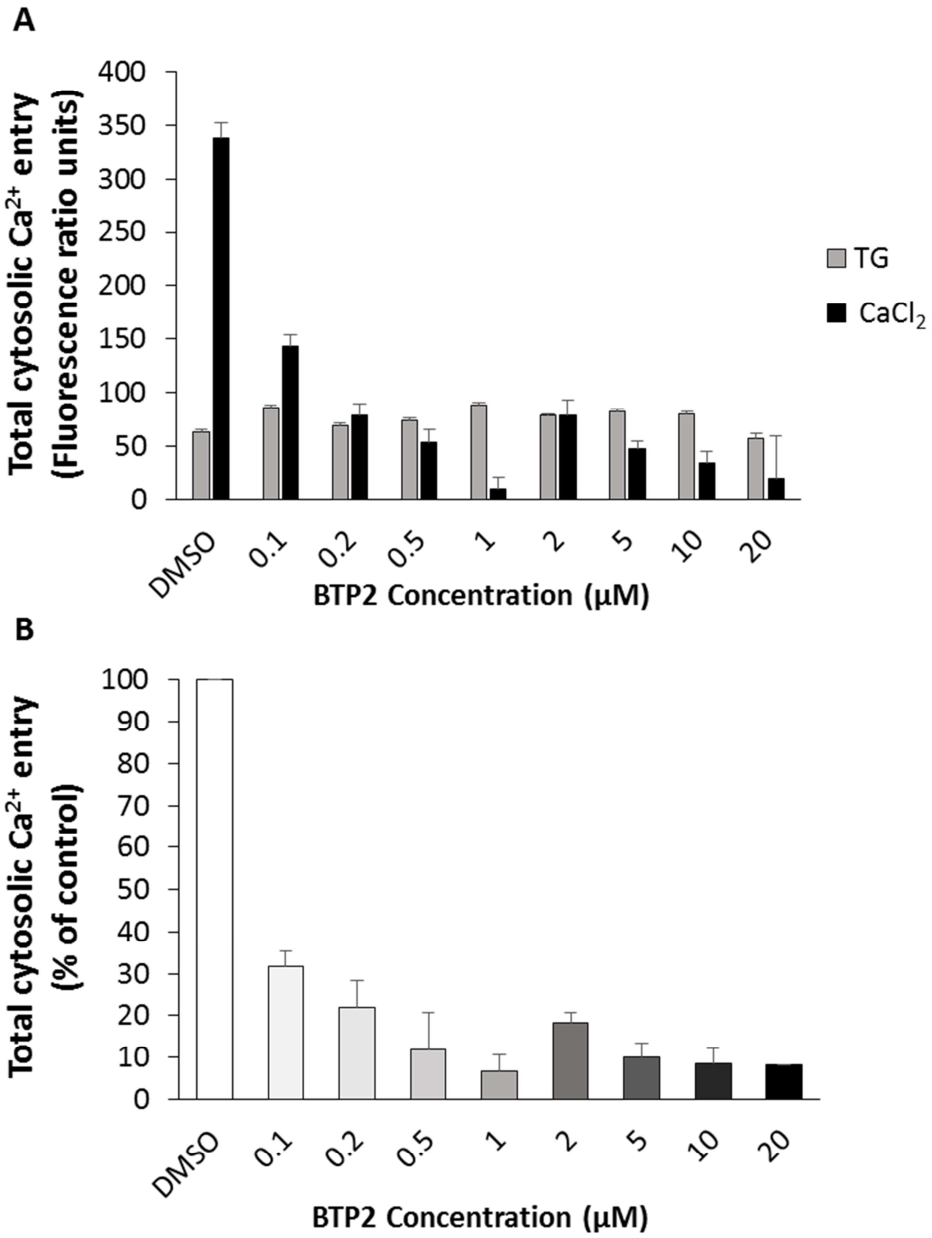

Figure A.ii. BTP2 drastically inhibits SOCE at low concentrations

N-type populations were treated for 24 hours with a range of concentrations of BTP (0.1 µM to 20 µM) or DMSO as a control. Changes in fluorescence ratio units (FRUs) are reflective of changes in $[Ca^{2+}]_i$ following addition of thapsigargin (TG) indicating Ca^{2+} store release and subsequent Ca^{2+}-addback ($CaCl_2$) indicating SOCE to replenish depleted stores. **(A)** DMSO (TG control) measurements were deducted from the experimental data. Compared to DMSO treatment, there was a significant effect of BTP2 treatment on total Ca^{2+} store release ($P<0.0001$) and total SOCE ($P<0.00001$). Cells treated with 0.1 µM BTP2 had a significant increase in total Ca^{2+} store release by

36.58% compared to DMSO treated cells (85.86 ± 1.82 and 62.87 ± 1.77 FRUs, respectively, P<0.0001****). Taking this change in store release into account, total SOCE ($CaCl_2$) was reduced by 68.90% in cells treated with 0.1 µM BTP2 compared to DMSO treated cells (143.41 ± 9.82 and 337.57 ± 14.60 FRUs, respectively). There was no significant difference in total Ca^{2+} store release between cells treated with 0.2 µM BTP2 (68.90 ± 2.52 FRUs) and DMSO treated cells (P=0.515) and total SOCE (78.76 ± 10.11 FRUs) was reduced by 78.71% (P<0.0001****). Cells treated with 0.5 µM BTP2 had a significant increase in total Ca^{2+} store release (73.36 ± 2.12 FRUs) by 16.70% compared to DMSO treated cells (P=0.005**) and total SOCE (53.06 ± 11.84 FRUs) was reduced by 86.53%. Cells treated with 1 µM BTP2 had a significant increase in total Ca^{2+} store release (88.25 ± 1.71 FRUs) by 40.38% compared to DMSO treated cells (P<0.0001****) and total SOCE (10.11 ± 10.36 FRUs) was reduced by 97.87%. Cells treated with 2 µM BTP2 had a significant increase in total Ca^{2+} store release (77.93 ± 1.82 FRUs) by 23.97% compared to DMSO treated cells (P<0.0001****) and total SOCE (78.34 ± 13.87 FRUs) was reduced by 81.28%. Cells treated with 5 µM BTP2 had a significant increase in total Ca^{2+} store release (82.38 ± 2.02 FRUs) by 31.04% compared to DMSO treated cells (P<0.0001****) and total SOCE (47.15 ± 7.25 FRUs) was reduced by 89.34%. Cells treated with 10 µM BTP2 had a significant increase in total Ca^{2+} store release (79.71 ± 2.56 FRUs) by 26.79% compared to DMSO treated cells (P<0.0001****) and total SOCE (34.43 ± 10.58 FRUs) was reduced by 91.96%. There was no significant difference in total Ca^{2+} store release between cells treated with 20 µM BTP2 (56.49 ± 4.72 FRUs) and DMSO treated cells (P=0.994) and total SOCE (19.74 ± 39.58 FRUs) was reduced by 93.49% (P<0.0001****). **(B)** The following percentages compare the average total SOCE of each BTP2 treated population with the average of DMSO populations taken to be 100%. Total SOCE was down-regulated by 68.24% at 0.1 µM BTP2, 77.96% at 0.2 µM BTP2, 88.19% at 0.5 µM BTP2, 93.19% at 1 µM BTP2, 81.70% at 2 µM BTP2, 89.95% at 5 µM BTP2, 91.47% at 10 µM BTP2 and 91.78% at 20 µM BTP2.

For DMSO n=539, 0.1 µM BTP2 n=339, 0.2 µM BTP2 n=191, 0.5 µM BTP2 n=234, 1 µM BTP2 n=336, 2 µM BTP2 n=270, 5 µM BTP2 n=295, 10 µM BTP2 n=221 and 20 µM BTP2 n=24. N≥3 except 20 µM BTP2 N=1.

A

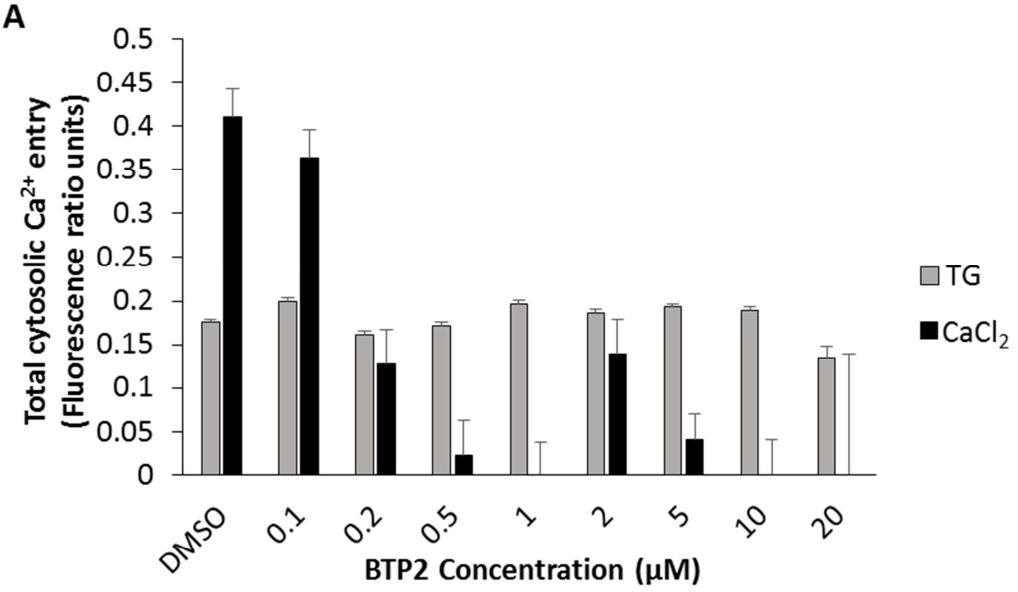

B

Rate of Rise (x 10^{-4} FRUs)									
		Concentration of BTP2 (µM)							
	DMSO	0.1	0.2	0.5	1	2	5	10	20
TG	11.61 ± 0.21	9.39 ± 0.21	9.25 ± 1.02	8.93 ± 0.27	9.02 ± 0.19	11.10 ± 0.21	11.50 ± 0.29	12.12 ± 0.30	6.24 ± 0.61
$CaCl_2$	100.91 ± 6.88	114.34 ± 7.90	42.15 ± 6.28	81.25 ± 9.18	48.49 ± 5.94	63.34 ± 5.31	34.66 ± 5.06	67.61 ± 7.95	148.65 ± 31.59

C

Rate of Decline (x 10^{-4} FRUs)									
		Concentration of BTP2 (µM)							
	DMSO	0.1	0.2	0.5	1	2	5	10	20
TG	2.79 ± 0.03	2.75 ± 0.04	2.20 ± 0.06	2.39 ± 0.05	2.68 ± 0.05	2.56 ± 0.04	2.50 ± 0.04	2.71 ± 0.06	1.92 ± 0.23
Total $CaCl_2$	3.31 ± 0.10	3.47 ± 0.17	2.11 ± 0.06	2.00 ± 0.16	1.42 ± 0.13	2.64 ± 0.17	1.05 ± 0.11	1.70 ± 0.16	2.85 ± 0.53
Initial $CaCl_2$	4.77 ± 0.28	10.18 ± 0.47	5.28 ± 0.47	6.22 ± 0.46	3.95 ± 0.35	7.31 ± 0.44	4.12 ± 0.31	5.18 ± 0.45	6.36 ± 1.17
Late $CaCl_2$	2.74 ± 0.08	0.79 ± 0.08	0.91 ± 0.11	0.54 ± 0.08	0.47 ± 0.06	0.88 ± 0.11	0.29 ± 0.04	0.36 ± 0.05	1.43 ± 0.36

Figure A.iii. BTP2 drastically alters SOCE dynamics at low concentrations

N-type populations were treated for 24 hours with a range of concentrations of BTP (0.1 µM to 20 µM) or DMSO as a control. Changes in fluorescence ratio units (FRUs) are reflective of changes in $[Ca^{2+}]_i$ following addition of thapsigargin (TG) indicating Ca^{2+} store release and subsequent Ca^{2+}-addback ($CaCl_2$) indicating SOCE to replenish depleted stores. **(A)** DMSO (TG control) measurements were deducted from the experimental data. Compared to DMSO treatment, there was a significant effect of BTP2 treatment on maximal Ca^{2+} store release ($P<0.0001$) and maximal SOCE ($P<0.00001$). Cells treated with 0.1 µM BTP2 had a significant 13.7% increase in maximal Ca^{2+} store release (TG) compared to DMSO treated cells (0.20 ± 0.004 and 0.18 ± 0.003 FRUs, respectively, $P<0.0001$****). Taking this change in store release into account, maximal SOCE ($CaCl_2$) was reduced by 22.06% in cells treated with 0.1

μM BTP2 compared to DMSO treated cells (0.36 ± 0.03 and 0.41 ± 0.03 FRUs, respectively). There was no significant difference in maximal Ca^{2+} store release between cells treated with 0.2 μM BTP2 (0.16 ± 0.005 FRUs) and DMSO treated cells (P=0.187) and maximal SOCE (0.13 ± 0.04 FRUs) was reduced by 66.01% (P<0.0001****). There was no significant difference in maximal Ca^{2+} store release between cells treated with 0.5 μM BTP2 (0.17 ± 0.005 FRUs) and DMSO treated cells (P=0.997) and maximal SOCE (0.02 ± 0.04 FRUs) was reduced by 94.57% (P<0.0001****). Maximal Ca^{2+} store release was increased by 11.93% in cells treated with 1 μM BTP2 (0.20 ± 0.004 FRUs) compared to DMSO treated cells (P=0.0003***) and maximal SOCE was completely abolished (P<0.0001****). There was no significant difference in maximal Ca^{2+} store release between cells treated with 2 μM BTP2 (0.19 ± 0.004 FRUs) and DMSO treated cells (P=0.449) and maximal SOCE (0.14 ± 0.04 FRUs) was reduced by 68.12% (P<0.0001****). Maximal Ca^{2+} store release was increased by 9.96% in cells treated with 5 μM BTP2 (0.19 ± 0.004 FRUs) compared to DMSO treated cells (P=0.011*) and maximal SOCE (0.04 ± 0.03 FRUs) was reduced by 91.04%. There was no significant difference in maximal Ca^{2+} store release between cells treated with 10 μM BTP2 (0.19 ± 0.005 FRUs) and DMSO treated cells (P=0.338) and maximal SOCE was completely abolished (P<0.0001****). There was no significant difference in maximal Ca^{2+} store release between cells treated with 20 μM BTP2 (0.13 ± 0.01 FRUs) and DMSO treated cells (P=0.088) and maximal SOCE was completely abolished (P=0.067). **(B)** Compared to DMSO treatment, there was a significant effect of BTP2 treatment on rate of Ca^{2+} store release (P<0.0001) and rate of SOCE (P<0.00001). The following are comparisons to DMSO treated cells. There was a significant decrease in rate of Ca^{2+} store release in cells treated with 0.1, 0.2, 0.5, 1 and 20 μM BTP2 (all P<0.0001) and no significant difference in cells treated with 2, 5 and 10 μM BTP2 (P=0.951, P>0.999 and P=0.972, respectively). There was a significant decrease in rate of SOCE in cells treated with 0.2, 1 and 5 μM BTP2 (all P<0.0001) and 2 and 10 μM BTP2 (P=0.002 and P=0.026, respectively). There was a non-significant decrease in rate of SOCE in cells treated with 0.5 M BTP2 (P=0.549) and a non-significant increase in rate of SOCE in cells treated with 0.1 and 20 μM BTP2 (P=0.838 and P=0.672, respectively). **(C)** Compared to DMSO treatment, there was a significant effect of BTP2 treatment on rate of decline of Ca^{2+} store release (P<0.0001), total SOCE (P<0.00001),

initial SOCE (P<0.00001) and late SOCE (P<0.00001). The following are comparisons to DMSO treated cells. There was a significant reduction in rate of decline of Ca^{2+} store release in cells treated with 0.2, 0.5, 5, and 20 µM BTP2 (all P<0.0001) and 2 µM BTP2 (P=0.002) and all other rates were non-significantly decreased. There was a significant reduction in rate of decline of SOCE in cells treated with 0.2, 0.5, 1, 5, and 10 µM BTP2 (all P<0.0001) and 2 µM BTP2 (P=0.009) and all other rates were not significantly altered. There was a significant increase in rate of decline of initial SOCE in cells treated with 0.1 and 2 µM BTP2 (both P<0.0001) whilst 0.2, 0.5, 10 and 20 µM BTP2 were non-significantly decreased and 1 and 5 µM BTP2 were non-significantly increased. There was a significant reduction in rate of decline of late SOCE in cells treated with all concentrations of BTP2 (all P<0.0001).

For DMSO n=539, 0.1 µM BTP2 n=339, 0.2 µM BTP2 n=191, 0.5 µM BTP2 n=234, 1 µM BTP2 n=336, 2 µM BTP2 n=270, 5 µM BTP2 n=295, 10 µM BTP2 n=221 and 20 µM BTP2 n=24. N≥3 except 20 µM BTP2 N=1.

Discussion

BTP2 (*N*-[4-[3,5-Bis(trifluoromethyl)pyrazol-1-yl]-4-methyl-1,2,3-thiadiazole-5-carboxamide) has been extensively utilised to investigate Ca^{2+} entry and inhibition (Zitt 2004; He 2005; Takezawa 2006; Ohga 2008; Law 2011; Schleifer 2012; Liu 2015). BTP2 has been shown to inhibit SOCE in sinoatrial node cells (Liu 2015), HEK293 cells (He 2005; Schleifer 2012), T cells (Zitt 2004; Takezawa 2006; Ohga 2008), DT40 B cells and A7r5 smooth muscle cells (He 2005). In this study, exposure to BTP2 for 24 hours induced a dose-dependent uncoupling of Ca^{2+} store release and SOCE in N-type populations that was evident in concentrations as low as 100 nM with a maximal inhibitory effect at 1 µM. BTP2 did not affect N-type cell morphology but did reduce cell viability and induce extensive cell death at concentrations above 10 µM.

Inhibition of Ca^{2+} entry by BTP2 is not solely SOCE specific and, whilst there are many agents that offer non-selective inhibition of SOCE (Putney 2001), there are currently no means for exclusive SOCE inhibition as other Ca^{2+} entry pathways may also be affected. However, whilst there is an inhibitory effect of BTP2 on ROCE, potency for SOCE inhibition has been found to be 7-fold greater than that of ROCE inhibition and direct inhibition of STIM1-Orai1-mediated CRAC currents was confirmed in HEK293 cells (Schleifer 2012). BTP2 specifically inhibited SOCE at low nanomolar concentrations (IC_{50} ~10 nM) in T cells with no effect on other SOCE-related pathways including ER Ca^{2+} store release, Ca^{2+} pumps, mitochondrial Ca^{2+} or K^+ channels (Zitt 2004). BTP2 was also found to reduce I_{CRAC} in Jurkat T cells and did not significantly affect K^+ or Cl^- channel activity (Takezawa 2006). Similarly, the imidazole compound SKF-96395 has been shown to inhibit SOCE through STIM1-Orai1 interactions (Putney 2001) and it was found that STIM1 overexpression in sinoatrial node cells caused an increase in SOCE that was almost completely inhibited by SKF-96395 (Liou 2005). Likewise, BTP2 inhibited SOCE in sinoatrial node cells in a similar manner to SKF-96395 (Liu 2015), suggesting that BTP2 may function through STIM1-Orai1 inhibition however, the mechanisms by which BTP2 exerts inhibition on the SOCE pathway is unclear. The trifluoromethyl group at the C3 position was found to be critical for BTP2 activity (Law 2011). It has also been suggested that the underlying mechanism by which BTP2 acts in lymphocytes is via TRPM4 interaction whereby Ca^{2+} acts on TRPM4 which regulates

Ca^{2+} signals through depolarisation of lymphocytes thereby reducing Ca^{2+} influx which is promoted by BTP2 (Takezawa 2006). BTP2 treatment of lymphocytes enhanced TRPM4 activity in a dose-dependent manner, however, this only occurred at low nanomolar concentrations and I_{CRAC} was blocked only at concentrations over 100-fold higher and it was concluded that BTP2 seemed to be the most potent and selective I_{CRAC} inhibitor of those investigated (Takezawa 2006).

Overall, the results from the discussed investigations and the effect of BTP2 on SOCE found here potentially demonstrate that the results from this study involving a down-regulation of SOCE observed with 9*c*RA-induced differentiation are likely due to changes in the SOCE-associated proteins STIM1 and Orai1.

II: RNA sequencing

STIM1 and Orai1 protein expression was down-regulated with differentiation of N-type populations, which may be caused by a change in gene expression. RNA from proliferating and differentiating N-type populations was sequenced under a collaboration with Professor Caroline Austin and Lauren Harkin. Preliminary RNAseq data is presented.

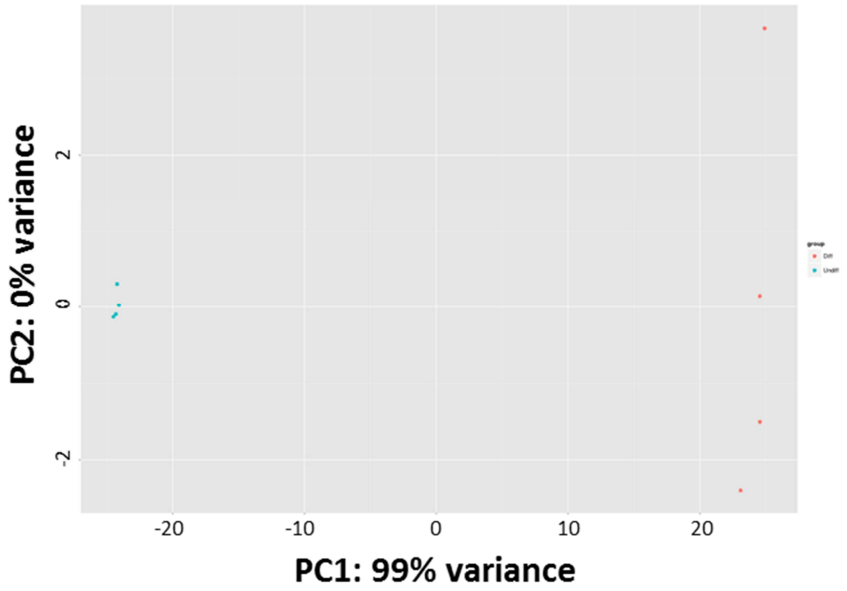

Figure A.iv. Overall gene expression is significantly altered with 9cRA-induced differentiation of N-type populations

PCA plot of normalised read counts for mapped to all genes expressed between proliferating N-type populations (blue, Undiff) and differentiating N-type populations (red, Diff). N=4 for each dataset.

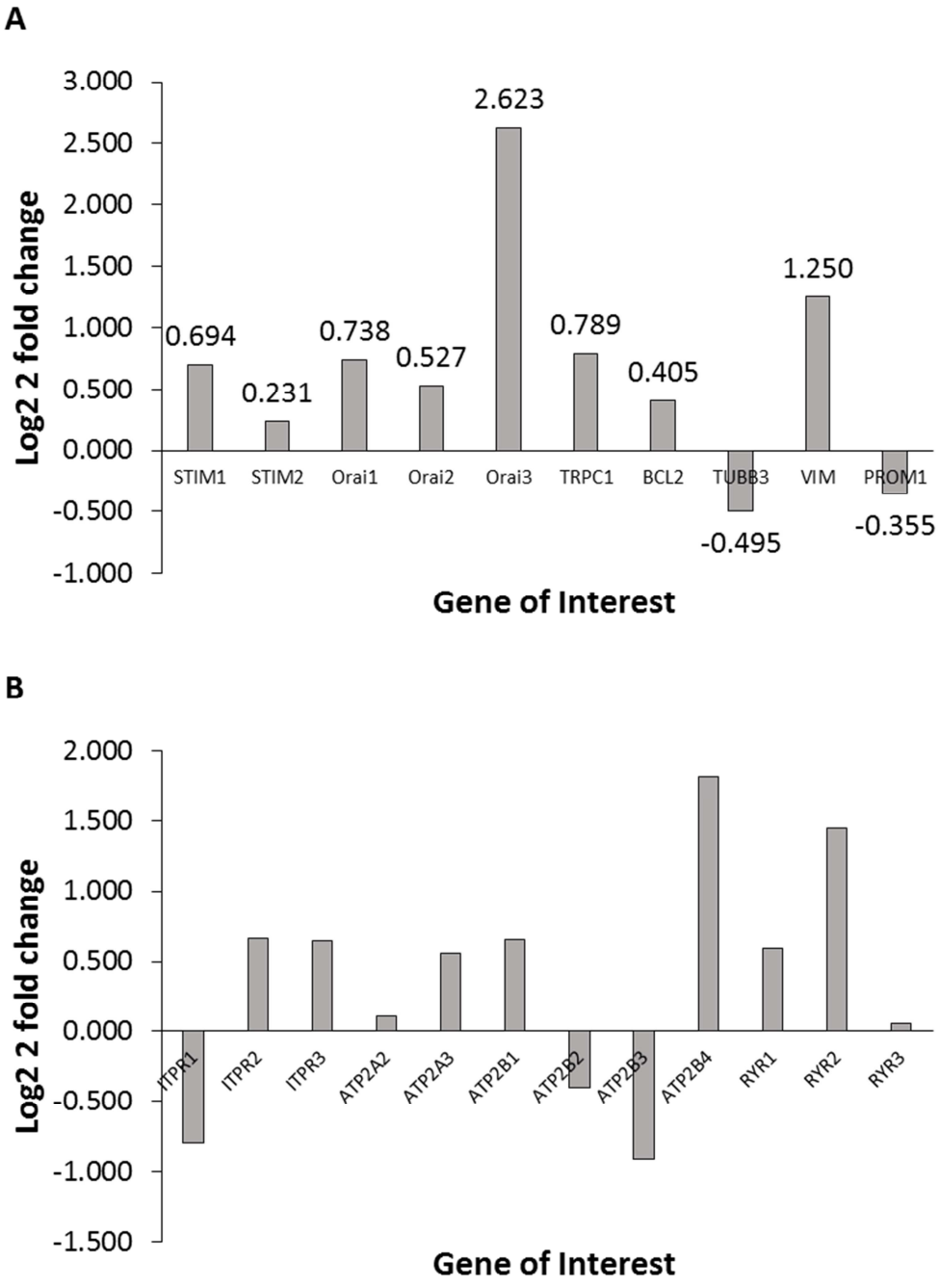

Figure A.v. Calcium signalling genes have significantly altered expression with 9cRA-induced differentiation of N-type populations

Log2 2 fold change in expression of genes of interest using DESeq analysis. All genes shown were significantly up- or down-regulated with adjusted P≤0.001. However, FDR was >0.05.

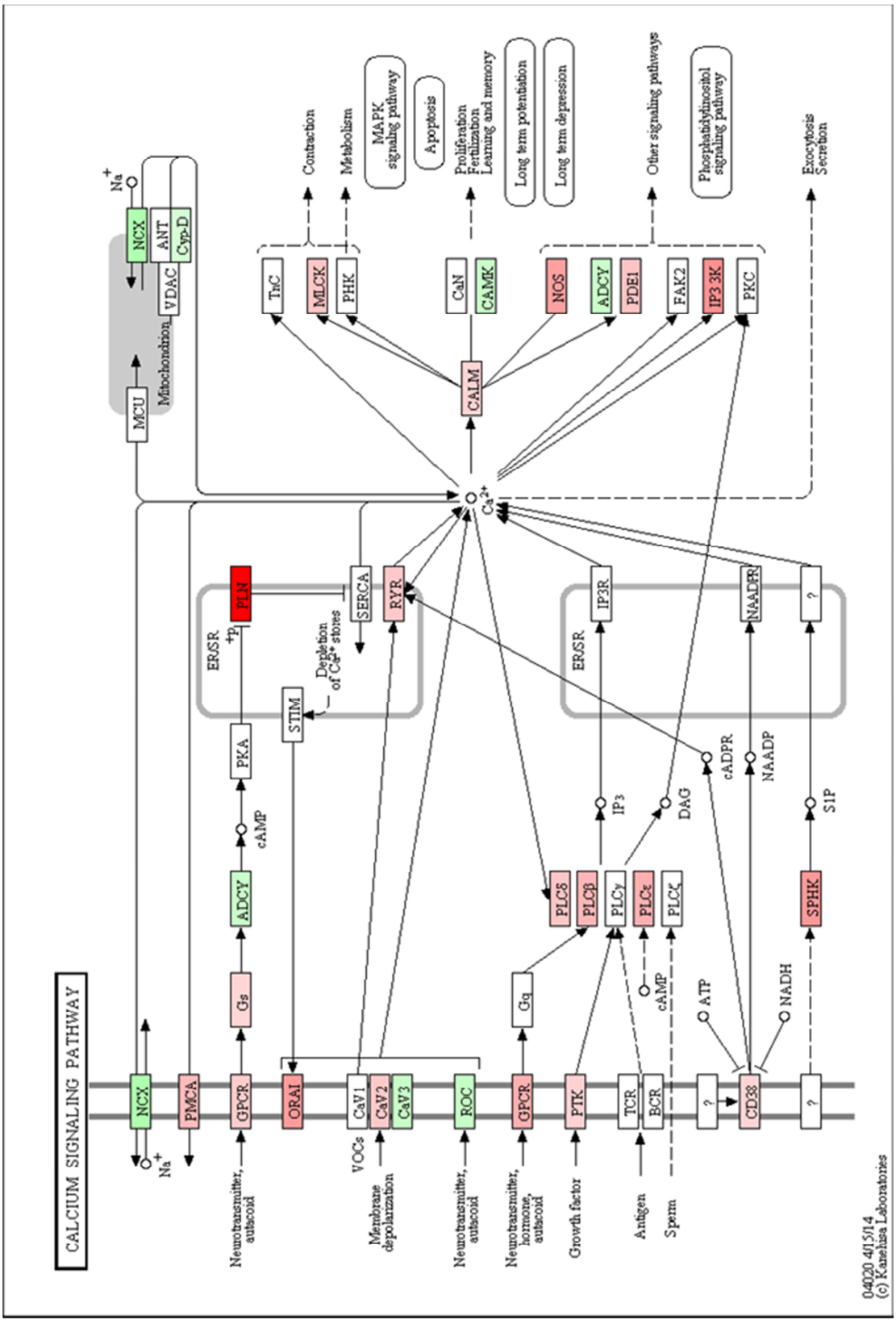
CALCIUM SIGNALING PATHWAY
Na+
NCX
ANT
Cyp-D
VDAC
Mitochondrion
MCU
Contraction
Metabolism
MAPK signaling pathway
Apoptosis
Proliferation Fertilization Learning and memory
Long term potentiation
Long term depression
Other signaling pathways
Phosphatidylinositol signaling pathway
Exocytosis Secretion
TnC
MLCK
PHK
CaN
CAMK
NOS
ADCY
PDE1
FAK2
IP3 3K
PKC
CALM
Ca2+
PLN
SERCA
RYR
ERSR
Depletion of Ca2+ stores
STIM
PKA
cAMP
IP3R
NAADPR
cADPR
NAADP
IP3
DAG
S1P
PLCδ
PLCβ
PLCγ
PLCε
PLCζ
SPHK
Gs
Gq
ATP
NADH
NCX
PMCA
GPCR
ORAI
CaV1
CaV2
CaV3
ROC
GPCR
PTK
TCR
BCR
?
CD38
?
Neurotransmitter, autacoid
VOCs
Membrane depolarization
Neurotransmitter, autacoid
Neurotransmitter, hormone, autacoid
Growth factor
Antigen
Sperm
04020 4/15/14
(c) Kanehisa Laboratories

Figure A.vi. Differential gene expression in the calcium signalling pathway with differentiation of N-type populations

Ingenuity Pathway Analysis (IPA) of changes in gene expression with differentiation of N-type populations. Red spectrum colouring represents an up-regulation in expression. Blue spectrum colouring represents a down-regulation in expression. Darker colours represent greater expression changes. White represents no significant change.

Chapter 9: Bibliography

Abdullaev, I.F., Bisaillon, J.M., Potier, M., Gonzalez, J.C., Motiani, R.K. & Trebak, M., 2008. Stim1 and orai1 mediate crac currents and store-operated calcium entry important for endothelial cell proliferation. *Circulation Research*, 103(11), pp.1289–1299.

Abeele, F. Vanden, Skryma, R., Shuba, Y., Van Coppenolle, F., Slomianny, C., Roudbaraki, M., Mauroy, B., Wuytack, F. & Prevarskaya, N., 2002. Bcl-2-dependent modulation of Ca2+ homeostasis and store-operated channels in prostate cancer cells. *Cancer Cell*, 1(2), pp.169–179.

Abemayor, E. & Sidell, N., 1989. Human neuroblastoma cell lines as models for the in vitro study of neoplastic and neuronal cell differentiation. *Environmental Health Perspectives*, 80, pp.3–15.

Acosta, S., Lavarino, C., Paris, R., Garcia, I., de Torres, C., Rodriguez, E., Beleta, H. & Mora, J., 2009. Comprehensive characterization of neuroblastoma cell line subtypes reveals bilineage potential similar to neural crest stem cells. *BMC Developmental Biology*, 9(1), p.12.

Agholme, L., Lindstrom, T., Kagedal, K., Mercusson, J. & Hallbeck, M., 2010. An In Vitro Model for Neuroscience: Differentiation of SH-SY5Y Cells into Cells with Morphological and Biochemical Characteristics of Mature Neurons. *Journal of Alzheimer's Disease*, 20(4), pp.1069–1082.

Alicia, S., Angélica, Z., Carlos, S., Alfonso, S. & Vaca, L., 2008. STIM1 converts TRPC1 from a receptor-operated to a store-operated channel: Moving TRPC1 in and out of lipid rafts. *Cell Calcium*, 44(5), pp.479–491.

Allenby, G., Bocquel, M.T., Saunders, M., Kazmer, S., Speck, J., Rosenberger, M., Lovey, a, Kastner, P., Grippo, J.F. & Chambon, P., 1993. Retinoic acid receptors and retinoid X receptors: interactions with endogenous retinoic acids. *Proceedings of*

the National Academy of Sciences of the United States of America, 90(1), pp.30–34.

Ambros, I.M., Zellner, A., Roald, B., Amann, G., Ladenstein, R., Printz, D., Gadner, H. & Ambros, P.F., 1996. Role of Ploidy, Chromosome 1p, and Schwann Cells in the Maturation of Neuroblastoma. *New England Journal of Medicine*, 334(23), pp.1505–1511.

Armstrong, J.L., Martin, S., Illingworth, N.A., Jamieson, D., Neilson, A., Lovat, P.E., Redfern, C.P.F. & Veal, G.J., 2012. The impact of retinoic acid treatment on the sensitivity of neuroblastoma cells to fenretinide. *Oncology Reports*, 27, pp.293–298.

Aubart, F.C., Sassi, Y., Coulombe, A., Mougenot, N., Vrignaud, C., Leprince, P., Lechat, P., Lompré, A.-M. & Hulot, J.-S., 2009. RNA interference targeting STIM1 suppresses vascular smooth muscle cell proliferation and neointima formation in the rat. *Molecular therapy : the journal of the American Society of Gene Therapy*, 17(3), pp.455–462.

Barletta, E., Mugnai, G. & Ruggieri, S., 1997. Inverse relationship between invasiveness and differentiative capacity in different human neuroblastoma cell lines. *International Journal of Cancer*, 70(5), pp.556–560.

Bell, E., Ponthan, F., Westermann, F., Whitworth, C., Thomas, H. & Redfern, C.P.F., 2013. Cell survival signalling through PPAR[delta] in neuroblastoma. *PLoS One*, 8(7), p.e68859.

Bell, N., 2011. Calcium signalling and differentiation in neuroblastoma cells. *PhD Thesis from the Institute for Cell and Molecular Biosciences*.

Bell, N., Hann, V., Redfern, C.P.F. & Cheek, T.R., 2013. Store-operated Ca2+ entry in proliferating and retinoic acid-differentiated N- and S-type neuroblastoma cells. *Biochimica et Biophysica Acta*, 1833, pp.643–651.

Bernal, S., Thompson, R., Gilbert, F. & Baylin, S.B., 1983. In Vitro and in Vivo Growth Characteristics of Two Different Cell Populations in an Established Line of Human Neuroblastoma. *Cancer Research*, 43(3), pp.1256–1260.

Berridge, M.J., 2010. Calcium hypothesis of Alzheimer's disease. *European Journal of Physiology*, 459(441-449).

Berridge, M.J., 1998. Neuronal Calcium Signaling. *Neuron*, 21, pp.13–26.

Berridge, M.J., Bootman, M.D. & Lipp, P., 1998. Calcium - a life and death signal. *Nature*, 395, pp.645–648.

Berridge, M.J., Lipp, P. & Bootman, M.D., 2000. The versatility and universality of calcium signalling. *Nature Reviews Molecular Cell Biology*, 1, pp.11–21.

Biagiotti, T., D'Amico, M., Marzi, I., Gennaro, P. Di, Arcangeli, A., Wanke, E. & Olivotto, M., 2006. Cell Renewing in Neuroblastoma: Electrophysiological and Immunocytochemical Characterization of Stem Cells and Derivatives. *Stem Cells*, 24, pp.443–453.

Biedler, J.L., Helson, L. & Spengler, B.A., 1973. Morphology and Growth, Tumorigenicity, and Cytogenetics of Human Neuroblastoma Cells in Continuous Culture. *Cancer Research*, 33(11), pp.2643–2652.

Biedler, J.L., Spengler, B.A. & Lyser, K.M., 1975. Morphological interconversion of human neuroblastoma cells. *In Vitro*, 10, p.380.

Bogeski, I., Kilch, T. & Niemeyer, B. a, 2012. ROS and SOCE: recent advances and controversies in the regulation of STIM and Orai. *The Journal of physiology*, 590(Pt 17), pp.4193–200.

Bojarski, L., Pomorski, P., Szybinska, A., Drab, M., Skibinska-Kijek, A., Gruszczynska-Biegala, J. & Kuznicki, J., 2009. Presenilin-dependent expression of STIM proteins and dysregulation of capacitative Ca2+ entry in familial Alzheimer's disease. *Biochimica et Biophysica Acta - Molecular Cell Research*, 1793(6), pp.1050–1057.

Bootman, M.D., Collins, T.J., Peppiatt, C.M., Prothero, L.S., MacKenzie, L., De Smet, P., Travers, M., Tovey, S.C., Seo, J.T., Berridge, M.J., Ciccolini, F. & Lipp, P., 2001. Calcium signalling-an overview. *Seminars in cell & developmental biology*, 12(1), pp.3–10.

Bourdeaut, F., Ribeiro, A., Paris, R., Pierron, G., Couturier, J., Peuchmaur, M. & Delattre, O., 2008. In neuroblastic tumours, Schwann cells do not harbour the genetic alterations of neuroblasts but may nevertheless share the same clonal origin. *Oncogene*, 27(21), pp.3066–3071.

Boyne, L.J., Fischer, I. & Shea, T.B., 1996. Role of vimentin in early stages of neuritogenesis in cultured hippocampal neurons. *International Journal of Developmental Neuroscience*, 14(6), pp.739–748.

Brandman, O., Liou, J., Park, W.S. & Meyer, T., 2007. STIM2 is a feedback regulator that stabilises basal cytosolic and endoplasmic reticulum Ca2+ levels. , 131(7), pp.1327–1339.

Brill, L.B. & Bennett, J.P., 2003. Dependence on electron transport chain function and intracellular signaling of genomic responses in SH-SY5Y cells to the mitochondrial neurotoxin MPP+. *Experimental Neurology*, 181(1), pp.25–38.

Brown, A.M., Riddoch, F.C., Robson, A., Redfern, C.P.F. & Cheek, T.R., 2005. Mechanistic and functional changes in Ca2+ entry after retinoic acid-induced differentiation of neuroblastoma cells. *Biochemical Journal*, 388, pp.941–948.

Cai, S., Fatherazi, S., Presland, R.B., Belton, C.M., Roberts, F.A., Goodwin, P.C., Schubert, M.M. & Izutsu, K.T., 2006. Evidence that TRPC1 contributes to calcium-induced differentiation of human keratinocytes. *Pflugers Archiv : European journal of physiology*, 452(1), pp.43–52.

Calì, T., Ottolini, D. & Brini, M., 2014. Calcium signaling in Parkinson's disease. *Cell and Tissue Research*, 357(2), pp.439–454.

Cancer Research UK, 2014. Childhood cancer incidence statistics. *http://www.cancerresearchuk.org/health-professional/cancer-statistics/childrens-cancers/incidence#undefined*, p.Accessed 22/09/2015.

Carafoli, E., 1987. Intracellular calcium homeostasis. *Annual Review of Biochemistry*, 56, pp.395–433.

Carmignoto, G., Pasti, L. & Pozzan, T., 1998. On the role of voltage-dependent calcium channels in calcium signaling of astrocytes in situ. *The Journal of neuroscience : the official journal of the Society for Neuroscience*, 18(12), pp.4637–4645.

Chambon, P., 1996. A decade of molecular biology of retinoic acid receptors. *FASEB journal : official publication of the Federation of American Societies for Experimental Biology*, 10, pp.940–54.

Chen, Y.-T.Y.-F., Chen, T.-T., Chiu, W.-T., Shen, M.-R., Chen, Y.-T.Y.-F., Chiu, W.-T. & Shen, M.-R., 2013. Remodeling of calcium signaling in tumor progression. *Journal of Biomedical science*, 20(23).

Cheung, Y.T., Lau, W.K.W., Yu, M.S., Lai, C.S.W., Yeung, S.C., So, K.F. & Chang, R.C.C., 2009. Effects of all-trans-retinoic acid on human SH-SY5Y neuroblastoma as in vitro model in neurotoxicity research. *NeuroToxicology*, 30(1), pp.127–135.

Ciccarone, V., Spengler, B.A., Meyers, M.B., Biedler, J.L. & Ross, R.A., 1989. Phenotypic Diversification in Human Neuroblastoma Cells: Expression of Distinct Neural Crest Lineages. *Cancer Research*, 49(1), pp.219–225.

Cimmino, F., Pezone, L., Avitabile, M., Acierno, G., Andolfo, I., Capasso, M. & Iolascon, A., 2015. Inhibition of hypoxia inducible factors combined with all-trans retinoic acid treatment enhances glial transdifferentiation of neuroblastoma cells. *Scientific Reports*, 5(May), p.11158.

Coco, S., Defferrari, R., Scaruffi, P., Cavazzana, A., Di Cristofano, C., Longo, L., Mazzocco, K., Perri, P., Gambini, C., Moretti, S., Bonassi, S. & Tonini, G.P., 2005. Genome analysis and gene expression profiling of neuroblastoma and

ganglioneuroblastoma reveal differences between neuroblastic and Schwannian stromal cells. *Journal of Pathology*, 207(3), pp.346–357.

Collins, A.T., Berry, P.A., Hyde, C., Stower, M.J. & Maitland, N.J., 2005. Prospective identification of tumorigenic prostate cancer stem cells. *Cancer research*, 65(23), pp.10946–10951.

Constantinescu, R., Constantinescu, A.T., Reichmann, H. & Janetzky, B., 2007. Neuronal differentiation and long-term culture of the human neuroblastoma line SH-SY5Y. *Journal of Neural Transmission*, 72, pp.17–28.

Courjaret, R. & Machaca, K., 2014. Mid-range Ca(2+) signalling mediated by functional coupling between store-operated Ca(2+) entry and IP3-dependent Ca(2+) release. *Nature communications*, 5(May), p.3916.

Darbellay, B., Arnaudeau, S., Bader, C.R., Konig, S. & Bernheim, L., 2011. STIM1L is a new actin-binding splice variant involved in fast repetitive Ca 2+ release. *Journal of Cell Biology*, 194(2), pp.335–346.

DeHaven, W.I., Jones, B.F., Petranka, J.G., Smyth, J.T., Tomita, T., Bird, G.S. & Jr, J.W.P., 2009. TRPC channels function independently of STIM1 and Orai1. *The Journal of Physiology*, 587(10), pp.2275–2298.

DeHaven, W.I., Smyth, J.T., Boyles, R.R. & Putney, J.W., 2007. Calcium inhibition and calcium potentiation of Orai1, Orai2, and Orai3 calcium release-activated calcium channels. *Journal of Biological Chemistry*, 282(24), pp.17548–17556.

Demuro, a., Penna, a., Safrina, O., Yeromin, a. V., Amcheslavsky, a., Cahalan, M.D. & Parker, I., 2011. Subunit stoichiometry of human Orai1 and Orai3 channels in closed and open states. *Proceedings of the National Academy of Sciences*, 108(43), pp.17832–17837.

Dráberová, E., Valle, L. Del, Gordon, J., Marková, V., Smejkalová, B., Bertrand, L., Chadarévian, J.P. de, Agamanolis, D.P., Legido, A., Khalili, K., Dráber, P. & Katsetos, C.D., 2008. Class III beta-tubulin is constitutively coexpressed with glial

fibrillary acidic protein and nestin in midgestational human fetal astrocytes: implications for phenotypic identity. *Journal of Neuropathology & Experimental Neurology*, 67(4), pp.341–354.

Dremina, E.S., Sharov, V.S., Kumar, K., Zaidi, A., Michaelis, E.K. & Schöneich, C., 2004. Anti-apoptotic protein Bcl-2 interacts with and destabilizes the sarcoplasmic/endoplasmic reticulum Ca2+-ATPase (SERCA). *The Biochemical journal*, 383, pp.361–370.

Dubey, M., Hoda, S., Chan, W.K.H., Pimenta, A., Ortiz, D.D. & Shea, T.B., 2004. Reexpression of vimentin in differentiated neuroblastoma cells enhances elongation of axonal neurites. *Journal of Neuroscience Research*, 78(2), pp.245–249.

Dwane, S., Durack, E. & Kiely, P. a, 2013. Optimising parameters for the differentiation of SH-SY5Y cells to study cell adhesion and cell migration. *BMC research notes*, 6(1), p.366.

Dziadek, M. a & Johnstone, L.S., 2007. Biochemical properties and cellular localisation of STIM proteins. *Cell calcium*, 42(2), pp.123–32.

Eckenrode, E.F., Yang, J., Velmurugan, G. V, Foskett, K. & White, C., 2010. Apoptosis protection by Mcl-1 and Bcl-2 modulation of inositol 1,4,5-trisphosphate receptor-dependent Ca2+ signaling. *The Journal of Biological Chemistry*, 285(18), pp.13678–13684.

Encinas, M., Iglesias, M., Liu, Y., Wang, H., Muhaisen, A., Cena, V., Gallego, C. & Comella, J.X., 2000. Sequential treatment of SH-SY5Y cells with retinoic acid and brain-derived neurotrophic factor gives rise to fully differentiated, neurotrophic factor-dependent, human neuron-like cells. *Journal of neurochemistry*, 75(3), pp.991–1003.

Feske, S., Gwack, Y., Prakriya, M., Srikanth, S., Puppel, S.-H., Tanasa, B., Hogan, P.G., Lewis, R.S., Daly, M. & Rao, A., 2006. A mutation in Orai1 causes immune deficiency by abrogating CRAC channel function. *Nature*, 441(7090), pp.179–185.

Fidler, I.J., 1978. Tumor Heterogeneity and the Biology of Cancer Invasion and Metastasis. *Cancer Research*, 38(9), pp.2651–2660.

Finklestein, J., Krailo, M., Lenarsky, C., Ladisch, S., Blair, G., Reynolds, C., Sitarz, A. & Hammond, G., 1992. 13-cis-retinoic acid (NSC 122758) in the treatment of children with metastatic neuroblastoma unresponsive to conventional chemotherapy: report from the Childrens Cancer Study Group. *Medical and Pediatric Oncology*, 20(4), pp.307–311.

Flourakis, M., Lehen'kyi, V., Beck, B., Raphaël, M., Vandenberghe, M., Abeele, F. V, Roudbaraki, M., Lepage, G., Mauroy, B., Romanin, C., Shuba, Y., Skryma, R. & Prevarskaya, N., 2010. Orai1 contributes to the establishment of an apoptosis-resistant phenotype in prostate cancer cells. *Cell death & disease*, 1, p.e75.

Foyouzi-Youssefi, R., Arnaudeau, S., Borner, C., Kelley, W.L., Tschopp, J., Lew, D.P., Demaurex, N. & Krause, K.H., 2000. Bcl-2 decreases the free Ca2+ concentration within the endoplasmic reticulum. *Proceedings of the National Academy of Sciences of the United States of America*, 97(11), pp.5723–5728.

Fukushima, M., Tomita, T., Janoshazi, A. & Putney, J.W., 2012. Alternative translation initiation gives rise to two isoforms of Orai1 with distinct plasma membrane mobilities. , pp.4354–4361.

Gaitonde, S. V, Qi, W., Falsey, R.R., Sidell, N. & Martinez, J.D., 2001. Morphologic conversion of a neuroblastoma-derived cell line by E6-mediated p53 degradation. *Cell growth & differentiation : the molecular biology journal of the American Association for Cancer Research*, 12(1), pp.19–27.

Galione, A., Morgan, A.J., Arredouani, A., Davis, L.C., Rietdorf, K., Ruas, M. & Parrington, J., 2010. NAADP as an intracellular messenger regulating lysosomal calcium-release channels. *Biochemical Society transactions*, 38(6), pp.1424–1431.

Gandhi, S., Wood-Kaczmar, A., Yao, Z., Plun-Favreau, H., Deas, E., Klupsch, K., Downward, J., Latchman, D.S., Tabrizi, S.J., Wood, N.W., Duchen, M.R. & Abramov, A.Y., 2009. PINK1-associated Pakinson's Disease is caused by neuronal vulnerability to calcium-induced cell death. *Molecular Cell*, 13(33), pp.627–638.

Gwack, Y., Srikanth, S., Feske, S., Cruz-Guilloty, F., Oh-hora, M., Neems, D.S., Hogan, P.G. & Rao, A., 2007. Biochemical and functional characterization of orai proteins. *Journal of Biological Chemistry*, 282(22), pp.16232–16243.

Han, G., Chang, B., Connor, M. & Sidell, N., 1995. Enhanced potency of 9-cis versus all-trans-retinoic acid to induce the differentiation of human neuroblastoma cells. *Differentiation*, 59(1), pp.61–69.

Hanada, M., Krajewski, S., Tanaka, S., Cazals-Hatem, D., Spengler, B.A., Ross, R.A., Biedler, J.L. & Reed, J.C., 1993. Regulation of Bcl-2 Oncoprotein Levels with Differentiation of Human Neuroblastoma Cells. *Cancer Research*, 53(20), pp.4978–4986.

Hao, B., Lu, Y., Wang, Q., Guo, W., Cheung, K.H. & Yue, J., 2014. Role of STIM1 in survival and neural differentiation of mouse embryonic stem cells independent of Orai1-mediated Ca2+ entry. *Stem Cell Research*, 12(2), pp.452–466.

He, L.P., Hewavitharana, T., Soboloff, J., Spassova, M. a. & Gill, D.L., 2005. A functional link between store-operated and TRPC channels revealed by the 3,5-bis(trifluoromethyl)pyrazole derivative, BTP2. *Journal of Biological Chemistry*, 280(12), pp.10997–11006.

Hero, B., Simon, T., Spitz, R., Ernestus, K., Gnekow, A.K., Scheel-Walter, H.-G., Schwabe, D., Schilling, F.H., Benz-Bohm, G. & Berthold, F., 2008. Localized Infant

Neuroblastomas Often Show Spontaneous Regression: Results of the Prospective Trials NB95-S and NB97. *Journal of Clinical Oncology* , 26 (9), pp.1504–1510.

Heyman, R.A., Mangelsdorf, D.J., Dyck, J.A., Stein, R.B., Eichele, G., Evans, R.M. & Thaller, C., 1992. 9-cis retinoic acid is a high affinity ligand for the retinoid X receptor. *Cell*, 68(2), pp.397–406.

Hodeify, R., Selvaraj, S., Wen, J., Arredouani, A., Hubrack, S., Dib, M., Al-Thani, S.N., McGraw, T. & Machaca, K., 2015. A STIM1-dependent “trafficking trap” mechanism regulates Orai1 plasma membrane residence and Ca2+ influx levels. *Journal of cell science*, pp.3143–3154.

Hong, J.H., Li, Q., Kim, M.S., Shin, D.M., Feske, S., Cheng, K.T., Ambudkar, I.S. & Muallem, S., 2011. Polarized but differential localization and recruitment of STIM1/Orai1 and STIM1/TRPC channels in secretory cells. *Traffic*, 12(2), pp.232–245.

Hoover, P.J. & Lewis, R.S., 2011. Stoichiometric requirements for trapping and gating of Ca2+ release-activated Ca2+ (CRAC) channels by stromal interaction molecule 1 (STIM1). *Proceedings of the National Academy of Sciences of the United States of America*, 108(32), pp.13299–13304.

Horinouchi, T., Higashi, T., Higa, T., Terada, K., Mai, Y., Aoyagi, H., Hatate, C., Nepal, P., Horiguchi, M., Harada, T. & Miwa, S., 2012. Different binding property of STIM1 and its novel splice variant STIM1L to Orai1, TRPC3, and TRPC6 channels. *Biochemical and Biophysical Research Communications*, 428(2), pp.252–258.

Huang, G.N., Zeng, W., Kim, J.Y., Yuan, J.P., Han, L., Muallem, S. & Worley, P.F., 2006. STIM1 carboxyl-terminus activates native SOC, I(crac) and TRPC1 channels. *Nature cell biology*, 8(9), pp.1003–1010.

Hwang, S.-Y. & Putney, J.W., 2012. Orai1-mediated calcium entry plays a critical role in osteoclast differentiation and function by regulating activation of the transcription factor NFATc1. *The FASEB Journal*, 26(4), pp.1484–1492.

Jamsa, A., Hasslund, K., Cowburn, R.F., Backstrom, A. & Vasange, M., 2004. The retinoic acid and brain-derived neurotrophic factor differentiated SH-SY5Y cell line as a model for Alzheimer's disease-like tau phosphorylation. *Biochemical and Biophysical Research Communications*, 319(3), pp.993–1000.

Jardin, I., Lopez, J.J., Salido, G.M. & Rosado, J. a., 2008. Orai1 mediates the interaction between STIM1 and hTRPC1 and regulates the mode of activation of hTRPC1-forming Ca2+ channels. *Journal of Biological Chemistry*, 283(37), pp.25296–25304.

Jardin, I., Salido, G.M. & Rosado, J.A., 2008. Role of lipid rafts in the interaction between hTRPC1, Orai1 and STIM1. *Channels (Austin, Tex.)*, 2(6), pp.401–403.

Jiang, H.-N., Zeng, B., Zhang, Y., Daskoulidou, N., Fan, H., Qu, J.-M. & Xu, S.-Z., 2013. Involvement of TRPC channels in lung cancer cell differentiation and the correlation analysis in human non-small cell lung cancer. *PloS one*, 8(6), p.e67637.

Joshi, S., Guleria, R., Pan, J., DiPette, D. & Singh, U.S., 2006. Retinoic acid receptors and tissue-transglutaminase mediate short-term effect of retinoic acid on migration and invasion of neuroblastoma SH-SY5Y cells. *Oncogene*, 25(2), pp.240–247.

Katsetos, C.D., Legido, A., Perentes, E. & Mork, S.J., 2003. Class III beta-tubulin isotype: a key cytoskeletal protein at the crossroads of developmental neurobiology and tumor neuropathology. *Journal of child neurology*, 18(12), pp.851–66; discussion 867.

Kawasaki, T., Lange, I. & Feske, S., 2009. A minimal regulatory domain in the C terminus of STIM1 binds to and activates ORAI1 CRAC channels. *Biochemical and Biophysical Research Communications*, 385(1), pp.1–11.

Kawasaki, T., Ueyama, T., Lange, I., Feske, S. & Saito, N., 2010. Protein kinase C-induced phosphorylation of Orai1 regulates the intracellular Ca2+ level via the store-operated Ca2+ channel. *Journal of Biological Chemistry*, 285(33), pp.25720–25730.

Kim, J.Y. & Muallem, S., 2011. Unlocking SOAR releases STIM. *The EMBO journal*, 30(9), pp.1673–1675.

Korecka, J. a., van Kesteren, R.E., Blaas, E., Spitzer, S.O., Kamstra, J.H., Smit, A.B., Swaab, D.F., Verhaagen, J. & Bossers, K., 2013. Phenotypic Characterization of Retinoic Acid Differentiated SH-SY5Y Cells by Transcriptional Profiling. *PLoS ONE*, 8(5), p.e63862.

Krishna, A., Biryukov, M., Trefois, C., Antony, P.M., Hussong, R., Lin, J., Heinäniemi, M., Glusman, G., Koeglsberger, S., Boyd, O., Berg, B.H.J. Van Den, Linke, D., Huang, D., Wang, K., Hood, L., Tholey, A., Schneider, R., Galas, D.J., Balling, R. & May, P., 2014. Systems genomics evaluation of the SH-SY5Y neuroblastoma cell line as a model for Parkinson's disease. *BMC Genomics*, 15(1154), pp.1–21.

Kuang, C., Yu, Y., Guo, R., Qian, D., Wang, K., Den, M., Shi, Y. & Huang, L., 2010. Silencing stromal interaction molecule 1 by RNA interference inhibits the proliferation and migration of endothelial progenitor cells. *Biochemical and biophysical research communications*, 398(2), pp.315–320.

LaRosa, G.J. & Gudas, L.J., 1988. Early retinoic acid-induced F9 teratocarcinoma stem cell gene ERA-1: alternate splicing creates transcripts for a homeobox-containing protein and one lacking the homeobox. *Molecular and cellular biology*, 8(9), pp.3906–3917.

Lasorella, A., Lavarone, A. & Israel, M.A., 1995. Differentiation of Neuroblastoma Enhances Bcl-2 Expression and Induces Alterations of Apoptosis and Drug Resistance. *Cancer Research*, 55(20), pp.4711–4716.

Law, M., Morales, J.L., Mottram, L.F., Iyer, A., Peterson, B.R. & August, A., 2011. Structural requirements for the inhibition of calcium mobilization and mast cell activation by the pyrazole derivative BTP2. *International Journal of Biochemistry and Cell Biology*, 43(8), pp.1228–1239.

Levy, C., Khaled, M. & Fisher, D.E., 2006. MITF: master regulator of melanocyte development and melanoma oncogene. *Trends in molecular medicine*, 12(9), pp.406–14.

Lewis, R.S., 2011. Store-operated calcium channels: new perspectives on mechanism and function. *Cold Spring Harbor perspectives in biology*, 3(12), pp.1–24.

Li, C., Wang, X., Vais, H., Thompson, C.B., Foskett, K. & White, C., 2007. Apoptosis regulation by Bcl-XL modulation of mammalian inositol 1,4,5-trisphosphate receptor channel isoform gating. *Proceedings of the National Academy of Sciences*, 104(30), pp.12565–12570.

Li, K.K.C., Goodall, J., Goding, C.R., Liao, S.-K., Wang, C.-H., Lin, Y.-C., Hiraga, H., Nojima, T., Nagashima, K., Schaefer, K.-L. & Lee, K. a W., 2003. The melanocyte inducing factor MITF is stably expressed in cell lines from human clear cell sarcoma. *British journal of cancer*, 89(6), pp.1072–8.

Li, M., Chen, C., Zhou, Z., Xu, S. & Yu, Z., 2012. A TRPC1-mediated increase in store-operated Ca 2+ entry is required for the proliferation of adult hippocampal neural progenitor cells. *Cell Calcium*, 51(6), pp.486–496.

Liang, Y., Mirnics, Z.K., Yan, C., Nylander, K.D. & Schor, N.F., 2003. Bcl-2 mediates induction of neural differentiation. *Oncogene*, 22(35), pp.5515–5518.

Liou, J., Fivaz, M., Inoue, T. & Meyer, T., 2007. Live-cell imaging reveals sequential oligomerization and local plasma membrane targeting of stromal interaction molecule 1 after Ca2+ store depletion. *Proceedings of the National Academy of Sciences of the United States of America*, 104(22), pp.9301–9306.

Liou, J., Kim, M.L., Heo, W. Do, Jones, J.T., Myers, J.W., Jr, J.E.F. & Meyer, T., 2005. STIM is a Ca2+ sensor essential for Ca2+-store-depletion-triggered Ca2+ influx. *Current Biology*, 15, pp.1235–1241.

Lis, A., Peinelt, C., Beck, A., Parvez, S., Monteilh-Zoller, M., Fleig, A. & Penner, R., 2007. CRACM1, CRACM2, and CRACM3 Are Store-Operated Ca2+ Channels with Distinct Functional Properties. *Current Biology*, 17(9), pp.794–800.

Liu, J., Xin, L., Benson, V.L., Allen, D.G. & Ju, Y.-K., 2015. Store-operated calcium entry and the localization of STIM1 and Orai1 proteins in isolated mouse sinoatrial node cells. *Frontiers in Physiology*, 6(March), pp.1–12.

Liu, S., Tian, Y., Chlenski, A., Yang, Q., Zage, P., Salwen, H.R., Crawford, S.E. & Cohn, S.L., 2005. Cross-talk between schwann cells and neuroblasts influences the biology of neuroblastoma xenografts. *American Journal of Pathology*, 166(3), pp.891–900.

Loercher, A.E., Tank, E.M.H., Delston, R.B. & Harbour, J.W., 2005. MITF links differentiation with cell cycle arrest in melanocytes by transcriptional activation of INK4A. *The Journal of cell biology*, 168(1), pp.35–40.

Lopes, F.M., Schröder, R., da Frota, M.L.C., Zanotto-Filho, A., Müller, C.B., Pires, A.S., Meurer, R.T., Colpo, G.D., Gelain, D.P., Kapczinski, F., Moreira, J.C.F., Fernandes, M.D.C. & Klamt, F., 2010. Comparison between proliferative and neuron-like SH-SY5Y cells as an in vitro model for Parkinson disease studies. *Brain Research*, 1337, pp.85–94.

Lopez, E., Jardin, I., Berna-Erro, A., Bermejo, N., Salido, G.M., Sage, S.O., Rosado, J. a. & Redondo, P.C., 2012. STIM1 tyrosine-phosphorylation is required for STIM1-Orai1 association in human platelets. *Cellular Signalling*, 24(6), pp.1315–1322.

Louis, M., Zanou, N., Van Schoor, M. & Gailly, P., 2008. TRPC1 regulates skeletal myoblast migration and differentiation. *Journal of cell science*, 121(Pt 23), pp.3951–3959.

Lovat, P.E., Irving, H., Annicchiarico-Petruzzelli, M., Bernassola, F., Malcolm, A.J., Pearson, A.D.J., Melino, G. & Redfern, C.P.F., 1997. Retinoids in neuroblastoma

therapy: distinct biological properties of 9-cis- and all-trans-retinoic acid. *European Journal of Cancer*, 33(12), pp.2075–2080.

Lovat, P.E., Irving, H., Malcolm, a J., Pearson, a D. & Redfern, C.P., 1997. 9-Cis Retinoic Acid-a better retinoid for the modulation of differentiation, proliferation and gene expression in human neuroblastoma. *Journal of neuro-oncology*, 31(1-2), pp.85–91.

Luik, R.M., Wang, B., Prakriya, M., Wu, M.M. & Lewis, R.S., 2008. Oligomerization of STIM1 couples ER calcium depletion to CRAC channel activation. *Nature*, 454(7203), pp.538–542.

Macara, I.G., 1985. Oncogenes, ions, and phospholipids. *American Journal of Physiology - Cell Physiology*, 248(1), pp.C3–C11.

Majewski, L. & Kuznicki, J., 2015. SOCE in neurons: Signaling or just refilling? *Biochimica et Biophysica Acta (BBA) - Molecular Cell Research*, 1853, pp.1940–1952.

Manji, S.S., Parker, N.J., Williams, R.T., van Stekelenburg, L., Pearson, R.B., Dziadek, M. & Smith, P.J., 2000. STIM1: a novel phosphoprotein located at the cell surface. *Biochimica et biophysica acta*, 1481(1), pp.147–55.

Maric, D., Maric, I. & Barker, J.L., 2000. Developmental changes in cell calcium homeostasis during neurogenesis of the embryonic rat cerebral cortex. *Cerebral cortex (New York, N.Y. : 1991)*, 10(6), pp.561–573.

Matthay, K.K., Reynolds, C.P., Seeger, R.C., Shimada, H., Adkins, E.S., Haas-Kogan, D., Gerbing, R.B., London, W.B. & Villablanca, J.G., 2009. Long-term results for children with high-risk neuroblastoma treated on a randomized trial of myeloablative therapy followed by 13-cis-retinoic acid: a Children's Oncology Group study . *Journal of Clinical Oncology*, 27, pp.1007–1013.

Mekahli, D., Bultynck, G., Parys, J.B., de Smedt, H. & Missiaen, L., 2011. Endoplasmic-reticulum calcium depletion and disease. *Cold Spring Harbor Perspectives in Biology*, 3(6), pp.1–30.

Mercer, J.C., Dehaven, W.I., Smyth, J.T., Wedel, B., Rebecca, R., Bird, G.S. & Jr, J.W.P., 2006. Large store-operated calcium-selective currents due to co-expression of Orai1 or Orai2 with the intacellular calcium sensor, STIM1. *Journal of Biological Chemistry*, 281(34), pp.24979–24990.

Messi, E., Florian, M.C., Caccia, C., Zanisi, M. & Maggi, R., 2008. Retinoic acid reduces human neuroblastoma cell migration and invasiveness: effects on DCX, LIS1, neurofilaments-68 and vimentin expression. *BMC cancer*, 8, p.30.

Middleton, G., Pinon, L.G., Wyatt, S. & Davies, A.M., 1998. Bcl-2 accelerates the maturation of early sensory neurons. *The Journal of neuroscience : the official journal of the Society for Neuroscience*, 18(9), pp.3344–3350.

Mignen, O., Thompson, J.L. & Shuttleworth, T.J., 2008. Orai1 subunit stoichiometry of the mammalian CRAC channel pore. *The Journal of physiology*, 586(2), pp.419–425.

Minucci, S., Leid, M., Toyama, R., Saint-Jeannet, J.P., Peterson, V.J., Horn, V., Ishmael, J.E., Bhattacharyya, N., Dey, a, Dawid, I.B. & Ozato, K., 1997. Retinoid X receptor (RXR) within the RXR-retinoic acid receptor heterodimer binds its ligand and enhances retinoid-dependent gene expression. *Molecular and cellular biology*, 17(2), pp.644–655.

Misonou, H., Morishima-Kawashima, M. & Ihara, Y., 2000. Oxidative Stress Induces Intracellular Accumulation of Amyloid β-Protein (Aβ) in Human Neuroblastoma Cells. *Biochemistry*, 39(23), pp.6951–6959.

Mizrak, D. & Brittan, M., 2008. CD133 : molecule of the moment. , pp.3–9.

Mollard, R., Viville, S., Ward, S.J., Décimo, D., Chambon, P. & Dollé, P., 2000. Tissue-specific expression of retinoic acid receptor isoform transcripts in the mouse embryo. *Mechanisms of Development*, 94(1-2), pp.223–232.

Mora, J., Cheung, N.-K. V, Juan, G., Illei, P., Cheung, I., Akram, M., Chi, S., Ladanyi, M., Cordon-Cardo, C. & Gerald, W.L., 2001. Neuroblastic and Schwannian Stromal Cells of Neuroblastoma Are Derived from a Tumoral Progenitor Cell. *Cancer Research*, 61(18), pp.6892–6898.

Morgan, J.I. & Curran, T., 1986. Role of ion flux in the control of c-fos expression. *Nature*, 322(6079), pp.552–555.

Mullins, F.M., Park, C.Y., Dolmetsch, R.E. & Lewis, R.S., 2009. STIM1 and calmodulin interact with Orai1 to induce Ca2+-dependent inactivation of CRAC channels. *Proceedings of the National Academy of Sciences of the United States of America*, 106(36), pp.15495–500.

Nakagawara, A., 1998. Molecular basis of spontaneous regression of neuroblastoma: role of neurotrophic signals and genetic abnormalities. *Human cell*, 11(3), pp.115–124.

Nakamura, K., Bindokas, V.P., Marks, J.D., Wright, D.A., Frim, D.M., Miller, R.J., Kang, U.N.J., N, C.N.K. & W, D.N.D.A., 2000. The Selective Toxicity of 1-Methyl-4-phenylpyridinium to Dopaminergic Neurons : The Role of Mitochondrial Complex I and Reactive Oxygen Species Revisited. *Molecular Pharmacology*, 58, pp.271–278.

Nakamura, Y., Hashimoto, R., Amano, M., Nagata, K., Matsumoto, N., Goto, H., Fukusho, E., Mori, H., Kashiwagi, Y., Kudo, T., Inagaki, M. & Takeda, M., 2000. Localized phosphorylation of vimentin by rho-kinase in neuroblastoma N2a cells. *Genes to cells : devoted to molecular & cellular mechanisms*, 5(10), pp.823–837.

Navalkele, P., O'Dorisio, M.S., O'Dorisio, T.M., Zamba, G.K.D. & Lynch, C.F., 2011. Incidence, survival, and prevalence of neuroendocrine tumors versus

neuroblastoma in children and young adults: Nine standard SEER registries, 1975–2006. *Pediatric Blood & Cancer*, 56(1), pp.50–57.

Navalkele, P., O'Dorisio, S., O'Dorisio, T.M., Zamba, G.K.D. & Lynch, C.F., 2011. Incidence, survival, and prevalence of neuroendocrine tumours versus neuroblastoma in children and young adults: nine standard SEER registries, 1975-2006. *Pediatric Blood Cancer*, 56, pp.50–57.

Nishihira, H., Toyoda, Y., Tanaka, Y., Ijiri, R., Aida, N., Takeuchi, M., Ohnuma, K., Kigasawa, H., Kato, K. & Nishi, T., 2000. Natural Course of Neuroblastoma Detected by Mass Screening: A 5-Year Prospective Study at a Single Institution. *Journal of Clinical Oncology*, 18(16), pp.3012–3017.

Ohga, K., Takezawa, R., Arakida, Y., Shimizu, Y. & Ishikawa, J., 2008. Characterization of YM-58483/BTP2, a novel store-operated Ca2+ entry blocker, on T cell-mediated immune responses in vivo. *International Immunopharmacology*, 8(13-14), pp.1787–1792.

Okazaki, T., Mochizuki, T., Tashima, M., Sawada, H. & Uchino, H., 1986. Role of intracellular calcium ion in human promyelocytic leukemia HL-60 cell differentiation. *Cancer Research*, 46(12), pp.6059–6063.

Olempska, M., Eisenach, P.A., Ammerpohl, O., Ungefroren, H., Fandrich, F. & Kalthoff, H., 2007. Detection of tumor stem cell markers in pancreatic carcinoma cell lines. *Hepatobiliary & pancreatic diseases international : HBPD INT*, 6(1), pp.92–97.

Pahlman, S., Ruusala, A.-I., Abrahamsson, L., Mattsson, M.E.K. & Esscher, T., 1984. Retinoic acid-induced differentiation of cultured human neuroblastoma cells: a comparison with phorbolester-induced differentiation. *Cell Differentiation*, 14, pp.135–144.

Parekh, A.B. & Putney, J.W., 2005. Store-operated Calcium Channels. *Physiological Reviews*, 85, pp.757–810.

Park, C.Y., Hoover, P.J., Mullins, F.M., Bachhawat, P., Covington, E.D., Raunser, S., Walz, T., Garcia, C.K., Dolmetsch, R.E. & Lewis, R.S., 2009. STIM1 clusters and activates CRAC channels via direct binding of a cytosolic domain to Orai1. *Cell*, 136(5), pp.876–890.

Parvez, S., Beck, A., Peinelt, C., Soboloff, J., Lis, A., Monteilh-Zoller, M., Gill, D.L., Fleig, A. & Penner, R., 2008. STIM2 protein mediates distinct store-dependent and store-independent modes of CRAC channel activation. *FASEB Journal*, 22(3), pp.752–761.

Peinelt, C., Vig, M., Koomoa, D.L., Beck, A., Nadler, M.J.S., Koblan-Huberson, M., Lis, A., Fleig, A., Penner, R. & Kinet, J.-P., 2006. Amplification of CRAC current by STIM1 and CRACM1 (Orai1). *Nature cell biology*, 8(7), pp.771–773.

Penna, A., Demuro, A., Yeromin, A. V, Zhang, S.L., Safrina, O., Parker, I. & Cahalan, M.D., 2008. The CRAC channel consists of a tetramer formed by Stim-induced dimerization of Orai dimers. *Nature*, 456, pp.116–120.

Petratos, S., Li, Q.X., George, A.J., Hou, X., Kerr, M.L., Unabia, S.E., Hatzinisiriou, I., Maksel, D., Aguilar, M.I. & Small, D.H., 2008. The beta-amyloid protein of Alzheimer's disease increases neuronal CRMP-2 phosphorylation by a Rho-GTP mechanism. *Brain*, 131(1), pp.90–108.

Picacentini, M., Piredda, L., Starace, D., Annicchiarico-Petruzzelli, M., Mattei, M., Oliverio, S., Farrace, M.G. & Melino, G., 1996. Differential growth of N- and S-type human neuroblastoma cells xenografted into SCID mice. Correlation with apoptosis. *Journal of Pathology*, 180, pp.415–422.

Pinton, P., Ferrari, D., Magalhaes, P., Schulze-Osthoff, K., Di Virgilio, F., Pozzan, T. & Rizzuto, R., 2000. Reduced loading of intracellular Ca2+ stores and downregulation of capacitative Ca2+ influx in Bcl-2-overexpressing cells. *Journal of Cell Biology*, 148(5), pp.857–862.

Ponthan, F., Borgstrom, P., Hassan, M., Wassberg, E., Redfern, C. & Kogner, P., 2001. The vitamin A analogues: 13-cis retinoic acid, 9-cis retinoic acid, and Ro 13-6307 inhibit neuroblastoma tumour growth in vivo. *Medical and Pediatric Oncology*, 36(1), pp.127–131.

Potier, M., Gonzalez, J.C., Motiani, R.K., Abdullaev, I.F., Bisaillon, J.M., Singer, H. a & Trebak, M., 2009. Evidence for STIM1- and Orai1-dependent store-operated calcium influx through ICRAC in vascular smooth muscle cells: role in proliferation and migration. *The FASEB journal : official publication of the Federation of American Societies for Experimental Biology*, 23(8), pp.2425–2437.

Potter, J.D., 2007. Morphogens, morphostats, microarchitecture and malignancy. *Nature Reviews Cancer*, 7, pp.464–474.

Pozo-Guisado, E., Casas-Rua, V., Tomas-Martin, P., Lopez-Guerrero, A.M., Alvarez-Barrientos, A. & Martin-Romero, F.J., 2013. Phosphorylation of STIM1 at ERK1/2 target sites regulates interaction with the microtubule plus-end binding protein EB1. *Journal of cell science*, 126(Pt 14), pp.3170–80.

Pozo-guisado, E. & Martin-romero, F.J., 2013. The regulation of STIM1 by phosphorylation. , (December), pp.1–5.

Prakriya, M., Feske, S., Gwack, Y., Srikanth, S., Rao, A. & Hogan, P.G., 2006. Orai1 is an essential pore subunit of the CRAC channel. *Nature*, 443(7108), pp.230–233.

Prakriya, M. & Lewis, R.S., 2006. Regulation of CRAC channel activity by recruitment of silent channels to a high open-probability gating mode. *The Journal of general physiology*, 128(3), pp.373–386.

Prevarskaya, N., Skryma, R. & Shuba, Y., 2011. Calcium in tumour metastasis: new roles for known actors. *Nature reviews. Cancer*, 11(8), pp.609–618.

Pritchard, J. & Hickman, J. a., 1994. Why does stage 4s neuroblastoma regress spontaneously? *Lancet*, 344(8926), pp.869–870.

Putney, J.W., 1986. A model for receptor-regulated calcium entry. *Cell Calcium*, 7(1), pp.1–12.

Putney, J.W., 2007. Multiple mechanisms of TRPC activation W. B. Liedtke & S. Heller, eds. *TRP ion channels function in sensory trasduction and cellular signaling cascades*.

Putney, J.W., 2001. The Pharmacology of Capacitative Calcium Entry. *Molecular Interventions*, 4(2), pp.84–94.

Putney, J.W., 2011. The Physiological Function of Store-operated Calcium Entry. *Neurochemical Research*, 36, pp.1157–1165.

Raz, A. & Ben-Ze'ev, A., 1987. Cell-contact and -architecture of malignant cells and their relationship to metastasis. *Cancer and Metastasis Reviews*, 6, pp.3–21.

Reboulleau, C.P., 1986. Extracellular calcium-induced neuroblastoma cell differentiation: involvement of phosphatidylinositol turnover. *Journal of Neurochemistry*, 46(3), pp.920–930.

Redfern, C.P., Lovat, P.E., Malcolm, a J. & Pearson, a D., 1994. Differential effects of 9-cis and all-trans retinoic acid on the induction of retinoic acid receptor-beta and cellular retinoic acid-binding protein II in human neuroblastoma cells. *The Biochemical journal*, 304 (Pt 1, pp.147–154.

Rees, J.L., Daly, A.K. & Redfern, C.P.F., 1989. Differential expression of the alpha and beta retinoic acid receptors in tissues of the rat. *Biochemical Journal*, 259, pp.917–919.

Reynolds, C.P., Matthay, K.K., Villablanca, J.G. & Maurer, B.J., 2003. Retinoid therapy of high-risk neuroblastoma. *Cancer Letters*, 197, pp.185–192.

Ricci-Vitiani, L., Lombardi, D.G., Pilozzi, E., Biffoni, M., Todaro, M., Peschle, C. & De Maria, R., 2007. Identification and expansion of human colon-cancer-initiating cells. *Nature*, 445(7123), pp.111–115.

Riddoch, F.C., Brown, A.M., Rowbotham, S.E., Redfern, C.P.F. & Cheek, T.R., 2007. Changes in functional properties of the caffeine-sensitive Ca2+ store during differentiation of human SH-SY5Y neuroblastoma cells. *Cell Calcium*, 41, pp.195–206.

Rizzuto, R., De Stefani, D., Raffaello, A. & Mammucari, C., 2012. Mitochondria as sensors and regulators of calcium signalling. *Nature Reviews Molecular Cell Biology*, 13(9), pp.566–578.

Da Rocha, J.F., da Cruz e Silva, O. a. B. & Vieira, S.I., 2015. Analysis of the Amyloid Precursor Protein (APP) role in neuritogenesis reveals a biphasic SH-SY5Y neuronal cell differentiation model. *Journal of Neurochemistry*, 134, pp.288–301.

Roos, J., DiGregorio, P.J., Yeromin, A. V, Ohlsen, K., Lioudyno, M., Zhang, S., Safrina, O., Kozak, J.A., Wagner, S.L., Cahalan, M.D., Velicelebi, G. & Stauderman, K.A., 2005. STIM1, an essential and conserved component of store-operated Ca2+ channel function. *The Journal of Cell Biology*, 169(3), pp.435–445.

Ross, R. a & Spengler, B. a, 2004. The conundrum posed by cellular heterogeneity in analysis of human neuroblastoma. *Journal of the National Cancer Institute*, 96(16), pp.1192–3.

Ross, R.A. & Biedler, J.L., 1985. Presence and Regulation of Tyrosinase Activity in Human Neuroblastoma Cell Variants in Vitro. *Cancer Research*, 45(4), pp.1628–1632.

Ross, R.A., Biedler, J.L. & Spengler, B.A., 2003. A role for distinct cell types in determining malignancy in human neuroblastoma cell lines and tumors. *Cancer Letters*, 197(1–2), pp.35–39.

Ross, R.A., Spengler, B. a, Dom, C., Rettig, W.J., Biedler, J.L., Domenech, C., Porubcin, M., Rettig, W.J. & Biedler, J.L., 1995. Human Neuroblastoma I-type Cells Are Malignant Neural Crest Stem Cells. *Cell Growth & Differentiation*, 6(April), pp.449–456.

Ross, R.A., Spengler, B.A. & Biedler, J.L., 1983. Coordinate morphological and biochemical interconversion of human neuroblastoma cells. *Journal of the National Cancer Institute*, 71(4), pp.741–747.

Sammels, E., Parys, J.B., Missiaen, L., Smedt, H.D. & Bultynck, G., 2010. Intracellular Ca2+ storage in health and disease: A dynamic equilibrium. *Cell Calcium*, 27, pp.297–314.

Sauc, S., Bulla, M., Nunes, P., Orci, L., Marchetti, a., Antigny, F., Bernheim, L., Cosson, P., Frieden, M. & Demaurex, N., 2015. STIM1L traps and gates Orai1 channels without remodeling the cortical ER. *Journal of Cell Science*, 128(8), pp.1568–1579.

Schleifer, H., Doleschal, B., Lichtenegger, M., Oppenrieder, R., Derler, I., Frischauf, I., Glasnov, T., Kappe, C., Romanin, C. & Groschner, K., 2012. Novel pyrazole compounds for pharmacological discrimination between receptor-operated and store-operated Ca $^{2+}$ entry pathways. *British Journal of Pharmacology*, 167(8), pp.1712–1722.

Schug, T.T., Berry, D.C., Shaw, N.S., Travis, S.N. & Noy, N., 2007. Opposing effects of retinoic acid on cell growth result from alternate activation of two different nuclear receptors. *Cell*, 129(4), pp.723–733.

Schwab, M., Westermann, F., Hero, B. & Berthold, F., 2003. Neuroblastoma: biology and molecular and chromosomal pathology. *The Lancet Oncology*, 4(8), pp.472–480.

Shaw, N., Elholm, M. & Noy, N., 2003. Retinoic acid is a high affinity selective ligand for the peroxisome proliferator-activated receptor beta/delta. *The Journal of Biological Chemistry*, 278(43), pp.41589–41592.

Shea, T.B., Beermann, M.L. & Fischer, I., 1993. Transient requirement for vimentin in neuritogenesis: Intracellular delivery of anti-vimentin antibodies and antisense oligonucleotides inhibit neurite initiation but not elongation of existing neurites in neuroblastoma. *Journal of Neuroscience Research*, 36(1), pp.66–76.

Sherbert, G. V, 2001. *Calcium Signalling in Cancer*, CRC Press.

Shi, Y., Song, M., Guo, R., Wang, H., Gao, P., Shi, W. & Huang, L., 2010. Knockdown of stromal interaction molecule 1 attenuates hepatocyte growth factor-induced endothelial progenitor cell proliferation. *Experimental Biology and Medicine* , 235 (3), pp.317–325.

Shin, H.Y., Hong, Y.H., Jang, S.S., Chae, H.G., Paek, S.L., Moon, H.E., Kim, D.G., Kim, J., Paek, S.H. & Kim, S.J., 2010. A role of canonical transient receptor potential 5 channel in neuronal differentiation from A2B5 neural progenitor cells. *PloS one*, 5(5), p.e10359.

Shuttleworth, T.J., 2012. Orai3--the "exceptional" Orai? *The Journal of physiology*, 590(Pt 2), pp.241–57.

Siegel, R., Naishadham, D. & Jemal, A., 2013. Cancer statistics, 2013. *CA: A Cancer Journal for Clinicians*, 63(1), pp.11–30.

Simpson, P.B., Bacha, J.I., Palfreyman, E.L., Woollacott, A.J., McKernan, R.M. & Kerby, J., 2001. Retinoic acid-evoked differentiation of neuroblastoma cells predominates over growth factor stimulation: an automated image capture and quantitation approach to neuritogenesis. *Analytical Biochemistry*, 298, pp.163–169.

Singh, S., Clarke, I., Terasaki, M., Bonn, V., Hawkins, C., Squire, J. & Dirks, P., 2003. Identificaiton of a Cancer Stem Cell in Human Brain Tumours. *Cancer Research*, 63, pp.5821–5828.

Smith, M., Adamson, P., Ballis, F., Feusner, J., Aronson, L., Murphy, R., Horowitz, M., Reaman, G., Hammond, G. & Fenton, R., 1992. Phase I and pharmacokinetic evaluation of all-trans-retinoic acid in pediatric patients with cancer. *Journal of Clinical Oncology*, 10(11), pp.1666–1673.

Smyth, J.T., Hwang, S.-Y., Tomita, T., DeHaven, W.I., Mercer, J.C. & Putney, J.W., 2010. Activation and regulation of store-operated calcium entry. *Journal of Cellular and Molecular Medicine*, 14(10), pp.2337–49.

Smyth, J.T., Petranka, J.G., Boyles, R.R., DeHaven, W.I., Fukushima, M., Johnson, K.L., Williams, J.G. & Jr, J.W.P., 2009. Phosphorylation of STIM1 Underlies Suppression of Store-operated Calcium Entry During Mitosis. *Nature Cell Biology*, 11(12), pp.1465–1472.

Smyth, J.T., Petranka, J.G., Boyles, R.R., DeHaven, W.I., Fukushima, M., Johnson, K.L., Williams, J.G. & Putney, J.W., 2009. Phosphorylation of STIM1 underlies suppression of store-operated calcium entry during mitosis. *Nature cell biology*, 11(12), pp.1465–72.

Soboloff, J., Spassova, M. a., Dziadek, M. a. & Gill, D.L., 2006. Calcium signals mediated by STIM and Orai proteins-A new paradigm in inter-organelle communication. *Biochimica et Biophysica Acta - Molecular Cell Research*, 1763(11), pp.1161–1168.

Stathopulos, P.B., Li, G.Y., Plevin, M.J., Ames, J.B. & Ikura, M., 2006. Stored Ca2+ depletion-induced oligomerization of stromal interaction molecule 1 (STIM1) via the EF-SAM region: An initiation mechanism for capacitive Ca2+ entry. *Journal of Biological Chemistry*, 281(47), pp.35855–35862.

Stathopulos, P.B., Zheng, L. & Ikura, M., 2009. Stromal interaction molecule (STIM) 1 and STIM2 calcium sensing regions exhibit distinct unfolding and oligomerization kinetics. *Journal of Biological Chemistry*, 284(2), pp.728–732.

Sundivakkam, P.C., Freichel, M., Singh, V., Yuan, J.P., Vogel, S.M., Flockerzi, V., Malik, A.B. & Tiruppathi, C., 2012. The Ca(2+) sensor stromal interaction molecule 1 (STIM1) is necessary and sufficient for the store-operated Ca(2+) entry function of transient receptor potential canonical (TRPC) 1 and 4 channels in endothelial cells. *Molecular pharmacology*, 81(4), pp.510–26.

Sundivakkam, P.C., Natarajan, V., Malik, A.B. & Tiruppathi, C., 2013. Store-operated Ca2+ entry (SOCE) induced by protease-activated receptor-1 mediates STIM1 protein phosphorylation to inhibit SOCE in endothelial cells through AMP-activated protein kinase and p38β mitogen-activated protein kinase. *The Journal of biological chemistry*, 288(23), pp.17030–41.

Suzuki, A. & Tsutomi, Y., 1998. Bcl-2 accelerates the neuronal differentiation: new evidence approaching to the biofunction of bcl-2 in the neuronal system. *Brain research*, 801(1-2), pp.59–66.

Tachibana, M., Takeda, K., Nobukuni, Y., Urabe, K., Long, J.E., Meyers, K.A., Aaronson, S.A. & Miki, T., 1996. Ectopic expression of MITF, a gene for Waardenburg syndrome type 2, converts fibroblasts to cells with melanocyte characteristics. *Nature genetics*, 14(1), pp.50–54.

Takahashi, Y., Murakami, M., Watanabe, H., Hasegawa, H., Ohba, T., Munehisa, Y., Nobori, K., Ono, K., Iijima, T. & Ito, H., 2007. Essential role of the N-terminus of murine Orai1 in store-operated Ca2+ entry. *Biochemical and Biophysical Research Communications*, 356(1), pp.45–52.

Takahashi, Y., Watanabe, H., Murakami, M., Ono, K., Munehisa, Y., Koyama, T., Nobori, K., Iijima, T. & Ito, H., 2007. Functional role of stromal interaction molecule 1 (STIM1) in vascular smooth muscle cells. *Biochemical and Biophysical Research Communications*, 361(4), pp.934–940.

Takenobu, H., Shimozato, O., Nakamura, T., Ochiai, H., Yamaguchi, Y., Ohira, M., Nakagawara, a & Kamijo, T., 2011. CD133 suppresses neuroblastoma cell differentiation via signal pathway modification. *Oncogene*, 30(1), pp.97–105.

Takezawa, R., Cheng, H., Beck, A., Ishikawa, J., Launay, P., Kubota, H., Kinet, J.-P., Fleig, A., Yamada, T. & Penner, R., 2006. A pyrazole derivative potently inhibits lymphocyte Ca2+ influx and cytokine production by facilitating transient receptor potential melastatin 4 channel activity. *Molecular pharmacology*, 69(4), pp.1413–1420.

Targos, B., Barańska, J. & Pomorski, P., 2005. Store-operated calcium entry in physiology and pathology of mammalian cells. *Acta biochimica Polonica*, 52(2), pp.397–409.

Tsokos, M., Scarpa, S., Ross, R.A. & Triche, T.J., 1987. Differentiation of Human Neuroblastoma Recapitulates Neural Crest Development Study of Morphology , Neurotransmitter Enzymes , and Extracellular Matrix Proteins. , 128(3), pp.484–496.

Valent, A., Bénard, J., Vénuat, A.M., Da Silva, J., Duverger, A., Duarte, N., Hartmann, O., Spengler, B. a. & Bernheim, A., 1999. Phenotypic and genotypic diversity of human neuroblastoma studied in three IGR cell line models derived from bone marrow metastases. *Cancer Genetics and Cytogenetics*, 112(2), pp.124–129.

Villablanca, J., Khan, A., Avramis, V., Seeger, R., Matthay, K., Ramsay, N. & Reynolds, C., 1995. Phase I trial of 13-cis-retinoic acid in children with neuroblastoma following bone marrow transplantation. *Journal of Clinical Oncology*, 13(4), pp.894–901.

Voigt, A. & Zintl, F., 2003. Effects of retinoic acid on proliferation, apoptosis, cytotoxicity, migration, and invasion of neuroblastoma cells. *Medical and Pediatric Oncology*, 40(4), pp.205–213.

Walton, J.D., Kattan, D.R., Thomas, S.K., Spengler, B. a., Guo, H.-F., Biedler, J.L., Cheung, N.-K. V. & Ross, R. a., 2004. Characteristics of Stem Cells from Human Neuroblastoma Cell Lines and in Tumors. *Neoplasia*, 6(6), pp.838–845.

Wessel, D. & Flugge, U., 1984. A method for the quantitative recovery of protein in dilute solution in the presence of detergents and lipids. *Analytical Biochemistry*, 138(1), pp.141–143.

Whitworth, C., 2012. Ca2+ signalling and differentiation in N- and S-type neuroblastoma cells. *MRes dissertation from the Institute for Cell and Molecular Biosciences*.

Wiesner, B., Roloff, B., Fechner, K. & Slominski, A., 2002. Intracellular calcium measurements of single human skin cells after stimulation with corticotropin-releasing factor and urocortin using confocal laser scanning microscopy. *Journal of cell science*, 116(Pt 7), pp.1261–1268.

Williams, R.T., Manji, S.S., Parker, N.J., Hancock, M.S., Van Stekelenburg, L., Eid, J.P., Senior, P. V, Kazenwadel, J.S., Shandala, T., Saint, R., Smith, P.J. & Dziadek, M. a, 2001. Identification and characterization of the STIM (stromal interaction molecule) gene family: coding for a novel class of transmembrane proteins. *The Biochemical journal*, 357(Pt 3), pp.673–685.

Williams, R.T., Senior, P. V., Van Stekelenburg, L., Layton, J.E., Smith, P.J. & Dziadek, M. a., 2002. Stromal interaction molecule 1 (STIM1), a transmembrane protein with growth suppressor activity, contains an extracellular SAM domain modified by N-linked glycosylation. *Biochimica et Biophysica Acta - Protein Structure and Molecular Enzymology*, 1596(1), pp.131–137.

Wu, M.M., Buchanan, J., Luik, R.M. & Lewis, R.S., 2006. Ca 2+ store depletion causes STIM1 to accumulate in ER regions closely associated with the plasma membrane. *Journal of Cell Biology*, 174(6), pp.803–813.

Wu, X., Zagranichnaya, T.K., Gurda, G.T., Eves, E.M. & Villereal, M.L., 2004. A TRPC1/TRPC3-mediated increase in store-operated calcium entry is required for differentiation of H19-7 hippocampal neuronal cells. *The Journal of biological chemistry*, 279(42), pp.43392–43402.

Yabe, J.T., Chan, W.K.-H., Wang, F.-S., Pimenta, A., Ortiz, D.D. & Shea, T.B., 2003. Regulation of the transition from vimentin to neurofilaments during neuronal differentiation. *Cell motility and the cytoskeleton*, 56(3), pp.193–205.

Yamashita, M., 2013. From neuroepithelial cells to neurons: Changes in the physiological properties of neuroepithelial stem cells. *Archives of Biochemistry and Biophysics*, 534(1-2), pp.64–70.

Yang, S., Zhang, J.J. & Huang, X.Y., 2009. Orai1 and STIM1 Are Critical for Breast Tumor Cell Migration and Metastasis. *Cancer Cell*, 15(2), pp.124–134.

Yin, S., Li, J., Hu, C., Chen, X., Yao, M., Yan, M., Jiang, G., Ge, C., Xie, H., Wan, D., Yang, S., Zheng, S. & Gu, J., 2007. CD133 positive hepatocellular carcinoma cells possess high capacity for tumorigenicity. *International journal of cancer. Journal international du cancer*, 120(7), pp.1444–1450.

Yuan, J.P., Kiselyov, K., Shin, D.M., Chen, J., Shcheynikov, N., Kang, S.H., Dehoff, M.H., Schwarz, M.K., Seeburg, P.H., Muallem, S. & Worley, P.F., 2003. Homer Binds TRPC Family Channels and Is Required for Gating of TRPC1 by IP3 Receptors. *Cell*, 114(6), pp.777–789.

Yuan, J.P., Lee, K.P., Hong, J.H. & Muallem, S., 2012. The closing and opening of TRPC channels by Homer1 and STIM1. *Acta Physiologica*, 204(2), pp.238–247.

Yuan, J.P., Zeng, W., Huang, G.N., Worley, P.F. & Muallem, S., 2007. STIM1 heteromultimerizes TRPC to determine their function as store-operated channels. *Nature Cell Biology*, 9(6), pp.636–645.

Zanou, N., Schakman, O., Louis, P., Ruegg, U.T., Dietrich, A., Birnbaumer, L. & Gailly, P., 2012. Trpc1 ion channel modulates phosphatidylinositol 3-kinase/Akt pathway during myoblast differentiation and muscle regeneration. *Journal of Biological Chemistry*, 287(18), pp.14524–14534.

Zhang, K.-Z., Westberg, J.A., Holtta, E. & Andersson, L.E., 1996. BCL2 regulates neural differentiation. *Proceedings of the National Academy of Sciences*, 93, pp.4504–4508.

Zhang, S.L., Ying, Y., Roos, J., Kozak, J.A., Deerinck, T.J., Ellisman, M.H., Stauderman, K.A. & Cah, 2005. STIM1 is a Ca2+ sensor that activates CRAC channels and migrates from the Ca2+ store to the plasma membrane. *Nature*, 437(7060), pp.902–905.

Zhang, W., Meng, H., Li, Z.-H., Shu, Z., Ma, X. & Zhang, B.-X., 2007. Regulation of STIM1, store-operated Ca2+ influx, and nitric oxide generation by retinoic acid in rat mesangial cells. *American journal of physiology. Renal physiology*, 292(3), pp.F1054–F1064.

Zheng, L., Roberg, K., Jerhammar, F., Marcusson, J. & Terman, A., 2006. Autophagy of amyloid beta-protein in differentiated neuroblastoma cells exposed to oxidative stress. *Neuroscience Letters*, 394, pp.184–189.

Zheng, L., Stathopulos, P.B., Li, G.Y. & Ikura, M., 2008. Biophysical characterization of the EF-hand and SAM domain containing Ca2+ sensory region of STIM1 and STIM2. *Biochemical and Biophysical Research Communications*, 369(1), pp.240–246.

Zhou, Y., Lewis, T.L., Robinson, L.J., Brundage, K.M., Schafer, R., Martin, K.H., Blair, H.C., Soboloff, J. & Barnett, J.B., 2011. The role of calcium release activated calcium channels in osteoclast differentiation. *Journal of Cellular Physiology*, 226(4), pp.1082–1089.

Zitt, C., Strauss, B., Schwarz, E.C., Spaeth, N., Rast, G., Hatzelmann, A. & Hoth, M., 2004. Potent Inhibition of Ca2+ Release-activated Ca2+ Channels and T-lymphocyte Activation by the Pyrazole Derivative BTP2. *Journal of Biological Chemistry*, 279(13), pp.12427–12437.

Zweifach, A. & Lewis, R.S., 1995. Rapid inactivation of depletion-activated calcium current (ICRAC) due to local calcium feedback. *The Journal of general physiology*, 105(2), pp.209–226.

Zweifach, A. & Lewis, R.S., 1995. Slow calcium-dependent inactivation of depletion-activated calcium current: Store-dependent and -independent mechanisms. *Journal of Biological Chemistry*, 270(24), pp.14445–14451.